Abstract

This Ph.D. thesis focuses on three main topics:

1) **Design and evaluation of new stable bidentate urea-type stationary phases for HPLC and UHPLC.** New totally synthetic bidentate urea-type phases were envisioned for HPLC and UHPLC, characterized by a high stability, a wide application range and an excellent suitability for LC-MS. Four conceptually new stationary phases have been developed for the separation of a wide variety of polar compounds by hydrophilic interaction chromatography (HILIC) through a facile one-pot two-step procedure with the aim of obtaining high hydrolytic stability in a variety of elution conditions. A full chemical characterization of the new materials has been obtained through solid-state NMR (both ^{29}Si and ^{13}C CPMAS) spectroscopy. A major application field of the bidentate urea-type stationary phase with free amino groups USP-HILIC-NH_2-sil was sugars analysis, usually hampered by α/β anomer peak splitting and instability of the stationary phases under conditions normally employed to suppress it. Complex mixtures of mono-, di- and oligosaccharides were successfully resolved under mild chromatographic conditions, which also allowed an

easy interface with mass spectrometry. The potential of such materials was shown in the separation of other highly polar compounds, including polyols, hydroxybenzoic acids, nucleobases, and vitamins. A parallel project was developed using a very similar synthetic scheme where enantiopure diamines were treated with (3-isocyanatopropyl) triethoxysilane to yield reactive ureido selectors that were eventually attached to unmodified silica particles through a stable, bidentate tether. The two steps were part of an easy and time-saving one-pot procedure, as was the case for the HILIC phases. These new monomeric *brush-type* chiral stationary phases, hereafter called "Crab-like" CSPs, are characterized by an excellent stability and enantioselectivity, a high permeability and efficiency, as well as an extended compatibility with all solvents and no memory effect, which allowed us to operate under normal phase, reversed phase and polar organic mode conditions. Comparative studies were performed with commmercial polymeric *brush-type* CSPs bearing the same chiral selector (1,2-diaminocyclohexane and 1,2-diphenyl-1,2-ethylenediamine) in order to evaluate the resolution and performance skills of the new "Crab-like" CSPs in different elution modes.

2) **Extending the use of "Inverted Chirality Columns Approach (ICCA)" for enantiomeric excess determination in absence of reference samples: application to a water-soluble camptothecin derivative.** The aim of the present study was to extend the use of the "Inverted Chirality Columns Approach (ICCA)" previously developed for the identification and quantitation of the trace enantiomer in highly enriched samples of the camptothecin (CPT) family of drugs to a novel water-soluble CPT derivative, namely namitecan (ST1968), currently undergoing phase I clinical trials as anticancer agent. Namitecan, identified from a series of hydrophilic 7-oxyiminomethyl derivatives, contains a free terminal amino group, which traditionally hampers the analysis under normal-phase HPLC conditions. Nevertheless, commercially available Pirkle-type chiral stationary phases (CSPs) available in both the enantiomeric forms (i.e., having the same bound selector with opposite configuration) mainly operate under normal-phase HPLC conditions. For this reason, namitecan was pre-columnN-derivatized with isocyanates A–D and their sulfur analogues E–H to reduce its polarity by converting the amino group into a fragment compatible with the chiral recognition mechanism (i.e., ureido and thioureido groups). Once the optimal columns system

and derivatizing agents were selected, an original enantioselective HPLC–MS/MS technique was developed on the Whelk-O1 CSPs.

3) **Kinetic and thermodynamic studies of the epimerization processes in Artemisinin-derived antimalarial drugs by Dynamic High Performance Liquid Chromatography (D-HPLC).**
Stereodynamic investigations have been performed on two active artemisinin derivatives having labile stereogenic centres, namely dihydroartemisinin (DHA), and an *in vivo* degradation product of DHA containing an endoperoxide, an aldehyde and a ketonic moiety, namely MKA (monoketoaldehyde). We were able to obtain MKA through pyrolysis or basic degradation of DHA and have fully characterized its structure through a variety o analytical techinques. The stereodynamic studies performed have focused on a stereolabile hemiacetalic function present in both molecules. Linear Solvation Energy Relationships (LSER) analysis was used to study the thermodynamics of the epimerization process in DHA and MKA. Computational studies have provided further data on the differential stability and acidity of the two epimeric forms of MKA, while a kinetic investigation is introduced.

List of publications

This thesis is mainly based on the following papers:

1. Badaloni, E.; Cabri, W.; Ciogli, A.; D'Acquarica, I.; Deias, R.; Gasparrini, F.; Giorgi, F.; Kotoni, D.; Villani, C. "Extending the use of "Inverted Chirality Columns Approach" for enantiomeric excess determination in absence of reference samples: application to a water-soluble camptothecin derivative". *J. Chromatog. A*, **2010**, *1217*, 1024-1032.

2. D'Acquarica, I.; Gasparrini, F.; Kotoni, D.; Pierini, M.; Villani, C.; Cabri, W. ; Di Mattia, M.; Giorgi, F. "Stereodynamic Investigation of Labile Stereogenic Centres in Dihydroartemisinin". *Molecules*, **2010**, *15*, 1309-1323.

3. Kotoni, D.; D'Acquarica, I.; Ciogli, A.; Villani, C.; Capitani, D.; Gasparrini, F. "Design and evaluation of hydrolytically stable bidentate urea-type stationary phases for hydrophilic interaction chromatography", *J. Chromatogr. A*, in press (available online since 14.december.2011).

4. D'Acquarica, I.; Gasparrini, F.; Kotoni, D.; Pierini, M.; Villani, C.; Cabri, W. ; Di Mattia, M.; Giorgi, F. "Stereolability of a Monoketoaldehyde (MKA) Active Derivative of Dihydroartemisinin, an Antimalarial Drug: A Thermodynamic and Kinetic Study.", in preparation for *J. Org. Chemistry.*

Contribution report

The author wishes to clarify her contributions to the listed papers:

Paper 1. Performed most of the chromatographic work as well as the pre-column derivatization, made contributions to the interpretation of the results and to the publication process.

Paper 2. Performed the chromatographic part of the experimental work and contributed to the manuscript preparation.

Paper 3. Contributed to the formulation of the research problem, performed all the synthetic and chromatographic work, made contributions to the interpretation of the results and cooperated in the writing of the manuscript.

Paper 4. Performed the complete study of the stereolabile compounds by dynamic HPLC and was in charge of the preparation and purification of the compound (MKA). Also contributed to the calculation of the interconversion barriers, as well as to the manuscript preparation.

Congress Communications

1. D. Kotoni, W. Cabri, A. Ciogli, I. D'Acquarica, M. Di Mattia, F. Gasparrini, F. Giorgi, A. Mazzanti, M. Pierini, M. Quaglia. *Kinetic and Thermodynamic Study of the Epimerization of Dihydroartemisinin and of a Monoketoaldehyde (MKA) Decomposition Product by Dynamic HPLC and UPLC.*
In abstracts of the e-WISPOC Winter School on Physical Organic Chemistry at Bressanone (Brixen), 2-6/02/2009, p. 558

2. C. Villani, F. Gasparrini, I. D'Acquarica, D. Kotoni, G. Palmieri, D. Wallworth, C. Cimarelli.
A rational approach to the design of new "Crab-like" Chiral Stationary Phases: Synthesis and Evaluation.
Presented at Chirality 2010, ISCD-22, Sapporo (Japan) 12-15/07/2010

3. M.Pierini, I. D'Acquarica, F. Gasparrini, D. Kotoni, M.Piras, C. Villani, W. Cabri, M. di Mattina, F. Giorgi, A. Mazzanti.
Stereolability of MKA, a rearrangement product of dihydroartemisinin endowed with antimalarial activity.
Presented at the XXXIII Convegno Nazionale della Divisione di Chimica Organica, San Benedetto del Tronto (Italy) 12-16/09/2010

4. D. Kotoni, I. D'Acquarica, F. Gasparrini, M. Pierini, C. Villani, W. Cabri, M. Di Mattia, F. Giorgi, A. Mazzanti.
Experimental and Theoretical Study of a New Dihydroartemisinin Derivative Containing a Labile Stereogenic Centre by Linear Solvation Energy Relationship (LSER) Analysis.
Presented at the Ischia Advanced School of Organic Chemistry at Ischia, 25-29/09/2010, p. P29. Winner of Grant of the Organizing Committee.
Oral Communication.

5. D. Kotoni, C. Villani, F. Gasparrini, I. D'Acquarica, D. Wallwarth.
A rational approach to the design of new "Crab-like" Chiral Stationary Phases: Synthesis and Evaluation.
Presented at X SAYCS, Pesaro, 18-20/10/2010
Oral Communication.
Awarded as best oral communication.
Prize: Silver Medal of the Società Chimica Italiana.

5. A. Ciogli, I. D'Acquarica, F. Gasparrini, D. Kotoni, C. Villani
Design and Evaluation of a New Tweezers-Like Stable Stationary Phase forHydrophilic Interaction Chromatography-Mass Spectrometry (HILIC-MS).

Presented at the HPLC 2011 international symposium in Budapest, 19-23/06/2011.

6. D. Kotoni, C. Villani, F. Gasparrini, I. D'Acquarica, D. Wallwarth.
A rational approach to the design of new "Crab-like" Chiral Stationary Phases for HPLC and UPLC: Synthesis and Evaluation
Presented at Chirality 2011, ISCD-23, Liverpool (UK) 10-13/07/2011

Table of contents

PART A

Design and evaluation of new bidentate urea-type stationary phases for HPLC and UHPLC.

Chapter 1

Design and evaluation of hydrolytically stable bidentate urea-type stationary phases for hydrophilic interaction chromatography

1.1 Introduction

The first HPLC separations of polar compounds such as carbohydrates on polar stationary phases were published in the 1970s [1], using mobile phases containing some water and a higher percentage of an organic solvent (typically acetonitrile). However, it was not until the early 1990s that new phases started emerging and Alpert [2] gave the practice a name by calling it "Hydrophilic Interaction Chromatography" (HILIC) to emphasize the presence of water in the mobile phase as the stronger eluting member, and the partition mechanism involved in the retention. Following twenty years of continuous development, HILIC is nowadays accepted as a common separation mode [3,4], essentially dedicated to the separation of very polar compounds, such as glycopeptides [5–8] amino acids [2,9] oligonucleotides [10,11] and highly polar natural products [12–15].

A major advantage of HILIC seems to be its easy coupling with mass spectrometry (MS) which extends its applicability to impurity

detection [16]. In fact, the use of a low aqueous/high acetonitrile mobile phase significantly improves detection sensitivity for compounds analyzed by LC/electrospray ionization (ESI) MS, thus overcoming the mismatch between normal-phase LC and ESI-MS [16–19].

The exact retention mechanism for HILIC is still open to considerable debate. The partitioning mechanism arises from the preferential adsorption of water on the polar stationary phase, which results in a relatively higher water content in the stagnant liquid phase on the stationary phase support than in the mobile phase [3,20]. Others reported that the separation in the HILIC mode is mainly governed by polar-polar interactions (i.e., hydrogen bonding, dipole-dipole, charge-dipole interactions) because of the strong dependence of the elution order on the number of polar functional groups involved [3,16,21,22]. In some cases, a combination of both partitioning and surface adsorption can take place, depending on the nature of the stationary phase (i.e., the hydration degree and charge), the properties of the solutes (i.e., the kind and number of polar functional groups) and the mobile phase composition [23]. Figure 1 shows a typical HILIC phase, namely aminopropyl-bonded silica stationary phase, and the possible separation mechanisms taking place. A comprehensive study of both retention and selectivity effects in HILIC

elution mode has just been published [24], showing the pivotal role of adsorptive solute-silanol interactions in the separation features of polar urea-type bonded phases.

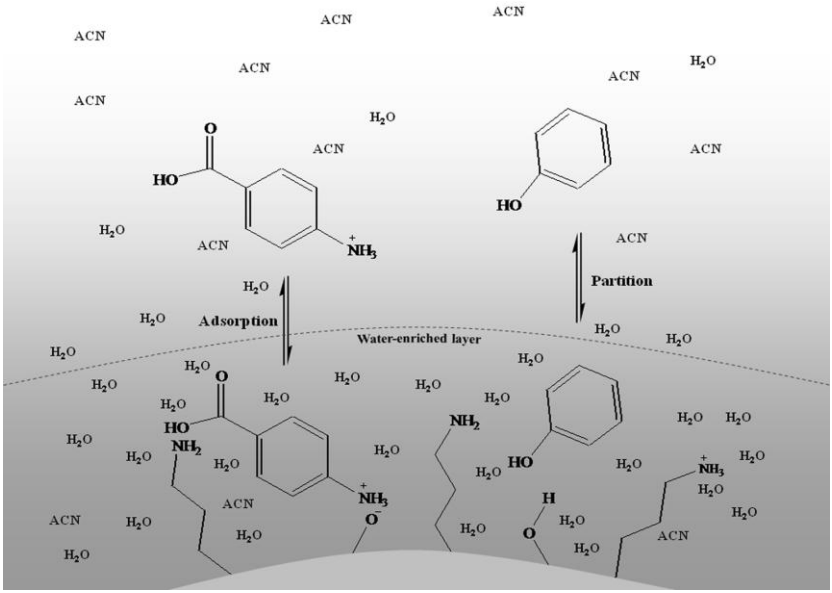

Figure 1. Mechanism of HILIC separation including partition and adsorption driven by hydrophilic and electrostatic interactions on an aminopropyl-bonded silica stationary phase with an acqueous-ACN mobile phase.

Although the number of commercially available columns especially designed for HILIC is dramatically growing [25], there still is not a substantial variety in stationary phases composition. Since HILIC was

considered as the aqueous normal-phase mode, it turns out that the first separations were performed using conventional unmodified silica gels, and actually a large fraction of the recently published works is still using such materials [3,4,16]. One of the properties that make underivatized silica inherently attractive in LC/MS analyses is the lack of ligands that may detach and show up as spurious peaks in the mass spectra.

However, severe irreversible adsorption has been observed on bare silica in HILIC mode. Recent bonded phase materials for HILIC seem to have addressed this issue, and various functionalized silica gels are today starting to become as common as unmodified silica in HILIC/MS applications [17–19].

A serious concern with bonded phases is the limited stability in basic aqueous eluents frequently used in HILIC that leads to fast bleeding and the concomitant exposure of free silanols. Earlier studies report the use of a “bidentate approach” in order to overcome hydrolytic instability of silica-based materials in reversed phase separations [26–28].

However, to our knowledge, there are no reports on the development of hydrolytically stable bidentate HILIC stationary phases. Herein, we report the preparation of a conceptually new stationary phase containing two bidentate urea-type functions suitable for the

separation of a wide variety of polar compounds by HILIC (polyols, sugars, hydroxybenzoic acids, nucleobases, vitamins). Bidentate Urea-type Stationary Phases (USP-HILIC) were envisioned and designed through a facile one-pot procedure with the aim of obtaining high stability in a variety of elution conditions, as well as a good selectivity towards the tested compounds. Moreover, a variant of the bidentate urea-type stationary phase was realized in which free amino groups were intentionally left on the silica surface to act as α/β sugar anomerization catalysts, a feature that proved beneficial to overcome the unwanted peak splitting observed when α and β anomers interconvert slowly on the chromatographic time scale.

In the last years, new sub-2 µm packings have been introduced in HILIC separations to be used under ultra-high performance liquid chromatography conditions. Neue and co-workers [29] have described the influence of mobile-phase composition and pH on analyte retention in these columns, demonstrating that reducing particle size in HILIC generates improvements in efficiency and, therefore, also in resolution, as observed in RPLC. Near to these completely porous supports, *core-shell* silica of $\sim$ 2.6 µm has been used to produce phases for UHPLC, yielding lower backpressure at the cost of slightly reduced efficiencies [30], which could be overcome by *in series* coupling of columns. Superficially porous particles are generally

composed of a 1.7-mm solid core surrounded by a 0.5-mm porous silica layer (d_p = 2.7 mm) [31, 32]. Chauve and co-workers have recently published a study where HILIC columns packed with porous sub-2 mm particles or with superficially porous particles of 2.7 mm were evaluated [33]. The authors concluded that the fused-core columns offer a backpressure two times lower than the sub-2-mm particle columns, but also a 30% lower efficiency.

Unfortunately, previous literature data are mainly concerned with bare silica supports in the UHPLC field, as only recently bonded phases for HILIC have been introduced in the market. A new amide phase was introduced by Waters under the name of BEH Amide [34-36], with the aim of enhancing the stability of the phases under a variety of conditions, especially alcaline pH. These new column exhibits a very wide range of applications and are particularly useful in sugars analysis.

Following the positive results obtained in the HPLC field, we decided to upgrade into the Rapid Speed LC field, with columns packed with particles with a d_p ranging between 2 and 3 µm. At this point, we would be able to evaluate the performance of our columns with the best UHPLC columns for HILIC applications present in the market. Two new phases for UHPLC were prepared according to the same procedure already used to prepare the HPLC phases. These new

phases proved highly competitive with two commercially available columns, namely the Acquity BEH Amide and the Phenomenex Kinetex HILIC, maintaining the high hydrolytic stability under basic conditions already observed with the HPLC phases. Furthermore, they represent one of the few bonded phases for RSLC-HILIC present in literature. Our future goal is to finally transit into the sub-2 µm range obtaining even more satisfying results in terms of efficiency and resolution, while maintaining the facile synthetic procedure as well as the high hydrolytic stability and wide range of applications.

1.2. Results and Discussion

1.2.1 Preparation of new bidentate urea-type stationary phases

When we first started designing the preparation of these new stationary phases, we had already been working on derivatizing silica gel through a facile procedure to obtain chemically and thermally stable glycopeptide-based chiral stationary phases that would prove useful under different separation modes [37]. These derivatization strategies rely on the use of di-isocyanate terminated spacers that react sequentially with surface anchored aminopropyl groups and with amino groups of the glycopeptides to yield a final stationary

phase where the chiral selector is secured to the silica surface through the spacer by two stable, polar ureidic bonds. Drawing inspiration from these synthetic schemes, we envisioned a new route to silica-based stationary phases, based on the one-pot reaction of a simple 1,2-diamine, an isocyanate-terminated organosilane and silica gel. The reaction sequence, sketched in Scheme 1, generates a highly polar, silica-based stationary phase that can be operated under HILIC conditions in the separation of polar compounds.

The new procedure is highly attractive as it is easy to realize in a reproducible manner and yields a final material that is very stable from the chemical and thermal points of view as a result of the two bidentate urea-type functions that represent the organic fragment anchored to the silica surface. Indeed, the bidentate technology was applied to a series of stationary phases to provide good hydrolytic stability in both low and high pH of the mobile phase [27]. The one-pot synthesis includes two steps: a first one where 1,2-ethylendiamine reacts with (3-isocyanatopropyl)triethoxysilane to yield an intermediate bis-urea with two pendant triethoxysilane functions. This step is easily performed by simply heating the two reacting partners in dry toluene and does not require any purification as no by product is generated during the urea bonds formation.

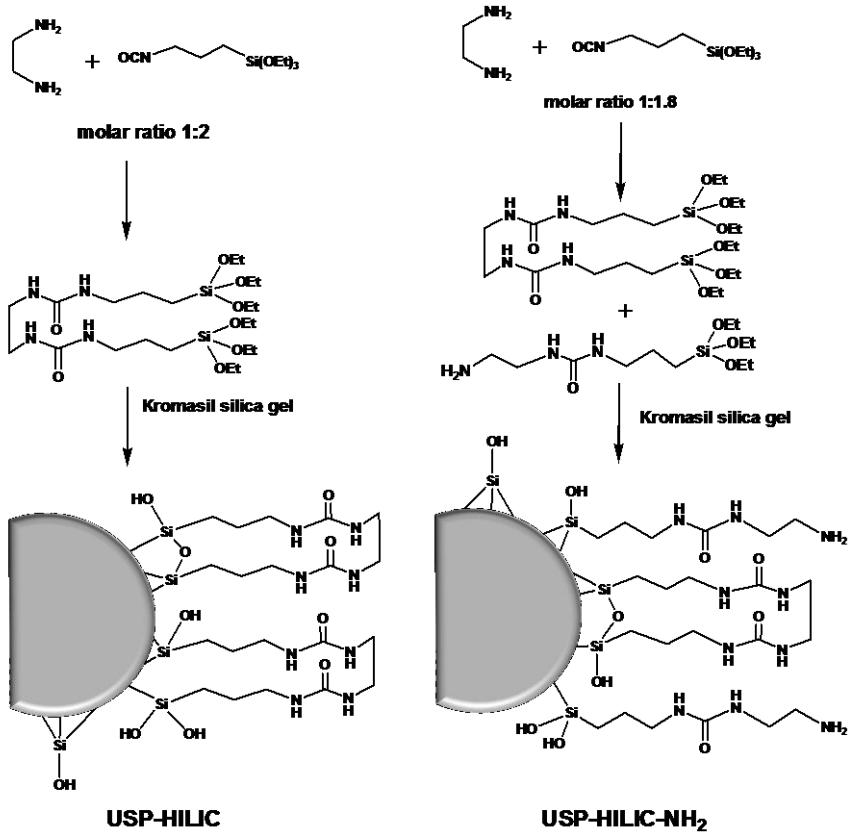

Scheme 1. Synthetic strategy for the preparation of the bidentate USP-HILIC and USP-HILIC-NH_2 stationary phases.

In the second step, performed in the same reaction flask, a slurry of hydrated silica is added to the bifunctional silane solution and the slurry is heated for 3 h to obtain the desired surface chemical modification. A weight ratio of 1 to 2.5 between the dimeric

ethylenediamine-isocyanate reagent and the previously hydrated silica gel was chosen in order to obtain a maximum degree of derivatization.

Hydrating the silica gel prior to the derivatizing procedure by treatment with ethanol 95% (by volume) aimed at creating a monomolecular water layer on the silica surface. In fact, during silanization, water plays a role in later stages, when hydrolysis of unreacted ethoxysilyl groups becomes crucial for further polymerization [38]. In such a way, hydration with a defined amount of water allows mainly horizontal polymerization, and the resulting silica shows enhanced surface density of silanes than the non-hydrated silica gel.

Four new bidentate stationary phases were prepared, namely an Urea-type Stationary Phase (USP-HILIC) and an urea-type phase bearing free amino groups (USP-HILIC-NH_2), as well as the corresponding silanized USP-HILIC-sil and USP-HILIC-NH_2-sil phases (Schemes 1 and 2).

The urea-type phase bearing free amino groups was specifically designed for applications to HILIC sugars analysis. Free amino groups on the silica surface have a potential catalytic effect on the α/β anomer interconversion of reducing sugars, and this effect in turn

translates in α/β anomer peaks averaging and collapse with concomitant simplification of the chromatographic pattern.

For the synthesis of the USP-HILIC phase and the corresponding silanized version, a molar ratio of 1.0 to 2.0 was used between 1,2-ethylenediamine and (3-isocyanatopropyl)triethoxysilane. In the preparation of USP-HILIC-NH_2 phase and the corresponding silanized version, a lower amount of (3-isocyanatopropyl) triethoxysilane was used (i.e., a 1 to 1.8 molar ratio, see Scheme 1).

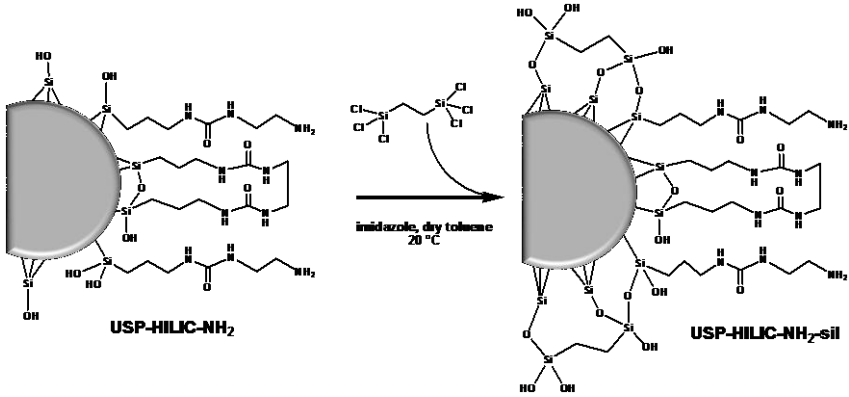

Scheme 2. Silanization reaction of the USP-HILIC-NH_2 stationary phase with 1,2-bis(trichlorosilyl)ethane yielding USP-HILIC-NH_2-sil.

In order to get a higher stability of the stationary phase, silanization with 1,2-bis(trichlorosilyl)ethane was used in the final stages of the synthesis. The silanized stationary phases showed good results in

terms of both stability and hydrophilicity, resulting from the formation of a hydrophilic stable coating through cross-linking between adjacent silanols. We believe that multiple attachments formed between ligands, the silica surface and the adjacent ligands produce a thin film on the surface which prevents silica dissolution at alkaline pH. In Scheme 2 is reported the silanization of USP-HILIC-NH_2 stationary phase with 1,2-bis(trichlorosilyl)ethane yielding USP-HILIC-NH_2-sil. As for Scheme 1, the depicted structures aim at representing the stationary phases from a qualitative point of view, and are coherent with the data obtained through solid state NMR spectroscopy (see Experimental Section).

1.2.2 NMR study of step 1 of the synthetic procedure

A complete characterization of the derivatizing bis- and mono-urea alkoxysilanes was performed using ^{1}H-NMR, ^{13}C-NMR spectroscopy as well as homo- and heterocorrelated 2D NMR experiments.

Two different ureido silanization reagents were prepared using, in the first case, 1 equivalent of ethylenediamine with 2 equivalents of (3-isocyanatopropyl) triethoxysilane in deuterated toluene (as reported for the synthesis of the USP-HILC phase), whereas, in the second case, the mixture was obtained by reacting 1 equivalent of

diamine with 1.5 equivalents of silane in the same solvent. Although the USP-HILIC-NH_2 was prepared using a 1:1.8 molar ratio (see Section 1.2.1), in this experiment a slightly higher ratio (1:1.5) was found useful to detect the desired mono-substituted compound. Structural assignment by NMR spectroscopy confirms that only the bis-substituted urea is formed in the first case, while two compounds are present in the second mixture.

In detail, the ^{1}H-NMR spectrum of the bi-component mixture in deuterated methanol showed a triplet at 2.68 ppm that was not present in the ^{1}H spectrum of the bis-substituted urea (see Fig. 2). A second triplet of the same intensity is visible at 3.16 ppm, albeit partially overlapped by the singlet corresponding to the four isochronous CH_2-N hydrogen atoms of the bis-substituted urea (3.17 ppm). These two triplets can be assigned to the two different CH_2-N of the mono-substituted urea (scalar coupling with the NH_2 is removed by the exchange of the NH_2 hydrogen atoms with the solvent). Also the multiplet at 3.07 ppm shows that two triplets with different intensity are present in the molecule. These signals correspond to the CH_2-N of the propyl chain, and the small triplet corresponds to the mono-substituted urea (for full NMR spectra, see Figs. 3–5).

Two 2D NMR spectra (see Figs. 6–7) were recorded to confirm this assignment. In particular, ^{1}H-^{1}H COSY confirmed that the two signals at 2.68 and 3.17 ppm are scalarly coupled, as expected for the mono-substituted compound. ^{1}H-^{13}C edited-HSQC confirmed that both the triplets correspond to secondary carbons, with chemical shift very similar to that of the bis-substituted compound.

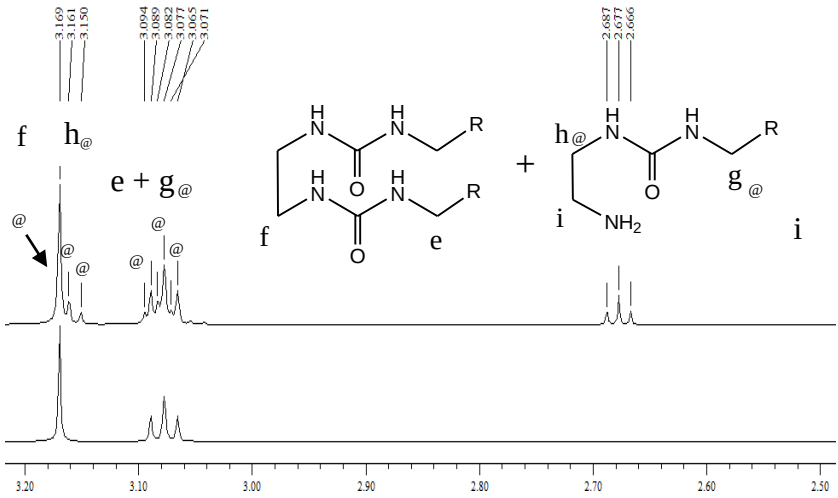

Figure 2. ^{1}H-NMR spectra in methanol-d_4 of reaction products obtained using a 1:1.5 molar ratio (top) and 1:2.0 molar ratio (bottom) of 1,2-ethylendiamine and (3-isocyanatopropyl)triethoxysilane. R = $(CH_2)_2$-$Si(OCH_2CH_3)_3$.

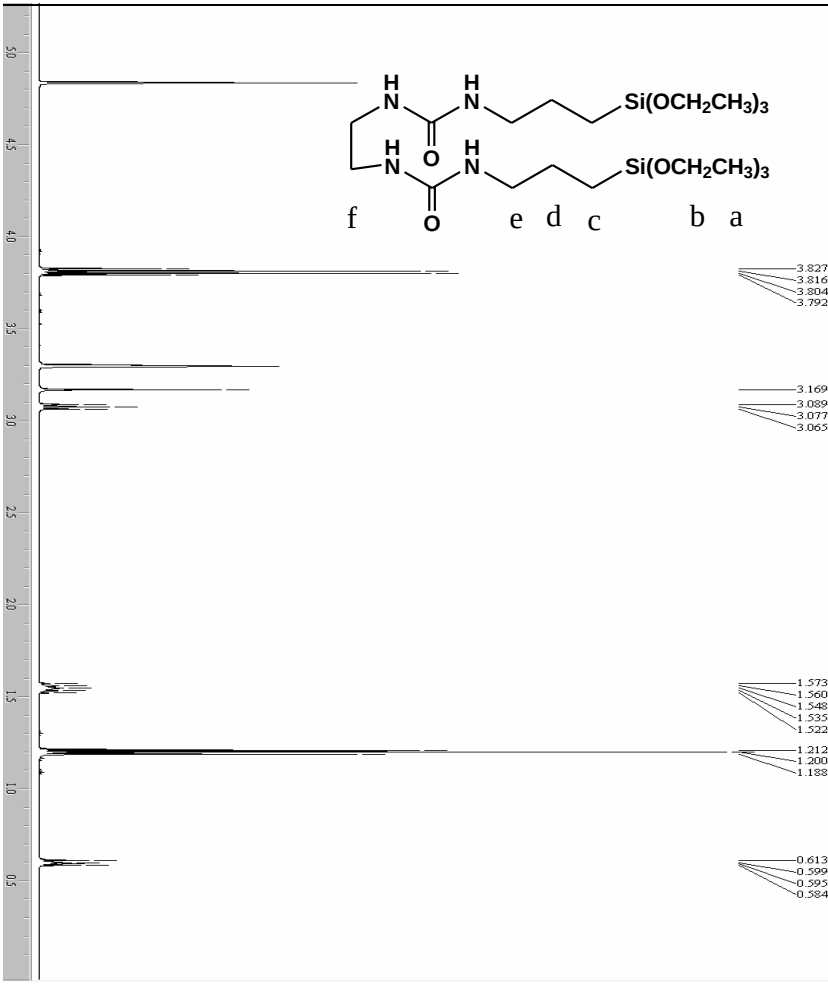

Figure 3. Full ^{1}H-NMR (600 MHz, CD_3OD) spectrum of bis-urea obtained from a 1:2 molar ratio of 1,2-ethylendiamine and (3-isocyanatopropyl) triethoxysilane. Signals: 0.60 ppm, pseudo-t, 4H(c); 1.20 ppm, t, 18H(a); 1.55 ppm, m(5), 4H(d); 3.07 ppm, t, 4H(e); 3.17 ppm, s, 4H(f); 3.80 ppm, q, 12H(b).

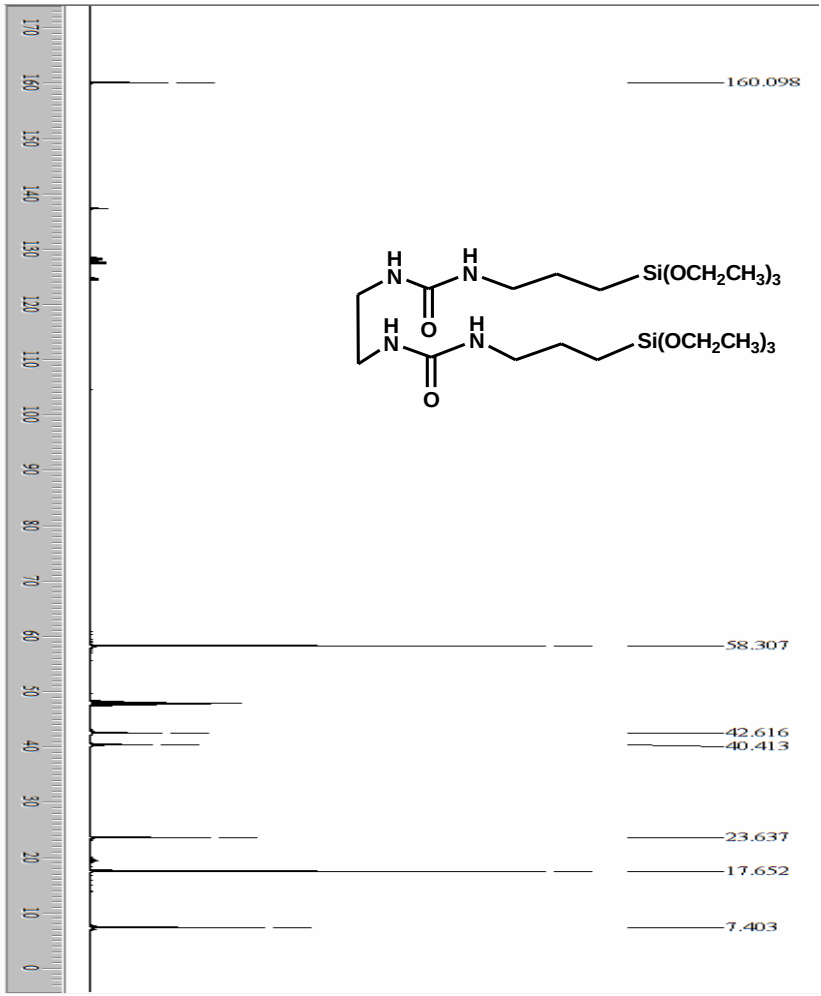

Figure 4. Full ^{13}C-NMR (150.8 MHz, CD_3OD) spectrum of bis-urea obtained from a 1:2 molar ratio of 1,2-ethylendiamine and (3-isocyanatopropyl) triethoxysilane. Signals: 7.40, 17.65, 23.64, 40.41, 42.62, 58.31, 160.10 ppm.

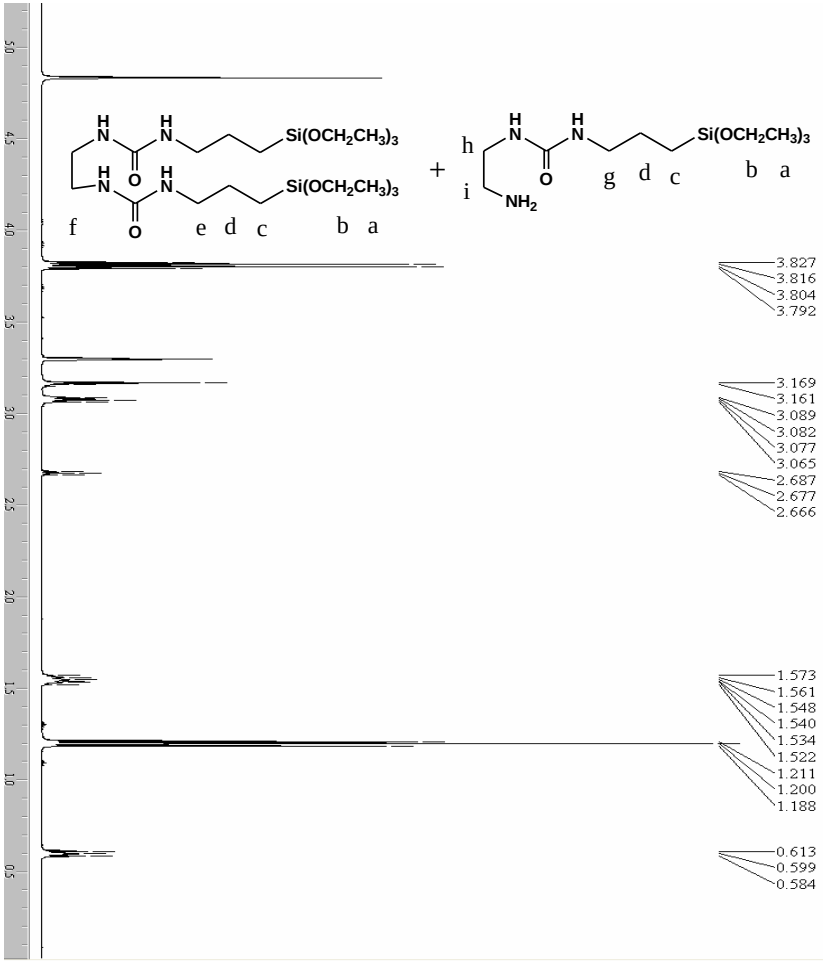

Figure 5. Full ^{1}H-NMR (600 MHz, CD_3OD) of bis-urea and mono-urea obtained from 1:1.5 molar ratio of 1,2-ethylendiamine and (3-isocyanatopropyl)triethoxysilane. Signals: 0.60 ppm, pseudo-t (c); 1.20 ppm, t (a); 1.55 ppm, m(5) (d); 2.68 ppm, t (i); 3.07 ppm, m (e,g); 3.16 ppm, t (h); 3.17 ppm, s (f); 3.80 ppm, q (b).

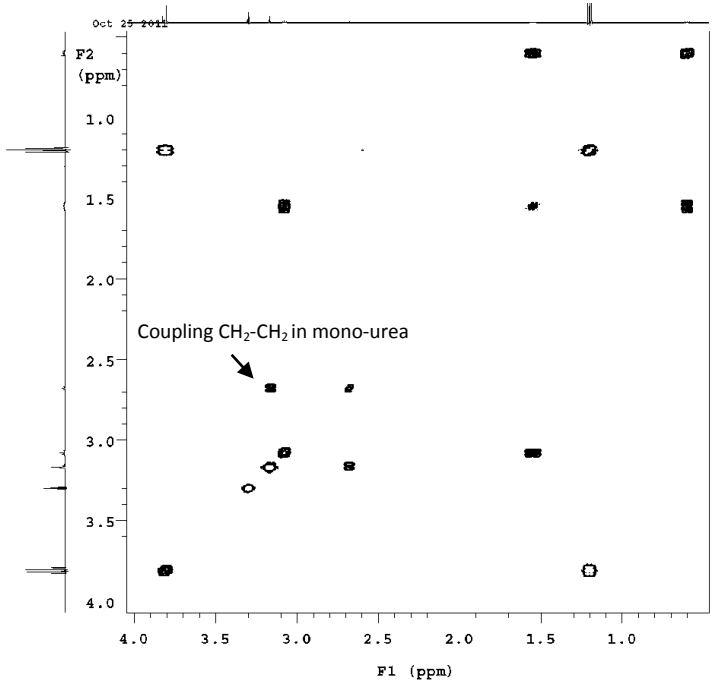

Figure 6. COSY-NMR spectrum of a reaction mixture obtained from 1:1.5 molar ratio of 1,2-ethylendiamine and (3-isocyanatopropyl)triethoxysilane.

1.2.3 Characterization of derivatized silica gels by solid state NMR and TGA

The outcome of surface modification was studied for each chemical step, including washing with a 10 mM NH_4OAc solution, by means of solid state ^{29}Si and ^{13}C CPMAS NMR spectroscopy. After each step of

chemical modification (introduction of ureido functions, washing with NH_4OAc solution, silanization with bis-silyl ethane bridge), the silica samples were characterized by solid state ^{29}Si and ^{13}C CPMAS NMR spectroscopy.

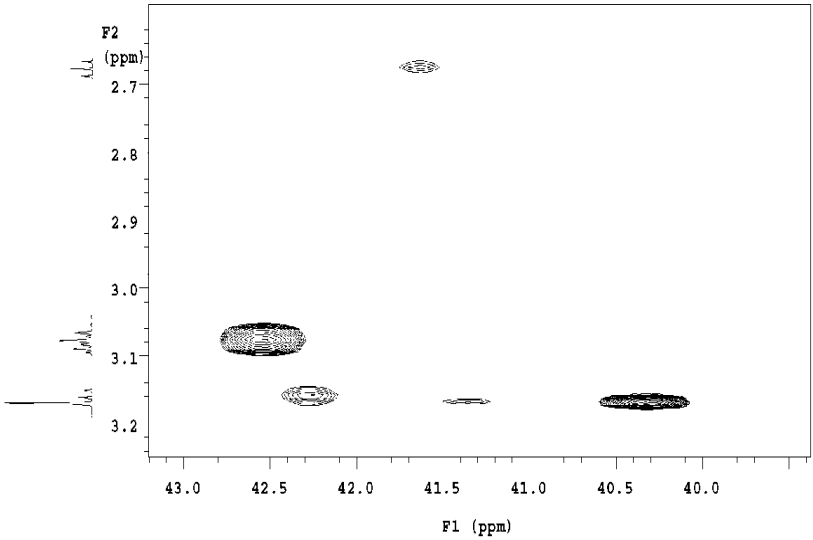

Figure 7. HSQC-NMR spectrum of a reaction mixture obtained from 1:1.5 molar ratio of 1,2-ethylendiamine and (3-isocyanatopropyl)triethoxysilane.

^{29}Si CPMAS NMR spectra of the investigated samples are shown in Fig. 8. All spectra show the resonances of structural elements of silica consisting of Q^2, Q^3, and Q^4 units, the superscripts indicating the number of Si-O-Si bonds. The resonance of bulk siloxane Q^4 units is

observed at -110 ppm, the resonance of Q^3 units of silanol groups and that of Q^2 units due to geminal silanol groups are observed at -101 and -90 ppm, respectively. Spectra of modified silica samples also show the typical signals of trifunctional silanes T [39]. In particular, resonances are observed at -49, -56, and -65 ppm due to silicon atoms of the silane molecules in which one (T^1), two (T^2), or three (T^3) hydroxyl groups are involved into reactions with hydroxyl moieties of silica surface. In accordance with these findings, T^2 and T^3 units of the modified silica samples are easily observed in the structures reported in Scheme 1. T^1 units are possibly ascribed to silane silicon atoms having two hydroxyl groups or one or two unreacted ethoxyl groups as substituents. Even if spectra acquired with cross-polarization are not directly quantitative, it is evident that the highest amount of T units with respect to Q units is found in USP-HILIC-sil (d) and USP-HILIC-NH_2-sil (g) silica gels; besides in these two samples, the highest amount of T^1 units is also found.

^{13}C CPMAS NMR spectra are shown in Fig. 9. The spectrum of the USP-HILIC silica gel (b) shows a resonance at 10.1 ppm ascribed to the methylene carbon atoms having the silane silicon atom of T^2 and T^3 units as a first neighbour. The resonance at 24.3 ppm is due to the methylene carbon atoms having the silane silicon atom as a second

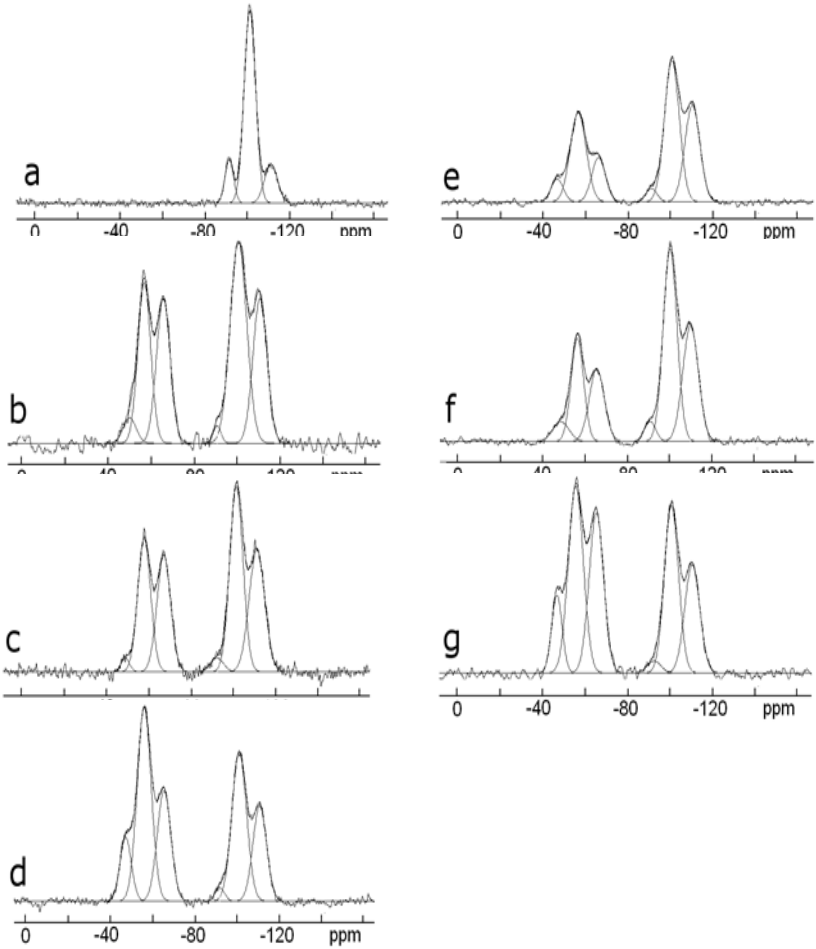

Figure 8. ^{29}Si CPMAS NMR spectra at 79.49 MHz of Kromasil (a), USP-HILIC (b), USP-HILIC washed (c), USP-HILIC-sil (d), USP-HILIC-NH_2 (e), USP-HILIC-NH_2 washed (f), USP-HILIC-NH_2-sil (g) silica gels. "Washed" refers to modified silica washed with a 10 mM NH_4OAc solution see Experimental Section). Deconvoluted spectra are superimposed to the experimental ones.

neighbour, the resonances at 42.7 ppm is due to the methylene carbon atoms having the NH group as a first neighbour, and the resonance at 161 ppm is due to the carbonyl carbon (see also Scheme 1). Resonances at 16 and 58 ppm are ascribed to methyl and methylene carbon atoms of unreacted ethoxyl groups.

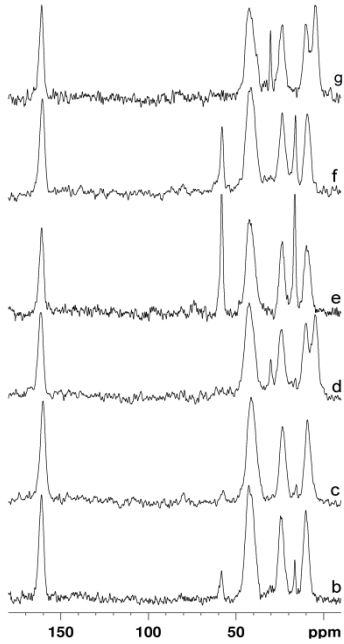

Figure 9. ^{13}C CPMAS NMR spectra at 100.63 MHz of USP-HILIC (b), USP-HILIC washed (c), USP-HILIC-sil (d), USP-HILIC-NH_2 (e), USP-HILIC-NH_2 washed (f), USP-HILIC-NH_2-sil (g) silica gels. "Washed" refers to modified silica washed with a 10 mM NH_4OAc solution (see Experimental Section).

These signals match the corresponding signals of the bis-urea silane recorded in solution (see Experimental Section), which are found at 7.41, 17.66, 23.64, 40.42, 42.63, 58.31 and 160.12 ppm (see Fig. 3). Signals of the non-equivalent carbon atoms close to the two different ureido nitrogens are seen in solution at 40.42 and 42.63 ppm, whereas a single unresolved signal is observed in the solid state at 42.7 ppm. The spectrum of USP-HILIC silica washed (c) shows a reduction of the intensity of the resonances of unreacted ethoxyl groups. Spectra of USP-HILIC-sil (d) and USP-HILIC-NH_2-sil (g) silica gels show an additional resonance at 4.4 ppm of methylene carbon atoms belonging to the bridge responsible of the cross-linking between adjacent silanols [40] (see also Scheme 2).

Spectra of USP-HILIC-NH_2 (e) and USP-HILIC-NH_2 (f) washed silica gels are very similar to that of HILIC silica (b), as the methylene carbon having the free amino group as a first neighbour may resonate at a chemical shift very close to that of the methylene carbon atoms having the NH group as a first neighbour [41]. All samples but USP-HILIC-NH_2-sil show a variable amount of unreacted ethoxyl groups.

Stability of the bidentate urea-type USP-HILIC-sil and USP-HILIC-NH_2-sil phases was attested by thermogravimetric analysis (TGA) in the 30–800 °C temperature range and both phases are stable up to 250 °C (Fig. 10).

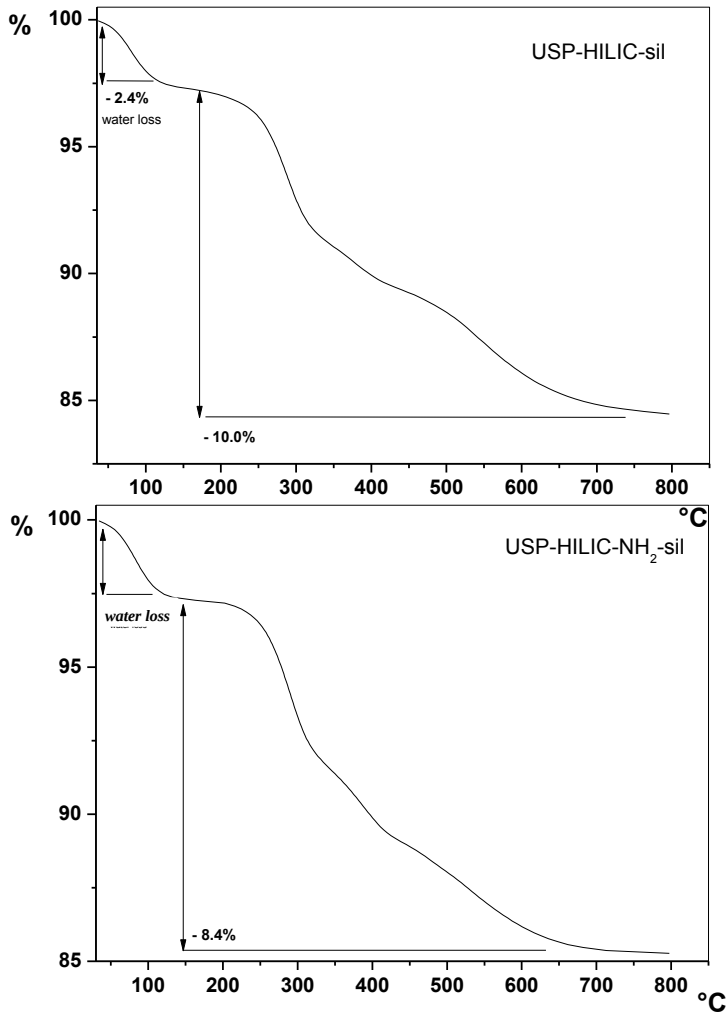

Figure 10. TGA curves of USP-HILIC-sil and USP-HILIC-NH2-sil phases.

The overall losses of organic matrix amount to 10.0% and 8.4% for USP-HILIC-sil and USP-HILIC-NH_2-sil respectively, while water

desorption for both samples accounts for the first step of weight loss up to around 150 °C (about 2.5%).

1.2.4 Chromatographic evaluation of the bidentate urea-type columns

To investigate the separation abilities of the bidentate urea-type columns in HILIC mode, chromatographic studies were performed with polar analytes as probes. A comparison was made with an aminopropyl-bonded silica (APS) column, which is the first bonded stationary phase to be routinely used for carbohydrate separations in HILIC mode [21]. The APS column used was a 150 mm × 4.0 mm I.D. Hypersil APS-2 silica (Si 120, 5 µm, surface area 170 m^2g^{-1}). A column packed with a diol-modified silica gel was also included in the comparative study, as the diol-modified silica has long been considered as nearly the ideal phase for HILIC applications owing to its high polarity and hydrogen-bonding properties. The diol-modified silica gel was prepared for this purpose from (3-glycidoxypropyl)trimethoxysilane and silica gel under acidic conditions using a one-pot procedure (see Experimental Section). Acid-catalyzed ring-opening reaction of the oxirane group gave the diol-modified silane which was grafted onto the silica surface to form

a siloxane-linked 2,3-dihydroxypropyl ligand. Finally, a 150 mm × 4.0 mm I.D. SeQuant ZIC-HILIC column (Si 200, 5 µm; specific surface area 135 m^2g^{-1}) was added to the study.

With the aim of evaluating the retention of highly polar compounds, a mixture of uracil, adenosine, and cytosine (see Fig. 11 for structures) was eluted with a mobile phase consisting of acetonitrile/water = 90:10 (v/v) through the different columns in order to perform a HILIC mode test (see Table 1). Naphthalene was added as an unretained marker of dead volume (k = 0 in all cases), and was always eluted before uracil, which is a common void volume marker in reversed phase HPLC. The number of theoretical plates per meter for the bidentate urea-type columns was calculated on uracil ($0.82 < k < 1.24$) and ranged from 36,000 to 80,000.

The Hypersil APS-2 and the DIOL columns, which have long been considered ideal under HILIC conditions, gave the lowest retention values, while the ZIC-HILIC column showed the highest ones. With regard to the bidentate urea-type columns, the USP-HILIC performed very well in terms of retention (always higher than the APS-2 and the DIOL columns) and selectivity (higher than APS-2 for the adenosine/uracil and cytosine/adenosine couples, but lower than the DIOL column). A sizeable increase in retention (9–19%) was observed

for the polar compounds moving to the USP-HILIC-NH_2 column, while selectivity and resolution remained almost unchanged.

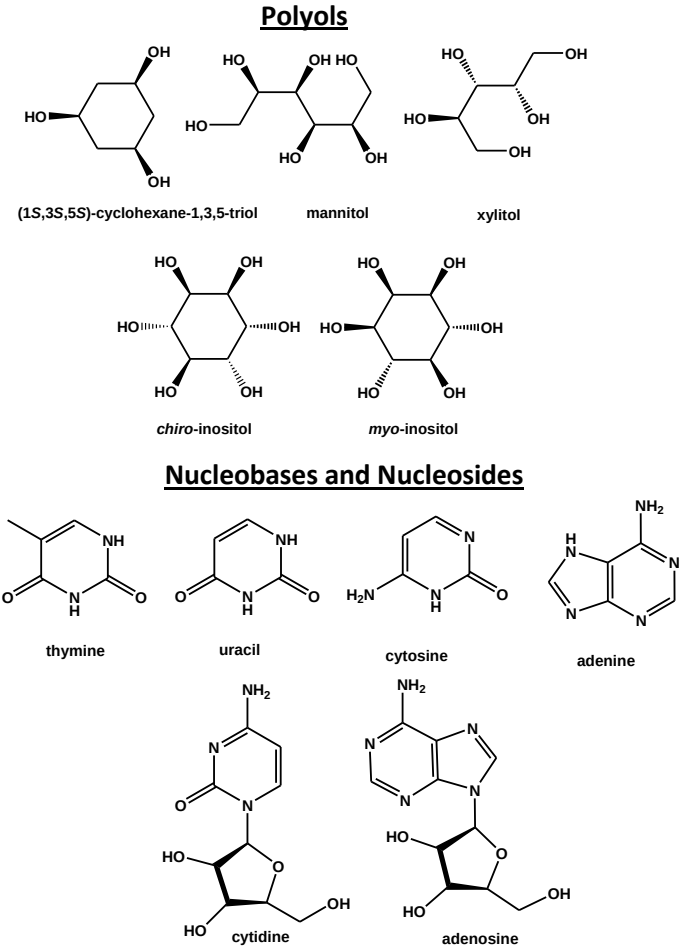

Figure 11. Structural formulas of the polyols, nucleobases and nucleosides analyzed on the bidentate urea-type columns.

The effect of silanization with 1,2-bis(trichlorosilyl)ethane on the USP-HILIC-NH_2 column led to a slight increment of retention (k) for adenosine (from 2.57 to 2.77) and cytosine (from 3.99 to 4.40), without significant influence on selectivity and resolution. Since it is known that salts can promote the retention of "non-charged" compounds under HILIC mode [11, 42], we added NH_4OAc to the above described mobile phase (final concentration 10 mM; ${}^{w}_{w}pH$ = 6.51; ${}^{s}_{w}pH$ = 8.05) and found for the USP-HILIC-sil column even better retention and selectivity values with respect to the non-silanized homologue phase. In fact, in the presence of NH_4OAc, the stagnant water-rich layer on the silica gel tends to thicken as the buffer attracts more water; thus, the liquid-liquid partitioning phenomena taking place become more consistent, leading to higher elution times. Moreover, in our case, hydrogen bonding formation between the urea functionality of the stationary phase and the acetate anion can be invoked (see Scheme 3), which indeed contribute to increase retention of the analytes. Salt addition proved useful also for the USP-HILIC-NH_2 columns, yielding increased retention and selectivity. The APS-2 showed a similar behaviour, while the DIOL column presented a decrement in the retention and selectivity values, probably due to a minor extent of the above-described hydrogen bonding interactions.

Table 1. Chromatographic data of the HILIC tests obtained on the bidentate urea-type columns in comparison with Hypersil APS-2, DIOL, and ZIC-HILIC columns.[a]

	Sample	USP-HILIC			USP-HILIC-sil			USP-HILIC-NH_2			USP-HILIC-NH_2-sil			Hypersil APS-2			DIOL			ZIC-HILIC		
		k[b]	α[c]	R_s[d]	k[b]	?[c]	R_s[d]	k[b]	?[c]	R_s[d]	k[b]	?[c]	R_s[d]	k[b]	?[c]	R_s[d]	k[b]	?[c]	R_s[d]	k[b]	?[c]	R_s[d]
No buffer	naphthalene	0.00			0.00			0.00			0.00			0.00			0.00			0.00		
			–	8.68		–	14.26		–	10.34		–	8.76		–	9.20		–	5.61		–	1.72
	uracil	1.04			0.82			1.24			1.16			0.91			0.57			0.64		
			2.26	8.59		2.17	8.55		2.07	8.29		2.39	7.46		2.01	6.00		3.03	9.58		2.03	–
	adenosine	2.35			1.78			2.57			2.77			1.83			1.73			1.30		
			1.49	5.55		1.58	5.95		1.55	6.55		1.59	5.32		1.25	2.46		1.59	6.02		2.41	–
	cytosine	3.50			2.81			3.99			4.40			2.29			2.76			3.13		
10 mM NH_4OAc	naphthalene	0.00			0.00			0.00			0.00			0.00			0.00			n.d.	n.d.	n.d.
			–	9.39		–	9.44		–	10.31		–	9.48		–	6.80		–	5.30			
	uracil	1.14			1.04			1.20			1.27			0.65			0.57			n.d.	n.d.	n.d.
			2.35	9.57		2.57	9.69		2.33	9.67		2.61	8.71		2.58	8.28		2.47	7.08			
	adenosine	2.68			2.67			2.80			3.31			1.68			1.41			n.d.	n.d.	n.d.
			1.47	5.93		1.54	6.08		1.61	7.61		1.56	5.70		1.54	5.59		1.59	5.58			
	cytosine	3.94			4.11			4.51			5.16$_s$			2.58			2.24			n.d.	n.d.	n.d.
	ε_T [e]		0.61			0.65			0.59			0.61			–			–			–	
	K_F [f]		2.46			3.33			3.08			2.46			3.29			2.61			–	

[a] Columns geometry: 150 mm × 4.0 mm I.D.; eluent: acetonitrile/water = 90:10 (v/v); flow rate: 1.0 ml/min; T = 25 °C; UV detection at 254 nm. [b] k = retention factor. [c] α = selectivity factor. [d] R_s = resolution, calculated as described in the Experimental Section. [e] ε_T = porosity. [f] K_F = permeability [10^{-14} m^2], calculated according to ref. [45].

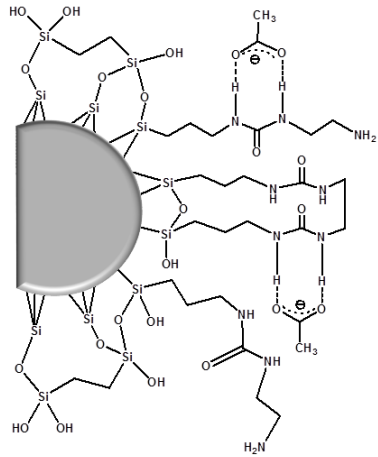

S**cheme 3.** Hydrogen bonding interactions between the urea functionality of the stationary phase and the acetate anion occurring during the HILIC retention mechanism.

1.2.5 Analysis of polyols

In order to evaluate the "sugarophilicity" of the bidentate urea-type columns, a preliminary test was devised, apt to determine their suitability in sugars analysis. We started our investigation by analyzing a mixture of four sugar alcohols and a cyclic polyol, namely 1,3,5-*cis*,*cis*-cyclohexanetriol (see Fig. 11 for structures) with a mobile phase composed of acetonitrile/water 85:15 (v/v). Since sugars alcohols and sugars in general do not have any significant UV

chromophore group, evaporative light-scattering detection (ELSD) was employed. Pulsed amperometric detection (PAD) coupled to anion exchange chromatography is an interesting alternative for the analysis of mono- and oligosaccharides; however, the main drawback is the predictable hydrolysis of methylated and acetylated oligosaccharides due to the high pH values of the eluent used for separation and detection [43].

Single sharp peaks were obtained for each analyte on the four bidentate urea-type columns (Fig. 12A–12D, solid lines), with good retention and selectivity data. The DIOL column showed very low "sugarophilicity" (Fig. 12F, solid lines) and the ZIC-HILIC column proved unstable after being used under basic (*vide infra*) conditions (data not shown). The APS-2 (Fig. 12E, solid lines) column retained slightly more the polyols, with respect to the lab-made columns.

As already checked in the HILIC test (see Section 1.2.4), addition of NH_4OAc to the above-described mobile phase (final concentration 10 mM) increased retention on the four bidentate urea-type columns, although the increment was more consistent for the USP-HILIC-NH_2 columns (Fig. 12C–12D, dot lines). In particular, *k* values of *myo*-inositol (the most retained analyte) were duplicated, passing from 6.18 to 11.46 on the USP-HILIC-NH_2 column and from 4.99 to 10.07 on the USP-HILIC-NH_2-sil column (see Table 2). Selectivity values also

showed a slight increment. Why is the increment in the *k* values more consistent for the USP-HILIC-NH_2 columns? This can be explained by considering that ammonium acetate buffer has a larger impact on the USP-HILIC-NH_2 phase due to the fact that at the operating pH (< pK_a of amino groups) ionic interactions are involved between the acetate moiety and the free amino group on the silica gel. In order to better solvate and stabilize such ion pairs, more water is attracted to the silica surface on the USP-HILIC-NH_2 phase, when compared to the USP-HILIC phase, resulting in a thickening of the water-layer and an increment of the time that the analyte spends in this water-layer, which is, indeed, the stationary phase in a HILIC mode separation. What we obtain is an increment in the retention polyols more evident than in the case of the USP-HILIC phase, where only the hydrogen bond formation can account for the thickening of the water-layer on the silica surface. The APS-2 column showed a similar behaviour (Fig. 12E, dot lines), with analysis time increasing from the initial 15 min up to 30 min. However, the high noise level was particularly high with this column, due to its high instability in the presence of mobile phases at ${}^{S}_{W}pH$ = 7.65. Such instability became more evident when increasing the ${}^{S}_{W}pH$ value to approximately 10 (data not shown).

Table 2. Chromatographic data obtained for a mixture of polyols (see Fig. 11 for structures) on the bidentate urea-type columns in comparison with Hypersil APS-2 and DIOL columns.[a]

	Sample	USP-HILIC			USP-HILIC-sil			USP-HILIC-NH_2			USP-HILIC-NH_2-sil			HYPERSIL APS-2			DIOL		
		$k^{[b]}$	$\alpha^{[c]}$	$R_s^{[d]}$	$k^{[b]}$	$\alpha^{[c]}$	$R_s^{[d]}$	$k^{[b]}$	$\alpha^{[c]}$	$R_s^{[d]}$	$k^{[b]}$	$\alpha^{[c]}$	$R_s^{[d]}$	$k^{[b]}$	$\alpha^{[c]}$	$R_s^{[d]}$	$k^{[b]}$	$\alpha^{[c]}$	$R_s^{[d]}$
No buffer added	1,3,5-*cis,cis*-cyclohexanetriol	1.39	1.54	4.86	1.41	1.52	4.72	1.36	1.73	6.22	1.36	1.58	4.29	1.02	2.07	7.48	0.85	1.14	<1
	mannitol	2.14	1.34_5	3.81	2.14	1.35_5	3.81	2.35	1.41	4.72	2.15	1.34	3.17	2.11	1.91	6.55	0.97	1.12	<1
	xylitol	2.88	1.39	5.08	2.90	1.42	5.24	3.32	1.53	6.91	2.89	1.43_5	4.54	4.04	1.55	6.77	1.08_5	1.12	<1
	chiro-inositol	4.00	1.17_5	3.10	4.11	1.20	3.19	5.08	1.22	3.62	4.15	1.20	2.62	6.26	1.44	6.47	1.22	1.17	<1
	myo-inositol	4.70			4.95			6.18			4.99			9.00			1.43		
10 mM NH_4OAc added	1,3,5-*cis,cis*-cyclohexanetriol	1.43	1.57	5.25	1.57	1.64	6.09	1.74_5	2.01	9.91	1.86	1.83	6.92	1.21	4.05	11.38	1.10	1.43	3.12
	mannitol	2.25	1.32	3.65	2.57	1.35	4.28	3.50_5	1.52	6.97	3.40	1.45	5.16	4.90	1.22	8.34	1.57	1.25	2.09
	xylitol	2.98	1.41	5.26	3.47	1.49	6.36	5.32	1.69	10.05	4.94	1.60	7.46	5.97	1.96	12.06	1.97	1.29	2.70
	chiro-inositol	4.21	1.20	3.03	5.17	1.23	3.69	8.97	1.28	5.17	7.91	1.27	4.32	11.69	1.56	8.91	2.54	1.26	2.53
	myo-inositol	5.04			6.34			11.46			10.07			18.19			3.21		

[a] Columns geometry: 150 mm × 4.0 mm I.D.; eluent: acetonitrile/water = 85:15 (v/v); flow rate: 1.0 ml/min; T = 25 °C; ELSD detection (T_{neb} = 50° C). [b] k = retention factor. [c] α = selectivity factor. [d] R_s = resolution, calculated as described in the Experimental Section.

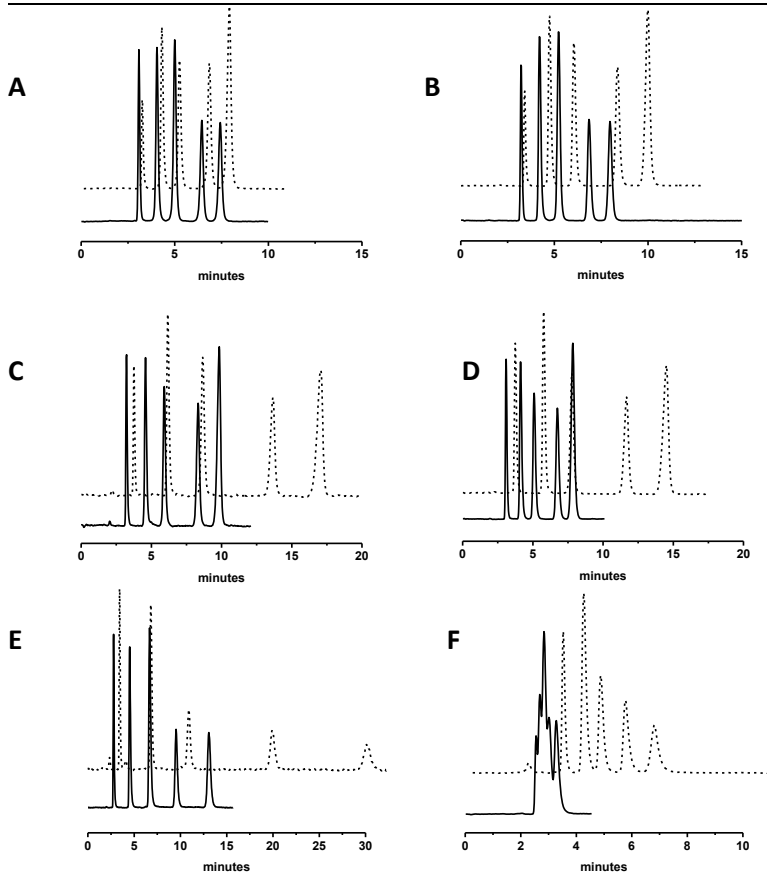

Figure 12. Analysis of a polyols mixture. Columns: A) USP-HILIC; B) USP-HILIC-sil; C) USP-HILIC-NH_2; D) USP-HILIC-NH_2-sil; E) APS-2; F) DIOL. Eluents: acetonitrile/water 85:15 (v/v) (solid lines) or acetonitrile/water 85:15 (v/v) plus 10 mM NH_4OAc (${}^{s}_{w}pH$ = 7.65) (dot lines). Flow rate: 1.0 ml/min, T = 25 °C, ELSD detection (T_{neb} = 50 °C). Elution order on all columns: (1) 1,3,5-cis,cis-cyclohexanetriol, (2) xylitol, (3) mannitol, (4) *chiro*-inositol, and (5) *myo*-inositol.

Finally, the DIOL column showed both a better retention and a baseline separation of the five polyols (Fig. 12F, dot lines), when compared to the previous analysis where no buffer was used. Nevertheless, peak shape was not satisfying, especially when compared to the bidentate urea-type columns.

1.2.6. Analysis of sugars

After evaluating the "sugarophilicity" of the bidentate urea-type columns, we examined their selectivity towards a complex mixture of nine sugars comprising two monosaccharides (namely, fructose and glucose), two disaccharides (namely saccharose and maltose) and a series of five maltose oligomers (see Fig. 13 for their structures). Since the diverse sugars of the test mixture show a broad range of adsorption affinities, the only practical method for their separation was gradient elution. Therefore, a 25 min linear gradient elution from 10% to 52% of water in acetonitrile was used in combination with ELSD detection, which indeed gave signal-to-noise ratios always much larger than UV detection, since ELSD response is only marginally affected by changes in the eluent composition (see Fig. 14 for representative chromatograms).

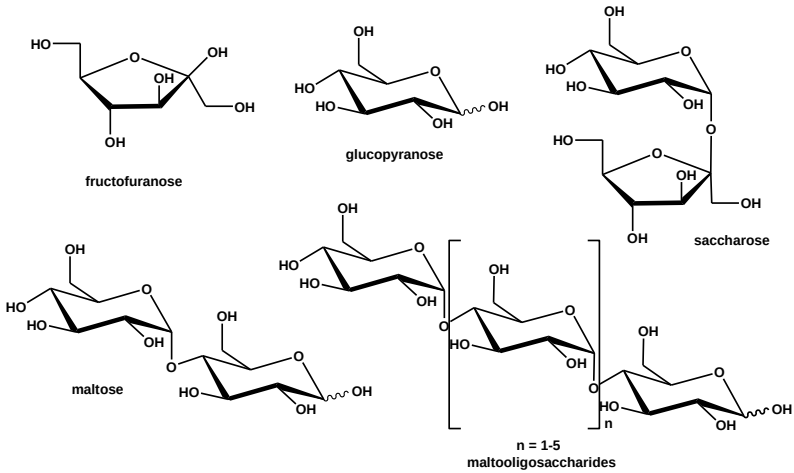

Figure 13. Structural formulas of the sugars analysed. Maltose oligomers: n = 1, maltotriose; n = 2, maltotetraose; n = 3, maltopentaose; n = 4, maltohexaose; n = 5, maltoheptaose.

By comparing the results obtained for the four bidentate urea-type columns with the APS-2, the DIOL, and the ZIC-HILIC columns (see Table 3), the USP-HILIC-NH_2-sil column proved the best for sugar analysis, in terms of both stability and selectivity. In fact, drift-free baselines were obtained under gradient elution conditions (see Fig. 14B), and satisfactory selectivity among couples of sugars belonging to homologue series: the monosaccharides were separated by a Δt_r of 2.26 min from the disaccharides, and the disaccharides were splitted from the series of maltose oligomers by Δt_r of 2.32 min. Retention increases roughly with the number of available hydroxyl groups in the

saccharide (i.e., maltooligosaccharides > disaccharides > monosaccharides), in accordance with the chromatographic behaviour of the overall HILIC mode. Notably, each analyte gave a single chromatographic peak (for a total of nine) for at least two reasons: (i) on-column anomerization (see Section 1.2.5.1) occurs faster than the chromatographic separation process, and (ii) the USP-HILIC-NH_2-sil column shows a low selectivity in discriminating among anomers. This did not happen on the USP-HILIC-sil column, where anomeric peaks were observed for fructose, glucose and maltose (Fig. 14A, *vide infra*).

With regard to the columns used as reference, the analysis on the APS-2 column was seriously hampered by the high noise level observed (Fig. 14C), despite the comparable retention (retention time ranging from 6.47 min to 18.75) and selectivity achieved among homologue series, with the individual sugars appearing as a single peak with no splitting due to α/β anomers. On the DIOL column (Fig. 14D), elution was too fast (retention time ranging from 3.87 to 11.65) and separation not complete, while on the ZIC-HILIC column anomerization occurred during the chromatographic run for at least seven of the nine sugars analyzed (Fig. 14E).

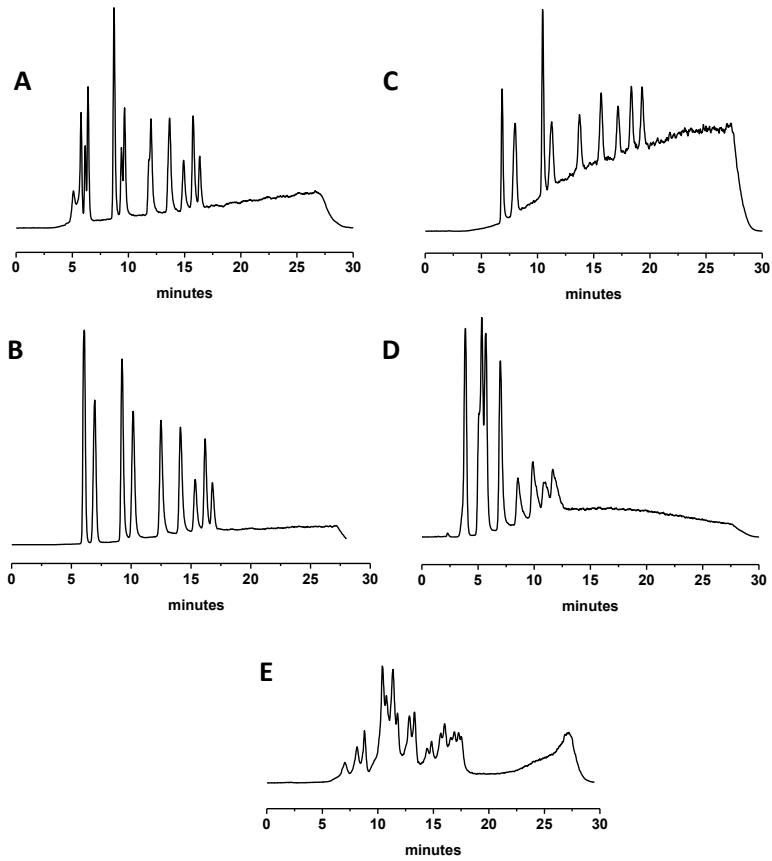

Figure 14. Analysis of the sugars mixture. Columns: A) USP-HILIC-sil; B) USP-HILIC-NH_2-sil; C) APS-2; D) DIOL; E) ZIC-HILIC. Eluent A: acetonitrile/water 90:10 (v/v); eluent B: water/acetonitrile 70:30 (v/v). Gradient elution from 100 to 30% A over 25 min (linear); back to 100% A in 1 min; 10 min re-equilibration time. Flow rate: 1.0 ml/min, T = 25 °C, ELSD detection (T_{neb} = 70° C). For the composition of the sample, see Table 3.

For this reason, chromatographic data reported for the ZIC-HILIC column in Table 3 were obtained by considering the averaged retention time of the two anomers. Starting from these results, we decided to perform further investigations on the on-column anomerization phenomena, in order to find suitable chromatographic conditions for controlling their effect on the final chromatographic results.

On-column anomerization of sugars

A major problem in the chromatographic separation of sugars, beside the low UV detectability, is that sugars exist in two anomeric forms that can interconvert slowly on the chromatographic time scale at neutral pH values, thus giving two peaks for each solute that can lead to overcrowding in the chromatogram. Such phenomena are observed when bare silica columns are used, whereas with amino-silica columns they are normally not observed, due to the basicity of such phases [21,44]. At high pH values, in fact, the interconversion of sugar anomers (i.e., anomerization) is rapid and only a single peak is detected. When analysis of reducing sugars is carried out on diol-modified silica, diisopropylethyl-amine (DIPEA) or TEA must be added to the mobile phase to enhance the kinetics of anomerization [3]. In

general, elevated temperatures (50–90 °C) or increases in the pH level by addition of 0.1% organic amines have been shown to facilitate the collapse of anomer peaks, thus resulting in one distinctive single peak.[45]

However, a factor to always keep in mind is the stability of the stationary phase under alkaline basic pHs. Many commercial columns, in fact, are not adequately stable under basic conditions and the corresponding chromatograms present peak shape deterioration, hampering the quality of analysis. This is exactly what we found after addition of 0.1% TEA (corresponding to a final concentration of 7 mM) in the mobile phase used for the separation of the above-mentioned sugars mixture: the DIOL, the APS-2 and the ZIC-HILIC columns proved highly unstable, as it can be seen by the steep drift of the baselines and the noise level resulted in clearly reduced peaks height (see Fig. 15B–15D). In particular, the ZIC-HILIC column (Fig. 15D) was seriously damaged after exposure to such alkaline basic conditions (> 10). The USP-HILIC-NH_2-sil column, instead, yielded very stable and drift-free baselines (Fig. 15A). The absence of anomeric peaks on the APS-2 column is attributed to a catalytic effect of free surface amino groups on the α/β anomer interconversion process [21]. The accelerated anomerization results in averaged, single peaks for each sugar, thus greatly simplifying the chromatographic profile.

Table 3. Chromatographic data obtained for a mixture of sugars (see Fig. 13 for structures) on the bidentate urea-type columns in comparison with Hypersil APS-2, DIOL, and ZIC-HILIC columns.[a]

Sugar	*USP-HILIC-sil*		*USP-HILIC-NH$_2$-sil*		*Hypersil APS-2*		*DIOL*		*ZIC-HILIC*	
	t_r[b]	Δt_r[c]	t_r[b]	Δt_r[c]	t_r[b]	Δt_r[c]	t_r[b]	Δt_r[c]	t_r[b]	Δt_r[c]
fructose	5.44		5.99		6.47		3.87		7.05	
		0.84		0.89		0.97		0.00		1.07
glucose	6.28		6.88		7.44		3.87		8.12	
		2.44		2.26		3.32		1.46		0.68
saccharose	8.72		9.14		10.76		5.33		8.80	
		0.80		0.94		0.57		0.36		2.77
maltose	9.52		10.08		11.33		5.69		11.57	
		2.49		2.32		1.99		1.30		1.49
maltotriose	12.01		12.40		13.32		6.99		13.06	
		1.65		1.63		1.91		1.55		1.58
maltotetraose	13.66		14.03		15.23		8.54		14.64	
		1.25		1.15		1.49		1.34		1.20
maltopentaose	14.91		15.18		16.72		9.88		15.84	
		0.84		0.80		1.11		0.97		0.89
maltohexaose	15.75		15.98		17.83		10.85		16.73	
		0.59		0.72		0.92		0.80		0.69
maltoheptaose	16.34		16.70		18.75		11.65		17.42	

[a] Columns geometry: 150 mm × 4.0 mm I.D.; eluent A: acetonitrile/water 90:10 (v/v); eluent B: water/acetonitrile 70:30 (v/v). Gradient elution from 100 to 30% A over 25 min (linear); back to 100% A in 1 min; 10 min re-equilibration time. Flow rate: 1.0 ml/min, T = 25 °C, ELSD (T_{neb} = 70 °C).

[b] t_r = retention time (min). [c] Δt_r = difference in retention time (min).

This is why we appositely prepared a bidentate urea-type stationary phase bearing some free amino groups (i.e., USP-HILIC-NH_2) in order to exploit such catalytic effect on sugar anomerization. As expected, the USP-HILIC-NH_2 column allowed detection of only nine

chromatographic peaks for our sugar mixture as a result of its activating effect on the kinetics of the interconversion process.

Chemical stability of the bidentate urea-type stationary phases

The different chromatographic profiles achieved after addition of 0.1 % TEA (corresponding to a final concentration of 7 mM) in the mobile phase used for the analysis of the sugars mixture were taken into account as a comparative stability test of the bidentate urea-type stationary phases at high pHs. Each injection was repeated several times until the noise level observed stopped diminishing all phases had reached their minimum noise level and the analysis was reproducible. Whilst the USP-HILIC column showed an excellent stability under basic conditions, the USP-HILIC-NH_2 phase, containing free amino groups, yielded a quite high noise level.

Silanization of such phase with 1,2-bis(trichlorosilyl)ethane, however, proved to increase its stability at high pHs, even after a high number of injections (more than 1000 injections were performed on the USP-HILIC-NH2-sil column, with negligible lowering of retention and selectivity factors without significant variation of retention and selectivity factors, that was in the range of ≤ 2%).

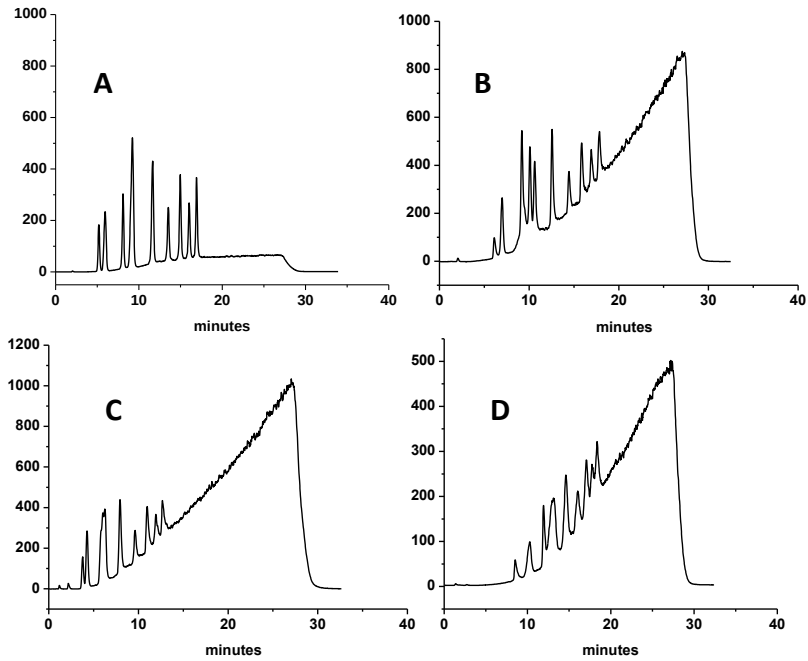

Figure 15. Effect of the addition of triethylamine (TEA) in the analysis of the sugars mixture. Columns: A) USP-HILIC-NH_2-sil; B) APS-2; C) DIOL; D) ZIC-HILIC. Eluent A: acetonitrile/water 90:10 (v/v) plus 7 mM TEA ($^{s}_{w}pH$ = 10.64); eluent B: water/acetonitrile 70:30 (v/v) plus 7 mM TEA ($^{s}_{w}pH$ = 10.88). Gradient elution from 100 to 30% A over 25 min (linear); back to 100% A in 1 min; 10 min re-equilibration time. Flow rate: 1.0 ml/min, T = 25° C, ELSD detection (T_{neb} = 70 °C). Sugars solutions (0.5 mg/ml) in acetonitrile/water 50/50 (v/v) were freshly prepared and allowed to equilibrate at T = 25 °C prior to injection. For the composition of the sample, see Table 3.

Easy interface with mass spectrometry

Carbohydrates are critical components of living systems and mediate a vast number of fundamental biological events - from complex cellular processes required to initiate and sustain life, to recognition phenomena that are responsible for autoimmune diseases, organ rejection, and inflammation. Such functional diversity is reflected in the diversity of carbohydrate structures. Hence, there is an increasing demand for easy access to glycoconjugates which can serve as probes in biochemical

studies and also as potential leads for new drugs against carbohydrate-based metabolic disorders. Since we used ELSD as the detection system in the analysis of sugars on the bidentate urea-type stationary phases, we predicted an easy interface with mass spectrometry, allowed by the use of volatile buffers: thus, we coupled an ESI-MS source to our chromatographic system and analyzed the test sugars mixture under the usual conditions. Direct infusion of 100 ppm solutions of maltotriose, maltotetraose, maltopentaose, maltohexaose, and maltoheptaose in acetonitrile/water 50/50 (v/v) containing 10 mM NH_4OAc, as well of mono- and disaccharides, into the ESI-MS instrument provided preliminary data to optimize the experimental mass conditions, which were then used in the HILIC/ESI-

MS method. In Fig. 16 is reported the HILIC/ESI-negative chromatogram obtained on the USP-HILIC-NH_2-sil column, by monitoring the total ion current (TIC) from 220 to 1500 amu (molecular weights of maltooligosaccharides range from 504 to 1152 Da).

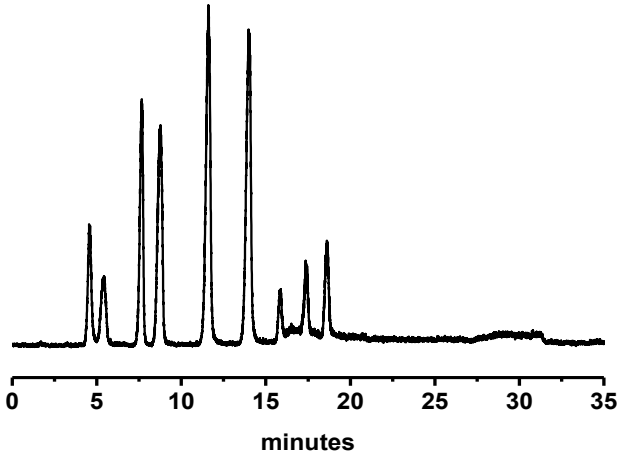

Figure 16. HILIC/ESI-MS (negative mode) separation of the sugars mixture on the USP-HILIC-NH_2-sil column. Eluent A: acetonitrile/water 90:10 (v/v) plus 10 mM NH_4OAc ($^{s}_{w}pH$ = 8.05); eluent B: water/acetonitrile 70:30 (v/v) plus 10 mM NH_4OAc ($^{s}_{w}pH$ = 6.80). Gradient elution from 100 to 30% A over 25 min (linear); back to 100% A in 1 min; 10 min re-equilibration time. Flow rate: 1.0 ml/min. T = 25 °C. ESI-MS detection (see Section 2.7). Total ion current (TIC) from 220 to 1500 amu was monitored. Sugars solutions (2 mg/ml) in acetonitrile/water 50/50 (v/v) were freshly prepared and allowed to equilibrate at *T* = 25 °C prior to injection. For the composition of the sample, see Table 3.

1.2.7. Analysis of organic aromatic acids

Encouraged by the results obtained during the analysis of complex mixtures of neutral compounds such as polyols and sugars, we decided to test the ability of the bidentate urea-type columns in separating acid and basic compounds. The analysis of organic acids is very interesting in the pharmaceutical field, but not always chromatographically easy to perform, since poor peak shape is often observed due to deprotonation. To this purpose, we prepared a test mixture containing 4-hydroxybenzenesulphonic acid, 4-hydroxybenzoic acid, 3,5-dihydroxybenzoic acid, 3,4,5-trihydroxybenzoic acid (or gallic acid) and the structurally related 3,4,5-trihydroxybenzamide (see Fig. 17 for their structures), which was isocratically eluted using a 85:15 (v/v) acetonitrile/water plus 30 mM NH_4OAc mixture ($^{s}_{w}pH$ = 7.73).

The best results in terms of peak shape were obtained with the silanized versions of both the bidentate urea-type columns (see Fig. 18), with a slight retention increment passing from the USP-HILIC-sil to the USP-HILIC-NH_2-sil column. Elution order of hydroxybenzoic acids followed the expected trend of HILIC mechanism of separation, i.e., 4-hydroxybenzoic acid (*k* ranging from 3.46 to 6.69) < 3,5-dihydroxybenzoic acid (*k* ranging from 4.49 to 9.18) < 3,4,5-

trihydroxybenzoic acid (*k* ranging from 7.81 to 17.22), the least retained compound being the benzamide (*k* ranging from 1.23 to 1.80), since it lacks the carboxylic acid function.

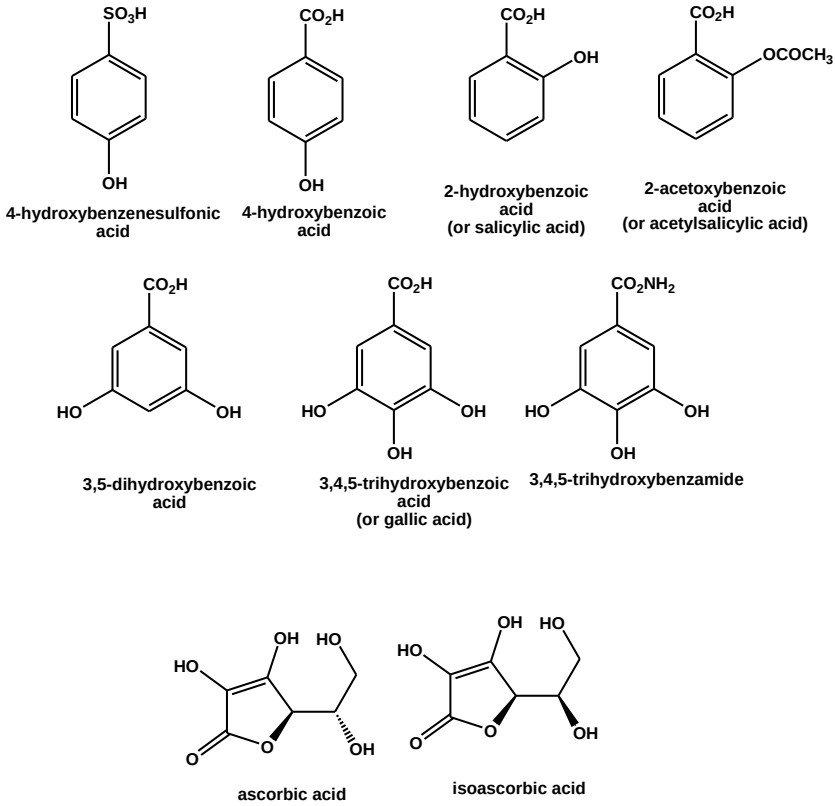

Figure 17. Structures of organic acids and related benzamide as well as lactones tested on HILIC columns.

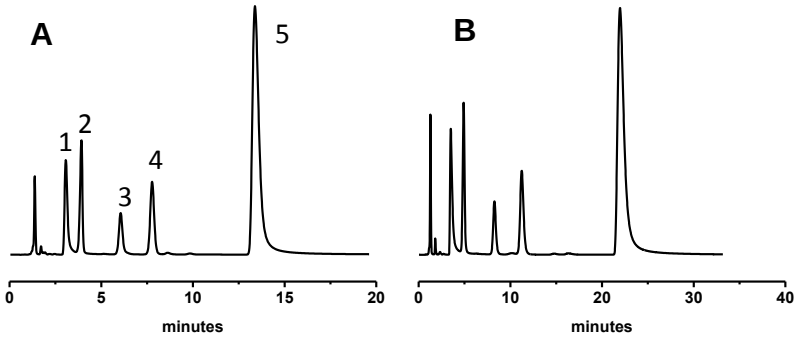

Figure 18. Analysis of a mixture of organic aromatic acids and a related "non-charged" compound (see Fig. 17 for structures). Columns: A) USP-HILIC-sil; B) USP-HILIC-NH_2-sil. Eluent: acetonitrile/water 85:15 (v/v) plus 30 mM NH_4OAc ($_w^s pH$= 7.73). Flow rate: 1.0 ml/min, *T* = 25 °C, UV detection at 254 nm. Peak 1) 3,4,5-trihydroxybenzamide; peak 2) 4-hydroxybenzenesulfonic acid; peak 3) 4-hydroxybenzoic acid; peak 4) 3,5-dihydroxybenzoic acid; peak 5) 3,4,5-trihydroxybenzoic acid (or gallic acid).

However, the HILIC-type interaction process cannot be invoked for the relative retention of 4-hydroxybenzoic and 4-hydroxybenzenesulphonic acids: in fact, retention of the former on the bidentate urea-type columns was always higher than that of the latter (*k* ranging from 2.08 to 3.89), despite its much lower polarity. Such an inverted elution order can be plausibly explained by taking into account superimposed non-HILIC interactions [24].

To further investigate the capability of the new columns of separating organic acids, a mixture made up of 2-hydroxybenzoic (or salicylic) and 2-acetoxybenzoic (or acetylsalicylic) acids (see Fig. 17 for their structures), containing also vitamin-like compounds (namely, ascorbic and isoascorbic acids) was separated using a mobile phase consisting of acetonitrile/water 80:20 (v/v) plus 5 mM KH_2PO_4 ($^{S}_{W}pH$ = 6.10). Indeed, under the chosen chromatographic conditions, the investigated columns (i.e., USP-HILIC-sil, USP-HILIC-NH_2-sil, APS-2, and DIOL) showed the same elution order (see Table 4), with 2-hydroxybenzoic acid always eluting first (*k* ranging from 0.42 to 0.48 on the bidentate urea-type columns) or not retained at all (as in the case of APS-2 and DIOL column, *k* = 0.00). The ascorbic acid (actually featuring a lactone ring rather than a carboxylic acid group) was always eluting last (*k* ranging from 3.04 on the USP-HILIC-sil to 4.09 on the USP-HILIC-NH_2-sil column), preceded by the isoascorbic acid peak (*k* ranging from 2.62 on the USP-HILIC-sil to 3.41 on the USP-HILIC-NH_2-sil column), which indeed differs from it only for the stereochemistry of one of the two stereogenic carbons (i.e., the two vitamins are diastereoisomers). Furthermore, the USP-HILIC-NH_2-sil column showed higher selectivity values in all cases, when compared to USP-HILIC-sil.

Table 4. Chromatographic data obtained for a mixture of pharmaceuticals and vitamins-like compounds (see Fig. 17 for structures) on the USP-HILIC-sil and the USP-HILIC-NH_2-sil columns in comparison with Hypersil APS-2 and DIOL columns.[a]

Sample	USP-HILIC-sil			USP-HILIC-NH_2-sil			Hypersil APS-2			DIOL		
	$k^{[b]}$	$\alpha^{[c]}$	$R_s^{[d]}$	$k^{[b]}$	$\alpha^{[c]}$	$R_s^{[d]}$	$k^{[b]}$	$\alpha^{[c]}$	$R_s^{[d]}$	$k^{[b]}$	$\alpha^{[c]}$	$R_s^{[d]}$
2-hydroxybenzoic acid (or salicylic acid)	0.48			0.42			0.00			0.00		
		2.17	3.98		2.29	3.06		–	2.87		–	2.19
2-acetoxybenzoic acid (or acetylsalicylic acid)	1.04			0.96			0.36			0.25		
		2.52	8.90		3.56	12.8		7.50	16.2		2.64	2.96
isoascorbic acid	2.62			3.41			2.69			0.66		
		1.16	1.79		1.20	2.27		1.30	3.89		1.24	0.90
ascorbic acid (or vitamin C)	3.04			4.09			3.49			0.82		

[a] Column geometry: 150 mm × 4.0 mm I.D.; eluent: acetonitrile/water = 80:20 (v/v) plus 5 mM KH_2PO4 ($^{s}_{w}pH$ = 6.10); flow rate: 1.0 ml/min, *T* = 25 °C; UV detection at 240 nm.[b] *k* = retention factor. [c] α = selectivity factor. [d] R_S = resolution, calculated as described in the Experimental Section

Finally, the USP-HILIC-NH_2-sil column behaves in a very similar manner to the APS-2 column, both in terms of peak shapes and retention: they indeed gave the same profiles, with salicylates eluting within the first three minutes of the chromatographic run, and vitamins-like compounds more strongly retained, with a separation between the two elution zones more marked for the APS-2 column (α

between acetylsalicylic and isoascorbic acid being 7.50) than the bidentate urea-type column (α = 3.56).

Such a simultaneous determination of drugs and vitamins-like compounds is highly desirable in the analysis of food and beverages, as well as of pharmaceutical preparations, and the bidentate urea-type columns proved a suitable alternative to previous approaches for such applications [46].

1.2.8. Analysis of nucleobases and nucleosides

In order to test the separation abilities of the bidentate urea-type phases over a wider range of analytes, a mixture containing four nucleobases (namely, thymine, uracil, adenine, cytosine) and two nucleosides (adenosine and cytidine) was eluted on the USP-HILIC-sil and USP-HILIC-NH_2-sil columns. The chromatographic profiles were then compared to the ones obtained by eluting the same mixture on the APS-2 and DIOL columns (see Fig. 19). The mobile phase consisted of acetonitrile-water 90:10 (v/v) containing a final 10 mM concentration of NH_4OAc. The elution order on all four columns was the same, with thymine always eluting before uracil. Surprisingly, adenosine was less retained than cytosine, despite the presence of ribose in the structure of the nucleoside.

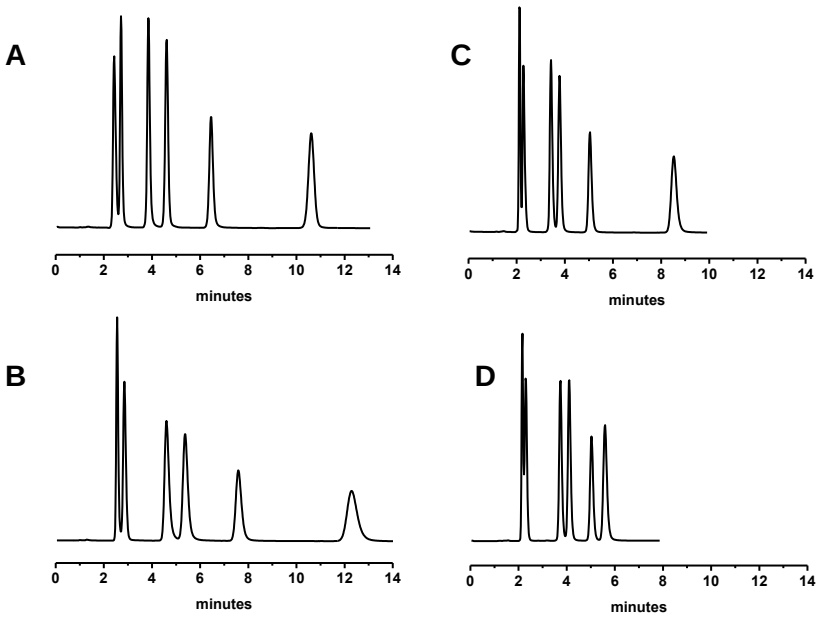

Figure 19. Analysis of a mixture of nucleobases and nucleosides (see Fig. 11 for structures). Columns: A) USP-HILIC-NH_2; B) USP-HILIC-NH_2-sil; C) APS-2; D) DIOL. Eluent: acetonitrile/water 90:10 (v/v) plus 10 mM NH_4OAc ($^{s}_{w}pH$ = 8.05). Flow rate: 1.0 ml/min, *T* = 25 °C, UV detection at 240 nm. Elution order: thymine, uracil, adenine, adenosine, cytosine, cytidine.

Cytidine was the most retained compound on all four columns. Retention and selectivity were higher on both urea-type columns when compared to the DIOL and the APS-2. A baseline separation of peak 3 (adenine) and peak 4 (adenosine) could only be obtained with the USP-HILIC-NH_2 phases, which also provided a considerably better

separation of thymine and uracil. When compared to the non silanized phase, USP-HILIC-NH_2-sil showed an increase in analysis time and similar selectivity values.

1.2.9 Transition from HPLC to RSLC and UHPLC.

Starting from the very promising results obtained in HPLC, we decided to prepare a 2.5 µm version of the USP-HILIC-NH_2 and the USP-HILIC-NH_2-sil phases. The stationary phase bearing a catalytic amount of free amino groups was selected as it proved more "sugarophilic" as well as more hydrophilic, with an increased retention of all tested analytes. Both the silanized and the non silanized versions of the phase were prepared and evaluated in order to have a more complete picture of the retention and stability of the phases.

As already observed, particularly in the case of the analysis of a mixture of organic acids, the retention mechanism is probably "mixed-mode", especially in the case of the USP-HILIC-NH_2 phases, with the amino groups playing an important role both through H-bond formation (see Scheme 3) and ionic interactions. Being such ionic interactions more consistent in the case of the USP-HILIC-NH_2 phases, they were chosen for the transition from traditional HPLC,

which uses 5 µm particles to Rapid Speed LC, with sub-3 µm particles, in our case 2.5 µm particles. The next step would be in this case the final transition to ultra-high performance LC, which is in fact one of the future goals of this project. As is well known, substantial increase in the sample throughput of a HPLC system can be in principle obtained by employing smaller particles packed in short columns and using high linear velocities of the eluent. Recently, an always increasing number of HILIC columns for UHPLC applications has been introduced in the market, but consist mainly of bare silica columns. To our knowledge, the only column with a wide application field which presents a bonded silica is the Acquity BEH Amide column, commercialized by Waters. At this point, although the two columns prepared were not in the sub-2 µm range, we decided to compare the results obtained with the Acquity BEH Amide and with a *fused-core* 2.6 µm column produced by Phenomenex, namely the Kinetex HILIC, which promises similar results with the UHPLC columns while yielding a lower back pressure. As described in the Experimental Section, the USP-HILIC-NH_2-2.5 and the USP-HILIC-NH_2-sil-2.5 phases were prepared following an identical synthetic procedure to the one already employed for the preparation of the 5 µm phases. Two columns (100 x 3.2 mm I.D.) were packed with these two new phases.

To investigate the separation abilities of the new bidentate urea-type columns in HILIC mode, chromatographic studies were performed with polar analytes as probes. Table 5 reports the results of the preliminary HILIC efficiency tests performed both with and without buffer.

As already observed with the HPLC columns, a considerable increase in retention was observed with the addition of ammonium acetate buffer to the mobile phase consisting of a 90:10 (v/v) mixture of acetonitrile:water, probably due to H-bond formation between the acetate molecule and the stationary phase (see Scheme 3). A similar test was performed on the two commercial columns, bearing a different geometry (100 x 2.1 mm I.D.), typical of the UHPLC columns. The reduced internal diameter lead us into using a flow rate of 0.4 ml/min with the two commercial columns, while a flow rate of 0.8 was used with the lab-made columns, as it is usually considered an optimum for columns with an internal diameter of 3.2 mm. As for the HPLC HILIC test, naphthalene was added as an unretained marker of dead volume (k = 0 in all cases), and was always eluted before uracil, which is a common void volume marker in reversed phase HPLC.

Table 5. Chromatographic data of the HILIC tests obtained on the bidentate urea-type-2.5 µm columns in comparison with Acquity BEH Amide and Kinetex HILIC columns.[a]

	Sample	USP-HILIC-NH_2-2.5			USP-HILIC-NH_2-sil-2.5			Acquity BEH Amide			Kinetex HILIC		
		k[b]	α[c]	R_s[d]	k[b]	α[c]	R_s[d]	k[b]	α[c]	R_s[d]	k[b]	α[c]	R_s[d]
No buffer added	naphthalene	0.00			0.00			0.00			0.00		
			–	9.42		–	11.94		–	4.80		–	3.25
	uracil	0.98			0.92			0.86			0.31		
			2.17	8.77		1.37	–		4.89_s	–		3.87	7.13
	adenosine	2.13			1.26			4.21			1.20		
			1.30	6.65		1.90	–		1.08	–		2.06	7.12
	cytosine	2.76_s			2.39			4.53			2.47		
10 mM NH_4OAc added	naphthalene	0.00			0.00			0.00			0.00		
			–	14.09		–	13.38		–	13.19		–	5.19
	uracil	1.00			0.96			1.27			0.46		
			2.41	12.21		2.59	12.24		2.49	12.70		3.06	7.65
	adenosine	2.41			2.49			3.16_s			1.41		
			1.53	7.59		1.62	8.03		1.34	5.70		1.76	6.35
	cytosine	3.68			4.04			4.24			2.48		

[a] Columns geometry for USP-HILIC-NH_2-2.5 and USP-HILIC-NH_2-sil-2.5 : 100 mm × 3.2 mm I.D.,); flow rate: 0.8 ml/min; columns geometry for Acquity BEH Amide and Kinetex HILIC : 100 x 2.1 mm I.D.; flow rate: 0.4 ml/min;eluent: acetonitrile/water = 90:10 (v/v) T = 25 °C; UV detection at 254 nm. [b] k = retention factor. [c] α = selectivity factor.

[d] R_s = resolution, calculated as described in the Experimental Section.

When compared to the HPLC results, retention of the two bidentate columns proved slightly lower; this is probably due to the fact that a different silica gel was used (Daisogel instead of Kromasil). The Kinetex column did not show any difference in retention after adding buffer to the mobile phase, probably due to the fact that being made up of bare silica gel, no H-bond formation can occur between the stationary phase and the acetate in the eluent. As far as the BEH-Amide column is concerned, a very poor peak shape was observed for adenosine and cytosine (peaks 3 and 4) as can be seen in Fig. 20 (*left*).

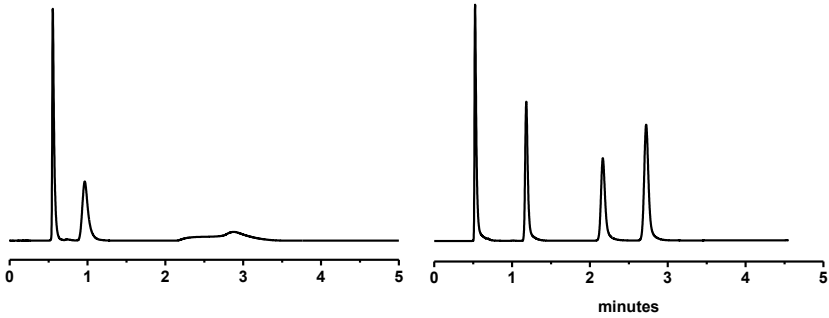

Figure 20. Chromatograms of HILIC test (see Fig. 11 for structures). Column: Acquity BEH Amide, 1.7 µm, 100 x 2.1 mm I.D. Eluent: on the left, acetonitrile/water 90:10 (v/v) and on the right, acetonitrile/water 90:10 (v/v) plus 10 mM NH_4OAc ($^{s}_{w}pH$ = 8.05). Flow rate: 0.4 ml/min, *T* = 25 °C, UV detection at 254 nm. Elution order: see Table 5.

The number of theoretical plates per meter for the bidentate urea-type columns was calculated on uracil ($0.92 < k < 1.00$) and ranged between 75'000 and 85'000 on both of them, which was higher than the one observed with the Kinetex HILIC (40'000) and the BEH Amide (65'000) columns, which was rather significant given the fact that these are both prepared for UHPLC applications.

1.2.9a Analysis of polyols

As with the HPLC columns, a preliminary "sugarophilicity" test was performed using the already described mixture of polyols (see Fig. 11 for structures and Table 6 for results). The *fused-core* column of bare silica (Fig. 21D) performed rather poorly both in terms of retention and especially on terms of efficiency, with N/m values lower than 60'000. The bidentate urea column in the silanized version (USP-HILIC-NH_2-sil-2.5, Fig. 21B) displayed a very high retention, comparable to the one obtained with the Acquity BEH Amide column (Fig. 21C), which displayed the highest number of theoretical plates as well as the highest retention and selectivity in the polyols series. It is noteworthy, however, that especially for mannitol, displaying an intermediate capacity factor, the efficiency of the lab-made 2.5 µm

Table 6. Chromatographic data of the HILIC tests obtained on the bidentate urea-type 2.5 µm columns in comparison with the Acquity BEH Amide and the Phenomenex Kinetex HILIC columns.[a]

Sample	USP-HILIC-NH_2-2.5 100 x 3.2 mm I.D. Flow-rate: 0.8 ml/min				USP-HILIC-NH_2-sil-2.5 100 x 3.2 mm I.D. Flow-rate: 0.8 ml/min				Acquity BEH Amide 100 x 2.1 mm I.D. Flow-rate: 0.4 ml/min				Kinetex HILIC 100 x 2.1 mm I.D. Flow-rate: 0.4 ml/min			
	k[b]	α[c]	R_s[d]	N/m[e]	k[b]	α[c]	R_s[d]	N/m[e]	k[b]	α[c]	R_s[d]	N/m[e]	k[b]	α[c]	R_s[d]	N/m[e]
1,3,5-*cis*,*cis*-Cyclohexanetriol	1.74	1.86	10.47	71'690	2.37	2.13	14.11	76'950	2.20	2.42	13.02	31'510	1.05	1.75	3.35	15'250
Xylitol	3.24	1.44	7.89	114'010	5.05	1.65	11.74	112'870	5.33	3.12	10.20	99'570	1.84	1.31	1.70	25'567
Mannitol	4.66	1.56	8.94	126'450	8.36	1.74	11.19	123'300	8.45	2.18	21.86	110'000	2.41	1.34	3.62	33'410
Chiro-inositol	7.26[5]	1.30	5.49	74'620	14.54	1.39	6.68	65'060	18.44	1.40	11.10	196'200	3.21	1.42	4.99	55'670
Myo-inositol	9.42			106'640	20.20			85'740	25.78			192'910	4.59			51'420

[a] Eluent: acetonitrile/water = 90:10 (v/v) plus 10 mM NH_4OAc ($^{s}_{w}pH$ = 8.05); T = 25 °C; UV detection at 254 nm.
[b] k = retention factor. [c] α = selectivity factor. [d] R_s = resolution, calculated as described in the Experimental Section.
[e] Theoretical plates per meter calculated ccording to the EU Pharmacopeia.

columns was not only comparable but also higher than the one obtained on the Acquity BEH Amide 1.7 µm column. The USP-HILIC-NH_2-sil-2.5 column RSLC proved highly promising in sugars analysis and comparable to UHPLC columns.

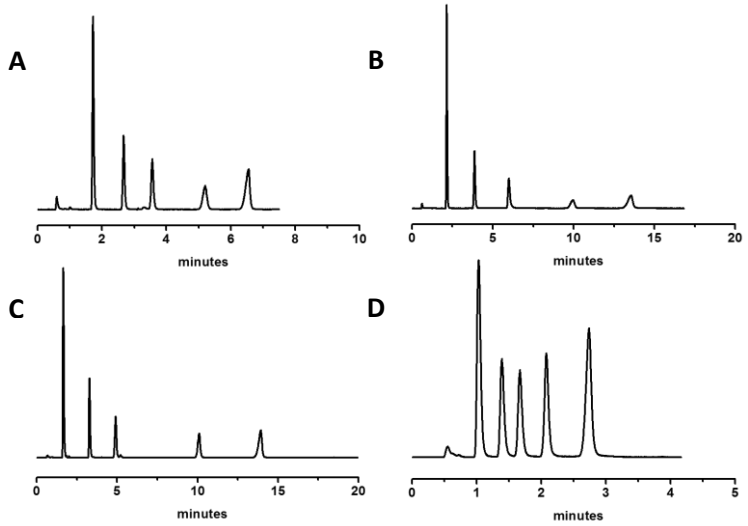

Figure 21. Analysis of a polyols mixture. Columns: A) USP-HILIC-NH_2-2.5; B) USP-HILIC-NH_2-sil-2.5; C) Acquity BEH Amide; D) Kinetex HILIC. Eluents: acetonitrile/water 85:15 (v/v) plus 10 mM NH_4OAc (${}^{s}_{w}pH$ = 7.65) Flow rate for A) and B): 0.8 ml/min, for C) and D): 0.4 ml/min. *T* = 25 °C, ELSD detection (T_{neb} = 50 °C). Samples were dissolved in acetonitrile/water 50/50 (v/v) and the solutions (1 mg/ml) were allowed to equilibrate at *T* = 25 °C prior to injection. Elution order on all columns: (1) 1,3,5-cis,cis-cyclohexanetriol, (2) xylitol, (3) mannitol, (4) *chiro*-inositol, and (5) *myo*-inositol.

1.2.9b Sugars Analysis

Sugars analysis has always been important in food analysis as well as in drug formulation but few analytical methods have been introduced since the APS-2 column was conceived. The APS-2 column historically represents the most used column in carbohydrate analysis, although recently new phases have been described in literature [34-36, 45, 47]; furthermore, the Acquity BEH Amide Columns applications Booklet presents a long list of applications in carbohydrate analysis, including complex mixtures. Given the ever increasing importance of proteomics and metabolomics, there is, at present, a growing interest in sugars analysis and "sugarophilicity" of stationary phases. As Prof. Hodgson stated in 1990 "*almost without exception, whenever two or more living cells interact in a specific way, cell surface carbohydrates will be involved*" [48]: it is therefore very important to be able to use columns with a good sugarophilicity. These columns should also be hydrolytically stable, especially in alkaline conditions, lack anomerization phenomena, show a high thermal stability and a good efficiency, along with the necessary selectivity and retentivity. All the above mentioned properties belong to the bidentate urea phases that have been prepared in our lab: transition into RSLC and, in the future, into UHPLC, would allow us to increase efficiency and reduce

analysis time, which is often important when analysing complex mixtures.

After evaluating the "sugarophilicity" of the bidentate urea-type columns, the silanized version was chosen for further applications due to its higher stability and higher retention. As previously described (see Section 1.2.6), we examined the selectivity of the column towards the already described complex mixture of nine sugars comprising two monosaccharides (namely, fructose and glucose), two disaccharides (namely saccharose and maltose) and a series of five maltose oligomers (see Fig. 13 for their structures). Ammonium acetate was added to the mobile phases (final concentration 10 mM) as the best results were obtained with the HPLC columns using buffered mobile phases.

In this case, a 15 min linear gradient elution from 10% to 40% of water in acetonitrile was used in combination with ELSD detection (see Fig. 22 for representative chromatograms). The same gradient elution was selected for the two commercial columns. It is noteworthy that both a reduced gradient time (15 min instead of the previous 25 min used in HPLC) and a smaller amount of water (most eluting solvent) were used, obtaining in all cases an excellent separation of all nine peaks on the lab-made and on the Acquity BEH Amide columns (see Fig 22A and 22B).

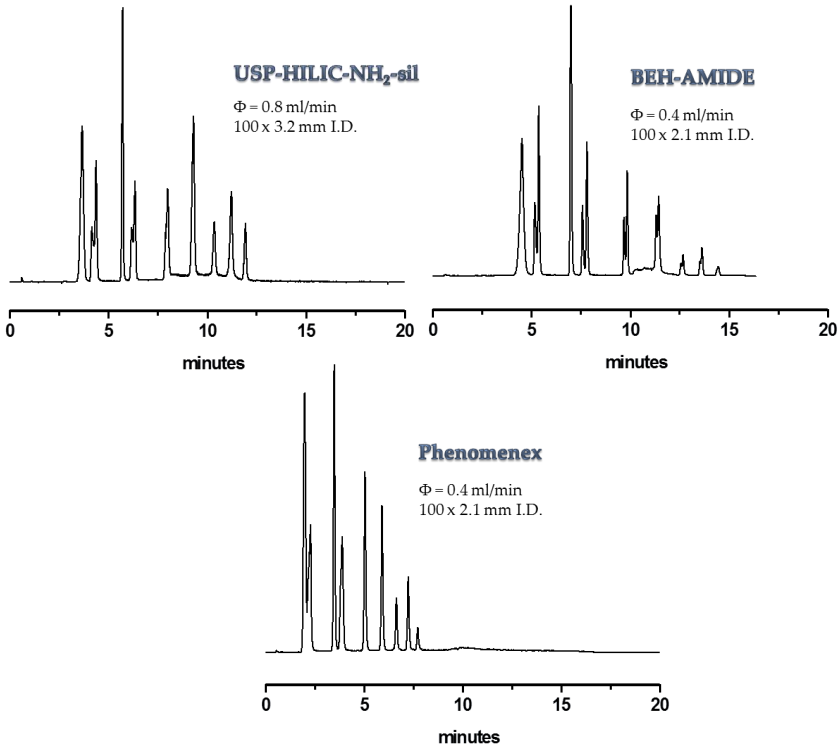

Figure 22. Analysis of the sugars mixture. Columns: A) USP-HILIC-NH2-sil-2.5; B) Acquity BEH-Amide; C) Phenomenex. Eluent A: acetonitrile/water 90:10 (v/v) plus 10 mM NH_4OAc ($^{s}_{w}pH$ = 8.05); eluent B: water/acetonitrile 70:30 (v/v) plus 10 mM NH_4OAc ($^{s}_{w}pH$ = 6.80). Gradient elution from 100 to 50% A over 15 min (linear); back to 100% A in 1 min; 10 min re-equilibration time. ELSD detection (T_{neb} = 70° C). Sugars solutions (0.5 mg/ml) in acetonitrile/water 50/50 (v/v) were freshly prepared and allowed to equilibrate at T = 25 °C prior to injection. For the composition of the sample, see Table 3.

The USP-HILIC-NH_2-sil-2.5 (Fig. 22B) also presented anomeric peaks for the lower MW sugars, while anomerization was not observed for maltopentose, maltohexose and maltoheptose. Kinetex HILIC *fused-core* showed a lower reten/tion of tested compounds (Fig. 22C), as was already the case for polyols, as well as an incomplete separation of peaks 1 and 2 corresponding to fructose and glucose, respectively. In order to obtain single sharp peaks for each analyte, the column temperature was raised from room temperature (25 °C) first to 40 and then to 50 and 60 °C. It is well known, in fact, that higher temperatures increment sugars anomerization rates, making anomeric peaks collapse into a single one. As it can be seen from Figure 23 (right), already at 40 °C, the USP-HILIC-NH_2-sil-2.5 did not show anomeric peaks while maintaining an excellent stability and low noise level even at 60 °C.

The Acquity BEH-Amide column, on the other hand, maintained its capacity to distinguish among anomeric peaks up to 50 °C (Fig 23 left), while still at 60 °C broad peaks were observed, while the noise level was always very low, proving the high thermal and chemical stability of the column.

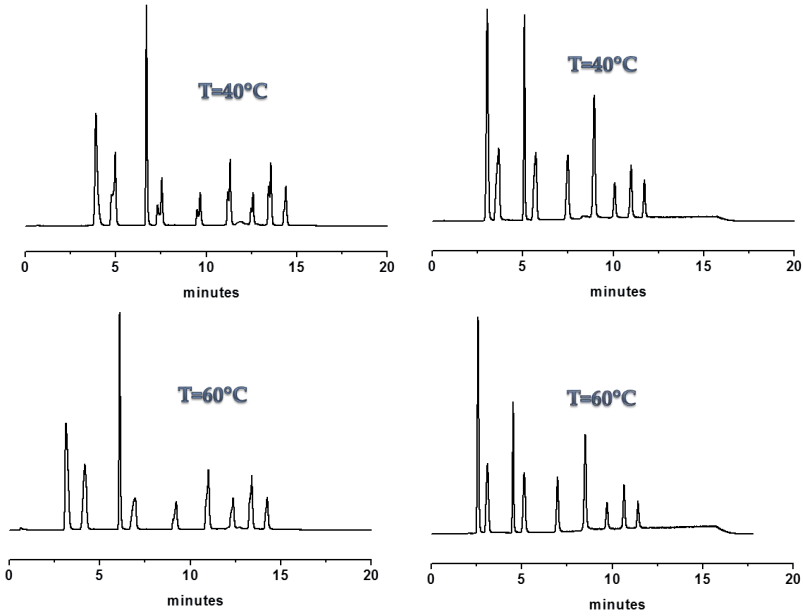

Figure 23. Effect of temperature on anomerization of reducing sugars. *Left:* Column: Acquity BEH-Amide; Flow-rate: 0.4 ml/min. *Right:* USP-HILIC-NH2-sil-2.5; Flow-rate: 0.8 ml/min; Eluent A: acetonitrile/water 90:10 (v/v) plus 10 mM NH_4OAc ($^{s}_{w}pH$ = 8.05); eluent B: water/acetonitrile 70:30 (v/v) plus 10 mM NH_4OAc ($^{s}_{w}pH$ = 6.80). Gradient elution from 100 to 50% A over 15 min (linear); back to 100% A in 1 min; 10 min re-equilibration time. ELSD detection (T_{neb} = 70° C). Sugars solutions (0.5 mg/ml) in acetonitrile/water 50/50 (v/v) were freshly prepared and allowed to equilibrate at T = 25 °C prior to injection. For the composition of the sample, see Table 3.

The results obtained through this comparative evaluation, allowed us to confirm the high stability and excellent "sugarophilicity" of the bidentate urea type columns also in RSLC applications. We believe that the most important advantage of the USP-HILIC-NH_2-sil-2.5 over the Acquity BEH-Amide column is the fact that the analysis of complex mixtures of sugars can be performed obtaining a good peak shape and a much clearer chromatographic profile, while showing a comparable stability, both under high temperature and alkaline pH (data not shown).

1.2.9c Other applications

Although we mainly focused on sugars analysis, further applications very similar to the one already performed on the HPLC columns were performed on the USP-HILIC-NH_2-sil-2.5 column. The mixture of four organic acids (see Section 1.2.7) as well as the one containing nucleobases and nucleosides (see Section 1.2.8) were tested on the RSLC columns. In particular, very interesting proved the results obtained analysing a mixture of 4-hydroxybenzoic acid, 3,5-dihydroxybenzoic acid, 3,4,5-trihydroxybenzoic acid (also named gallic acid) and 4-benzenesulphonic acid. Using a mobile phase identical to the one used in section 1.2.7, namely a 85/15 (v/v)

mixture of acetonitrile: water plus 30 mM ammonium acetate, we were able to obtain an excellent separation of all four acids in 8 minutes, considerably faster than with the HPLC correspondent column (25 min). In Fig. 24 the results obtained with the USP-HILIC-NH_2-sil-2.5 are compared to the ones given by the commercial columns. A partial separation of peaks 2 and 3 (α = 1.11) was obtained with the Kinetex HILIC column (Fig. 24B), which also showed a low retention of the analytes, with *k* ranging between 0.40 and 2.00. The Acquity BEH-Amide column (Fig. 24A) displayed a good retention for the first three compounds (*k* ranging between 1.76 and 4.12) and an excellent baseline separation could be obtained ($\alpha_{1,2}$ = 1.55 and $\alpha_{2,3}$ = 1.51). However, the fourth peak corresponding to gallic acid could only be identified through enrichment with the standard as it was extremely broad in shape, notwithstanding the 30 mM concentration of the buffer. We believe, in fact, that gallic acid is adsorbed on the silica gel of the column, making it inadequate for the analysis of similar acid compounds, bearing a considerable number of polar groups.

On the contrary, our column (Fig. 24C) showed a satisfactory chromatographic profile for all peaks, as well as an excellent selectivity (α values of 1.99, 1.24 and 1.82, respectively) and good retention values (*k* between 1.66 and 7.48).

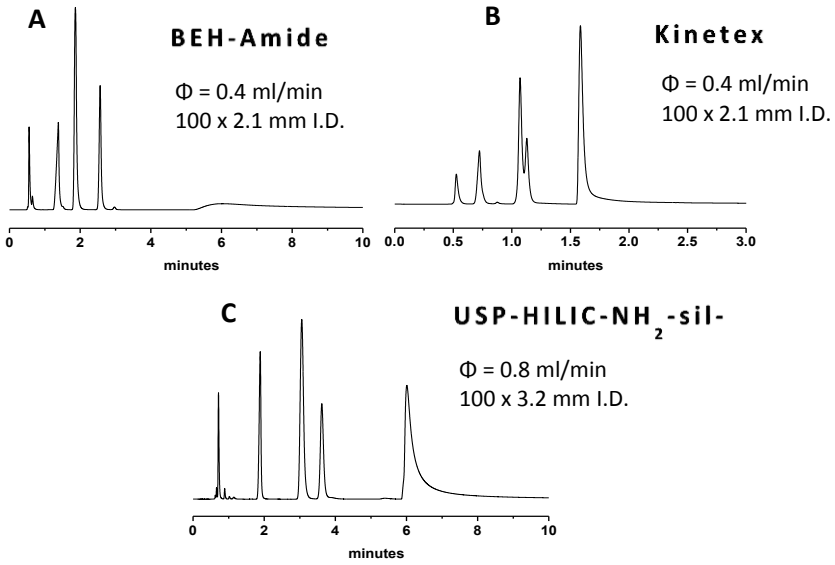

Figure 24. Analysis of a mixture of organic aromatic acids (see Fig. 11 for structures). Columns: A) Acquity BEH Amide; B) Kinetex HILIC; C) USP-HILIC-NH_2-sil-2.5. Eluent: acetonitrile/water 85:15 (v/v) plus 30 mM NH_4OAc ($_w^spH$= 7.73). *T* = 25 °C, UV detection at 254 nm. Peak 1) 4-hydroxybenzenesulfonic acid; peak 2) 4-hydroxybenzoic acid; peak 3) 3,5-dihydroxybenzoic acid; peak 4) 3,4,5-trihydroxybenzoic acid (or gallic acid).

It should be noted that in this case a mixed mode separation mechanism can be observed including both H bond formation, typical hydrophilic interaction, and ion exchange, particularly between the ionizable free amino groups on the stationary phase and the carboxylic functions of the analytes.

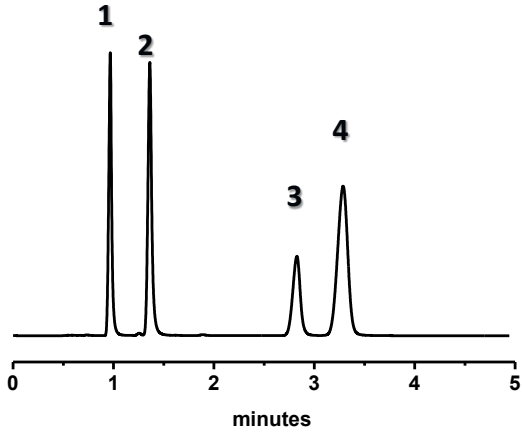

Figure 25. Analysis of a mixture of pharmaceuticals and vitamins-like compounds (see Fig. 17 for structures) on the USP-HILIC-NH_2-sil-2.5 column. Eluent: acetonitrile/water = 80:20 (v/v) plus 5 mM KH_2PO_4 ($^{s}_{w}$pH = 6.10); flow rate: 0.8 ml/min, *T* = 25 °C; UV detection at 240 nm. Peak 1) 2-hydroxybenzoic acid (salicylic acid); peak 2) 2-acetoxybenzoic acid; peak 3) isoascorbic acid and peak 4) ascorbic acid.

Finally, other applications similar to the ones performed in HPLC were carried out (data not reported) An example can be seen in Fig. 25, reporting separation of a mixture made up of ascorbic and isoascorbic acid together with salicylic and acetylsalicylic acids. Such applications are the RSLC equivalent of the ones already observed in HPLC.

1.3 Conclusions

New liquid chromatography stationary phases suited for HILIC applications have been prepared, packed into HPLC columns and evaluated using a large set of polar test solutes. The original synthetic procedure exploits the preliminary preparation of a bidentate alkoxysilane incorporating urea fragments, and its subsequent immobilization onto silica surface yielding double-tethered, hydrolytically stable urea-type stationary phases. A variant of the urea-type HILIC phase featuring some free amino groups on the silica surface was prepared and shown to be particularly suited for the analysis of sugars, whereby α/β anomer interconversion was accelerated by the residual basic sites and single sharp peaks were obtained for each individual sugar. The new HILIC stationary phases are chemical and thermally stable and showed good selectivities for a broad set of chemically diverse, polar compounds. Chemical inertness of the new urea-type HILIC stationary phases facilitated their use in LC-MS applications, giving drift-free chromatograms as a result of negligible release of bonded ligands during chromatographic elution.
Finally, technological upgrade to RSLC was obtained by using 2.5 µm particles to prepare a stable urea-type stationary phase following the one-pot procedure already used during the preparation of the HPLC

phases. The new RSLC column proved very efficient and was able to compete with the best HILIC UHPLC columns present in the market. As for the HPLC columns, the 2.5 µm column presented similar chemical inertness and thermal stability, as well as a wide range of applications.

1.4 Experimental Section

1.4.1 Apparatus

Two different arrangements were optimized for chromatographic runs: UHPLC and HPLC systems. The Acquity® UPLC consisted of a binary solvent manager, sample manager, a "homemade temperature controller" column compartment and PDA
[200–400 nm] detector with a 500 nl flow cell (Waters, Milford, MA, USA). The PDA was set with filter time constant of 0.05 s and a sampling rate of 80 points/s. HPLC separations were performed on a chromatographic system consisting of a Waters Alliance 2695 pump and an autosampler equipped with a model 996 PDA detector. A model Sedex-55 evaporative light scattering detection (ELSD) system (S.E.D.E.R.E., France) was also used. Chromatographic data were collected and processed using the Empower 2.0 software (Waters).

To reduce the extracolumn volumes, connecting tubes of 0.1 mmI.D. for UHPLC arrangement and standard tubes of 0.25 mm I.D. for HPLC system were employed.

LC-MS was performed using a Thermo Fischer Scientific HPLC separation module (San Jose, CA, USA) consisting of an Accela 1250 Pump, an autosampler and a PDA detector, coupled to a Thermo Finnigan LXQ linear ion trap mass spectrometer, equipped with an ESI ion source bearing a steel needle. Chromatographic and mass spectrometric data were collected and processed using the Thermo Xcalibur Chromatography Manager software, version 2.1.

FT-IR spectra (KBr pellets) were recorded on a Jasco 430 Fourier transform IR spectrometer (Jasco Europe, Cremella, Italy) at a resolution of 4 cm^{-1}.

The mobile phase pH was measured with a Metrohm Model 632 pH-meter (Metrohm, Heriscan, Switzerland).

^{1}H-NMR and ^{13}C-NMR solution spectra were recorded on a Varian INOVA spectrometer operating at a field of 14.4 T (600 MHz for ^{1}H, 150.8 MHz for ^{13}C) with an indirect-triple resonance probe.

Solid state ^{29}Si and ^{13}C CPMAS NMR spectra were measured on a Bruker Avance III spectrometer at 79.49 MHz and 100.63 MHz, respectively. Samples were packed into 4 mm zirconia rotors, and sealed with Kel-F caps. The spin rate was 8 kHz. The cross-polarization

(CP) was performed by applying the variable spin-lock sequence RAMP-CPMAS [49]; the RAMP was applied on the ^{1}H channel and during the contact time the amplitude of the RAMP was increased from 50 to 100% of the maximum value. ^{29}Si CPMAS spectra were obtained with a contact time optimized at 3 ms, the recycle delay being 4 s. ^{13}C CPMAS spectra were obtained with a contact time optimized at 6 ms, the recycle delay being 3 s. All spectra were acquired with a time domain of 1024 data points, zero filled and Fourier transformed with a size of 4096 data points, applying an exponential multiplication with a line broadening of 4 Hz. ^{29}Si and ^{13}C chemical shifts were referenced to tetramethylsilane used as an external reference. The deconvolution of ^{29}Si CPMAS spectra was performed by using the dm2006 software package [50]. Each resonance was modelled by a gaussian lineshape, and characterized by the amplitude, the chemical shift and the width at half height.

Thermogravimetric analysis (TGA) was carried out and certified by REDOX snc laboratories (Monza, Italy). The percent values of weight losses are extrapolated from the TGA curves by tangential-mode integration.

1.4.2. Chemicals and reagents

Spherical Kromasil Si 100 silica gel (pore size 100 Å, particle size 5.0 µm, specific surface area 340 m^2g^{-1}) was purchased from Eka Nobel (Bohus, Sweden). Spherical Daisogel Si 120-2.5P silica gel (pore size 120 Å, particle size 2.6 µm, specific surface area 343 m^2g^{-1}) was a kind gift of Daiso (Japan). Ethylenediamine, (3-isocyanatopropyl)triethoxysilane, 4-(dimethylamino)pyridine (or 4-DMAP), dry toluene, 1,2-bis(trichlorosilyl)-ethane, toluene-d_8, methanol-d_4, maltotriose, maltotetraose, malto-pentaose, maltohexaose and maltoheptaose as well as 1,3,5-cis,cis-cyclohexanetriol, xylitol, chiro-inositol, myo-inositol, thymine, uracil, cytosine, adenine, cytidine, adenosine, acetylsalicylic acid, salicylic acid, 4-hydroxybenzoic acid, 3,5-dihydroxybenzoic acid, 4-hydroxybenzene-sulfonic acid, and gallic acid were from Sigma Aldrich (St. Louis, MO, USA). Mannitol, maltose, saccharose, ascorbic and isoascorbic acids, and triethylamine (TEA) for HPLC were from Fluka (Buchs, Switzerland). Ammonium acetate (NH_4OAc) was supplied from Baker (Division of Mallinckrodt Baker Inc., Phillipsburg, NJ). HPLC gradient grade water, acetonitrile, hexane, tetrahydrofuran, chloroform stabilized with ethanol were purchased

from Sigma Aldrich. Other polar analytes were available from earlier studies.

1.4.3 Preparation of the bidentate urea-type USP-HILIC stationary phases

A solution of 1,2-ethylenediamine (0.29 ml; 4.3 mmol) in dry toluene (70 ml) was heated at 110 °C under a nitrogen atmosphere. After distillation of 5 ml of solvent, a solution of (3-isocyanatopropyl)triethoxysilane (2.13 ml; 8.6 mmol) in dry toluene (10 ml) was added and the solution was stirred under nitrogen for 4 h at 100 °C. Six grams of dried silica (Kromasil Si 100, 5.0 µm, specific surface area 340 m^2g^{-1}) were suspended in ethanol 95% by volume (250 ml) and kept overnight under stirring. Hydrated silica gel, washed and dispersed in 40 ml of dry toluene, was added to the above reaction flask and the mixture was heated at 90 °C under continuous stirring for 3 h. Finally, 4-DMAP (0.64 g; 5.2 mmol) was added and the slurry was kept under continuous stirring for 16 h at 90 °C. After cooling at room temperature, the modified silica gel (Urea-type Stationary Phase or USP-HILIC) was isolated by filtration, washed with methanol and dichloromethane, and dried *in vacuo* (0.1 mbar) at T = 60 °C to constant weight (7.1 g; weight increment =

19%). FT-IR (KBr):3329, 2978, 2933, 1876, 1645, 1560, 1076, 955 cm^{-1}. Elemental analysis: C 7.04%, H 1.43%, N 2.71%, corresponding to 574 µmol of substrate per gram of silica or 1.71 µmol/m^2 (based on nitrogen). Calculation based on carbon content yielded similar values, i.e., 580 µmol and 1.71 µmol/m^2, respectively.

Two grams of USP-HILIC were dispersed in a 10 mM NH_4OAc solution in water-acetonitrile 70:30, v/v (60 ml). The slurry was kept overnight under continuous stirring at 30 °C, then filtered, washed with water, acetone, methanol and dichloromethane and dried *in vacuo* (0.1 mbar) at T = 60 °C. After the washing procedure, the dried silica was added to a reaction flask containing imidazole (0.100 g; 1.45 mmol) dissolved in dry toluene (20 ml). A solution of 1,2-bis(trichlorosilyl)ethane (0.5 ml; 2.5 mmol) in dry toluene (5 ml) was added dropwise to the slurry and was allowed to react for 2 h under a nitrogen atmosphere and continuous stirring at room temperature. Finally, the silanized silica gel (USP-HILIC-sil) was filtered, washed with toluene, chloroform, methanol and dichloromethane, and dried *in vacuo* (0.1 mbar) at T = 60 °C. FT-IR (KBr): 3352, 2943, 2887, 1869, 1635, 1566, 1053, 806 cm^{-1}. Elemental analysis: C 6.96%, H 1.37%, N 2.60%.

1.4.4 Preparation of the bidentate urea-type USP-HILIC-NH_2 stationary phases

A bidentate urea-type stationary phase bearing some free amino groups (USP-HILIC-NH_2) was prepared as reported for USP-HILIC (see Section 1.4.3) starting from three grams of hydrated Kromasil Si 100 silica gel and using a different molar ratio between (3-isocyanatopropyl)triethoxysilane (1.08 ml; 4.4 mmol) and ethylenediamine (0.16 ml; 2.4 mmol). After identical work-up, the modified silica gel (USP-HILIC-NH_2) was washed with 50-ml portions of methanol and dichloromethane, and dried *in vacuo* (0.1 mbar) at *T* = 60 °C to constant weight (3.58 g; weight increment = 12.7 %). FT-IR (KBr): 3329, 2938, 2880, 1867, 1635, 1560, 1053, 800 cm–1. Elemental analysis: C 7.42%, H 1.37%, N 3.17% corresponding approximately to 619 µmol of substrate per gram of silica or 1.82 µmol/m^2 (based on carbon), calculated assuming -($CH_2CH_2CH_2NH$-CO-NH-CH_3)$_2$ as the ligated fragment.

Two grams of USP-HILIC-NH_2 silica gel were silanized as reported for USP-HILIC (see Section 1.4.3). After identical work-up, the silanized silica gel (USP-HILIC-NH_2-sil) was filtered, washed with 50-ml portions of toluene, chloroform, methanol and dichloromethane and dried *in vacuo* (0.1 mbar) at *T* = 60 °C. FT-IR (KBr): 3334, 2935, 2882, 1876,

1633, 1567, 1095, 804 cm–1. Elemental analysis: C 7.26%, H 1.42%, N 2.73%.

1.4.5 Preparation of the bidentate urea-type USP-HILIC-NH_2-2.5 stationary phases

The same synthetic procedure was used as the one reported for the 5 µm phases. In this case, a 2.5 µm Daisogel silica gel (specific surface area: 343 m^2g^{-1}, pore size 120 Å) was used.

A solution of 1,2-ethylenediamine (0.07 ml; 1.04 mmol) in dry toluene (15 ml) was heated at 110 °C under a nitrogen atmosphere. After distillation of 3 ml of solvent, a solution of (3-isocyanatopropyl)triethoxysilane (0.46 ml; 1.87 mmol) in dry toluene (5 ml) was added and the solution was stirred under nitrogen for 4 h at 100 °C. 1.45 grams of dried silica (Daisogel Si 120, 2.5 µm, specific surface area 343 m^2g^{-1}) were suspended in ethanol 95% by volume (60 ml) and kept overnight under stirring. Hydrated silica gel, washed and dispersed in 10 ml of dry toluene, was added to the above reaction flask and the mixture was heated at 90 °C under continuous stirring for 3 h. Finally, 4-DMAP (0.15 g; 1.24 mmol) was added and the slurry was kept under continuous stirring for 16 h at 90 °C. After cooling at room temperature, the modified silica gel (USP-HILIC-NH_2-

2.5) was isolated by filtration, washed with methanol and dichloromethane, and dried *in vacuo* (0.1 mbar) at *T* = 60 °C to constant weight (1.66 g; weight increment = 15%). FT-IR (KBr): 3367, 2978, 1645, 1559, 1079, 968, 789 cm^{-1}. Elemental analysis: C 5.83%, H 1.26%, N 2.57%.

0.76 grams of USP-HILIC-NH_2-2.5 silica gel were silanized as reported for USP-HILIC (see Section 1.4.3). After identical work-up, the silanized silica gel (USP-HILIC-NH_2-sil) was filtered, washed with 20-ml portions of toluene, chloroform, methanol and dichloromethane and dried *in vacuo* (0.1 mbar) at *T* = 60 °C. FT-IR (KBr): 3299, 2935, 2882, 1635, 1558, 1095, 791 cm–1. Elemental analysis: C 6.28%, H 1.36%, N 2.21%.

1.4.6 Preparation of the diol-modified silica gel

Three grams of dried silica (Kromasil Si 100; 5 µm, specific surface area: 340 m^2g^{-1}) was suspended in methanol (35 ml) containing H_2SO_4 80% (0.1 ml). A solution of (3-glycidoxypropyl)trimethoxysilane (0.5 ml; 2.3 mmol) in methanol (10 ml) was added dropwise in an argon atmosphere. The slurry was heated to 70 °C for 2 h with continuous mechanical stirring. After cooling to room temperature, the diol-modified silica was isolated by filtration; washed with 30-ml portions

of methanol, water, methanol, and acetone; and dried under reduced pressure (0.1 mbar) at *T* = 60 °C. Elemental analysis: C 3.18%, H 0.77%, corresponding to 326.3 µmol of substrate per gram of silica or 1.40 µmol/m^2.

1.4.7 Chromatographic set-up

HPLC columns: Stainless steel (150 mm × 4.0 mm I.D.) columns were packed with the four bidentate urea-type USP-HILIC, USP-HILIC-sil, USP-HILIC-NH_2 and USP-HILIC-NH_2-sil stationary phases using a slurry packing procedure already described [51]. A Kromasil Si 100, 5 µm diol-modified silica gel was *ad hoc* prepared (see Section 1.4.6) and packed as well into a stainless steel (150 mm × 4.0 mm I.D.) column. For comparative purposes, two more commercial columns (150 mm × 4.0 mm I.D.) were used, namely Hypersil APS-2 (Si 120, 5 µm; specific surface area: 170 m^2g^{-1}) from Thermo Fischer Scientific and ZIC-HILIC (Si 200, 5 µm; specific surface area 135 m^2g^{-1}) from SeQuant (Sweden). All chromatographic runs were carried out under isocratic or gradient elution with the flow rate set to 1.0 ml/min.

RSLC columns: Stainless steel (100 mm × 3.2 mm I.D.) columns were packed with the two bidentate urea-type USP-HILIC-NH_2 and USP-

HILIC-NH_2-sil stationary phases using a slurry packing procedure already described [51].

All chromatographic runs were carried out under isocratic or gradient elution with the flow rate set to 0.8 ml/min for the lab made columns. A flow rate of 0.4 ml/min was selected for the two UHPLC commercial columns (Acquity BEH Amide and Kinetex HILIC).

Eluents were composed of acetonitrile and water or aqueous buffers in a volume ratio of 90 to 10 or 85 to 15. The aqueous buffers were prepared by dissolving appropriate amounts of NH_4OAc, KH_2PO_4 or TEA in water so that the final concentration in the hydro-organic mixture amounted to 5–30 mM of the desired additive.

The pH was measured both in aqueous buffer prior mixing with acetonitrile (namely, ${}^{w}_{w}pH$) and in the final hydro-organic solvent mixture (${}^{s}_{w}pH$). Sample solutions were prepared in the mobile phase (0.5–2 mg/ml) and allowed to equilibrate at T = 25 °C prior to injection into the HPLC system (2–5 µl aliquots).

The column hold-up volumes (V_0) were determined by static pycnometry (*pyc*) using the following equation: $V_{0,pyc} = (w_{CHCl3}-w_{THF})/(\rho_{CHCl3}-\rho_{THF})$, where w and ρ are the masses of the columns filled with solvents and solvent density, respectively [52,53]. The number of theoretical plates per meter was calculated by built-in functions in the Empower software using 50% peak width. Resolution values were

calculated by built-in functions in the Empower software using the equation $(t_2 - t_1) \times 1.18/(w_2 + w_1)$ where t_2 and t_1 are retention times and w_2 and w_1 are peak widths at 50% of peak height.

1.4.8 HILIC/ESI-MS analysis

HILIC/MS was performed by electrospray ionization (ESI) using an ion trap analyzer operated under the following conditions: ion polarity, negative; capillary temperature, 275 °C; source voltage, 4.0 kV; capillary voltage, -44.5 V; tube lens offset, 44.0 V; sheath gas, 10 arbitrary units; auxiliary gas, 5 arbitrary units. Total ion current (TIC) from 220 to 1500 amu was monitored.

1.5 References and Notes

[1] Rabel, R.M.; Caputo, A.G.; Butts, E.T. *J. Chromatogr.* **1976**, *126*, 731-740.

[2] Alpert, A.J. *J. Chromatogr.* **1990**, *499*, 177-196.

[3] Hemström, P.; Irgum, K. *J. Sep. Sci.* **2006**, *29*, 1784-1821, and references cited therein.

[4] Dejaegher, B.; Vander Heyden, Y.; *J. Sep. Sci.* **2010**, *33*, 1-18 and references cited therein.

[5] Takegawa, Y.; Deguchi, K.; Ito, H.; Keira, T.; Nakagawa, H.; Nishimura, S.-I. *J. Sep. Sci*. **2006**, *29*, 2533-2540.

[6] Takegawa, Y.; Deguchi, K.; Ito, H.; Keira, T.; Nakagawa, H.; Nishimura, S.-I. *J. Chromatogr. A* **2006**, *1113*, 177-181.

[7] Takegawa, Y.; Deguchi, K.; Ito, H.; Keira, T.; Nakagawa, H.; Nishimura, S.-I. *J. Sep. Sci*. **2008**, *31*, 1585-1593.

[8] Takegawa, Y.; Deguchi, K.; Ito, H.; Keira, T.; Nakagawa, H.; Nishimura, S.-I. *J. Sep. Sci*. **2008**, *31*, 1594-1597.

[9] Martens-Lobenhoffer, J.; Postel, S.; Tröger, U.; Bode-Böger, S.M. *J. Chromatogr. B* **2007**, *855*, 271-275.

[10] Holdšendová, P.; Suchánková, J.; Bunček, M.; Bačkovská, V.; Coufal, P. *J. Biochem. Biophys. Methods* **2007**, *29*, 23-29.

[11] Guo, Y.; Gaiki, S. *J. Chromatogr. A* **2005**, *1074*, 71-80.

[12] Strege, M.A. *Anal. Chem.* **1998**, *70*, 2439-2445.

[13] Tolstikov, V.V.; Fiehn, O. *Anal. Biochem.* **2002**, *301*, 298-307.

[14] Diener, M.; Erler, K.; Christian, B.; Luckas, B. *J. Sep. Sci.* **2007**, *30*, 1821-1826.

[15] Zhang, H.; Guo, Z.; Zhang, F.; Xu, Q.; Liang, X. *J. Sep. Sci.* **2008**, *31*, 1623-1627.

[16] Nguyen, H.P.; Schug, K.A. *J. Sep. Sci.* **2008**, *31*,1465-1480, and references cited therein.

[17] Dell'Aversano, C.; Hess, P.; Quilliam, M.A. *J. Chromatogr. A* **2005**, *1081*, 190-201.

[18] Ciminiello, P.; Dell'Aversano, C.; Fattorusso, E.; Forino, M.; Magno, G.S.; Tartaglione, L.; Quilliam, M.A.; Tubaro, A.; Poletti, R. *Rapid Commun. Mass Spectrom.* ***2005****, 19*, 2030-2038.

[19] Naidong, W. *J. Chromatogr. B* **2003**, *796*, 209-224.

[20] Ikegami, T.; Tomomatsu, K.; Takubo, H.; Horie, K.; Tanaka, N. *J. Chromatogr. A* **2008**, *1184*, 474-503.

[21] Orth, P.; Engelhardt, H. *Chromatographia* **1982**, *15*, 91-96.

[22] Nikolov, Z.L.; Reilly, P.J. *J. Chromatogr.* **1985**, *325*, 287-293.

[23] Karatapanis, A.E.; Fiamegos, Y.C.; Stalikas, C.D. *J. Chromatogr. A* **2011**, *1218*, 2871-2879.

[24] Bicker, W.; Wu, J.Y.; Yeman, H.; Albert, K.; Lindner, W. *J. Chromatogr. A* **2011**, *1218*, 882-895.

[25] Lämmerhofer, M. *J. Sep. Sci.* **2010**, *33*, 679-680.

[26] Kirkland, J.J.; van Straten, M.A.; Claessens, H.A. *J. Chromatogr. A* **1998**, *797,* 111-120.

[27] Kirkland, J.J.; Adams, J.B.; van Straten, M.A.; Claessens, H.A. *Anal. Chem.* **1998**, *70*, 4344-4352.

[28] Liu, X.; Bordunov, A.V.; Pohl, C.A. *J. Chromatogr. A* **2006**, *1119*, 128-134.

[29] Grumbach, E. S., Diehl, D. M., Neue, U. D., *J. Sep. Sci.* **2008**, *31*, 1511–1518.

[30] Cunliffe, J. M., Maloney, T. D., *J. Sep. Sci.* **2007**, *30*, 3104–3109.

[31] DeStefano, J. J., Langlois, T. J., Kirkland, J. J., *J. Chromatogr. Sci.* **2008**, *46*, 254–260.

[32] Salisbury, J. J., *J. Chromatogr. Sci.* **2008**, *46*, 883–886.

[33] Chauve, B.; Guillarme, D.; Cleon, P.; Veuthy, J.-L. *J. Sep. Sci.* **2010**, *33*, 1-13.

[34] Neue, U.D.; Iraneta, P.C.; Hudalla, C.J.; Turner, J.; Alden, B.A.; Boissel, C.; Wheat, T.; Gillece-Castro, B.; Tran, K.; Wyndham, K.; Walsh, D. *Presentation at HPLC 2009*

[35] Waters Corporation ACQUITY UPLC BEH Amide Columns applications Booklet WA64081, www.waters.com

[36] Neue, U.D.; Iraneta, P.C.; Hudalla, C.J. *J. Sep. Sci.* **2010**, *33*, 838-340.

[37] D'Acquarica, I.; Gasparrini, F.; Misiti, D.; Pierini, M.; Villani, In *Advances in Chromatography*; Eds.; E. Grushka, N. Grinberg, CRC Press: Taylor & Francis Group, Boca Raton, FL, **2008**; Vol. *46*, p. 108-173.

[38] Krasnoslobodtsev, A.V.; Smirnov, S.N. *Langmuir* **2002**, *18*, 3181-3184.

[39] Albert, K. *J. Sep. Sci.* **2003**, *26*, 215-224.

[40] Yim, J.-H.; Lyu, Y.-Y.; Jeong, H.-D.; Mah, S.K.; Hyeon-Lee, J.; Hahn, J.-H.; Kim, G.S.; Chang., S.; Park, J.-G. *J. Appl. Polym. Sci.* **2003**, *90*, 626-634.

[41] Yang, J.J.; El-Nahhal, I.M.; Ssuer Chuang, I.; Maciel, G.E. J. *Non-Cryst. Solids* **1997**, *209*, 19-39.

[42] Bicker, W.; Wu, J.Y.; Lämmerhofer, M.; Lindner, W. *J. Sep. Sci.* **2008**, *31*, 2971-2987.

[43] Olechno, J.D.; Carter, S.R.; Edwards, W.T.; Gillen, D.G. *American Biotech. Lab.* **1987**, *5*, 38-50.

[44] Moriyasu, M.; Kato, A.; Okada, M.; Hashimoto, Y. *Anal. Lett.* **1984,** *17*, 689-699 and 1533-1538.

[45] Moni, L.; Ciogli, A.; D'Acquarica, I.; Dondoni, A.; Gasparrini, F.; Marra, A. *Chem. Eur. J.* **2010**, *16*, 5712-5722.

[46] Nováková, L.; Solich, P.; Solichová, D. *Tr. Anal. Chem.* **2008**, *27*, 942-958.

[47] Schuster, G.; Lindner, W. *Anal Bioanal Chem.* **2011**, *400*, 2539-2554.

[48] Hodgson, J. *Bio/Technology* **1990**, *8*, 625-628.

[49] Metz, G.; Wu, X.; Smith, S.O. *J. Magn. Reson.* **1994**, *110*, 219-227.

[50] Massiot, D.; Fayon, F.; Capron, M.; King, I.; LeCalvé, S.; Alonso, B.; Durand, J.O.; Bujoli, B.; Gan, Z.; Hoatson, G. *Magn. Reson. Chem.* **2002**, *40*, 70-76.

[51] D'Acquarica, I.; Gasparrini, F.; Giannoli, B.; Badaloni, E.; Galletti, B.; Giorgi, F.; Tinti, M.O.; Vigevani, A. *J. Chromatogr. A* **2004**, *1061*, 167-173.

[52] Rustamov, I.; Farcas, T.; Ahmed, F.; Chan, F.; LoBrutto, R.; McNair, H.M.; Kazakevich, Y.V. *J. Chromatogr. A* **2001**, *913*, 49-63.

[53] Gritti, F.; Kazakevich, Y.V.; Guiochon, G. *J. Chromatogr. A* **2007**, *1161*, 157-169.

Chapter 2

A rational approach to the design of new "Crab-like" chiral stationary phases for HPLC and UHPLC: synthesis and evaluation

2.1 Introduction

Liquid chromatographic resolution of enantiomers on chiral stationary phases (CSPs) is currently the most accurate and convenient means used in chiral separations. As prof. Ward shows in his biannual review, "HPLC is by far the most popular method of choice for performing chiral separations, with applications using this technique appearing twice as often as all the other techniques combined". [1]. In his 2010 review, he estimates around 1000 publications appearing between 2008 and 2010 where enantioselective HPLC (e-HPLC) is involved. Given the well-known importance of enantiomeric determination and purity, there is continuous strive for new CSPs. There are different types of CSPs available, including polysaccharide-based and cyclodextrin-based CSPs (introduced by Armstrong)[2], phases with macrocyclic antiobiotics such as vancomycin and teicoplanin, crown ether CSPs, protein CSPs, ligand-exchange CSPs (developed by

Davankov) [3], and *brush-type* CSPs, introduced by prof. Pirkle of the University of Illinois, in the late '70s.[4]

Pirkle-type CSPs are totally synthetic phases bearing selectors of low molecular weight, usually derived from aminoacids, which are covalently bonded to silica particles of high superficial area. In their design, Pirkle and co-workers used their knowledge on chiral auxiliaries in the field of NMR. Such auxiliaries showed enantioselectivity in solution and were the first selectors to be immobilized on silica gel and successfully separate sulfoxides and related compounds bearing an aromatic π-basic ring. While applying the reciprocity concept [5,6] (the interactions that allow the single enantiomer A to separate the enantiomers of B can be used by one of the two enantiomers of compound B to separate the enantiomeric pair A), new CSPs were designed and are now commercially available (by Regis Technologies, Inc. and Sumimoto). The most common type of interaction in π-bonding between aromatic rings present both in the CSP and in the analyte. Typical brush-type CSPs include amongst others, the Whelk-O1 and Whelk-02 phases, the DACH-DNB CSP introduced by prof. Gasparrini's group in 1986 [7], leucine and phenylglycine CSPs, ULMO and Pirkle 1-J phases.

The advantages of Pirkle-type CSPs include:

- Robustness and stability of the stationary phase, due to the covalent bonds immobilizing the selector on the silica particles.
- Thermal stability.
- High permeability.
- High chromatographic efficiency.
- Given the high loading, an easy scale-up to preparative LC is possible.
- Compatibility with a wide range of solvents (*brush-type* columns can operate under normal phase, reversed phase and polar organic mode).
- Availability of both chiral forms of the selector which allows the inversion of the elution order by switching the chirality of the column (an aspect which has been fully investigated and applied in Part B of this thesis, under the name of *Inverted Chirality Columns Approach*). [8,9] Being totally synthetic, the two columns are totally equivalent from a chemical point of view and only differ in the chirality of the selector.

For the above mentioned reasons, *brush-type* CSPs have proved highly competitive in e-HPLC and are now used for a wide range of applications.

A polymeric *brush-type* phase was introduced in 2005 by Gasparrini and co-workers: it unites the advantages of a typical monomeric Pirkle-type phase (stability, permeability, efficiency, loading, possibility of having both enantiomeric forms) with the high selectivity of non-synthetic polymeric phases.[10] The selector chosen is an enantiopure diacryloyl derivative of *trans*-1,2-Diaminocyclohexane (DACH-ACR) and the separation mechanism involves H-bond formation and steric effects. This CSP is currently commercialized by Supelco under the name of Astec P-CAP. Soon after, prof. Armstrong introduced a similar CSP bearing the diacryloyl derivative of *trans*-1,2-Diphenyl-1,2-ethylenediamine, which gives the phase the possibility to establish π-π interactions with the analytes.[11] This CSP is also commercialized by Supelco with the name Astec P-CAP-DP.

In this work, the design and preparation of two monomeric CSPs is described. New "Crab-like" totally synthetic, *brush-type* chiral stationary phases (CSPs) were envisioned for enantioselective HPLC and UHPLC (Figure 1). Our goal was to synthesize highly efficient CSPs containing a ureidic bond which would grant them stability, extended applicability to a variety of analytes, and LC-MS^n potentials in a range of eluents. Such columns, based on totally synthetic selectors, are ideal candidates for Inverted Chirality Columns Approach (ICCA),

previously developed in our laboratories. Chiral selectors were chosen among diamines and aminoalcohols; in particular, a set of chiral diamines, including 1,2-diaminocyclohexane (DACH) and 1,2-diphenyl-1,2-ethylenediamine (DPEDA) were the first candidates.

Figure 1. "Crab-Like" chiral stationary phases

Enantiopure diamines were treated with (3-isocyanatopropyl)-triethoxysilane, to yield reactive ureido selectors that were eventually attached to unmodified silica particles through a stable, bidentate tether. The new CSPs proved promising for the enantioseparation of a wide range of racemates (including benzodiazepines, N-derivatized aminoacids, and chiral drugs) both in normal phase (NP) and polar organic mode (POM), which uses 100% organic solvents such as acetonitrile, methanol and ethanol or combos. Comparative studies were operated with polymeric P-CAP[and P-CAP-DP columns in order

to evaluate the resolution and performance skills of the new CSPs in different elution modes.

2.2. Results and Discussion

2.2.1 Preparation of new "Crab-like" chiral stationary phases

In the past two years we have envisioned bidentate urea-type phases, where the selector, being either a chiral molecule or an achiral one (as in the case of the HILIC phases described in Chapter A-1 of this thesis) is covalently bonded on the silica gel through a stable bidentate tether. The chemistry would be in both cases very simple and the derivatization process can take place following a "two-step one-pot" procedure. The same procedure was used in the past by our group to obtain chemically and thermally stable glycopeptide-based chiral stationary phases that would prove useful under different separation modes [12]. Drawing inspiration from these synthetic schemes, we envisioned a new route to silica-based stationary phases, based on the one-pot reaction of a simple 1,2-diamine (either chiral or achiral), an isocyanate-terminated organosilane and silica gel. The new procedure is highly attractive as it is easy to realize in a reproducible manner and yields a final material that is very stable

from the chemical and thermal points of view as a result of the two bidentate urea-type functions that represent the organic fragment anchored to the silica surface. Indeed, the bidentate technology was applied to a series of stationary phases to provide good hydrolytic stability in both low and high pH of the mobile phase [13-15].

In Scheme 1 we report the general synthetic scheme of the "Crab-like" CSPs. It was the particular bidentate attack on the silica surface, reminiscent of a crab, that inspired the name of these CSPs.

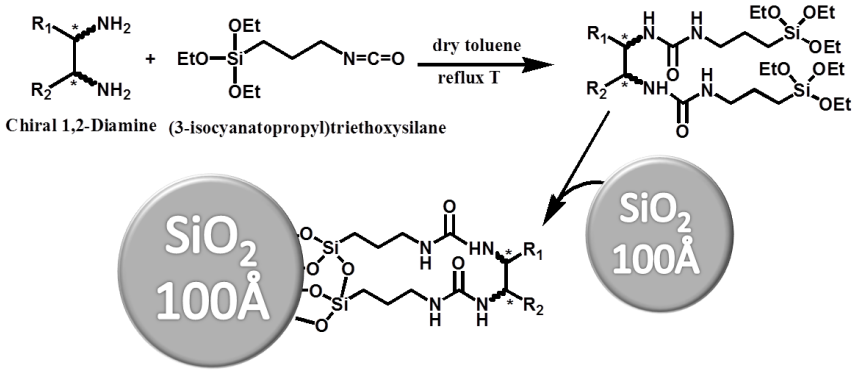

Scheme 1. General synthetic pathway for the synthesis of CSP-1 and CSP-2.

The reaction pathway proposed in Scheme 1 is a general one, which however, applies perfectly to various diamines. In the future, we are planning to substitute the diamines with aminoalcohols.

Two different chiral 1,2-diamines were used: (*R*,*R*)-1,2-Diamino-cyclohexane or (*R*,*R*)-DACH and (*R*,*R*)-1,2-Diphenyl-1,2-ethylene-diamine or (*R*,*R*)-DPEDA, whose structures are reported in Figure 2.

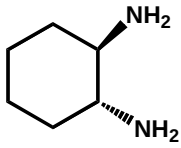

(1*R*,2*R*)-(-)-1,2-Diaminocyclohexane
(*R*,*R*)-DACH

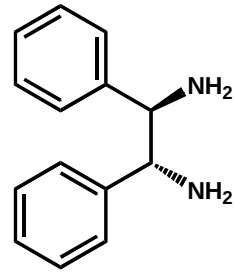

(1*R*,2*R*)-(+)-1,2-diphenyl-
1,2-ethylenediamine
(*R*,*R*)-DPEDA

Figure 2. Chemical structure of the two chiral selectors used for the preparation of CSP-1 (*on the left*) and CSP-2 (*on the right*).

A 1:2 ratio between the chiral diamine and (3-isocyanatopropyl) triethoxysilane was used (as in the case of HILIC phases, the completeness of the first step was monitored by ^{1}HNMR) to form the intermediate ureido selector. At this point, underivatized silica particles (Kromasil Si 100, 5 µm) were added to the reaction mixture in dry toluene and the reaction was quenched by filtration after 20 h, to obtain CSP-1 and CSP-2 (see Scheme 2). The two phases were

finally endcapped with N-(trimethylsilyl)imidazole to enhance the stability of the phases.

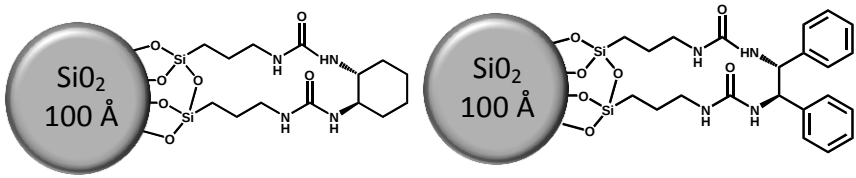

Scheme 2. Structures of CSP-1 (*left*) and CSP-2 (*right*).

2.2.2 Achiral efficiency tests on the "Crab-like" columns

The newly synthesized "Crab-like" stationary phases were packed into columns of 250 x 4.0 mm I.D. and their efficiency and retentivity were studied through a set of achiral tests in NP, RP and HILIC mode. Given the chemical nature of the bonded selector, in fact, these new CSPs show a high hydrophilicity, which can be better understood by performing an achiral test under HILIC conditions. It should not be forgotten that these CSPs are very tightly related to the HILIC phases presented in Chapter A-1 of this thesis.

Firstly, a NP achiral test was performed by injecting a mixture of 5 aromatic compounds (benzene, nitrobenzene, methyl benzoate, acetophenone and 1,3-dinitrobenzene) using a mobile phase made up of *n*-hexane-chloroform (ethanol stabilized), 90:10 (v/v). The

chromatograms obtained can be seen in Figure 3, showing clearly that CSP-2, bearing DPEDA as chiral selector, retains the analytes more strongly. Retention values for the CSP-1 range between 0.13 and 2.04, while *k* values observed with the CSP-2 vary between 0.16 and 4.23 (see Table 1). Baseline separation was obtained for all five compounds on both columns, making them excellent candidates for NP applications.

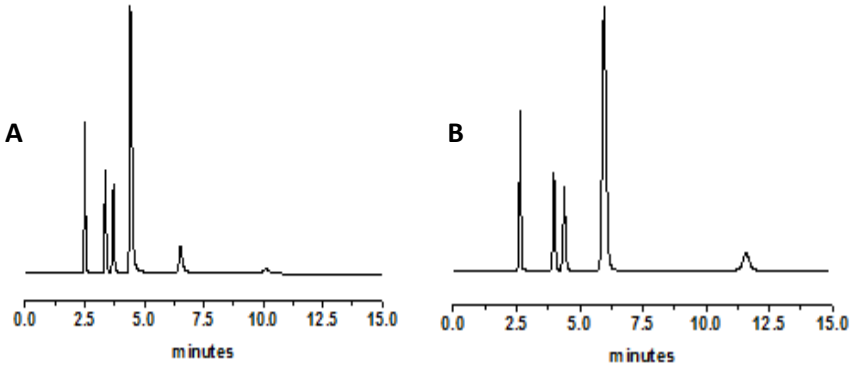

Figure 3. Chromatograms of a mixture of aromatic NP test compounds on: A) CSP-1; B) CSP-2. Column: 250 x 4.0 mm I.D., 5 µm. Eluent: *n*-hexane-$CHCl_3$ (ethanol stabilized), 90:10 (v/v); flow rate: 1.0 ml/min; *T* = 25 °C, UV detection at 254 nm. Elution order: benzene, nitrobenzene, methyl benzoate, acetophenone, 1,3-dinitrobenzene.

The different retention observed on the "Crab-like" columns is probably due to the presence of the aromatic moiety in DPEDA which

Table 1. Chromatographic data of the achiral NP efficiency test performed on the "Crab-like" CSPs. [a]

Sample	CSP-1				CSP-2			
	$k^{(b)}$	$\alpha^{(c)}$	$R_s^{(d)}$	N/m[(e)]	$k^{(b)}$	$\alpha^{(c)}$	R_s[(d)]	N/m[(e)]
Benzene	0.13			33'464	0.16			25'216
		4.15	7.73			4.86	9.39	
Nitrobenzene	0.54			54'656	0.77			43'912
		1.30	2.73			1.24	2.51	
Acetophenone	0.70			52'576	0.95			42'224
		1.48_5	4.67			1.75	7.46	
Methyl Benzoate	1.04			37'664	1.67			35'748
		1.96	9.81			2.53	15.79	
1,3-Dinitrobenzene	2.04			44'784	4.23			40'428
$\varepsilon_T^{(f)}$			0.67				0.70	
$K_F^{(g)}$			3.76				4.14	

[a] Columns geometry: 250 mm × 4.0 mm I.D.; eluent: *n*-hexane-$CHCl_3$ (ethanol stabilized) = 90:10 (v/v); flow rate: 1.0 ml/min; T = 25 °C; UV detection at 254 nm. [b] *k* = retention factor. [c] α = selectivity factor.
[d] R_s = resolution, calculated as described in the Experimental Section. [e] Theoretical plates per meter. Plate Count based on peak width at 50.0% of peak height (using the constant 5.54) as specified by the European Pharmacopeia. [f] ε_T = porosity. [g] K_F = permeability [10^{-14} m^2], calculated according to ref. [16].

allows for an extra type of interaction when compared to the DACH-based CSP: π-stacking is, in fact, possible in the case of CSP-2,

between the analytes and the stationary phase and becomes a particularly important type of interaction in NP chromatography. The chromatographic efficiency data obtained for the two columns represent the typical values obtained for 5 µm-Pirkle-type columns.

The RP achiral test, on the other hand, gave very similar results for the two CSPs. The results obtained are reported in Table 2 and Figure 4.

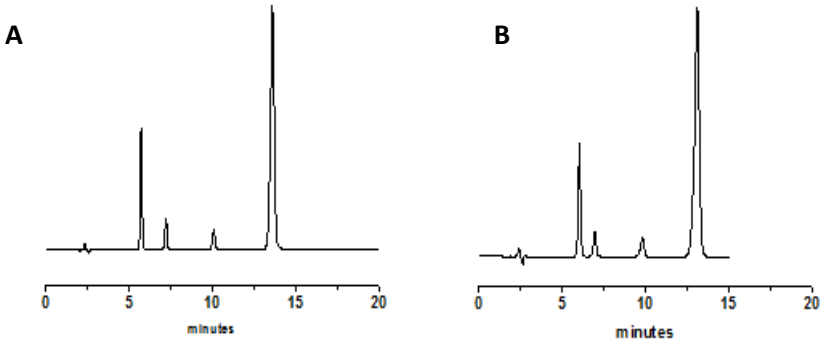

Figure 4. Chromatograms of a mixture of RP aromatic test compounds on: A) CSP-1; B) CSP-2. Column: 250 x 4.0 mm I.D., 5 µm. Eluent: H_2O/acetonitrile, 60:40 (v/v); flow rate: 1.0 ml/min; *T* = 25 °C, UV detection at 254 nm. Elution order: benzene, toluene, biphenyl, naphthalene.

Finally, a HILIC mode test was performed by injecting a mixture of highly polar compounds consisting of uracil, adenosine and cytosine (see fig. 5 for chromatograms). Naphthalene was added as an unretained marker of dead volume (*k* = 0), and was always eluted

before uracil, which is a common void volume marker in reversed phase HPLC.

Table 2. Chromatographic data of the achiral RP efficiency test performed on the "Crab-like" CSPs. [a]

Sample	CSP-1				CSP-2			
	$k^{(b)}$	$\alpha^{(c)}$	$R_s^{(d)}$	N/m$^{(e)}$	$k^{(b)}$	$\alpha^{(c)}$	$R_s^{(d)}$	N/m$^{(e)}$
Benzene	1.57			63'652	1.71			39'564
		1.46	7.43			1.26	3.57	
Toluene	2.30			67'456	2.18			40'264
		1.61	10.87			1.64	8.72	
Biphenyl	3.70			68'880	3.58			42'576
		1.47	4.67			1.45	7.39	
Naphthalene	5.43			67'800	5.18			42'052

[a] Columns geometry: 250 mm × 4.0 mm I.D.; eluent: H_20:acetonitrile = 60:40 (v/v); flow rate: 1.0 ml/min; T = 25 °C; UV detection at 254 nm.

[b] *k* = retention factor. [c] α = selectivity factor.

[d] R_s = resolution, calculated as described in the Experimental Section.

[e] Theoretical plates per meter. Plate Count based on peak width at 50.0% of peak height (using the constant 5.54) as specified by the European Pharmacopeia.

Retention values proved quite different for the two columns under HILIC conditions: CSP-1, in fact, retained the analytes only poorly ($0.34<k<0.84$) while CSP-2 showed considerably higher *k* value

(between 0.36 and 1.62), thus proving more hydrophilic (see Table 3). It should be noted, at this point, that CSP-2 also retained more in the NP test, which would seem to contradict the results of the HILIC test. We should not, in fact, consider only polarity of the stationary phase but also the specific interactions taking place, namely π-bonding between the aromatic moiety of DPEDA and the aromatic moieties in the analytes, as well as possible steric effects.

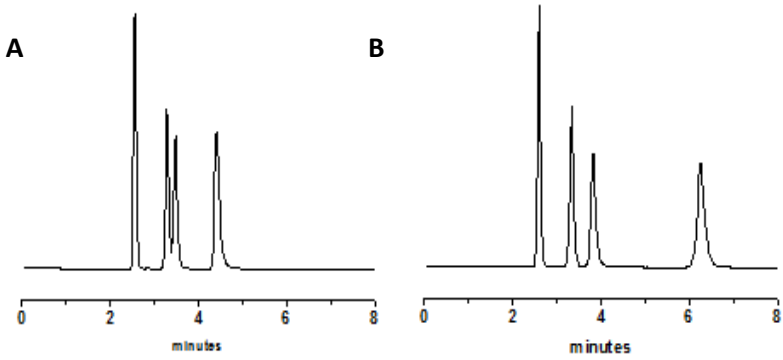

Figure 5. Chromatograms of HILIC test on: A) CSP-1; B) CSP-2. Column: 250 x 4.0 mm I.D., 5 µm. Eluent: acetonitrile/H_2O, 90:10 (v/v); flow rate: 1.0 ml/min; *T* = 25 °C, UV detection at 254 nm. Elution order: naphthalene, uracil, adenosine, cytosine.

Furthermore, an incomplete separation of peaks 2 and 3 (corresponding to uracil and adenosine, respectively) was observed

on CSP-1 while a baseline separation of all four compounds was obtained on CSP-2.

Table 3. Chromatographic data of the achiral RP efficiency test performed on the "Crab-like" CSPs. [a]

Sample	CSP-1			CSP-2		
	$k'^{(b)}$	$\alpha^{(c)}$	$R_s^{(d)}$	$k'^{(b)}$	$\alpha^{(c)}$	$R_s^{(d)}$
Naphthalene	0.00			0.00		
		-	5.90		-	5.43
Uracil	0.34			0.36		
		1.23_5	1.33		1.58	2.83
Adenosine	0.42			0.57		
		2.00	5.40		2.84	10.00
Naphthalene	0.84			1.62		

[a] Columns geometry: 250 mm × 4.0 mm I.D.; eluent: H_20:acetonitrile = 60:40 (v/v); flow rate: 1.0 ml/min; T = 25 °C; UV detection at 254 nm.

[b] *k* = retention factor. [c] α = selectivity factor.

[d] R_s = resolution, calculated as described in the Experimental Section.

The achiral tests performed on the "Crab-like" CSPs further underline their compatibility with all solvents, a typical property of the *brush-type* columns. They can be useful in separating a wide range of compounds, having different solubility characteristics. Moreover, the columns show no memory effect, meaning that we were able to pass from NP to RP or HILIC and back to NP several times, without any

changes in terms of retention and resolution. Finally, the excellent permeability make them good candidates for preparative chromatography.

2.2.3 Chiral applications in NP-HPLC.

When considering *brush-type* phases, chiral method development is typically carried out either in normal phase or polar organic mode, which mostly uses water free mixtures of acetonitrile and methanol (or ethanol) for the separation of a wide variety of chiral compounds.
In Figure 6, examples of chiral separations in NP can be seen. 1,1'-Bi-2,2'-naphthol is a racemate that is usually injected in our lab as a chiral probe apt to determine the ability of a new column to separate chiral compounds. As seen in Fig. 6A an excellent enantioseparation was obtained on both columns, with CSP-2 showing the highest enantioselectivity value (α = 2.31). Given this first positive result, a series of benzodiazepines and benzodiazepine-derived molecules were tested on the two columns. Oxazepam (Fig. 6B) was very neatly separated on the DACH-based CSP (mobile phase made up of dichloromethane/methanol; 97:3), while only a partial separation could be obtained on CSP-2 (α = 1.06).

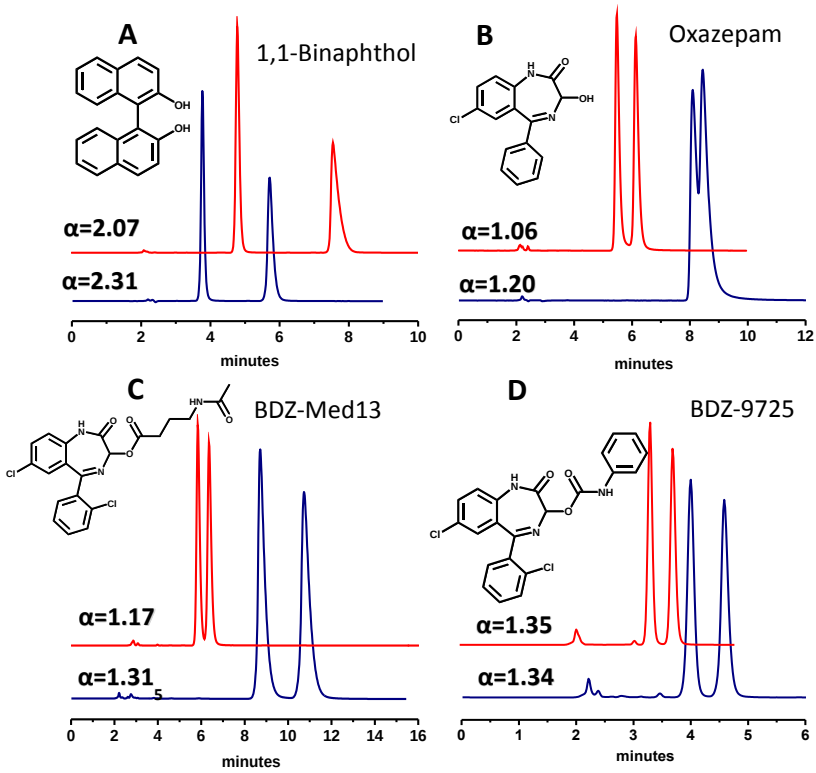

Figure 6. Chromatograms of chiral separations in NP on CSP-1 (red line) and CSP-2 (blue line): A) 1,1-Binaphthol; B) Oxazepam; C) BDZ-Med13; D) BDZ-9725. Column: 250 x 4.0 mm I.D., 5 µm. Eluent: CH_2Cl_2/MeOH, 97:3 (v/v); flow rate: 1.0 ml/min; *T* = 25 °C, UV detection at 254 nm.

On the other hand, a benzodiazepine-derived compound, BDZ-Med 13 (Fig. 6C) was better separated on the DPEDA-based column, with

an α = 1.31_5 (1.17 on CSP-1). Finally, BDZ-9725 (Fig. 6D) was excellently separated in both phases with similar α values.

At this point, we decided to compare these results with the ones obtained on a *poly-brush*-DACH-ACR column (*poly*-CSP-3). This *brush-type* polymeric phase is a totally synthetic phase introduced by prof. Gasparrini and co-workers with the aim of producing polymeric materials forming a thin, ordered layer on the silica surface without altering the pores morphology. Classic polymeric CSPs may suffer from slow analyte mass transfer kinetics and reduced efficiency if the degree of polymerization, grafting density and polymer architecture are not properly controlled. [10] At the purpose, a *grafting-from* polymerization approach was introduced, instead of the classic *grafting-to* approach used to obtain the synthetic polymeric materials usually produced for HPLC (see Fig. 7). The *grafting-from* approach grants the phase a high degree of polymerization across the surface and accounts for the excellent reproducibility and stability observed with the *poly-brush*-DACH-ACR phase. Supelco commercializes the phase under the name of P-CAP. In NP applications we did not use the commercial column, but a lab-made one, prepared according to the patented procedure [17] described in ref. 10.

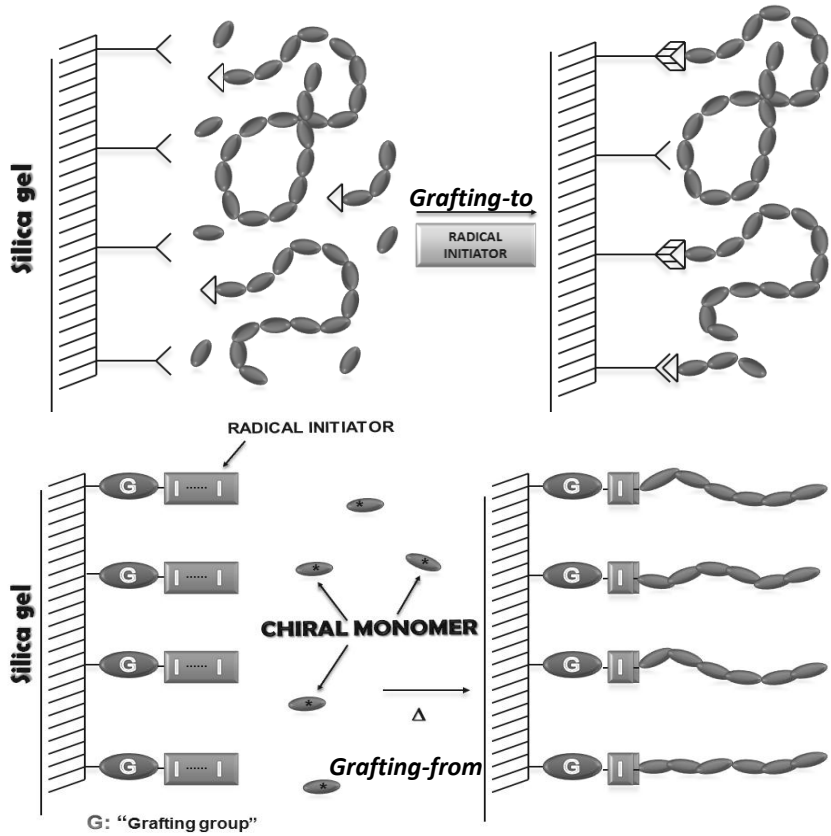

Figure 7. *Grafting-to* approach used in classical polymeric phases (top) and *grafting-from* approach used in the preparation of *poly-brush-type*-DACH-ACR phase (bottom).

The results obtained in NP for the three columns are reported in Table 4. Although *poly*-CSP-3 showed an impressive α of 2.40 for

temazepam and especially of 4.85 for BDZ-9725, it was not able to separate neither oxazepam or diltiazem. All compounds were separated on CSP-2 (α ranging between 1.06 and 2.31) and only CSP-1 was able to better separate oxazepam.

Table 4. Chromatographic data obtained for the NP chiral applications of the "Crab-like" CSPs and *poly*-CSP-3. [a]

Sample	CSP-1			CSP-2			*Poly*-CSP-3		
	k_1[b]	α[c]	R_s[d]	k_1[b]	α[c]	R_s[d]	k_1[b]	α[c]	R_s[d]
1,1-Binaphthol	1.16	2.07	9.65	0.64	2.31	8.96	1.50	1.85	6.91
BDZ-Med-13	0.98	1.17	1.76	2.79	1.31_5	3.43	0.97	1.22	1.79
BDZ-GV-142066X				0.31	1.13		0.36	1.44	2.55
BDZ-9725	0.55	1.35	2.52	0.74	1.34	2.64	1.18_5	4.85	1.73
Oxazepam	1.47	1.20	2.48	2.52	1.06				
Temazepam				0.12	1.42	7.19	0.05	2.40	1.26
Diltiazem				0.19	1.21				

[a] Columns geometry: 250 mm × 4.0 mm I.D.; eluent: CH_2Cl_2/MeOH, 97:3 (v/v); flow rate: 1.0 ml/min; T = 25 °C; UV detection at 254 nm.

[b] *k* = retention factor. [c] α = selectivity factor.

[d] R_s = resolution, calculated as described in the Experimental Section.

2.2.4 Chiral applications in Polar Organic Mode (POM-HPLC).

Together with NP applications, this project was mainly concerned with separating chiral compounds using polar organic mode (POM). In 1993 prof. Armstrong *et al.* introduced a polar—organic mobile phase system composed of acetonitrile, with small portions of hydrogen bonding modifiers, for the enantiomeric separation of chiral molecules on cyclodextrin-bonded phases. [18] This mobile phase allows for the separation of a wide variety of analytes which cannot be resolved in either traditional normal- or reversed-phase chromatography on cyclodextrin-bonded phases. It provides additional opportunities for chiral selectivity should other types of mobile phases fail. Acetonitrile is the dominant solvent and bases/acids/buffers are added to suppress ionization; through POM different interaction mechanisms can be exploited. Furthermore, usually less baseline noise is observed in UV detection. It is, also, often easier to perform sample preparation (especially for polar or ionisable compounds) and scale-up. Finally, acetonitrile and methanol make LC-MS compatible mobile phases, which is nowadays becoming increasingly important. Although POM was introduced for cyclodextrin-based phases, it is used for a wide range of stationary

phases, such as polysaccharidic CSPs, teicoplanin-based CSPs, P-CAP and P-CAP-DP CSPs, cinchona based CSPs, etc.

A mobile phase made up of MeCN/MeOH (85:15; v/v) + 10 mM ammonium formate buffer ($^{S}_{W}pH$ = 7.45) was used to separate 13 different N-derivatized aminoacids (see Table 5) on the two "Crab-like" CSPs and the commercial Astec P-CAP column (250 x 4.6 mm I.D.) under POM conditions. The aminoacids used were N-derivatized through 4 different protecting groups, namely N-*tert*-butoxycarbonyl (BOC), fluorenylmethyloxycarbonyl (FMOC), carboxybenzyl (Z) and 3,5-dinitrobenzoyl (DNB), whose structures are showed in Figure 8.

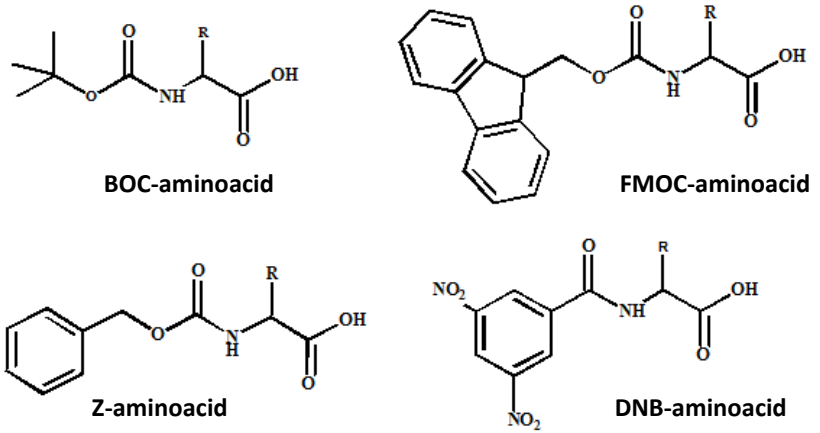

Figure 8. N-derivatized aminoacids analyzed in POM.

Table 5. N-derivatized aminoacid separated under POM conditions on CSP-1, CSP-2 and commercial Astec-(*S,S*)-P-CAP columns.[a]

	Samples	(R,R)-CSP-1			(R,R)-CSP-2			Astec-(*S,S*)-P-CAP		
		k_1	α	R_s	k_1	α	R_s	k_1	α	R_s
1	Z-alanine	2.31	1.16	2.48	2.68	1.28	2.29	3.06	1.13	1.68
2	Z-leucine	1.92	1.12_5	1.86	1.49	1.27	1.83	2.22	1.28	2.73
3	Z-phenylalanine	2.31	1.12	1.89	1.77_5	1.27	2.26	2.94	1.17	2.15
4	BOC-methionine	1.97	1.07	1.14	1.46	1.10	1.04	2.06	1.27	2.76
5	BOC-phenylalanine	2.07	1.10	0.93	1.56	1.11_5	1.16	2.20	1.15	1.74
6	DNB-alanine	2.40	1.32_5	4.39	2.61	1.41	3.92	3.92	1.15	1.57
7	DNB-valine	1.88	1.19	2.68	1.51	1.21	1.36	2.50	1.16	1.39
8	DNB-leucine	1.99	1.30	4.20	1.47	1.35	2.95	4.28	1.33	2.80
9	DNB-isoleucine	1.82	1.18	2.61	1.34	1.19	1.58	2.47	1.28	2.33
10	Fmoc-leucine	2.10	1.14	2.15	1.62	1.17	1.98	2.56	1.42	3.85
11	Fmoc-methionine	2.39	1.11	1.79	2.07	1.18	1.90	3.26	1.42	4.18
12	Fmoc-phenylalanine	2.62	1.12	1.95	2.16	1.22	2.23	3.35	1.22	2.48
13	Fmoc-serine	4.42	1.14	2.13	4.51_5	1.13	1.51	7.16	1.19	2.06

[a] Columns geometry: 250 mm × 4.0 mm I.D. for CSP-1 and CSP-2; 250 mm × 4.6 mm I.D. for Astec-(*S,S*)-P-CAP column. Eluent: MeCN/MeOH (85:15; v/v) + 10 mM ammonium formate buffer ($^{s}_{w}pH$ = 7.45); flow rate: 1.0 ml/min for CSP-1 and CSP-2; 1.3 ml/min for Astec-(*S,S*)-P-CAP; *T* = 25 °C; UV detection at 254 nm. [b] *k* = retention factor. [c] α = selectivity factor. [d] R_s = resolution, calculated as described in the Experimental Section.

As it can be seen from Table 5, a good separation of all 13 aminoacidic derivatives was obtained both “Crab-like” columns, with α values ranging between 1.10 and 1.41. In particular, the racemates which were best separated on both columns were the N-DNB-derivatized aminoacids. On the DPEDA column, these analytes showed the highest enantioselectivity values (up to 1.41). A very good separation of *Z*-aminoacids was also possible on the CSP-2 column, while the BOC-aminoacids yielded the lowest α values.

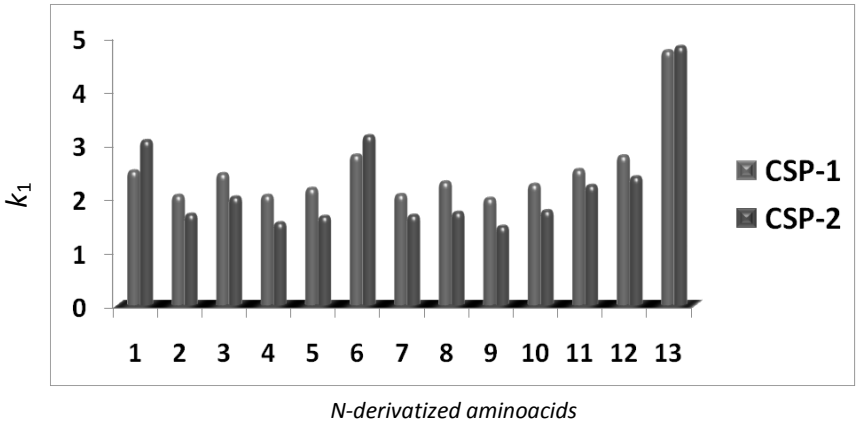

Figure 9. Comparison of retention factors (k_1) of 13 N-derivatized aminoacids (see Table 5 for sample names and experimental conditions) on CSP-1 and CSP-2.

The FMOC-protected aminoacids were all baseline separated, on both "Crab-like" columns. When compared to CSP-1, the CSP-2 column showed a slightly lower retentivity in 10 out of 13 analytes (only Z-alanine, DNB-alanine and FMOC-serine were more strongly retained on the CSP-2 column). However, it also yielded higher enantioselectivity values compared to CSP-1 for all N-derivatized aminoacids, except for FMOC-Serine (α = 1.14 on CSP-1 against a very similar α of 1.13 on CSP-2). Figure 9 graphically compares the retentivity of the two columns, while in fig. 10 a comparison of α values is shown.

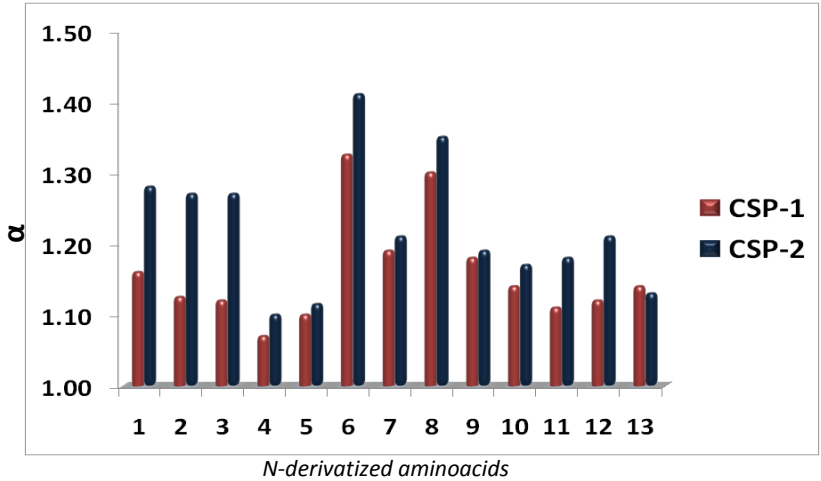

Figure 10. Comparison of enantioselectivity values (*α*) of 13 N-derivatized aminoacids (see Table 5 for sample names and experimental conditions) on CSP-1 and CSP-2.

In Figure 11 are reported overlays of chromatograms obtained on CSP-1 and CSP-2.

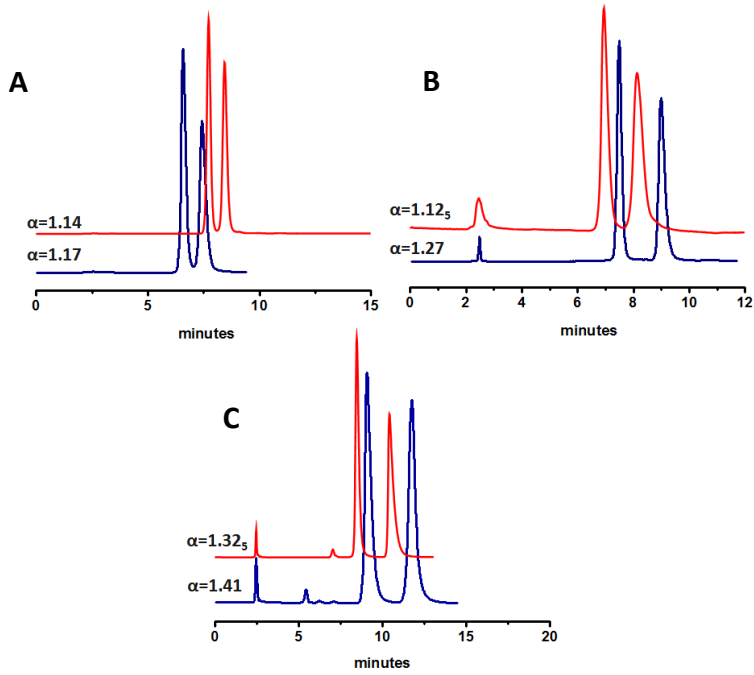

Figure 11. Examples of chromatograms of A) FMOC-leucine; B) Z-leucine and C) DNB-alanine on CSP-1 (red line) and CSP-2 (blue line). For experimental conditions see Tab. 5.

After the encouraging results obtained for the CSP-2 phase, we decided to compare our column with a *brush-type* polymeric column, which is often used in the analysis of chiral molecules in POM-HPLC.

In fact, typical applications of Astec P-CAP include N-derivatized aminoacids.

After injecting, under the same experimental conditions used for the "Crab-like" columns, all 13 compounds (see Table 5), we were able to conclude that, although the P-CAP column showed higher capacity factors, it was mostly complementary to the CSP-2 column. In particular, Z-alanine, Z-phenylanine, DNB-alanine, DNB-leucine and DNB-valine were better separated on the CSP-2 column (see Table 5).

At this point, a fourth column was introduced in the study, the P-CAP-DP column, a polymeric *brush-type* column which presents a DPEDA selector in its structure. We confronted this column with our monomeric *brush-type* CSP-2 column, having a DPEDA selector, as well. The same experimental conditions and samples used in the previous study were also used for the P-CAP-DP column. Full experimental data can be observed in Table 6, while Fig. 12 reports three overlays of chromatograms obtained on the two columns.

Surprisingly, only six compounds showed a some kind of enantioseparation on the commercial P-CAP-DP column, while as well as seven enantiomeric pairs coeluted ($\alpha = 1.00$). Furthermore, the P-CAP-DP displayed a very low retention of the tested compounds.

We concluded that the P-CAP-DP column is not capable of separating compounds such as N-derivatized aminoacids. In fact, it is not the first

study where this column performs poorly. Literature data have proved that both the P-CAP and the DEAVB columns better separate sulfoxides and binaphthols [19,20], while efforts have been made to optimize the enantiorecognition mechanism of P-CAP-DP by substituting the phenyl ring with more substituted aromatic moieties (Cl-P-CAP-DP, 3Me-P-CAP-DP and Naph-P-CAP-DP).[21]

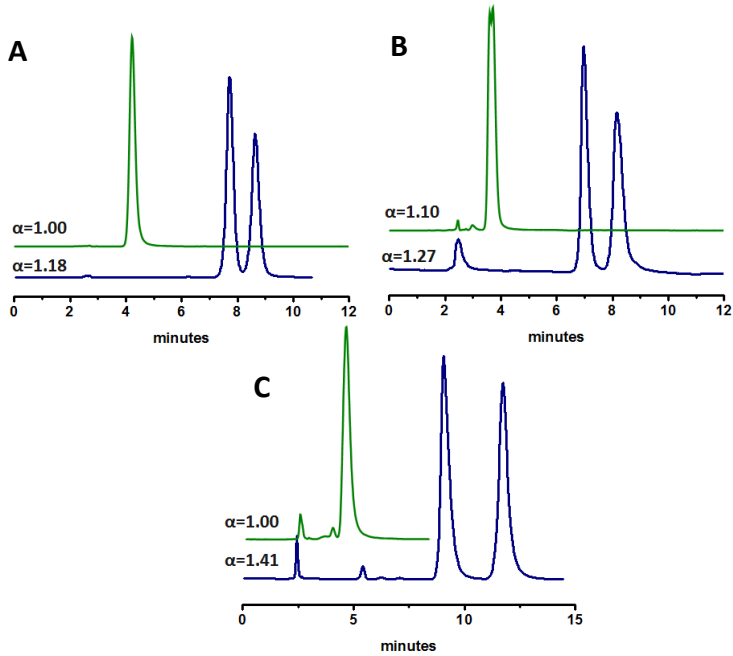

Figure 12. Examples of chromatograms of A) FMOC-methionine; B) Z-leucine and C) DNB-alanine on P-CAP-DP (green line) and CSP-2 (blue line). For experimental conditions see Tab. 6.

Table 6. N-derivatized aminoacid separated under POM conditions on CSP-2 and commercial Astec-P-CAP-DP columns.[a]

	Samples	(R,R)-CSP-2			P-CAP-DP		
		k_1	α	R_s	k_1	α	R_s
1	Z-alanine	2.68	1.28	2.29	0.65	1.09	
2	Z-leucine	1.49	1.27	1.83	0.43_5	1.10	
3	Z-phenylalanine	1.77_5	1.27	2.26	0.48_5	1.30	0.83
4	BOC-methionine	1.46	1.10	1.04	0.35	1.00	
5	BOC-phenylalanine	1.56	1.11_5	1.16	0.38	1.10_5	
6	DNB-alanine	2.61	1.41	3.92	0.80	1.00	
7	DNB-valine	1.51	1.21	1.36	0.41_5	1.00	
8	DNB-leucine	1.47	1.35	2.95	0.56	1.00	
9	DNB-isoleucine	1.34	1.19	1.58	0.34	1.00	
10	Fmoc-leucine	1.62	1.17	1.98	0.47	1.00	
11	Fmoc-methionine	2.07	1.18	1.90	0.68	1.00	
12	Fmoc-phenylalanine	2.16	1.21	2.23	0.57_5	1.16_5	
13	Fmoc-serine	4.51_5	1.13	1.51	1.35	1.13	

[a] Columns geometry: 250 mm × 4.0 mm I.D. for CSP-2; 250 mm × 4.6 mm I.D. for Astec-P-CAP-DP column. Eluent: MeCN/MeOH (85:15; v/v) + 10 mM ammonium formate buffer ($^{s}_{w}pH$ = 7.45); flow rate: 1.0 ml/min for CSP-2; 1.3 ml/min for Astec-P-CAP-DP; *T* = 25 °C; UV detection at 254 nm. [b] *k* = retention factor. [c] α = selectivity factor. [d] R_s = resolution, calculated as described in the Experimental Section.

We believe that the CSP-2 column conjugates an excellent stability with the presence of aromatic moieties, capable of participating in π-bonding interactions. It is, we believe, an excellent substitute for the commercial P-CAP-DP column, to be used together with the P-CAP phase, with which it showed a good complementarity.
At this point, however, further analytical data and especially a more wide range of analytes are needed to better understand the application field of this new, promising “Crab-like” CSP.

2.2.5 Transition from e-HPLC to e-UHPLC.

One of the most widely used chromatographic methods to separate and quantitate enantiomers is based on their direct HPLC resolution on chiral stationary phases [22–24]. Standard eHPLC columns are normally packed with 3–5 micron silica based spherical particles and have standard geometries (length: 150-250 mm and internal diameter: 2–4.6 mm). A substantial increase in the sample throughput of an enantioselective HPLC (e-HPLC) system can be in principle obtained by employing smaller particles packed in short columns and using high linear velocities of the eluent [25-34]. The small particle size approach is now feasible as manufacturers can produce silica based materials with narrow size distributions at the

sub-2-micron regime. Several hardware designs together with dedicated particulate materials have been introduced in the last years, together with the corresponding acronyms (UHPLC, ultra-high pressure liquid chromatography; RRLC, rapid resolution liquid chromatography,etc).

As was clearly underlined in a previous article by Gasparrini and coworkers,[35] many practical difficulties have arised with the use of new sub-2-micron particles, mainly correlated to the particle size reduction and to the adaptation of the surface modification chemistry of classical CSPs to smaller particles. The column permeability reduction results in a considerable increase of the column backpressure (Δp is, in fact, proportional to the inverse of the particle diameter squared). It is easily concluded that the full potential of high speed separations can only be exploited on chromatographic hardware that can withstand elevated pressures (UHPLC). Moreover, the increased propensity of smaller silica particles to aggregate during the synthetic procedure should be considered in the preparation of the sub-2-micron CSPs. Finally, mechanical resistance and long term stability of the packed bed are also of major concern when high flow (and hence high pressure) applications are planned.

However, these practical difficulties are worthwile overcoming when one considers the advantages of UHPLC separations. They are in fact, extremely time saving, as the chiral separations become consistently faster (reaching even the sub-minute range) and use a lower amount of eluents (and therefore have a great reduction in the amount of waste produced), which is certainly extremely cost-saving as well as environmental-friendly. Finally, the injection volume is sensibly smaller in UHPLC when compared to HPLC, which usually allows for a higher mass sensitivity.

To the purpose, a Thermo Syncronis 1.7 µm was used following an identical synthetic procedure to the one already described for the 5 µm version of CSP-2 (see experimental section). The new CSP-2-1.7 µm was packed into a 75 x 3.2 mm ID stainless steel tube and was then tested for its enantioselectivity and compared to the CSP-2-5 µm column. Examples of separations obtained are shown in Figure 13 and Table 7. The first consideration to be made is on the enantioselectivity of the new phase: it was, in fact, observed that the α values of the UHPLC column were superior to the ones observed in HPLC, with the exception of Z-phenylalanine, BOC-phenylalanine and FMOC-methionine. However, the retention was lower for the 1.7 µm column, probably due to the different properties of the silica matrix used for the preparation of the two phases.

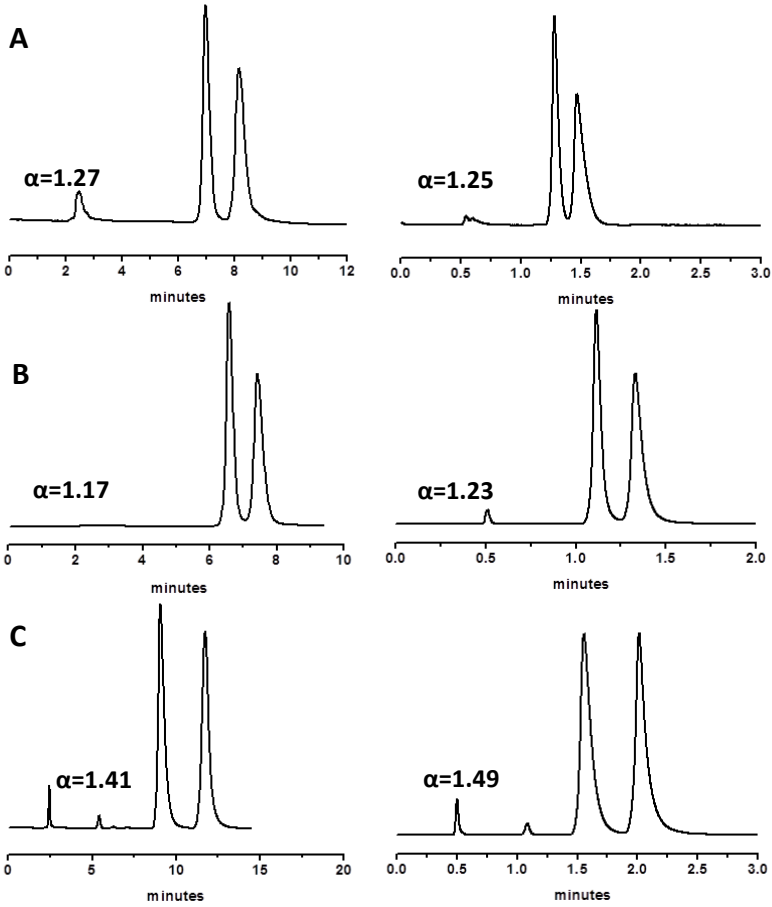

Figure 13. Examples of chromatograms of A) Z-phenylalanine; B) FMOC-phenylalanine and C) DNB-alanine on CSP-2-5 µm (left) and CSP-2-1.7µm (right) columns. [a] Columns geometry: 250 mm × 4.0 mm I.D. (left) and 75 mm × 3.2 mm I.D. (right). Eluent: MeCN/MeOH (85:15; v/v) + 10 mM ammonium formate buffer ($^{s}_{w}pH$ = 7.45); flow rate: 1.0 ml/min (left) and 0.8 ml/min (right); *T* = 25 °C; UV detection at 254 nm.

Table 7. N-derivatized aminoacid separated under POM conditions on CSP-2-5 µm and CSP-2-1.7 µm columns.

Samples	*CSP-2-5 µm 250 x 4.0 mm ID*			*CSP-2-1.7 µm 75 x 3.2 mm ID*		
	k_1	α	R_s	k_1	α	R_s
Z-alanine	2.68	1.28	2.29	1.85	1.42	2.89
Z-leucine	1.49	1.27	1.83	1.12	1.27	1.56
Z-phenylalanine	1.77_5	1.27	2.26	1.41_5	1.25	1.59
BOC-methionine	1.46	1.10	1.04	1.18	1.14	-
BOC-phenylalanine	1.56	1.11_5	1.16	1.11	1.10	-
DNB-alanine	2.61	1.41	3.92	1.94	1.44	3.12
DNB-valine	1.51	1.21	1.36	1.12	1.23	1.42
DNB-leucine	1.47	1.35	2.95	1.10	1.37	2.38
DNB-isoleucine	1.34	1.19	1.58	1.05	1.20	1.25
Fmoc-leucine	1.62	1.17	1.98	1.31	1.23	1.42
Fmoc-methionine	2.07	1.18	1.90	1.59	1.16	1.20
Fmoc-phenylalanine	2.16	1.21	2.23	1.65	1.27	1.52
Fmoc-serine	4.51_5	1.13	1.51	3.22	1.17	1.79

[a] Eluent: MeCN/MeOH (85:15; v/v) + 10 mM ammonium formate buffer ($^{s}_{w}pH$ = 7.45); flow rate: 1.0 ml/min for CSP-2-5 µm and 0.8 ml/min for CSP-2-1.7 µm. *T* = 25 °C; UV detection at 254 nm. [b] *k* = retention factor. [c] α = selectivity factor. [d] R_s = resolution, calculated as described in the Experimental Section.

However, the most interesting fact in the transition from HPLC to UHPLC was the reduction of the analysis time, with separations in the sub-2 minute range. By using a higher flow, sub-minute separations can be obtained.

Starting from these very promising initial results, we believe that future developments will allow us to prepare a highly efficient and stable CSP for UHPLC. It should be noted, in fact, that at the moment no chiral supports are available for UHPLC applications.

2.3 Conclusions

New "Crab-like" CSPs have been successfully designed and prepared through a facile one-pot procedure. Two enantiopure diamines, namely 1,2-diaminocyclohexane (DACH) and 1,2-diphenyl-1,2-ethylene-diamine (DPEDA), were used as chiral selectors for these new *brush-type* CSPs containing a stable bidentate urea-type structure. The new "Crab-like" phases allow for different mechanisms of separation: normal-phase, reversed-phase and polar organic mode. CSP-2 bearing DPEDA as chiral selector showed good selectivity and resolution values over a wide range of racemates including benzodiazepines, N-derivatized amino acids and chiral drugs but also in the separation of otherwise difficult to separate

diastereomeric compounds (data not shown). The excellent stability as well as the compatibility with POM mobile phases make it an extremely interesting CSP for future LC-MS^n applications. The transition from HPLC to UHPLC clearly demonstrates the general applicability of the synthetic procedure. UHPLC columns, in fact, proved both time-saving and cost-saving as well as environmental friendly. Finally, the availability of both enantiomeric forms of the chiral selector makes these CSPs suitable for Inverted Columns Chirality Approach (ICCA), a method which will be extensively described in part B of this thesis.

2.4 Experimental Section

2.4.1 Apparatus

Two different arrangements were optimized for chromatographic runs: UHPLC and HPLC systems. The Acquity® UPLC consisted of a binary solvent manager, sample manager, a "homemade temperature controller" column compartment and a PDA [200–400 nm] detector with a 500 nl flow cell (Waters, Milford, MA, USA). The PDA was set at a filter time constant of 0.05 s and a sampling rate of 80 points/s. HPLC separations were performed on a chromatographic

system consisting of a Waters Alliance 2695 pump and an autosampler equipped with a model 996 PDA detector. Chromatographic data were collected and processed using the Empower 2.0 software (Waters). To reduce the extracolumn volumes, connecting tubes of 0.1 mm I.D. for the UHPLC arrangement and standard tubes of 0.25 mm I.D. for the HPLC system were employed.

2.4.2. Chemicals and reagents

Spherical Kromasil Si 100 silica gel (pore size 100 Å, particle size 5.0 µm, specific surface area 340 m^2g^{-1}) was purchased from Eka Nobel (Bohus, Sweden). Spherical Syncronis Si 100-1.7P silica gel (pore size 100 Å, particle size 1.7 µm, specific surface area 320 m^2g^{-1}) was a kind gift of Thermo Scientific (San Jose, CA, USA). (*R*,*R*)-1,2-Diaminocyclohexane, (*R*,*R*)-1,2-Diamino-1,2-ethylenediamine, (3-isocyanatopropyl)triethoxysilane, 4-(dimethylamino)pyridine (or 4-DMAP), N-(trimethylsilyl)imidazole, and dry toluene were from Sigma Aldrich (St. Louis, MO, USA). Ammonium formate as well as all aminoacid derivatives were purchased from Fluka (Buchs, Switzerland). HPLC gradient grade water, acetonitrile, hexane, tetrahydrofuran, chloroform stabilized with ethanol were purchased

from Sigma Aldrich. Other polar analytes were available from earlier studies.

2.4.3 Preparation of CSP-1

A solution of (*R*,*R*)-DACH (0.219 g; 1.93 mmol) in 30 ml of dry toluene was heated at 120 °C under a nitrogen atmosphere. After distillation of 3 ml of solvent, a solution of (3-propyl-isocyanate)triethoxysilane (3.86 mmoles; 0.95 ml) in 5 ml of anhydrous toluene was added dropwise. The solution was kept under continuous stirring for 4h. Kromasil Si-100 silica gel, previously hydrated with ethanol 96° and thus washed and dispersed in 40 ml of toluene, was then added (2.962 g; 5 µm) and the reaction was kept for 4 hours under continuous stirring at 100°C. The derivatized silica was then treated with 4-DMAP (0,187 g; 1.53 mmol) overnight. The reaction was quenched by filtration. The silica gel was washed with dichloromethane and dried at reduced pressure (0.1 mbar, *T* = 80°C) (3.647 g; weight increment = 23.2%). FT-IR (KBr): 3892, 3589, 3355 2978, 2937, 2864, 1876, 1637, 1558, 1448, 1086, 960, 891, 795. Elemental analysis: C = 9.49%; H = 1.92%; N = 2.04% corresponding approximately to 448 µmol of substrate per gram of silica or 1.32 µmol/m^2.

End-capping procedure: To a dispersion of the dried silica gel (3.647 g) in 60 ml of dry toluene was added 1 ml of N-(trimethylsilyl)imidazole and the reaction was kept under continuous stirring overnight at 80°C. The silica gel was then filtered and washed with toluene, dichloromethane, methanol and dichloromethane and dried at reduced pressure (0.1 mbar, *T* = 60°C) to obtain 3.557 g of end-capped CSP-1.

2.4.3 Preparation of CSP-2

A solution of (*R*,*R*)-DPEDA (0.285 g; 1.34 mmol) in 20ml of dry toluene was heated at 120°C under a nitrogen atmosphere. After distillation of 3 ml of solvent, a solution of (3-isocyanatpropyl)triethoxysilane (2.68 mmol; 0.70 ml) in 5 ml of anhydrous toluene was added. The solution was kept under continuous stirring for 4h. Kromasil Si-100 silica gel, previously hydrated with ethanol 96° and thus washed and dispersed in 30 ml of toluene, was then added (2.373 g; 5 μm) and the reaction was kept for 14 hours under continuous stirring at 90 °C. The derivatized silica was then treated with 4-DMAP (0.138 g; 1.13 mmol) for 4 h. The reaction was quenched by filtration. The silica gel was washed with dichloromethane and dried *in vacuo* (0.1 mbar, *T* = 80°C) (2.836 g; weight increment = 19.5%). FT-IR (KBr): 3629, 3361,

2978, 2933, 1867, 1643, 1564, 1454, 1076, 953, 793. Elemental analysis: C = 9.39%; H = 1.23%; N = 1.70% corresponding approximately to 361 μmol of substrate per gram of silica or 1.06 μmol/m^2.

End-capping procedure: To a dispersion of the dried silica gel (2.820 g) in 60 ml of dry toluene, 1 ml (6.82 mmol) of 1-trimethylsilyl imidazole was added and the reaction was kept under continuous stirring overnight at 80°C. The silica gel was then filtered and washed with toluene, dichloromethane, methanol and dichloromethane and dried at reduced pressure (0.1 mbar, *T* = 60°C) obtaining 2.760 g of end-capped CSP-2.

2.4.5 Preparation of CSP-2-1.7P

The same one-pot procedure used for the preparation of CSP-2 was used to prepare the 1.7 μm version of CSP-2. In this case a spherical Syncronis Si 100-1.7P silica gel (pore size 100 Å, particle size 1.7 μm, specific surface area 320 m^2g^{-1}) was employed. Elemental analysis: C 10.94%, H 1.47% and N 2.37%.

2.4.7 Chromatographic set-up

HPLC columns: Stainless steel (250 mm × 4.0 mm I.D.) columns were packed with CSP-1, CSP-2 and *poly*-DACH-ACR phases using a slurry packing procedure already described.[36] The two commercial columns, Astec P-CAP and Astec P-CAP-DP (geometry: 250 × 4.6 mm I.D.) were a kind gift of Supelco. All chromatographic runs were carried out under isocratic elution with the flow rate set to 1.0 ml/min for the lab made columns and 1.3 ml/min for the commercial columns.

RSLC columns: A stainless steel (75 mm × 3.2 mm I.D.) column was packed with CSP-2-1.7P phase using a slurry packing procedure already described [36]. All chromatographic runs were carried out under isocratic or gradient elution with the flow rate set to 0.8 ml/min.

For chiral applications in polar organic mode, eluents were composed of acetonitrile and methanol in a volume ratio of 85 to 15, plus ammonium formate in a final 10 mM concentration. In normal phase, the mobile phase consisted of dichloromethane/methanol, 97/3 v/v. Sample solutions were prepared in the mobile phase (0.5–2 mg/ml) and allowed to equilibrate at T = 25 °C prior to injection into the HPLC system (1–5 µl aliquots).

Achiral efficiency tests were carried out under normal phase, reversed phase and HILIC mode conditions.

The column hold-up volumes (V_0) were determined by static pycnometry (*pyc*) using the following equation: $V_{0,pyc} = (w_{CHCl3}-w_{THF})/(\rho_{CHCl3}-\rho_{THF})$, where w and ρ are the masses of the columns filled with solvents and solvent density, respectively [37,38]. The number of theoretical plates per meter was calculated by built-in functions in the Empower software using 50% peak width. Resolution values were calculated by built-in functions in the Empower software using the equation $(t_2 - t_1) \times 1.18/(w_2 + w_1)$ where t_2 and t_1 are retention times and w_2 and w_1 are peak widths at 50% of peak height.

1.5 References and Notes

[1] Ward, T.J.; Ward, K.D. *Anal. Chem.* **2010**, *141*, 313-353.

[2] Armstrong, D.; DeMond, W. *J. Chromatogr. Sci.* **1984**, *22*, 411-415.

[3] Davankov, V.A; Semechkin, A.V. *J. Chromatogr.* **1977**, *141*, 313-353.

[4] Pirkle, W. H.; House, D.W. *J. Org. Chem.*, **1979,** *44*, 1957-1960.

[5] Pirkle, W. H.; Pochapsky, T.C. *Chem. Rev.,* **1989**, *89*, 347-362.

[6] Pirkle, W.H.; Welch, C.J.; Lamm, B. *J. Org. Chem.*, **1992,** *57*, 3854-3860.

[7] Gargaro, G.; Gasparrini, F.; Misiti, D.; Palmieri, G.; Pierini M.; Villani C. *Chromatographia*, **1987,** *24*, 505-509.

[8] Badaloni, E.; Cabri, W.; Ciogli, A.; Deias, R.; Gasparrini, F.; Giorgi, F.; Vigevani, A.; Villani, C. *Anal. Chem.* **2007**, *79*, 6013-6019.

[9] Badaloni, E.; Cabri, W.; Ciogli, A.; D'Acquarica, I.; Deias, R.; Gasparrini, F.; Giorgi, F.; Kotoni, D.; Villani, *J. Chromatogr. A* **2010**, *1217*, 1024-1032.

[10] Gasparrini, F.; Misiti, D.; Rompietti, R.; Villani, C. *J. Chromatogr A* **2005,** *1064*, 25-38.

[11] Zhong, Q.; Han, X.; He, L.; Beesley, T. E.; Trahanovsky, W.S.; Armstrong, D. W. *J. Chromatogr A* **2005,** *1066*, 55-70.

[12] D'Acquarica, I.; Gasparrini, F.; Misiti, D.; Pierini, M.; Villani, In *Advances in Chromatography*; Eds.; E. Grushka, N. Grinberg, CRC Press: Taylor & Francis Group, Boca Raton, FL, **2008**; Vol. *46*, p. 108-173.

[13] Kirkland, J.J.; van Straten, M.A.; Claessens, H.A. *J. Chromatogr. A* **1998**, *797,* 111-120.

[14] Kirkland, J.J.; Adams, J.B.; van Straten, M.A.; Claessens, H.A. *Anal. Chem.* **1998**, *70*, 4344-4352.

[15] Liu, X.; Bordunov, A.V.; Pohl, C.A. *J. Chromatogr. A* **2006**, *1119*, 12-134.

16] Moni, L.; Ciogli, A.; D'Acquarica, I.; Dondoni, A.; Gasparrini, F.; Marra, A. *Chem. Eur. J.* **2010**, *16*, 5712-5722.

[17] F. Gasparrini, D. Misiti, C. Villani. PCT Int. Appl. (2003) 25 pp. CODEN: PIXXD2 WO 2003079002. Columns packed with CSPs prepared in this way (P-CAP) are commercially available from Supelco (Sigma Aldrich, Milano, Italy)

[18] Chang, S.C.; Reid, G.L.; Chen, S.; Chang, C.D.; Armstrong, D.W. *Trends in Analytical Chemistry*, **1993**, *12*, 144-153.

[19] Laurenço, T.C.; Armstrong, D. W.; Cass, Q.B. *Chromatographia* **2010**, *71*, 361-372.

[20] Loukotková, L.; Tesařova, E.; Bosáková, Z.; Repko, P., Armstrong, D. W. *J. Sep. Sci.* **2010**, *33*, 1-11.

[21] Payagal, T.; Wanigasekara, E.; Armstrong, D. W. *Anal. Bioanal. Chem.* **2011**, *399*, 2445-2461.

[22] Allenmark, S. *Chromatographic Enantioseparation, Methods and Applications*, Ellis Horwood, New York, 1991.

[23] Francotte, E.; Lindner, W. (Eds.), *Chirality in Drug Research*, Wiley-VCH VerlagGmbH & Co. KGaA, Weinheim, 2006.

[24] Subramanian, G. (Ed.), *Chiral Separation Techniques—A Practical Approach*, 3rd ed., Wiley-VCH, Weinheim, 2007.

[25] Giddings, J.C. *Anal. Chem.* **1965**, *37*, 60-63.

[26] Knox, J.H. *J. Chromatogr. Sci.* **1977**, *15*, 352-353.

[27] Poppe, H. *J. Chromatogr. A* **1997**, *778*, 3-21.

[28] Wu, N.; Lippert, J.A.; Lee, M.L. *J. Chromatogr. A* **2001**, *911*, 1-12.

[29] Jerkovich, A.D.; Mellors, J.S.; Jorgenson, J.W. *LC–GC Eur.* **2003**, *16*, 20-23.

[30] Majors, R.E. *LC–GC N. Am.* **2005**, *23*, 1248-1255.

[31] Majors, R.E. *LC–GC N. Am.* **2006**, *24*, 248-266.

[32] Desmet, G.; Gzil, P.; Nguyen, D.T.-T.; Guillarme, D.; Rudaz, S.; Veuthey, J.-L.; Vervoort, N.; Torok, G.; Cabooter, D.; Clicq, D. *Anal. Chem.* **2006**, *78*, 2150-2162.

[33] Guillarme, D.; Nguyen, D.T.-T.; Rudaz, S.; Veuthey, J.-L. *J. Chromatogr. A* **2007**, *1149*, 20-29.

[34] Carr, P.W.; Wang, X.; Stoll, D.R. *Anal. Chem.* **2009**, *81*, 5342-5353.

[35] Cancelliere, G.; Ciogli, A.; D'Acquarica, I.; Gasparrini, F.; Kocergin, J.; Misiti, D.; Pierini, M.; Ritchie, H.; Simone, P. Villani, C. *J. Chromatogr. A* **2010**, *1217*, 990-999.

[36] D'Acquarica, I.; Gasparrini, F.; Giannoli, B.; Badaloni, E.; Galletti, B.; Giorgi, F.; Tinti, M.O.; Vigevani, A. *J. Chromatogr. A* **2004**, *1061,* 167-173.

[37] Rustamov, I.; Farcas, T.; Ahmed, F.; Chan, F.; LoBrutto, R.; McNair, H.M.; Kazakevich, Y.V. *J. Chromatogr. A* **2001**, *913*, 49-63.

[38] Gritti, F.; Kazakevich, Y.V.; Guiochon, G. *J. Chromatogr. A* **2007**, *1161*, 157-169.

PART B

Extending the use of "Inverted Chirality Columns Approach (ICCA)" for enantiomeric excess determination in absence of reference samples: application to a water-soluble camptothecin derivative.

1. Introduction

Previous studies were performed in our lab aimed at describing an original enantioselective HPLC-MS/MS technique for the identification and quantitation of the trace enantiomer in highly enriched samples of the Camptothecin (CPT) family of drugs, even in absence of reference samples [1]. The approach we developed, designated as "Inverted Chirality Columns Approach (ICCA)", is based on the reversal of the elution order of a given enantiomeric pair [2] as a result of the columns switching, under identical chemical conditions. This technique, which is not available when naturally occurring selectors such as polysaccharides or proteins are employed, is very useful for enantiomeric trace analysis when the minor enantiomer follows the major one and is partially hidden by the tailing of the leading enantiomer: on the chiral stationary phase (CSP) with opposite configuration the trace enantiomer is eluted first, thus enabling a more precise and accurate quantitation by peak area integration.[3] ICCA was developed to respond to important incoming needs in the field of pharmaceutical analysis: (*i*) the complete assignment of the stereoisomeric composition of chiral drugs [4,5], including natural products and synthetic intermediates, as established by the International Conference on Harmonization (ICH)

guidelines [6]; in such cases, however, only one enantiomer is available as the reference, and the racemate could be prepared by means of expensive and multistep, time-consuming total syntheses; (*ii*) extreme enantiomeric excesses (ee > 99%) must be estimated with large accuracy, which is a critical point in any of the available techniques [4]; (*iii*) low limits of detection (LODs) and quantitation (LOQs) in highly enriched samples contained in complex mixtures are strongly required to yield an unequivocal peak identification. Application of the ICCA to semi-synthetic derivatives of CPT endowed with anticancer activity [1] clearly showed its selectivity and specificity in the accurate determination of extreme ee, even when only one enantiomer was available. The success of the approach was assured by the combination of Pirkle-type CSPs with multistage mass spectrometry (APCI-MS/MS) detection.

The accomplished familiarity in the ICCA pathway prompted us to approach a novel water-soluble CPT derivative, namely namitecan (ST1968) [7-10], currently undergoing phase I clinical trials as anticancer agent (for structure see Fig. 1). [11] The CPT family of drugs appears to have a unique mechanism of action by inhibiting the nuclear enzyme topoisomerase I (topo I), resulting in the formation of a ternary complex between CPT, topo I and DNA [12]. As topo I was found to be over expressed in colorectal, prostate and other tumours

compared to non malignant tissues [13], this has led to a resurgence of studies on this drug family. Both semi- and totally synthetic CPT derivatives have been prepared in recent years [14], and a number of CPT analogues are currently undergoing clinical evaluation. From structure-activity (SAR) studies [15], it appears that the lactone ring and the natural 20S-configuration of CPTs are essential for anticancer activity. In particular, researchers have focused on modifying CPT at the 7-position to synthesize agents with improved pharmacological and toxicological profiles.

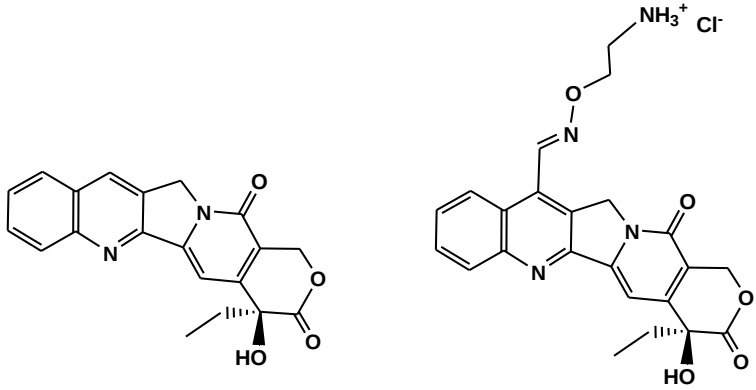

Figure 1. Chemical structures of Campthotecin CPT (left) and Namitecan (ST1968, right).

Namitecan, identified from a series of hydrophilic semi-synthetic 7-oxyiminomethyl derivatives, exhibited a remarkable ability to stabilize

the cleavable topo I-DNA complex and its *in vivo* activity was found promising [8].

2. Results and discussion

2.1 Extension of the "Inverted Chirality Columns Approach (ICCA)".

The main limitation of the ICCA method previously developed [1] is that it can be exploited only with stationary phases based on totally synthetic selectors, since complex natural selectors such as polysaccharides, proteins or glycopeptides are not suitable to yield CSPs in both the enantiomeric versions. On the contrary, Pirkle-concept CSPs are ideally suited to these purposes, since some of them have been developed and commercialized in both the enantiomeric forms. This is the case of the DACH-DNB columns family [18], that we indeed applied in the analysis of CPT and some lipophylic derivatives endowed with anticancer activity [1], and of the Whelk-O1 columns, introduced by the Pirkle group a few years after the DACH-DNB [19]. A distinctive feature of the above columns is that they have been designed to undergo simultaneous H-bonding, face-to-face, and face-to-edge aromatic interactions with the analytes, and mainly operate under normal-phase HPLC conditions.

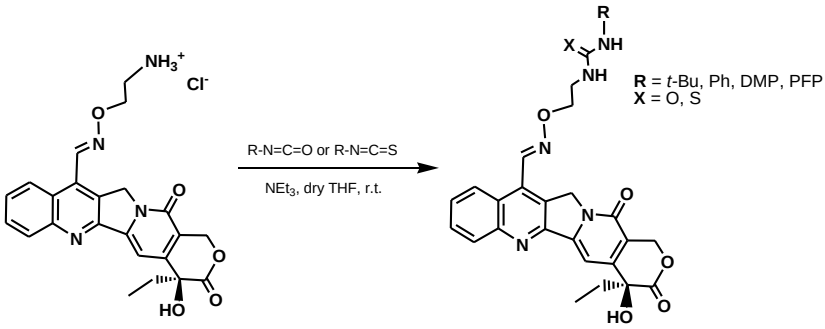

Figure 2. Synthetic scheme for the N-terminal derivatization of namitecan (ST1968).

With the aim of extending the use of the ICCA method to the novel water-soluble CPT derivative namitecan (ST1968; Fig. 1), we faced the problem of the presence of a free terminal amino group, which traditionally hampers the analysis under normal-phase conditions and in our case would certainly decrease the enantiorecognition ability of the CSPs. It is known, in fact, that polar sites where non specific (i.e., non enantioselective) interactions may occur are detrimental to chiral recognition, and the amino group in our CPT derivatives, remote from the stereogenic centre at C20 (see Fig.1), is such a site. For this reason, namitecan was pre-column N-protected (see Fig. 2) with a set of isocyanates (A–D in Fig. 3) in alkaline medium, to reduce its polarity by converting the amino group into a fragment compatible

with the chiral recognition mechanism (i.e., ureido groups). We also decided to study isothiocyanates E–H as derivatizing agents (Fig. 3) because we expected to improve the overall performances of the HPLC separation in terms of enantioselectivity and peak shapes.

Compared to the urea derivatives, the thiourea analogues have reduced superfluous interactions with the chiral selector of the stationary phase and diminished interactions with the underlying silica support: indeed, the sulfur atom is less electronegative and larger than oxygen, and the thiourea function has decreased H-bonding ability compared to the corresponding urea, leading to an overall improvement of the solute-stationary phase adsorption equilibria.

3.2 Choice of the proper chiral columns system

Initially, we decided to begin our investigation by referring to the previous work [1], where the DACH-DNB columns family was employed. Thus, we pre-column derivatized namitecan with isocyanate A (Fig. 3) by a standard procedure (see Fig. 2 and Section 2.3 for details) [20].

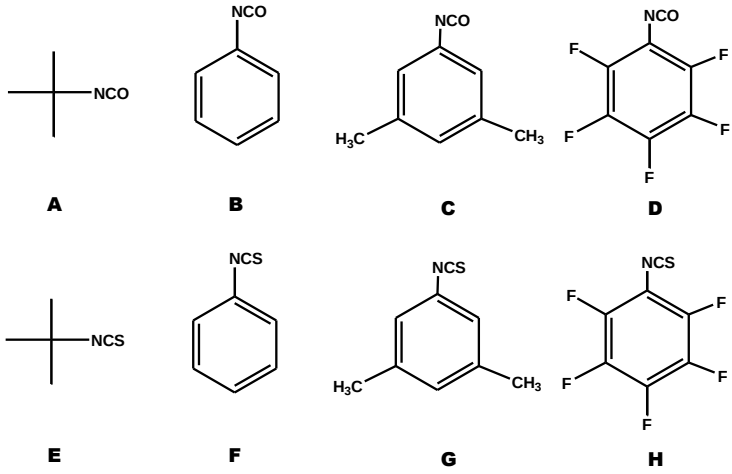

Figure 3. Chemical structures of isocyanates and their sulfur analogues used as N-protecting reagents. A = *tert*-butyl isocyanate (*t*-BuI); B = phenyl isocyanate (PhI); C = 3,5-dimethylphenyl isocyanate (DMPI); D = pentafluorophenyl isocyanate (PFPI); E = *tert*-butyl isothiocyanate (*t*-BuIS); F = phenyl isothiocyanate (PhIS); G = 3,5-dimethylphenyl isothiocyanate (DMPIS), and H = pentafluorophenyl isothiocyanate (PFPIS).

For namitecan, neither the racemate nor the (*R*)-enantiomer were easily available as reference, since total synthesis is a complex and expensive task. Thus, the position of the minor enantiomer peak was assessed by computer reprocessing of chromatograms obtained by running the single (*S*)-enantiomer on (*R*,*R*)- and (*S*,*S*)-DACH-DNB CSPs alternatively (Fig. 4A and 4B, respectively), to give the "virtual

racemate" shown in Fig. 4C (obtained by ElabChrom, a lab-made software that merges two independent chromatograms) [1]. As expected, elution order was the same as already found for the whole CPT series and confirmed by CD spectra [ibid.], i.e., (*S*)-enantiomers (leading peaks) were better retained by the stationary phase with (*S*,*S*)-configuration. For this reason, detection of the trace (*R*)-enantiomer was achievable only on such CSP, where the trace was eluted first. The results of the HPLC separations of the N-protected-namitecan derivatives on the (*R*,*R*)- and (*S*,*S*)-DACH-DNB CSPs are presented in Table 1. Unfortunately, enantioselectivity (α) values between the two namitecan enantiomers as *t*-butyl-ureido derivatives were quite low (α = 1.10), when compared with the previous results obtained for lipophylic CPT derivatives (α = 1.22–1.50) [1]; no significant increase of such value was obtained by introducing in the analyte an aromatic moiety (DMP) close to the ureido functionality (i.e., by pre-derivatizing namitecan with isocyanate C), whereas a sizeable increase in retention was observed, with capacity factors (*k'*) growing up from 1.83 to 3.20 for the trace (*R*)-enantiomer (see Table 1 and Fig. 4).

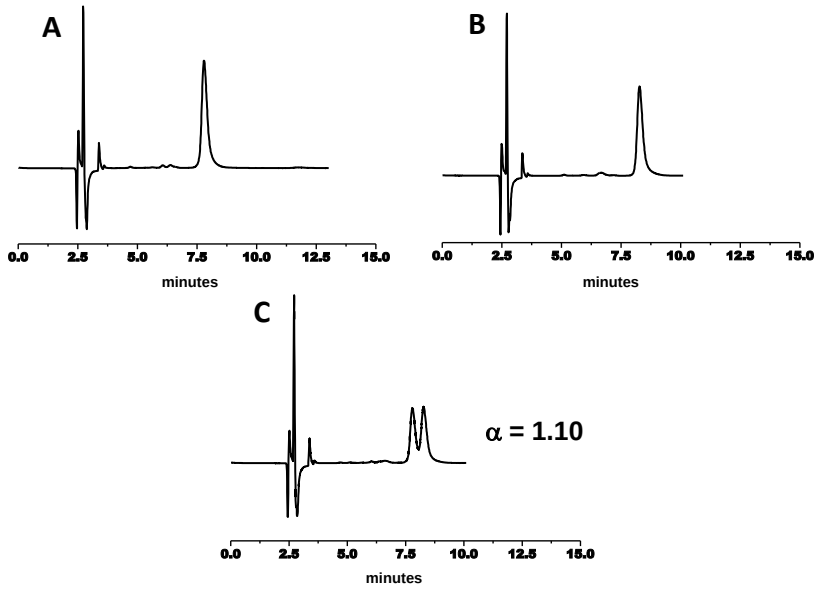

Figure 4. (A) Chromatogram of (*S*)-namitecan as NH-CO-NH-DMP derivative on (*R*,*R*)-DACH-DNB column. (B) Chromatogram of (*S*)-namitecan as NH-CO-NH-DMP on (*S*,*S*)-DACH-DNB column. (C) Computer-generated chromatogram of the "virtual racemate". Eluent: *n*-hexane-dichloromethane (EtOH stabilized) (40:60, v/v) + 3% methanol; flow-rate: 1.00 ml/min; T = 25 °C; UV detection at 370 nm.

These unhelpful preliminary results prompted us to explore the second typology of Pirkle-type columns system, i.e., the Whelk-O1 family, containing the 4-(3,5-dinitrobenzamido)-1,2,3,4-tetrahydro-phenanthrene as selector [17,19].

Table 1. Chromatographic data for the analysis of namitecan as ureido derivatives on (*R*,*R*)- and (*S*,*S*)-DACH-DNB columns

CSP config.	Sample	Chromatographic peak	$k'^{(a)}$	$\alpha^{(b)}$	$R_s^{(c)}$
(*R*,*R*)	*(S)*-namitecan	(*S*)-namitecan-NH-C(O)-NH-*t*-Bu	1.83	–	–
(*S*,*S*)	*(S)*-namitecan	*(S)*-namitecan-NH-C(O)-NH-*t*-Bu	2.01	–	–
(*S*,*S*)	Virtual (*R*,*S*)-namitecan	(*R*)-namitecan-NH-C(O)-NH-*t*-Bu	1.83	1.10	1.08
		(S)-namitecan-NH-C(O)-NH-*t*-Bu	2.01		
(*R*,*R*)	(*S*)-namitecan	(*S*)-namitecan-NH-C(O)-NH-DMP	3.20	–	–
(*S*,*S*)	(*S*)-namitecan	(*S*)-namitecan-NH-C(O)-NH-DMP	3.49	–	–
(*S*,*S*)	Virtual (*R*,*S*)-namitecan	(*R*)-namitecan-NH-C(O)-NH-DMP	3.20	1.09	1.15
		(*S*)-namitecan-NH-C(O)-NH-DMP	3.49		

(*a*) Retention factor. (*b*) Enantioselectivity factor. (*c*) Resolution factor.

First of all, we analyzed CPT samples for which the racemate was available as reference. The CSP gave easy access to the two enantiomers, with attractive enantioselectivity (α = 1.50) and time of analysis (10–15 mins), under the same chromatographic conditions (see Fig. 5). Notably, we found the opposite elution order with respect to the DACH-DNB columns family, i.e., (*S*)-CPT was better retained by the stationary phase with (*R*,*R*)-configuration. For this reason, detection of the trace (*R*)-enantiomer was achievable only on such CSP, where the trace was eluted first. Since preliminary experiments with namitecan as *t*-butyl- and DMP-ureido derivatives showed larger retention and enantioselectivity values (see Table 2

and Fig. 5), the Whelk-O1 columns family was selected to perform a more in-depth investigation.

Table 2. Chromatographic data for the analysis of namitecan as ureido derivatives on (*R*,*R*)- and (*S*,*S*)-Whelk-O1 columns

CSP config.	Sample	Chromatographic peak	$k'^{(a)}$	$\alpha^{(b)}$	$R_s^{(c)}$
(*R*,*R*)	(*S*)-namitecan	(*S*)-namitecan-NH-C(O)-NH-*t*-Bu	3.93	–	–
(*S*,*S*)	(*S*)-namitecan	(*S*)-namitecan-NH-C(O)-NH-*t*-Bu	2.82	–	–
(*S*,*S*)	Virtual (*R*,*S*)-namitecan	(*R*)-namitecan-NH-C(O)-NH-*t*-Bu (*S*)-namitecan-NH-C(O)-NH-*t*-Bu	3.93 2.82	1.39	3.59
(*R*,*R*)	(*S*)-namitecan	(*S*)-namitecan-NH-C(O)-NH-Ph	6.86	–	–
(*S*,*S*)	(*S*)-namitecan	(*S*)-namitecan-NH-C(O)-NH-Ph	5.64	–	–
(*S*,*S*)	Virtual (*R*,*S*)-namitecan	(*R*)-namitecan-NH-C(O)-NH-Ph (*S*)-namitecan-NH-C(O)-NH-Ph	6.86 5.64	1.22	2.97
(*R*,*R*)	(*S*)-namitecan	(*S*)-namitecan-NH-C(O)-NH-DMP	5.72	–	–
(*S*,*S*)	(*S*)-namitecan	(*S*)-namitecan-NH-C(O)-NH-DMP	4.43	–	–
(*S*,*S*)	Virtual (*R*,*S*)-namitecan	(*R*)-namitecan-NH-C(O)-NH-DMP (*S*)-namitecan-NH-C(O)-NH-DMP	5.72 4.43	1.29	3.75
(*R*,*R*)	(*S*)-namitecan	(*S*)-namitecan-NH-C(O)-NH-PFP	1.87	–	–
(*S*,*S*)	(*S*)-namitecan	(*S*)-namitecan-NH-C(O)-NH-PFP	1.31	–	–
(*S*,*S*)	Virtual (*R*,*S*)-namitecan	(*R*)-namitecan-NH-C(O)-NH-PFP (*S*)-namitecan-NH-C(O)-NH-PFP	1.87 1.31	1.43	3.08

(*a*) Retention factor. (*b*) Enantioselectivity factor. (*c*) Resolution factor.

2.3 Check of the chromatographic equivalence of columns with opposite configuration

As already stated in our previous work [1], the two columns with opposite selector configuration used in the ICCA technique must be

perfectly equivalent both chemically (i.e., same retention and selectivity) and geometrically (i.e., identical dimensions, particle size, packing efficiency, etc.). (*R*,*R*)- and (*S*,*S*)-Whelk-O1 columns equivalence was demonstrated by running the (*R*,*S*)-CPT sample on the two columns: chromatograms were found to be superimposable (see Fig. 5A and 5B). Afterwards, the same sample was analyzed on a tandem-columns arrangement, i.e., on the two columns connected in series via a zero dead-volume column coupler. In such case, the two CPT enantiomers were coeluted (α = 1.00), yielding a single peak with double area and retention times which were the sum of the averaged values obtained on the single columns (Fig. 5C).

2.4 Choice of N-protecting groups of namitecan

In the present study four isocyanates (A–D in Fig. 3) were at first investigated as potential N-protecting groups of the free terminal amine of namitecan, ranging from alkyl- (A) to aryl-substituted (B), in the latter case containing electron-rich (C) or electron-poor (D) moieties. Later, we included in the study the corresponding isothiocyanates (E–H in Fig. 3), in order to explore the role of sulfur in terms of intermolecular H-bonding interaction, polarity and steric hindrance with respect to oxygen.

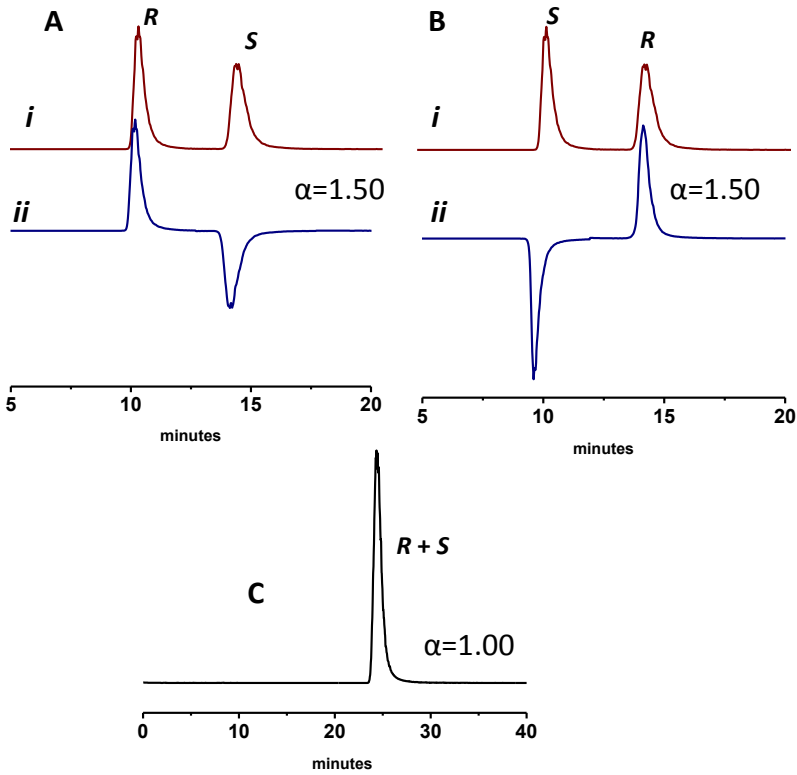

Figure 5. (A) Chromatogram of (*R*,*S*)-CPT on (*R*,*R*)-Whelk-O1 column (k'_R = 3.41; k'_S = 5.11; α = 1.50). (B) Chromatogram of (*R*,*S*)-CPT on (*S*,*S*)-Whelk-O1 column (k'_S = 3.43; k'_R = 5.14; α = 1.50). (C) Chromatogram of (*R*,*S*)-CPT on tandem (*R*,*R*)-Whelk-O1 plus (*S*,*S*)-Whelk-O1 columns arrangement (k'_R = k'_S = 4.17; α = 1.00). Eluent: *n*-hexane-dichloromethane (amylene stabilized) (40:60, v/v) + 5% methanol; flow-rate: 1.00 ml/min; T = 25 °C; UV and CD detection at 370 nm.

In general, both alkyl- and aryl-derivatizing agents reacted rapidly with namitecan; however, isothiocyanate E gave an excess of impurities and was discarded. Derivatization solutions were stable for at least three hours, with the exception of isocyanate D, which worked in the proper way only if freshly prepared (less than 30 minutes before injection).

With regard to the chromatographic behaviour of the diversely N-protected analytes on the Whelk-O1 columns family (see Tables 2 and 3), the presence of an aromatic moiety bonded to the ureido function (Table 2 and Fig. 6) yielded much higher capacity factors (k' = 5.64 for the trace (R)-enantiomer), with respect to the *t*-butyl substituent (k' = 2.82). This is likely due to the more efficient π-stacking interactions between analytes and the chiral selector. Notably, with electron-donor substituents (such as 3,5-DMP) on the aromatic ring retention slightly decreased to 4.43 (probably for steric hindrance), whereas with electron-withdrawing groups (i.e., PFP) it drastically dropped to 1.31. Enantioselectivity approximately showed the opposite trend, i.e., it increased with the lowering of retention: α changed from 1.22 to 1.43 going from the most retained derivative, i.e., -NH-CO-NH-Ph (k' = 5.64) to the less retained, i.e., -NH-CO-NH-PFP (k' = 1.31).

As expected, with isothiocyanate derivatives (Table 3 and Fig. 7) we observed the same trend, i.e., the less the retention factor, the

highest the enantioselectivity: in fact, α changed from 1.28 to 1.34 going from the most retained derivative, i.e., -NH-CS-NH-Ph (*k'* = 4.06) to the less retained, i.e., -NH-CS-NH-PFP (*k'* = 1.61).

Table 3. Chromatographic data for the analysis of namitecan as thioureido derivatives on (*R*,*R*)- and (*S*,*S*)-Whelk-O1 columns.

CSP config.	Sample	Chromatographic peak	$k'^{(a)}$	$\alpha^{(b)}$	$R_s^{(c)}$
(*R*,*R*)	(*S*)-namitecan	(*S*)-namitecan-NH-C(S)-NH-Ph	5.19	–	–
(*S*,*S*)	(*S*)-namitecan	(*S*)-namitecan-NH-C(S)-NH-Ph	4.06	–	–
(*S*,*S*)	Virtual (*R*,*S*)-namitecan	(*R*)-namitecan-NH-C(S)-NH-Ph	5.19	1.28	3.13
		(*S*)-namitecan-NH-C(S)-NH-Ph	4.06		
(*R*,*R*)	(*S*)-namitecan	(*S*)-namitecan-NH-C(S)-NH-DMP	4.79	–	–
(*S*,*S*)	(*S*)-namitecan	(*S*)-namitecan-NH-C(S)-NH-DMP	3.67	–	–
(*S*,*S*)	Virtual (*R*,*S*)-namitecan	(*R*)-namitecan-NH-C(S)-NH-DMP	4.79	1.30	3.13
		(*S*)-namitecan -NH-C(S)-NH-DMP	3.67		
(*R*,*R*)	(*S*)-namitecan	(*S*)-namitecan-NH-C(S)-NH-PFP	2.15	–	–
(*S*,*S*)	(*S*)-namitecan	(*S*)-namitecan-NH-C(S)-NH-PFP	1.61	–	–
(*S*,*S*)	Virtual (*R*,*S*)-namitecan	(*R*)-namitecan-NH-C(S)-NH-PFP	2.15	1.34	2.72
		(*S*)-namitecan-NH-C(S)-NH-PFP	1.61		

(*a*) Retention factor. (*b*) Enantioselectivity factor. (*c*) Resolution factor.

In general, the change from oxygen to sulfur on the derivatizing agent yielded to lower retentivity, whereas enantioselectivity was almost insensitive to the O $\rightarrow$ S displacement.

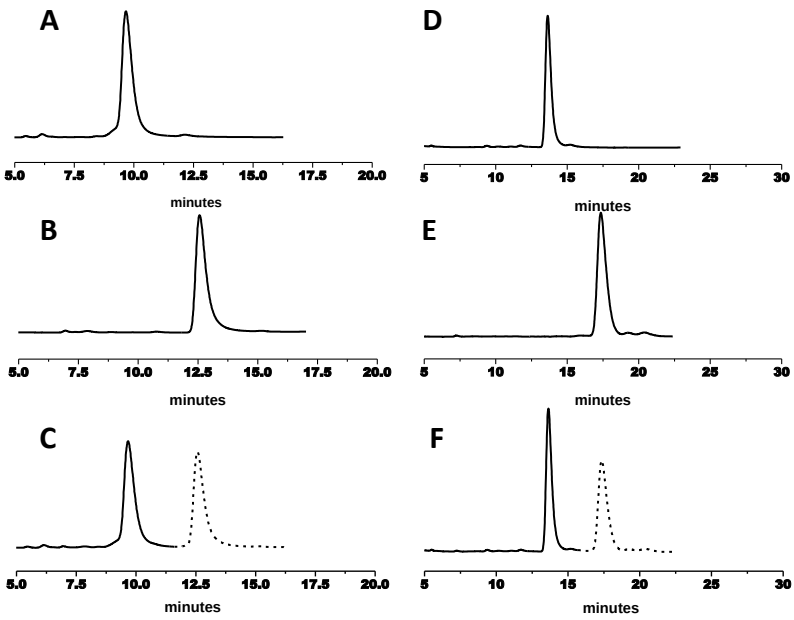

Figure 6. (A) Chromatogram of (*S*)-namitecan as NH-CO-NH-*t*-Bu derivative on (*R*,*R*)-Whelk-O1 column. (B) Chromatogram of (*S*)-namitecan as NH-CO-NH-*t*-Bu on (*S*,*S*)-Whelk-O1 column. (C) Computer-generated chromatogram of the "virtual racemate". (D) Chromatogram of (*S*)-namitecan as NH-CO-NH-DMP derivative on (*R*,*R*)-Whelk-O1 column. (E) Chromatogram of (*S*)-namitecan as NH-CO-NH-DMP on (*S*,*S*)-Whelk-O1 column. (F) Computer-generated chromatogram of the "virtual racemate". Eluent: *n*-hexane-dichloromethane (amylene stabilized) (40:60, v/v) + 5% methanol; flow-rate: 1.00 ml/min; T = 25 °C; UV detection at 370 nm.

This preliminary screening of potential N-protecting groups of ST1968 allowed us to select four amenable candidates to submit to APCI-

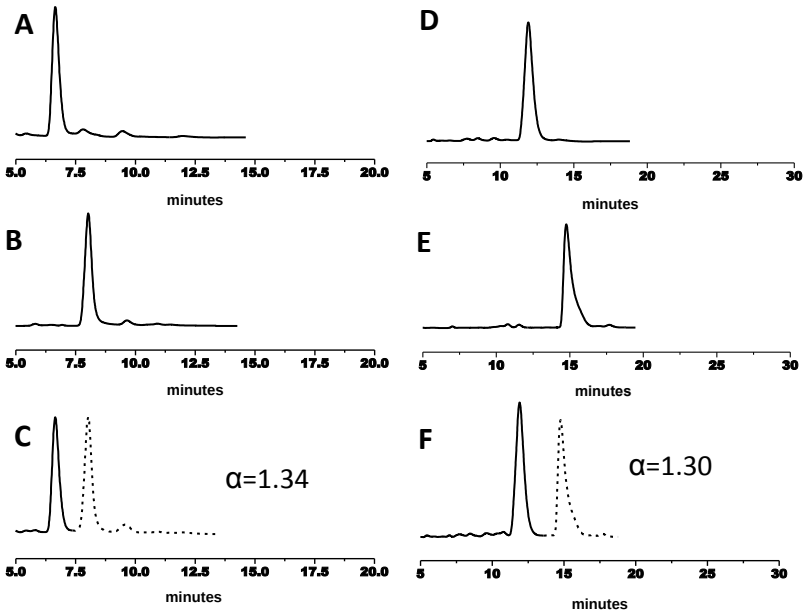

Figure 7. (A) Chromatogram of (*S*)-namitecan as NH-CS-NH-PFP derivative on (*R*,*R*)-Whelk-O1 column. (B) Chromatogram of (*S*)-namitecan as NH-CS-NH-PFP on (*S*,*S*)-Whelk-O1 column. (C) Computer-generated chromatogram of the "virtual racemate". (D) Chromatogram of (*S*)-namitecan as NH-CS-NH-DMP derivative on (*R*,*R*)-Whelk-O1 column. (E) Chromatogram of (*S*)-namitecan as NH-CS-NH-DMP on (*S*,*S*)-Whelk-O1 column. (F) Computer-generated chromatogram of the "virtual racemate". Eluent: *n*-hexane-dichloromethane (amylene stabilized) (40:60, v/v) + 5% methanol; flow-rate: 1.00 ml/min; T = 25 °C; UV detection at 370 nm.

MS/MS detection: two ureido derivatives, namely NH-CO-NH-*t*- Bu (α = 1.39) and NH-CO-NH-DMP (α = 1.29), and two thioureido derivatives, i.e., NH-CS-NH-PFP (α = 1.34) and NH-CS-NH-DMP (α = 1.31).

The selection was made on the grounds of both enantiodiscrimination ability and chemical stability: although the namitecan derivative prepared from isocyanate D exhibited the highest enantioselectivity values of all the series of derivatizing agents (α = 1.43), its elevated chemical instability was considered as a detrimental factor; on the contrary, its sulfur analogue, which indeed gave the highest α amongst the sulfur series, was shown to be an easy to handle analyte.

2.5 Chromatographic APCI-MS/MS method development

An APCI interface was chosen since it is known to be well suited to detect non polar and medium polarity molecules with masses between 100 and 1000 Da, and to be compatible with analytical flow-rates, offering a wide linear dynamic range for quantitative purposes [21]. The precursor and product ions for each analyte of interest were

determined by direct infusion of single analyte solutions. The mass spectra recorded in full scan acquisition mode showed the protonated molecular ions $[M+H]^+$ as base peaks, with mass-to-charge ratios (m/z) as reported in Table 4.

Table 4. Precursor and product ions for the four ST1968 derivatives obtained by APCI-MS/MS detection.

	$[M+H]^+$ *m/z*	**Product ions**	
		m/z	**Attribution**
(*S*)-namitecan-NH-C(O)-NH-*t*-Bu	533	435	$[namitecan+H]^+$
(*S*)-namitecan-NH-C(O)-NH-DMP	582	435	$[namitecan+H]^+$
(*S*)-namitecan-NH-C(S)-NH-PFP	660	435	$[namitecan+H]^+$
		477	$[M+H-C_6HNF_5]^+$
(*S*)-namitecan-NH-C(S)-NH-DMP	598	435	$[namitecan+H]^+$
		477	$[M+H-C_6H_4Me_2N]^+$

The fragmentation pattern obtained by isolation of the different $[M+H]^+$ ions from isocyanate derivatives gave an MS/MS spectrum containing a major fragment at m/z = 435, arising from the loss of the N-protecting groups. The following ion transitions were chosen for the SRM acquisition: 534 $\rightarrow$ 435 and 582 $\rightarrow$ 435, for *t*-butyl-ureido and DMP-ureido derivatives, respectively. Figure 8 shows a typical chromatogram of (*S*)-namitecan as NH-CO-NH-*t*-Bu derivative

obtained on (*R*,*R*)-Whelk-O1 column with APCI-MS/MS detection: as it can be easily seen, the trace (*R*)-enantiomer was easily identified and quantified (0.003%). Notably, the fragmentation pattern obtained by isolation of the different [M+H]+ ions from isothiocyanate derivatives gave an MS/MS spectrum containing, beside the above mentioned peak at m/z = 435, another major fragment at m/z = 477, corresponding to the loss of an aniline-substituted moiety, i.e., $[M+H\text{-}C_6F_5NH_2]^+$ and $[M+H\text{-}C_6H_3Me_2NH_2]^+$ for PFP-thioureido and DMP-thioureido derivatives, respectively.

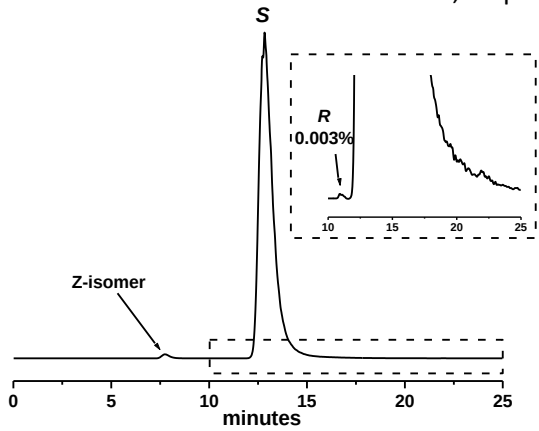

Figure 8. Chromatogram of (*S*)-namitecan as NH-CO-NH-*t*-Bu derivative on (*R*,*R*)-Whelk-O1 column. The ion transition 534 → 435 was chosen for the SRM acquisition. Eluent: *n*-hexane-dichloromethane (amylene stabilized) (40:60, v/v) + 5% methanol; flow-rate: 1.00 ml/min; *T* = 25 °C; APCI-MS/MS detection (for conditions, see Experimental Section).

The following ion transitions were chosen for the SRM acquisition: 660 → 435 and 660 → 477 for the PFP-thioureido derivative, and 598 → 435 and 598 → 477 for the DMP-thioureido derivative. A typical chromatogram obtained on (*R*,*R*)-Whelk-O1 column by MS detection in SRM mode for namitecan as DMP-thioureido derivative is shown in Figure 9.

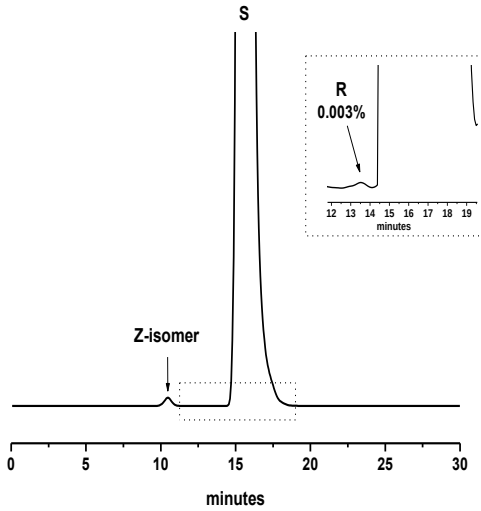

Figure 9. Chromatogram of (*S*)-ST1968 as NH-CS-NH-DMP derivative on (*R*,*R*)-Whelk-O1 column. The ion transitions 598 → 435 and 598 → 477 were chosen for the SRM acquisition. Eluent: *n*-hexane-dichloromethane (amylene stabilized) (40:60, v/v) + 5% methanol; flow-rate: 1.00 ml/min; *T* = 25 °C; APCI-MS/MS detection (for conditions, see Experimental Section).

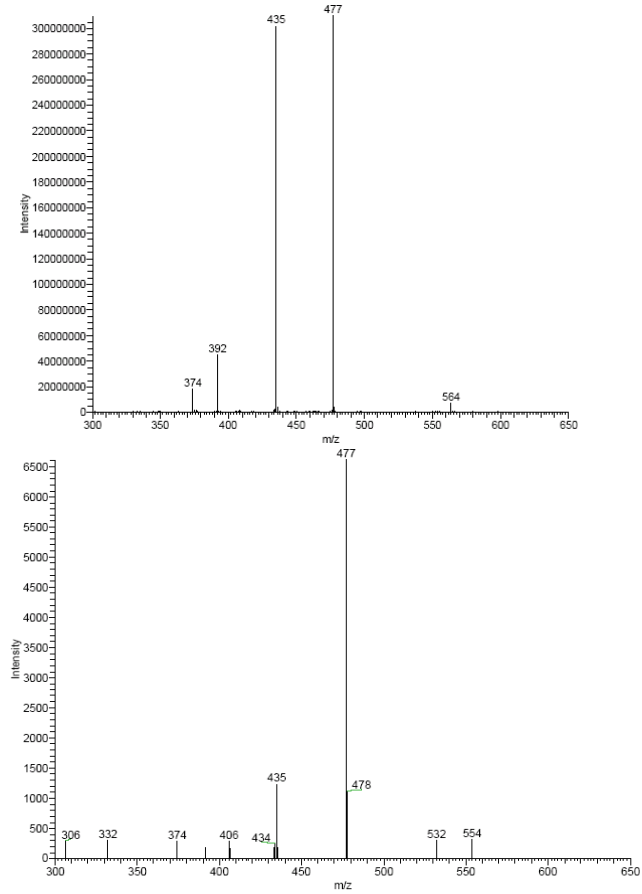

Figure 10. APCI-MS/MS spectra of (*S*)-ST1968 as NH-CS-NH-DMP derivative. Fragmentation was obtained by isolation of the $[M+H]^+$ ion at 598 *m*/*z*, with a collision energy of 35% (arbitrary units), corresponding to chromatographic peak of (*S*)-ST1968 (top) and to its (*Z*)-isomer (bottom).

An interesting benefit of the thioureido derivatives with respect to the ureido is that the (*Z*)-impurity of namitecan can be easily detected with high selectivity and sensitivity since it gave a fragmentation pattern where the peak at m/z = 477 was the major one (Fig. 10). This behaviour was not observed with the oxygen derivatives.

2.6 Chromatographic APCI-MS/MS method validation

The method was evaluated according to the criteria described in Section 2.6. LOD was determined at 50 pg injected, whereas LOQ at 150 pg. The accuracy and precision (n = 6) obtained at LOQ level were 67.7% and 22.0%, respectively. Linearity was verified throughout the tested range with the following linear relationship and correlation coefficient (R^2): $y = 6.48 \times 10^8 x + 2.07 \times 10^8$, $R^2 = 0.9976$. As it can be observed, the wide dynamic linearity range obtained (five orders of magnitude) enabled the quantitation of the trace (*R*)-enantiomer down to 0.003% of the main compound, corresponding to enantiomeric excess values up to 99.994%.

3. Conclusions

A set of alkyl- and aryl-substituted isocyanates and isothiocyanates were investigated as potential N-protecting groups of the free terminal amine of namitecan (ST1968), a novel water-soluble CPT derivative currently undergoing phase I clinical trials as anticancer agent. Successful separations on the Whelk-O1 columns could be obtained with all protecting groups (α ranging from 1.22 to 1.43), although those including pentafluoroaryl moieties were found to yield higher enantioselectivities (α = 1.43) than those with aliphatic residues (α = 1.39). However, pentafluoroaryl derivatives gave the lowest retention values, and hence did not show chemoselectivity towards eventual impurities, such as the (*Z*)-diastereoisomer of ST1968. As expected, the change from oxygen to sulfur on the derivatizing agent yielded to lower retentivity, whereas enantioselectivity was almost insensitive to the O $\rightarrow$ S displacement.

The screening of potential N-protecting groups of namitecan allowed us to identify an interesting candidate for further investigations on namitecan: the NH-CS-NH-DMP derivative indeed exhibited satisfying enantioselectivity (α = 1.30) and chemoselectivity towards the (*Z*)-diastereoisomer of ST1968, as well as a good chemical stability. Moreover, it showed a good response for the protonated molecule in

the positive ion mode APCI-MS/MS detection. The successful application of the ICCA technique combined with multistage mass spectrometry (APCI-MS/MS) detection enabled us to detect the trace (*R*)-enantiomer of namitecan on the (*R*,*R*)-Whelk-O1 CSP at 0.003% level, corresponding to enantiomeric excess values up to 99.994%.

It is worthy of note that the procedure we developed is not limited to the CPT class of compounds but can be easily applied to other chiral amines, allowing their separation on commercially available Pirkle-type CSPs under normal-phase HPLC conditions.

4. Experimental Section

4.1 Instrumentation

Liquid chromatography was performed using a Thermo HPLC separation module (San José, CA, USA) consisting of a Surveyor MS micro pump, a Surveyor AS autosampler equipped with a Rheodyne Model 7725i-20 μL injector, and a Surveyor PDA Photodiode Array Detector, coupled to a Thermo Finnigan LCQ Deca XP Plus ion trap mass spectrometer, equipped with an orthogonal APCI ion source. Chromatographic data were collected and processed using the Thermo Xcalibur Chromatography Manager software, version 1.2. A

Jasco PU-980 Intelligent HPLC pump coupled with a Jasco 995 UV/CD detector was also used, and data were collected using the Borwin software (Jasco, Europe). The (*S*,*S*)- and (*R*,*R*)-DACH-DNB (250 × 4.6 mm I.D.), 5 μm particle size chromatographic columns used were purchased by Regis Technologies (Morton Grove, IL, USA). (*S*,*S*)- and (*R*,*R*)-Whelk-O1 (5 μm particle size) CSPs, obtained from Regis Technologies, were packed into 250 × 4.6 mm I.D. stainless steel columns using a slurry packing procedure already described [16], with *n*-hexane as pressurizing agent (700 bar for 20 min). Notably, although sold as the (*S*,*S*)-Whelk-O1, the true configuration is (3*R*,4*S*). The incorrect assignment is a remnant of the original Whelk-O CSP wherein the selector was bound to silica via an undecyl linkage and thus correctly assigned the (*S*,*S*)-configuration [17].

4.2 Chemicals and reagents

Purified samples of (*S*)-CPT and (*R*,*S*)-CPT were purchased from Boehringer Ingelheim Pharma KG, Germany. 7-(*E*)-(2-Aminoethyloxy-imino)methyl camptothecin hydrochloride or namitecan (ST1968) was supplied by sigma-tau S.p.A. (Pomezia, Italy) [7-10].

HPLC-grade *n*-hexane, methanol, dichloromethane, triethylamine (Et_3N), dry tetrahydrofuran (THF), dry toluene, isocyanates A–D, as well as phenyl isothiocyanate (F) and pentafluorophenyl isothiocyanate (H) were purchased from Sigma-Aldrich (St. Louis, MO, USA), whereas tert-butyl isothiocyanate (E) and 3,5-dimethylphenyl isothiocyanate (G) were from Fluorochem (Derbyshire, UK).

4.3 Derivatization procedures

All the solutions of namitecan were prepared in amber glass volumetric flasks, since the *E* and *Z* diastereoisomers of the oxime group in position 7 undergo light-induced interconversion at room temperature. Special care was taken in the handling of CPT and derivatives because of the carcinogenic nature of the compounds. All samples were sequestered and disposed of according to the material safety data sheet (MSDS) and sigma-tau S.p.A. hazardous handling and waste policy.

The various pre-column N-terminal derivatizations of ST1968 were carried out as follows: approximately 100 μl aliquots of the proper isocyanate (A, B, and D) or isothiocyanate (E–H) in dry toluene (19.7–27.6 mmol in 10 ml) were added to a solution (500 μl) of ST1968 in dry and degassed THF (2.1×10^{-3} mmol in 5 ml) containing

Et_3N (2.4×10^{-2} mmol) in an amber screw-cap vial, resulting in analyte concentration of approximately 0.42 mmol/l. For isocyanate C, a more diluted dry toluene solution was prepared (7.1 mmol in 10 ml), due to lower solubility. The mixture was vortexed for 5 minutes at room temperature, and directly injected into the HPLC system (10–20 µl). ST1968 derivatives from isocyanates A–C were stable for at least three hours, whereas the reaction mixture with D proved instable within a few minutes. Isothiocyanates F–H gave also stable derivatives, while derivatization reaction with E yielded a mixture of side-products, and was discarded.

4.4 Chromatographic conditions

HPLC separations were carried out under normal-phase conditions on both DACH-DNB and Whelk-O1 columns family. In the first case, the mobile phase was made up of 40% *n*-hexane and 60% dichloromethane (stabilized with ethanol ~ 0.25%), plus 3% methanol added (v/v). For Whelk-O1 columns family, the polar modifier was increased to 5%, since amylene stabilized dichloromethane was employed. The flow-rate was set to 1.00 ml/min and the columns were thermostated at 25 °C. All derivatization reaction mixtures were directly injected without further dilution. Aliquots of 10–20 µl were

injected. The chromatograms were recorded by monitoring the UV trace at 370 nm (200–400 nm PDA range). Columns hold-up time (t_0) was determined from the elution time of an unretained marker (1,3,5-tri-*t*-butylbenzene) using as eluent a mixture made up of 95% dichloromethane (amylene stabilized) and 5% methanol, at T = 25 °C, flow-rate 1.00 ml/min and UV detection at 254 nm. Hold-up times, obtained as mean value of three injections, were 2.75 and 2.55 min on the DACH-DNB and Whelk-O1 columns family, respectively.

4.5 APCI-MS/MS detection

MS detection was performed by an Atmospheric Pressure Chemical Ionization (APCI) interface, the sheath and auxiliary gases (high purity nitrogen) being 80 and 10 (arbitrary units), respectively. MS parameters were optimized as follows: APCI vaporizer T = 450 °C, corona discharge current 5.00 mA, tube lens offset 30.0 V, source voltage 4.5 kV and current 80 μA, capillary voltage 15 V at T = 250 °C. The acquisition was operated in positive ion mode and identification and quantitation were based on selected reaction monitoring (SRM) detection; in particular the scan range for the parent scan was 250-650 atomic mass units (amu), each scan consisting of three microscans with a maximum ion injection time of 50 ms while the

SRM scan consisted of one microscan and a 50 ms injection time; the precursor isolation window was set at 2 amu and collision energy at 35% (arbitrary units).

4.6 Method validation for the DMP-thioureido derivative of namitecan

Method validation based on sensitivity, linearity, accuracy, and precision was performed only for the DMP-thioureido derivative of namitecan (ST1968). Sensitivity was evaluated by determining the limit of detection (LOD) and quantitation (LOQ) according to the signal-to-noise ratio approach. Signal-to-noise ratios of at least 3:1 for LOD and 9:1 for LOQ were considered acceptable. Linearity was investigated by calculation of the regression line by the least squares method and expressed by the correlation coefficient (R^2). In particular, it was checked on different (*S*)-enantiomer solutions at nine concentration levels in a range from 0.0025 to 250 μg/ml (five orders of magnitude). Accuracy and precision were assessed at the LOQ value on six replicated injections. Accuracy was expressed as the percent recovery of the analyte with respect to the nominal concentration of the (*S*)-enantiomer solutions which were considered as the theoretical value. Precision was expressed as RSD%.

5. References and Notes

[1] Badaloni, E.; Cabri, W.; Ciogli, A.; Deias, R.; Gasparrini, F.; Giorgi, F.; Vigevani, A.; Villani, C. *Anal. Chem.* **2007**, *79*, 6013-6019.

[2] Okamoto, M. *J. Pharm. Biomed. Anal.* **2002**, 27, 401-407.

[3] Cancelliere. G.; D'Acquarica, I.; Gasparrini, F.; Misiti, D.; Villani, C. *Pharm. Sci. Technol. Today* **1999**,*2*, 484-492.

[4] Maier, N. M.; Franco, P.; Lindner, W. *J. Chromatogr. A*, **2001**, *906*, 3-33.

[5] *Chirality in Drug Research*; E. Francotte, W. Lindner, Eds.; Wiley-VCH, Verlag GmbH & Co. KGaA: Weinheim, Germany, **2006**.

[6] International Conference on Harmonization (ICH) of technical requirements for registration of pharmaceuticals for human use, Q6A October **1999**.

[7] (a) Penco, S.; Merlini, L.; Zunino, F.; Carminati, P. *PCT Int. Appl.* **2000**, 68 pp., WO 2000053607 A1 20000914; (b) Pisano, C.; Vesci, L.; Zunino, F. *PCT Int. Appl.* **2008**, 15 pp., WO 2008098701 A1 20080821.

[8] De Cesare, M.; Beretta, G. L.; Tinelli, S.; Benedetti, V.; Pratesi, G.; Penco, S.; Dallavalle, S.; Merlini, L.; Pisano, C.; Zunino, F. *Biochem. Pharm.* **2007**, *73*, 656-664.

[9] Pisano, C.; De Cesare, M.; Beretta, G. L.; Zuco, V.; Pratesi, G.; Penco, S.; Vesci, L.; Foderà, R.; Ferrara, F. F.; Guglielmi, M. B.;

Carminati, P.; Dallavalle, S.; Morini, G.; Merlini, L.; Orlandi, A.; Zunino, F. *Mol. Cancer Ther.* **2008**, *7*, 2051-2059.

[10] Pisano, C.; Zuco, V.; De Cesare, M.; Benedetti, V.; Vesci, L.; Foderà, R.; Bucci, F.; Aulicino, C.; Penco, S.; Carminati, P.; Zunino, F. *Eur. J. Cancer* **2008**, *44*, 1332-1340.

[11] 2009 ASCO Annual Meeting *J. Clin. Oncol* **2009**, *27:15s*, (suppl; abstr 2570).

[12] Hsiang, Y.-H.; Hertzberg, R.; Hecht, S.; Liu, L. F. *J. Biol. Chem.* **1985**, *260*, 14873-14878.

[13] Husain, I.; Mohler, J. L.; Seigler, H. F.; Besterman, J. M. *Cancer Res.* **1994**, *54*, 539-546.

[14] Pommier, Y. *Chem. Rev.* **2009**, *109*, 2894-2902.

[15] Kawato, Y.; Terasawa, H. *Recent Advances in the Medicinal Chemistry and Pharmacology of Camptothecin. In Progress in Medicinal Chemistry;* G. P. Ellis, D. K. Luscombe, Eds.; Elsevier: London, **1997**; pp 70–100.

[16] D'Acquarica, I.; Gasparrini, F.; Giannoli, B.; Badaloni, E.; Galletti, B.; Giorgi, F.; Tinti, M. O.; Vigevani, A. *J. Chromatogr. A* **2004**, *1061*, 167-173.

[17] Job, G. E.; Shvets, A.; Pirkle, W. H.; Kuwahara, S.; Kosaka, M.; Kasai, Y.; Taji, H.; Fujita, K.; Watanabe, M.; Harada, N. *J. Chromatogr. A* **2004**, *1055*, 41-53.

[18] Gasparrini, F.; Misiti, D.; Villani, C. *Italian Patent* No. 21584 A, August 29, **1989**.

[19] Pirkle, W. H.; Welch, C. J.; Lamm, B. *J. Org. Chem.* **1992**, *57*, 3854-3860.

[20] K. Blau, J. M. Halket, Eds.; Handbook of Derivatives for Chromatography. Second Edition, **1993**.

[21] Niessen, W. M. A.; Tinke, A. P. *J. Chromatogr. A* **1995**, *703*, 37-57.

PART C

Kinetic and Thermodynamic Studies of the Epimerization Processes in Artemisinin-derived Antimalarial Drugs by Dynamic High Performance Liquid Chromatography (D-HPLC)

Chapter 1

Stereodynamic investigation of labile stereogenic centres in Dihydroartemisin.

1.1 Introduction

1.*1.1 Artemisinin and Dihydroartemisinin*

Malaria is a mosquito-borne infectious disease caused by eukaryotic protists of the genus *Plasmodium*. It is widespread in tropical and subtropical regions, including Sub-Saharan Africa, Asia and the Americas. The cause of the disease is a protozoa, discovered in 1880 by Charles Louis Alphonse Laveran, who observed the parasites in a blood smear taken from a patient deceased from malaria, in the military hospital of Constantine, Algeria. The disease results from the multiplication of malaria parasites within red blood cells, causing fever and headache and progressing to coma and death in more severe cases, largely caused by *Plasmodium falciparum*, the most virulent species. Each year, there are approximately 350-500 million cases of malaria worldwide, killing around 781,000 people each year according to the World Health Organisation's 2010 World Malaria

Report [1], 2.23% of deaths worldwide. The majority of deaths are young children in Sub-Saharan Africa. [2]

In the past years, the combination of artemisinin derivatives in combination with other conventional antimalarial drugs (artemisinin-based combination therapies or ACTs) was developed and is now the treatment of choice for the most lethal forms of malaria. [3]

Artemisinin (Qinghaosu, **1**, Figure 1) is a sesquiterpene lactone endoperoxide isolated from *Artemisia annua L.* that Chinese herbalists have traditionally used to treat malaria [4,5]. Since its identification in the early 1970s, artemisinin, as well as its semi-synthetic derivatives [6] and synthetic trioxanes [7], have been used in therapy. Reduction of artemisinin by sodium borohydride in methanol [8] produces dihydroartemisinin (DHA, **2**, Figure 1), which is also its main *in vivo* metabolite and provides improved antimalarial potency [7,9,10]. The synthesis of **2** has opened pathways for further derivatization at C-10 to give ether (**3**-**5** in Figure 1) and ester (**6** in Figure 1) derivatives, largely exploited by the China Cooperative Research Group [11] with the aim of tuning water and/or oil solubility and improving bioavailability.

Conversion of the lactone carbonyl group at C-10 of artemisinin into the hydroxyl (hemiacetal) group in **2** yielded a new stereochemically labile centre in the molecule, which, in turn, provided two

interconverting lactol hemiacetal epimers, namely **2α** and **2β** (See Scheme 1).

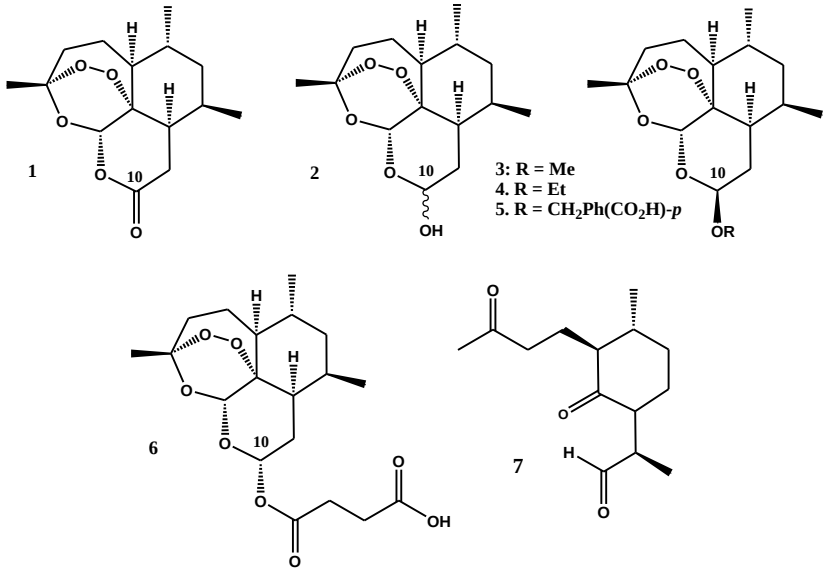

Figure 1. Chemical structures of artemisinin (**1**), dihydroartemisinin (DHA, **2**), artemether (**3**), arteether (**4**), artelinic acid (**5**), artesunic acid (**6**), and a ubiquitous thermal decomposition product of **2** designated as diketoaldehyde (DKA, **7**).

The α-epimer bears the hydroxyl group in the equatorial position (absolute stereochemistry at C-10: R), whereas the 2β-epimer possesses an axial hydroxyl group [12], as shown by the polytube models in Figure 2.

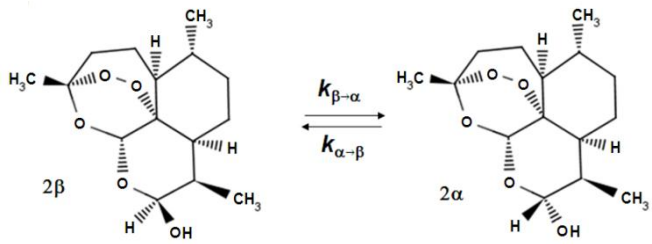

Scheme 1. Chemical structures of the two interconverting epimers of DHA (2): the 2α-epimer bears the hydroxyl group in the equatorial position (absolute stereochemistry at C-10: R), whereas the 2β-epimer possesses an axial hydroxyl group.

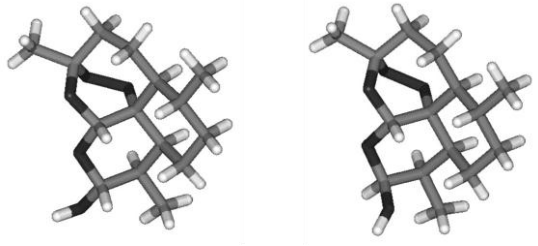

Figure 3. Polytube models of the two interconverting epimers of DHA (2): the 2β-epimer (right) was obtained by computer editing of the X-Ray data of crystalline 2β [10]; the model for the 2α-epimer (left) was derived by molecular mechanics optimization (MMFF force field as implemented in SPARTAN 04) by inverting the configuration at C-10.

Although **2** has a chair-like pyranose ring, such a nomenclature is the reverse of that normally used for designating the stereochemistry of sugars and glycosides, in which, for example, D-glucopyranose possesses an axial hydroxyl group [13].

Bulk solid **2** consists exclusively of the β-epimer, as illustrated by an X-ray crystallographic study on crystalline **2.**[14] However, upon dissolution in various solvents, the initial solution consisting of **2β** slowly equilibrates to mixtures of **2α** and **2β** epimers with different solvent-dependent compositions [13, 14-16].

Dissolution of vacuum-dried, bulk solid **2** in $CDCl_3$ provides a solution consisting exclusively of **2β**, which equilibrates to an about 1:1 mixture of **2β** and **2α** within 10 h [14,15]. The rate and extent of interconversion in solution is solvent-dependent: in non-polar solvents such as CD_2Cl_2, the equilibrium ratio of **2α**/**2β** is 1:1.35, reaching values of 2:1 in methanol and acetone, and 3:1 in dimethylsulfoxide [15,16], in accordance with the increased solvent polarity. In hydro-organic solvents, a 4.5:1 equilibrium ratio for **2α/2β** was reached after a minimum of 18 h following dissolution in 50% (v/v) ethanol in water at 4° C [17]. HPLC determinations of the **2α**/**2β** ratio showed that a stable value (3.3:1) is achieved after 10–12 h in mobile phases comprising 50% (v/v) acetonitrile in 0.1 M acetate buffer (pH 4.8) [18,19]. Finally, the **2α**/**2β** ratio was also determined

in vivo, in a study aimed at obtaining information on protein binding of DHA: a preferential existence of the α-DHA epimer (**2α**/**2β** ratio of about 6:1) was assayed by HPLC with radiochromatographic detection in patients with malaria infection.[20].

Computational studies, performed by Haynes and co-workers with AM1 and PM3 semiempirical methods, showed that the DHA epimers have very close heats of formation, *i.e.*, have similar thermodynamic stabilities [13,15]. These studies also showed that acylations where the hydroxyl group of DHA acts as the nucleophile exclusively yield the α epimer for kinetic reasons. The biological implication of such a process is the observation that Phase II glucuronidation of **2** exclusively provides the α-DHA-β-glucuronide.[21,22]

Thus, a deeper understanding of the kinetic, thermodynamic and mechanistic features of the **2α**/**2β** equilibration, including its stereochemical implications, may have a great importance in the investigation of the mechanism of action and/or toxicity of the drug at a molecular level. Moreover, since a previous study [23] on the equilibrium between **2α** and **2β** showed that interconversion of the two epimers occurrs on a chromatographic time-scale, this prompted a thorough investigation of the phenomena as a crucial requisite of any analytical method aimed at quantitating this family of drugs.

This work describes the use of DHPLC in the stereodynamic investigations of DHA by dynamic HPLC.

1.1.2 HPLC Analytical methods for DHA

Numerous HPLC methods [17-35] have been developed for the analysis and plasma levels monitoring of **2**, formerly based on two main detection strategies due to the lack of strong ultraviolet absorption or fluorescent chromophores: reductive electrochemical (EC) [17, 24-26,34] and UV detection [18,19,29] with pre- or post-column derivatization. The latter approach lacks specificity in that metabolites of the drug are also converted, in many instances, to products having overlapping UV spectra. On the other hand, HPLC-EC provides excellent specificity and sensitivity, although it suffers from some inherent difficulties, i.e., rigorous deoxygenation of samples and mobile phases, and special laboratory facilities are needed. To overcome these shortcomings, evaporative light scattering detection (ELSD) was also coupled to the HPLC analysis of artemisinin and related analogues [32]. The high sensitivity and selectivity of mass spectrometry (MS) opened the way to a large production of analytical methods based on the HPLC-MS coupling [28-31,33,35] for the plasma monitoring of **2**, either based on atmospheric pressure

chemical ionization (APCI) [29,33] or electrospray ionization (ESI) mode.[28,30,31,35] Radiochromatographic detection [20] was exploited as well in a recent HPLC study aimed at determining the **2α/2β** ratio in vivo and evaluating the protein binding of dihydroartemisinin.

Notwithstanding such large availability in literature of robust HPLC methods suitable for the analysis of DHA, none of them considers the effects of epimers equilibration on the analytical response. Actually, the very first study showing that interconversion of the two DHA epimers (Figure 2) occurred in a chromatographic time-scale (i.e., on-column epimerization could be detected) was performed in 1986 by investigating the multiple-peaks of the drug by reversed-phase HPLC [23], but no other related papers followed. Moreover, the author of the study reported a largely overestimated activation energy barrier of 280 kJ mol^{-1} for the interconversion of the two DHA epimers, which cannot be related to dynamic events occurring on the chromatographic time-scale at room temperature [36]. Only recently [37], this issue was considered by our research group with the aim of providing improved and reliable HPLC procedures suited for either isolation of pure **2α** and **2β** or their quantification in solution and in complex mixtures, under conditions of suppressed interconversion. In such study, an effective analytical approach was developed to

overcome the intrinsic shortcomings of the International Pharmacopoeia guidelines on antimalarial drugs.

1.1.3 Pharmacopoeia guidelines on Antimalarial drugs

In the International Pharmacopoeia monograph on Artenimolum or Artenimol (i.e., dihydroartemisinin) [38], the method currently recommended is an HPLC assay based on the use of a stainless steel column (100 mm × 4.6 mm I.D.) packed with a reversed-phase (RP) C18 stationary phase (3.0 μm particle size). The mobile phase is acetonitrile-water 60:40 (v/v), delivered at a flow-rate of 0.6 ml min^{-1} and the detection system used is an ultraviolet spectrophotometer set at a wavelength of about 216 nm. The aim of the pharmacopoeial method is to quantitate DHA (**2**) in the presence of artemisinin (**1**) as related substance. The monograph does not account for any other related substance. The final requirement is that "the test is not valid unless the relative retention of α-artenimol compared with artemisinin is about 0.6, and the resolution between the peaks is not less than 2.0. […] Measure the areas of the peak (twin-peak) responses and calculate the percentage content of $C_{15}H_{22}O_5$ (i.e., artemisinin) with reference to the dried substance".

Four main issues should be taken into account when considering the above method: (i) the column temperature is not specified, (ii) no mention is made of the interconversion between the two epimers of **2**, which indeed occurs on the chromatographic time-scale, (iii) the conditions are not very selective towards DKA (**7**, Figure 1), which is a ubiquitous contaminant of **2**, and (iv) since signal-to-noise ratios in the presence of plateau zones are always smaller than in normal elution profiles, quantitation of species eventually eluting in the plateau area would be negatively affected. The main drawback of the method, however, is that the presence of a visible plateau between the two DHA epimers (called twin-peak in the monography) is completely neglected. In addition, stationary phases may have a retarding or activating effect on the kinetics of the dynamic process involving stereolabile species [39], and this feature should be taken into account as well.

1.1.4. On-column interconversions studies through Dynamic High Performance Liquid Chromatography

Investigations of dynamic molecular processes and determination of their kinetic parameters are commonly performed by dynamic nuclear magnetic resonance (DNMR) spectroscopy [40-43], which

yields quite reliable values for the corresponding free energies of activation ($\Delta G^{\#}$). Pertinent kinetic parameters might also be determined by chromatography, specifically for two species that interconvert during their passage through the column itself (i.e., on-column interconverting species).

Chromatographic retention of a species, in its simplest form, is related to the equilibrium constant for its distribution between the mobile and stationary phases (Figure 4).

$$K_D^A = \frac{\phi}{k'_A} \quad ; \quad K_D^B = \frac{\phi}{k'_B}$$

$$k_1^{app} = \frac{1}{1+k'_A}\, k_1^m + \frac{k'_A}{1+k'_A}\, k_1^s$$

$$k_{-1}^{app} = \frac{1}{1+k'_B}\, k_{-1}^m + \frac{k'_B}{1+k'_B}\, k_{-1}^s$$

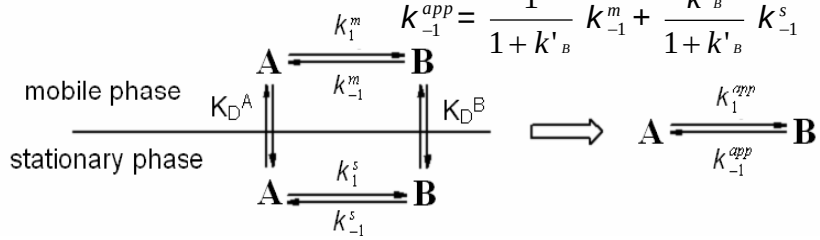

Figure 4. Primary (vertical arrows) and secondary (horizontal arrows) equilibria taking place during chromatography of two interconvertible species A and B on a stationary phase. *Left*: actual interconversions occurring in the mobile and stationary phases; right: the apparent equilibria. k'_A and k'_B are the retention factors of the first (A) and second (B) eluting species, k_1^m and k_{-1}^m the rate constants for the forward and backward interconversion in mobile phase, respectively, and k_1^s and k_{-1}^s are the rate constants for the forward and backward interconversion in stationary phase, respectively.

Chromatography of two interconverting species, however, leads to the establishment of a secondary equilibrium. When an analyte is subjected to a secondary equilibrium, its retention is a weighted average of the retention of the two species [39]. If the interconversion rate is slow compared to the chromatographic process, two resolved peaks are observed due to the occurrence of little or no interconversion. If the rate of interconversion is fast compared to the chromatographic process, only one peak is observed due to the extensive interconversion.

However, if the interconversion is on a similar time-scale to that of the chromatographic process, band spreading and peak distortion may be observed (Figure 5). The two peaks may be joined by an elevated baseline (plateau). This elevated baseline represents species which have undergone at least one interconversion cycle during elution through the column.Stereolabile species can therefore be conveniently investigated by Dynamic High Performance Liquid Chromatography (DHPLC), either in the form of variable temperature or variable flow chromatography.

A quite comprehensive view of milestone works on dynamic chromatography and its applications is given in refs 44-57, including gas and liquid chromatography. DHPLC has been recently used for the study of internal molecular dynamics of a range of chiral stereolabile

compounds, and for the determination of kinetic parameters for the pertinent equilibrium (i.e., the reversible isomerization of one enantiomer into the other, or enantiomerization).

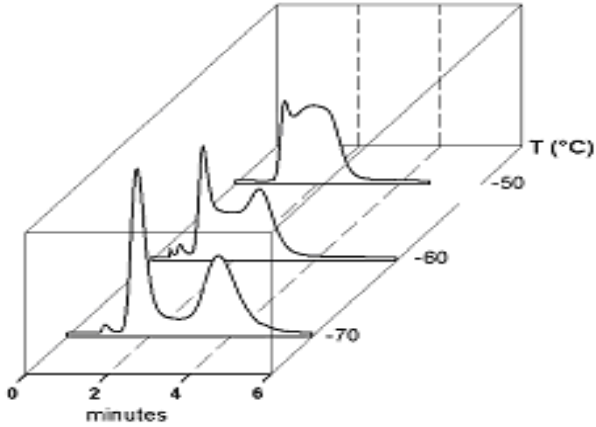

Figure 5. DHPLC traces of a tertiary amide in the form of variable temperature HPLC.

In a general DHPLC experiment, the chromatographic column acts at once as chemical reactor and separation device: first-order, reversible processes where the interconversion rates are on the same time-scale as the column separation rate typically yield temperature- and flow-dependent chromatographic profiles, with an interference regime between the two resolved peaks (Figure 5). Computer simulation of the experimental deformed profiles can be used to

obtain overall rate constants for the interconversion process occurring during HPLC (Figure 6).

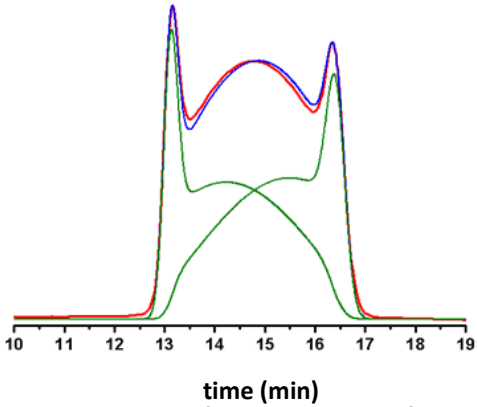

Figure 6. Computer-simulation of experimental deformed profiles of two interconverting species. Red line: experimental profile. Blue line: computer-simulated profile. Green lines: computer-simulated profiles of the individual interconverting species.

These rate constants are averaged values that bring contributions from the process occurring in the mobile phase (k_1^m and k_{-1}^m, for the forward and backward interconversion, respectively) and in the stationary phase k_1^s and k_{-1}^s, for the forward and backward interconversion, respectively). If one of the two constants (usually km) is available from independent measurements, the missing rate constant can be obtained by simulation [49]. Several methods have been used to extract kinetic data from experimental elution profiles

(the theoretical plate model [49], the stochastic model [48,55], the continuous flow model [47], peak deconvolution methods [53,54], approximation functions [52], and the unified equation [57]), and each method exploits a different theoretical framework to describe the dynamic system in which primary and secondary equilibria take place inside the column (Figure 4). The theoretical plate model portrays the chromatographic separation as a discontinuous process, by assuming that all the steps continually proceed in separate uniform sections of a column consisting of N plates. Each theoretical plate is then considered as a distinct chemical reactor in which three events take place: distribution of the species between the mobile and stationary phases, interconversion in both phases, and shifting of the mobile phase onto the next plate [49]. The stochastic model describes the chromatographic separation using time-dependent distribution functions [48,55]. The elution profile of two interconverting species is given by the sum of the distribution functions of the non-interconverted species and the probability of density functions of the interconverted species. In the continuous flow model, general analytical expressions based on the dimensionless Damköhler (Da) number describe the chromatographic mass distribution at the column outlet for a solute subjected to secondary equilibria [47]. In contrast to these ab initio-type

simulations, semiempirical peak deconvolution methods have also been developed to estimate rate constants of enantiomerization and isomerization.[54,55] A direct calculation of enantiomerization barriers from chromatographic parameters based on an approximation function was also attempted,[53] limited to equilibrated and degenerated first-order reactions, i.e., enantiomerizations. Later on, a unified equation has been derived [57] to calculate rate constants of reversible as well as irreversible (pseudo-) first-order reactions by a few iterative steps, without the need of performing a computationally extensive simulation of elution profiles. This calculation method is a valuable tool for the investigation of first-order reactions, in particular the stereochemical integrity of enantiomeric, epimeric, and isomeric compounds. In this context, it is worthy of noting that we have developed a lab-made computer program, Auto DHPLC y2k, which implements both stochastic [48,55] and theoretical plate [49] models, and may take into account all types of first-order interconversions, i.e. enantiomerizations as well as diastereomerizations or constitutional isomerizations (e.g. pseudo first-order tautomerizations), as well as tailing effects.[37, 58-62] With non-enantiomeric isomerizations, forward and backward processes occur at different rates in the achiral mobile phase, where the two isomerizing species are usually

present in differing amounts. According to the thermodynamic cycle involved inside a virtual chromatographic theoretical plate for a generic first-order isomerization process concomitant with the chromatographic distribution equilibria (see Figure 4), we applied the following general equation in the algorithm:

$$\frac{k_{-1}^{m}}{k_{1}^{m}} \times \frac{k_{1}^{s}}{k_{-1}^{s}} = \frac{k'_{B}}{k'_{A}}$$

where k'_A and k'_B are the retention factors of the first (A) and second (B) eluting species, k_1^m and k_{-1}^m are the rate constants for the forward and backward interconversion in mobile phase, respectively, and k_1^s and k_{-1}^s, are the rate constants for the forward and backward interconversion in the stationary phase, respectively. Program functionality was validated on several first-order isomerizations (both enantiomerization and non-enantiomerization) by comparing DHPLC results with those obtained by DNMR technique [58-61] or by classical method [62]. The algorithm also implements the chance of taking tailing effects into account. Both chromatographic and kinetic parameters can be automatically optimized by simplex algorithm until obtaining the best agreement between experimental and simulated dynamic chromatograms.

1.2 Results and Discussion

1.2.1 On-Column epimerization of DHA

To overcome the intrinsic shortcomings of the International Pharmacopoeia and try to address the four points raised when considering such method, we performed a systematic investigation on the influence of chromatographic conditions (stationary phase and column temperature) on the simultaneous reversed-phase HPLC determination of artemisinin (**1**), α-DHA (**2α**), β-DHA (**2β**), and a thermal decomposition product of **2** (DKA, **7**), taking into consideration for the first time the *on-column* epimerization of **2** [37]. Nine commercial RP-C18 (see Table 1 for colums details) columns with different pore size, surface area, carbon load and permeability were evaluated according to the International Pharmacopoeia monograph on DHA (see Figure 7), and compared on the basis of their stationary phase effect towards the interconversion between **2α** and **2β.** In particular, we defined the Catalytic Effect of Stationary Phases (CESP) as the percentage increasing (positive) or decreasing (negative) of the epimerization rate constant, with respect to the analogous value measured in mobile phase.

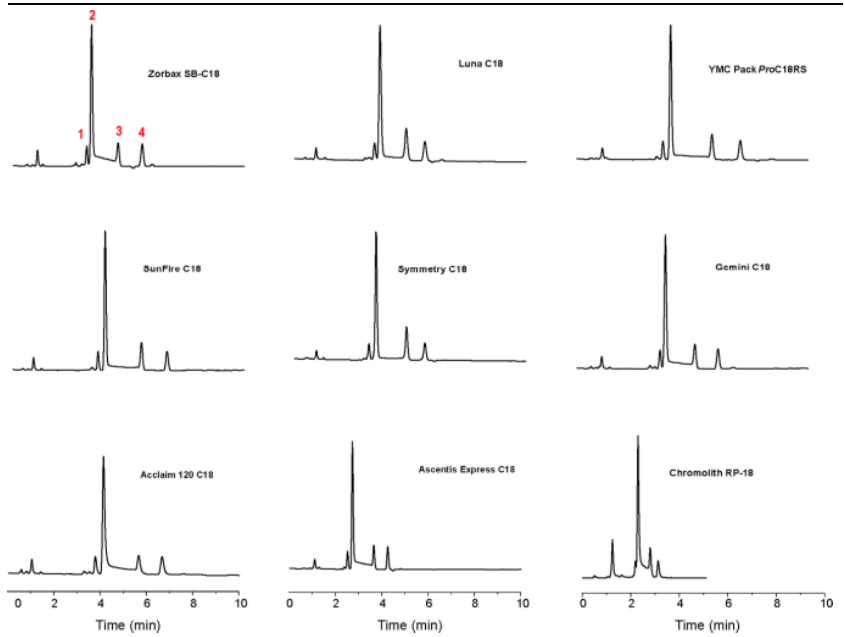

Figure 7. Typical room temperature chromatograms obtained for a standard mixture of **1** and **2** (containing **7** as impurity). Peak 1 corresponds to DKA (**7**), peak 2 to the 2α-epimer, peak 3 to the 2β-epimer, and peak 4 to artemisinin (**1**).

Activation free energies of the process, obtained by computer simulation of the experimentally obtained elution profiles (see Figure 8), showed that the Symmetry C18 column among the nine analyzed has an inhibiting effect on epimerization ($\Delta G^{\#}$ = 22.1 for **2α→ 2β** and 21.6 kcal mol^{-1} for the backward process, compared to ($\Delta G^{\#}$ = 21.7 and 21.0 kcal mol^{-1} for the same processes in free solution). The

column was therefore selected for the development of a cryo-HPLC method aimed at minimizing on-column interconversion.

Table 1. Physicochemical data of the tested commercial RP-C18 columns

Column	Dimension (mm×mm)	Particle size (μm)	Pore size (Å)	Surface area ($m^2 g^{-1}$)	End-capped	k_0 ×10^{14} (m^2)	Carbon load %	Carbon load (μmol m^{-2})	Hold-up time[a] (min)
Zorbax SB-C18	150×4.6	5.0	80	180	No	4.41	-	2.00	1.56
Luna C18	150×4.6	5.0	100	440	Yes	2.56	19.00	3.00	1.70
YMC-Pack ProC18 RS	150×4.6	5.0	80	500	Yes	2.36	21.90	-	1.61
SunFire C18	150×4.6	3.5	96	331	Yes	1.31	16.62	3.76	1.63
Symmetry C18[b]	150×4.6	3.5	100	340	Yes	1.70	19.67	3.15	1.56
Gemini C18	150×4.6	3.0	110	375	Yes	1.30	14.00	-	1.78
Acclaim 120 C18	150×4.6	3.0	120	300	Yes	1.56	18.00	3.20	1.79
Ascentis Express C18	150×4.6	2.7	90	300	Yes	1.18	-	3.50	1.45
Chromolith RP-18	150×4.6	-	-	150	Yes	5.95	18.00	3.60	1.54

Variable temperature (from 40 to 0 °C) separations performed on the Symmetry C18 column allowed to detect plateau zones only at T > 20 ° C. For this reason, only simulations of the chromatograms registered from 40 to 25 °C were made, by using the classical stochastic model, as implemented within the Auto DHPLC y2k program [58-62]. Since the **2α/2β** ratio was shown to be temperature-independent within

the explored range, a constant value of the relative abundances of the two epimers was set in all the performed relevant simulations.

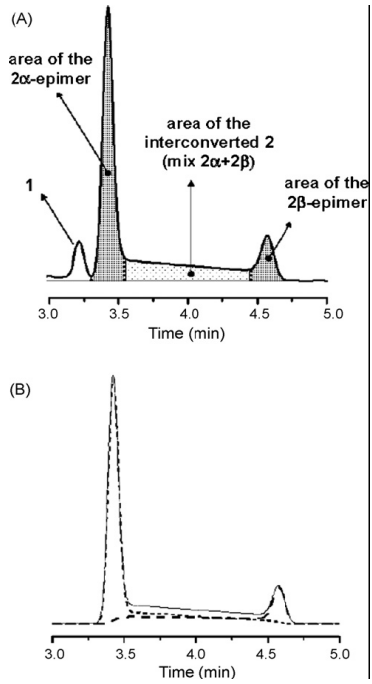

Figure 8. (A) Schematic representation of the integration model used for the calculation of **2α-** and **2β-**epimers areas. (B) Computer simulated profiles of **2α** (dotted line), **2β** (dashed line), and of the mixture **2α** + **2β** (solid line).

On the basis of the epimerization rate constants extrapolated at T < 25 °C, we calculated a marginal plateau area (< 2%) only close to T = 0 °C for the Symmetry C18 column, clearly showing that low column

temperatures are necessary to suppress interconversion. Figure 9 shows the superimposed experimental and simulated chromatographic profiles with the measured activation free energies.

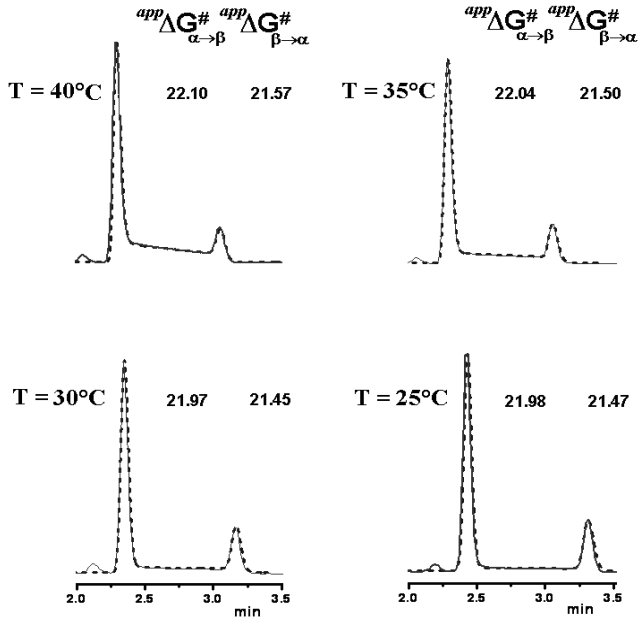

Figure 9. Variable temperature chromatographic profiles obtained on the Symmetry C18 column. Solid line: experimental chromatograms. Dotted line: computer simulated profiles obtained with the measured free energy activation barriers for the on-column epimerization process.

Van't Hoff analyses of the obtained data were also carried out to evaluate the enthalpic and entropic contributions to the epimerization barrier. We found that only a small contribution to

$\Delta G^{\#}_{\alpha-\beta}$ and $\Delta G^{\#}_{\beta-\alpha}$ is due to entropy ($\Delta S^{\#}$ values < 10 u.e.). This suggested that a monomolecular process may be involved in the rate-determining step, reasonably, the ring opening of either the protonated or deprotonated α- or β-hemiacetalic form of **2**, generated in a previous reversible step by reaction with an acid or a base, respectively. Such kinetic pathway would be in agreement to what already reported.[37]

1.3 Conclusions

Artemisinin derivatives such as DHA, artesunate, and artemether are nowadays playing an increasing role in the treatment of drug-resistant malaria. They are the most potent antimalarials available, rapidly lethal to all asexual stages of the parasite *Plasmodium falciparum*. DHA is the main metabolite of artemisinin, and contains a stereochemically labile centre at C-10, which, in turn, provides two interconverting lactol hemiacetal epimers, namely α and β. DHA consists exclusively of the β-epimer in the solid state. Upon dissolution in various solvents, however, the initial solutions slowly equilibrate to mixtures of α- and β-epimers with different solvent-dependent composition. Thus, a deeper understanding of the kinetic, thermodynamic and mechanistic features of the DHA equilibration

(i.e., epimerization) may prove of great importance in the investigation of the mechanism of action and/or toxicity of the drug at a molecular level. Moreover, since the equilibrium between the two DHA epimers occurs on a chromatographic time-scale, a crucial requisite of any analytical method aimed at quantitating this family of drugs is the identification of the optimal conditions (such as stationary phase and column temperature) able to suppress or at least minimize *on-column* epimerization, while achieving the best selectivity and efficiency of separation. In the International Pharmacopoeia monograph on DHA, the drug is quantitated in the presence of artemisinin as related substance, while no other related substance is contemplated. The main drawback of the method, however, is that the presence of a visible plateau between the two interconverting epimers is completely neglected. Despite the large availability in literature of robust HPLC methods suitable for the analysis of DHA, none of them takes into account the effects of the equilibration of epimers on the analytical response.

Our goal was to tackle the issue with the aim of providing improved and reliable HPLC procedures suited for either isolation of pure **2α** and **2β** or their quantification in solution and in complex mixtures. Computer simulation was employed to gain insight on the Catalytic Effect of the Stationary Phase (CESP). Activation free energies of the

process, obtained by computer simulation of the experimentally obtained elution profiles, showed that the Symmetry C18 column among the nine analyzed has an inhibiting effect on epimerization ($\Delta G^{\#}$ = 22.1 for **2α→2β** and 21.6 kcal mol^{-1} for the backward process). The column was selected for the development of a cryo-HPLC method aimed at minimizing on-column interconversion. On the basis of the epimerization rate constants extrapolated at T<25°C, we calculated a marginal plateau area (<2%) only close to T=0°C for the 150 mm × 4.6 mm column geometry. Dynamic High Performance Liquid Chromatography (DHPLC) and computer simulation of the experimental deformed profiles clearly showed that low column temperatures are necessary to suppress interconversion between DHA epimers. The results described in this chapter were published in 2010 in *Molecules* Special Issue on Artemisinin.

1.4 Experimental Section

1.4.1 Apparatus

Liquid chromatography was performed using a Waters Model 2695 HPLC separation module (Waters, Milford, MA, USA) coupled with a Waters 996 Photodiode Array Detector. Chromatographic data were

collected and processed using Empower2 software (Waters). Variable temperature HPLC was performed by using a thermally insulated container cooled by the expansion of liquid carbon dioxide (CO_2). Flow of liquid CO_2 and column temperature were regulated by a solenoid valve, thermocouple, and electric controller. Temperature variations after thermal equilibration were within ±0.1 °C.

1.4.2 Chemicals and reagents

Artemisinin (**1**), dihydroartemisinin (DHA, **2**), and diketoaldehyde (DKA, 3) samples were supplied by sigma-tau S.p.A., Pomezia (Italy). HPLC-grade acetonitrile, methanol, and water were purchased from Carlo Erba (Italy). Deuterium oxide was from Sigma–Aldrich (St. Louis, MO, USA). The following commercially available reversed-phase C18 HPLC columns were used: Zorbax SB-C18 (Agilent Technologies, Santa Clara, CA, USA); Luna C18 (Phenomenex, Inc., Torrance, CA, USA); YMC-Pack ProC18 RS (YMC Europe GmbH, Dinslaken, Germany); SunFire C18 (Waters); Symmetry C18 (Waters); Gemini C18 (Phenomenex, Inc.); Acclaim 120-C18 (Dionex Corporation, Sunnyvale, CA, USA); Ascentis Express C18 (Sigma–Aldrich); Chromolith RP-18 (Merck).

2.4.7 Simulation of dynamic chromatograms

Simulation of variable-temperature experimental chromatograms was performed by using the lab-made [37, 58-62] computer program Auto DHPLC y2k which implements both stochastic and theoretical plate models. The developed algorithm may take into account all types of first-order interconversions, i.e., enantiomerizations as well as diastereomerizations or constitutional isomerizations (e.g., pseudo first-order tautomerizations). Within non-enantiomeric isomerizations, forward and backward interconversion occur at different rates in the achiral mobile phase, where the two isomerizing species are present in differing amounts. According to the thermodynamic cycle involved inside a virtual chromatographic theoretical plate for a generic first-order isomerization concomitant with the chromatographic repartition equilibrium, we applied in the algorithm the following general equation:

$k_{-1}^{m}/k_{1}^{m} \times k_{1}^{s}/k_{-1}^{s} = k'_B/k'_A$,

where k'_A and k'_B are the retention factors of the first (A) and the second (B) eluting species, k_{-1}^{m} and k_{1}^{m} are the rate constants for the backward and forward interconversion in mobile phase, respectively,

and k_1^S and k_{-1}^S are the rate constants for the forward and backward interconversion in stationary phase, respectively.

Program functionality was validated on several first-order isomerizations (both enantiomerization and non-enantiomerization) by comparing DHPLC results with those obtained by DNMR technique or by classical method. The algorithm developed also allowed to take tailing effects into account.

1.5 References and Notes

[1] WHO world malaria report. World Health Organization, **2010**. http://www.who.int/malaria/world_malaria_report_2010/en/ index.html

[2] Snow, R.W.; Guerra, C.A.; Noor, A.M.; Myint, H.Y.; Hay, S.I. *Nature*, **2005**, *434*, 214-217.

[3] Ashley, E.A.; White, N.J. *Curr. Opin. Infect. Dis.* **2005**, *18*, 531–536.

[4] Klayman, D.L. *Science* **1985**, *228*, 1049–1055.

[5] Chaturvedi, D.; Goswami, A.; Saikia, P.P.; Barua, N.C.; Rao, P.G. *Chem. Soc. Rev.* **2010**,*39*, 435-454.

[6] O'Neill, P.M. *Expert Opin. Invest. Drugs* **2005**, *14*, 1117-1128.

[7] (a) O'Neill, P.M.; Posner, G.H. *J. Med. Chem.* **2004**, *47*, 2945-2964.

(b) Bez, G.; Kalita, B.; Sarmah, P.; Barua, N.C.; Dutta, D.K. *Curr. Org. Chem.* **2003**, *7*, 1231-1255.

[8] Li, Y.; Yu, P.-L.; Chen, Y.-X.; Li, L.-Q.; Gai, Y.-Z.; Wang, D.-S.; Zheng, Y.-P. *Chin. Sci. Bull.* **1979**, *24*, 667–669.

[9] Posner, G.H.; Paik, I.-H.; Chang, W.; Borstnik, K.; Sinishtaj, S.; Rosenthal, A. S.; Shapiro, T.A. *J. Med. Chem.* **2007**, *50*, 2516-2519.

[10] Li, Q.G.; Peggins, J.O.; Fleckenstein, L.L.; Masonic, K.; Heiffer, M.H.; Brewer, T.G. *J. Pharm. Pharmacol.* **1998**, *50*, 173-182.

[11] China Cooperative Research Group on Qinghaosu and its Derivatives as Antimalarials. *J. Tradit. Chin. Med.* **1982**, *2*, 9-16.

[12] Pathak, A.K.; Jain, D.C.; Sharma, R.P. *Indian J. Chem., Sect. B: Org. Chem. Incl. Med. Chem.* **1995**, *34*, 992-993.

[13] Haynes, R.K.; Chan, H.-W.; Cheung, M.-K.; Chung, S.T.; Lam, W.-L.; Tsang, H.W.; Voerste, A.; Williams, I.D. *Eur. J. Org. Chem.* **2003**, 2098-2114.

[14] Luo, X.; Yeh, H. J.C.; Brossi, A.; Flippen-Anderson, J.L.; Gilardi, R. *Helv. Chim. Acta* **1984**, *67*, 1515-1522.

[15] Haynes, R.K.; Chan, H.-W.; Cheung, M.-K.; Lam, W.-L.; Soo, M.-K.; Tsang, H.-W.; Voerste, A.; Williams, I.D. *Eur. J. Org. Chem.* **2002**, 113-132.

[16] Haynes, R.K. *Curr. Topics Med. Chem.* **2006**, *6*, 509-537.

[17] Navaratnam, V.; Mordi, M. N.; Mansor, S. M. *J. Chromatogr. B* **1997**, *692*, 157–162.

[18] Batty, K. T.; Davies, T. M. E.; Thu, L. T.; Binh, T. Q.; Anh, T. K.; Ilett, K. F. *J. Chromatogr. B* **1996**, *677*, 345–350.

[19] Batty, K. T.; Ilett, K. F.; Davis, T. M. E. *J. Pharm. Pharmacol.* **1996**, *48*, 22–26.

[20] Batty, K. T.; Ilett, K. F.; Davis, T. M. E. *Br. J. Clin. Pharmacol.* **2004**, *57*, 529-533.

[21] Maggs, J. L.; Madden, S.; Bishop, L. P.; O'Neill, P. M.; Park, K. B. *Drug Metab. Dispos.* **1997**, *25*, 1200-1204.

[22] Ramu, K.; Baker, J. K. *J. Med. Chem.* **1995**, *38*, 1911-1921.

[23] Shishan, Z. *Chromatographia* **1986**, *22*, 77-80.

[24] Zhou, Z.M.; Anders, J.C.; Chung, H.; Theoharides, A.D. *J. Chromatogr.* **1987**, *414*, 77-90.

[25] Karbwang, J.; Na-Bangchang, K.; Molunto, P.; Banmairuroi, V.; Congpuong, K. *J. Chromatogr. B* **1997**, *690*, 259-265.

[26] Sandrenan, N.; Sioufi, A.; Godbillon, J.; Netterb, C.; Danker, M.; van Valkenburg, C. J. *Chromatogr. B* **1997**, *691*, 145-153.

[27] Avery, B.A.; Venkatesh , K.K.; Avery, M.A. *J. Chromatogr. B* **1999**, *730*, 71-80.

[28] Ortelli, D.; Rudaz, S.; Cognard, E.; Veuthey, J.L. *Chromatographia* **2000**, *52*, 445-450.

[29] Souppart, C.; Gauducheau, N. ; Sandrenan, N. ; Richard, F. *J. Chromatogr. B* **2002**, *774*, 195-203.

[30] Sabarinath, S.; Rajanikanth, M.; Madhusudanan, K.P.; Gupta, R.C. *J. Mass Spectrom.* **2003**, *38*, 732-742.

[31] Rajanikanth, M.; Madhusudanan, K.P.; Gupta, R.C. *Biomed. Chromatogr.* **2003**, *17*, 440-446.

[32] Kotecka, B.M.; Rieckmann, K.H.; Davis, T.M.E.; Batty, K.T.; Ilett, K.F. *Acta Trop.* **2003**, *87*, 371-375.

[33] Naik, H.; Murry, D.J.; Kirsch, L.E.; Fleckenstein, L. *J. Chromatogr. B* **2005**, *816*, 233-242.

[34] Lai, C.-S.; Nair, N.K.; Mansor, S.M.; Olliaro, P.L.; Navaratnam, V. J. *Chromatogr. B* **2007**, *857*, 308-314.

[35] Liu, Y.; Zeng, X.; Deng, Y.; Wang, L.; Feng, Y.; Yang, L.; Zhou, D. *J. Chromatogr. B* **2009**, *877*, 465-470.

[36] Cabri, W.; D'Acquarica, I.; Simone, P.; Di Iorio, M.; Di Mattia, M.; Gasparrini, F.; Giorgi, F.; Mazzanti, A.; Pierini, M.; Quaglia, M.; Villani, C. *J. Org. Chem.* **2011**, *76*, 1751-1758.

[37] Cabri, W.; Ciogli, A.; D'Acquarica, I.; Simone, P.; Di Iorio, M.; Di Mattia, M.; Gasparrini, F.; Giorgi, F.; Mazzanti, A.; Pierini, M.; Quaglia, M.; Villani, C. *J. Chromatogr. B* **2008**, *875*, 180-191.

[38] International Pharmacopoeia, Monographs for Antimalarial Drugs, 4th Ed., WHO Press: Geneva, **2006**; pp. 215-218.

[39] D'Acquarica, I.; Gasparrini, F.; Pierini, M.; Villani, C.; Zappia, G. *J. Sep. Sci* **2006**, *29*, 1508-1516.

[40] Jackman, L.M.; Cotton F.A. *Dynamic Nuclear Magnetic Resonance Spectroscopy;* Academic Press: New York, NY, USA, 1975

[41] Kaplan, J.I.; Fraenkel, G.; *NMR of Chemically Exchanging Systems;* Academic Press: New York, 1980.

[42] Sandström, J. *Dynamic NMR Spectroscopy*; Academic Press: London, UK, 1982.

[43] Oki, M. *Applications of Dynamic NMR Spectroscopy to Organic Chemistry*; VCH: Deerfield Beach, FL, USA, 1985.

[44] 21. Giddings, J.C. *J. Chromatogr.* **1960**, *3*, 443–453.

[45] Kramer, R. *J. Chromatogr.* **1975**, *107*, 241–252.

[46] Schurig, V.; Burkle, W. *J. Am. Chem. Soc.* **1982**, *104*, 7573–7580.

[47] Burkle, W.; Karfunkel, H.; Schurig, V. *J. Chromatogr.* **1984**, *288*, 1–14.

[48] Jacobson, J.; Melander, W.; Vaisnys, G.; Horváth, C. *J. Phys. Chem.* **1984**, *88*,4536–4542.

[48] Veciana, J.; Crespo, M.I. *Angew. Chem. Int. Ed. Engl.* **1991**, *30*, 74–77.

[49] Jung, M.; Schurig, V. *J. Am. Chem. Soc.* **1992**, *114*, 529–534.

[50] Cabrera, K.; Jung, M.; Fluck, M.; Schurig, V. *J. Chromatogr. A* **1996**, *731*, 315–321.

[51] Oxelbark, J.; Allenmark, S. *J. Chem. Soc. Perkin Trans*. **1999**, *2*, 1587–1589.

[52] Trapp, O.; Schoetz, V.; Schurig, V. *Chirality* **2001**, *13*, 403–414.

[53] Trapp, O.; Schurig, V. *J. Chromatogr. A* **2001**, *911*, 167–175.

[54] Kiesswetter, R.; Brandl, F.; Kastner-Pustet, N.; Mannschreck, A. *Chirality* **2003**, *15*, S40–S49.

[55] Krupcik, J.; Oswald, P.; Májek, P.; Sandra, P.; Armstrong, D.W. *J. Chromatogr. A* **2003**, *1000*, 779–800.

[56] Wolf, C. *Dynamic Stereochemistry of Chiral Compounds—Principles and Applications*; RSC Publishing: Cambridge, UK, 2008.

[57] Trapp, O. *Anal. Chem.* **2006**, *78*, 189–198.

[58] Gasparrini, F.; Lunazzi, L.; Misiti, D.; Villani, C. *Acc. Chem. Res.* **1995**, *28*, 163–170.

[59] Dell'Erba, C.; Gasparrini, F.; Grilli, S.; Lunazzi, L.; Mazzanti, A.; Novi, M.; Pierini, M.; Tavani, C.; Villani, C. *J. Org. Chem.* **2002**, *67*, 1663–1668.

[60] Gasparrini, F.; Grilli, R.; Leardini, L.; Lunazzi, L.; Mazzanti, A.; Nanni, D.; Pierini, M.; Pinamonti, M. *J. Org. Chem.* **2002**, *67*, 3089–3095.

[61] Dalla Cort, A.; Gasparrini, F.; Lunazzi, L.; Mandolini, L.; Mazzanti, A.; Pasquini, C.; Pierini, M.; Rompietti, R.; Schiaffino, L. *J. Org. Chem.* **2005**, *70*, 8877–8883.

[62] Cirilli, R.; Ferretti, R.; La Torre, F.; Secci, D.; Bolasco, A.; Carradori, S.; Pierini, M.

J. Chromatogr. A **2007**, *1172*, 160–169.

[63] D'Acquarica. I.; Gasparrini, F.; Kotoni, D.; Pierini, M.; Villani, C.; Cabri, W.; Di Mattia, M.; Giorgi, F. *Molecules* **2010**, *15*(3), 1309-1332.

Chapter 2

Stereolability of a monoketoaldehyde (MKA) active derivative of Dihydroartemisinin, an antimalarial Drug: a thermodynamic and kinetic study.

2.1 Introduction

In the previous chapter of this PhD thesis, a new HPLC method was presented in order to overcome the shortcomings of the International Pharmacopeia in the analysis of dihydroartemisinin **2** (DHA). The best experimental conditions for the quantitavite determination of both α- and β-DHA through cryo-HPLC were obtained. The combined use of DHPLC and computer simulation of the experimental deformed profiles using lab-made AutoDHPLC y2k software proved helpful in the characterization of the two epimers.

In the past years, our research also focused on products deriving from the degradation of DHA. The peroxide group in the 1,2,4-trioxane ring of artemisinin (**1**) and its derivatives confers them antimalarial activity, but also makes artemisinins more difficult to handle in a drug-development setting compared to other conventional

antimalarial drugs, as it is both a chemically and thermally sensitive group.[1] Starting from the 1980s a long series of scientific publications have studied the decomposition of artemisinin **1** and dihydroartemisinin **2** under a variety of conditions. Artemisinin has been reported to be labile under acidic or basic treatment, but unexpectedly stable in neutral solvents when heated up to 150 °C.[2] However, considerable changes were detected when heating was extended to 190 °C for ten minutes [3], with no prevalent product being formed (isolation yields ranging between 4 and 12%). In contrast, thermolysis of DHA **2** at 190 °C for three minutes produced mainly 2-desoxyartemisinin **3** (Figure 1, 30% yield) and the diketoaldehyde **4** (DKA, Figure 1, 50% yield) as a temperature dependent mixture of stereoisomers, assumed to be epimeric at C-6.[4]

Twenty years later, these same compounds were recovered, albeit with lower yields, by heating solid **2** at 100 °C for 14 h under a nitrogen atmosphere.[5] In this case other minor compounds were observed, such as the already known peroxyhemiacetal **5** (Figure 1, 7% yield) and an hitherto unknown dicarbonyl compound **6** (Figure 1, 2% yield), also independently identified by another research group,[6] and most likely formed by oxidation and subsequent decarboxylation of its putative precursor **4**. Haynes and collaborators reported that

comparable yields were observed when performing the reaction under air. Higher yields of **5** (48%) were obtained by decomposition of **2** under aqueous acidic solution.[6]

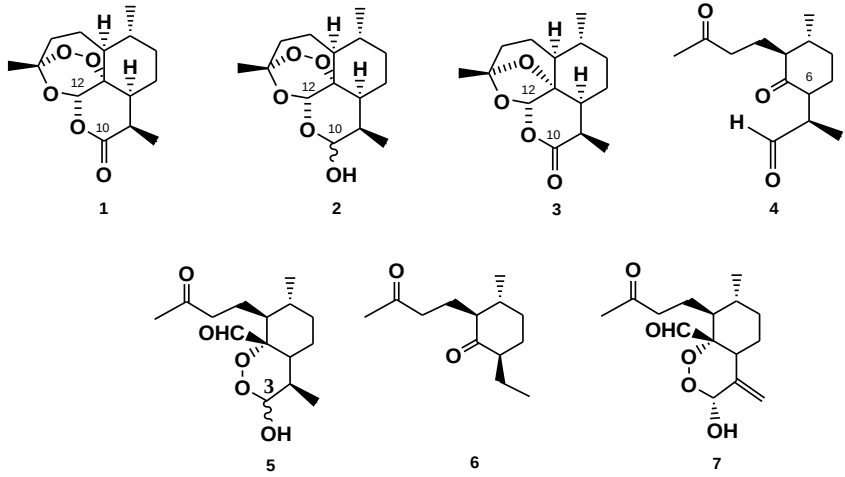

Figure 1. Chemical structures of artemisinin **1**, dihydroartemisinin **2** (DHA), 2-desoxyartemisinin **3**, diketoaldehyde **4** (DKA), monoketo-aldehyde **5** (MKA), a new dicarbonyl compound **6** and an α-MKA-ene **7**, bearing an α configuration in the solid phase.[6]

Peroxyhemiacetal **5** (hereafter named monoketo-aldehyde, MKA, for the presence of one ketone and one aldehyde group in its structure, in contrast with DKA), was isolated for the first time in 1993 by the group of professor Baker through exposure of the ethyl ether analogue of **2** (called β-arteether) to simulated stomach acid, and was

reported to have significant antimalarial activity in an *in vitro* assay (IC_{50} in the 0.99–2.2 ng/ml range). [7] Being a hemiacetal like **2**, MKA was also expected to occur in solution as a mixture of epimers (at position C-3), namely, **5α** and **5β** (Figure 2). In their work, Baker and co-workers compare MKA **5** with a reference compound **7** [8], bearing an olefinic moiety in position C-4. Such compound **7**, has been crystallized and appears to have an α configuration in the solid state. In 1995, Acton and Roth also obtained MKA **5** in a 25 % yield through acid decomposition of both β-arteether and DHA **2**. No further information are present in literature about the configuration of MKA **5** as it has never been crystallized.

We have recently found [9] that the interconversion of the two MKA epimers occurrs on a chromatographic time scale; for this reason, separation of the two interconverting species must be a prerequisite of any analytical method aimed at quantitating the drug in active ingredients, pharmaceutical formulations, and biological fluids. Moreover, the fact that **5** is active *in vitro* on a ng-scale and that it seems to have a lower neurotoxicity when compared to DHA [10], make it a very interesting compound for future pharmaceutical formulations, as such or after appropriate derivatization.

This chapter deals with the isolation and on-column epimerization of **5** at C-3. It provides a thermodynamic and kinetic investigation of the

5α/**5β** equilibration, including their stereochemical implication, which may have great importance in better understanding the metabolism of dihydroartemisinin **2** and in providing the scientific community with a new candidate for malaria treatment. Following a complete characterization of the scarcely investigated structure of MKA, a comprehensive thermodynamic investigation of the epimerization process has been performed by correlating the data obtained through an in-depth linear solvation energy relationships (LSER) analysis with molecular modelling supported by empirical data and NMR measurements. A preliminary study of the epimerization process from a kinetic point of view has also been achieved, determining the activation parameters ($\Delta G^{\#}$, $\Delta H^{\#}$ and $\Delta S^{\#}$) as a function of ionic strength, general and specific acid and base catalysts and temperature in different solvents by dynamic HPLC (DHPLC)*.

Finally, convincing rationalization of the results has been obtained by a synergic integration of experimental and theoretical data.An analogous work was previously performed by our lab on dihydroartemisinin **2** and has been recently published in the *Journal of Organic Chemistry*. [11,12] During my PhD internship, my work focused on obtaining similar information on MKA (**5**) and comparing the final results with those obtained for DHA.

* For a complete list of pubblications on DHPLC see Chapter 1 of Part C.

2.2 Results and Discussion

2.2.1 Preparation of MKA

In our initial studies, dihydroartemisinin **2** was submitted to pyrolysis in order to obtain a series of by-products reported in literature, such as DKA **4** and MKA **5**. Following heating at 120 °C for 1h, a complex mixture was obtained, containing, amongst others, MKA and DKA.

Periodic withdrawals of the reaction mixture were made for the UHPLC monitoring, under reversed-phase (RP) conditions, using a C_{18} Acquity column (100 x 2.1 mm I.D.). The brown mixture obtained was allowed to cool to room temperature and separation was carried out by semi-preparative NP-HPLC, to give MKA **5** as one of the major products (Figure 3). Purification of the reaction mixture proved rather tricky, however, and MKA could not be obtained in high yields (13%, even after repeated semi-preparative HPLC experiments). At this point, a new preparation process was devised: **5** was obtained directly from dihydroartemisinin **2** by adding a catalytic amount of NaOH to a solution of DHA in a water:acetonitrile (30:70; v/v) mixture, at room temperature. Monitoring of the reaction through RP-HPLC, using a Symmetry C_{18} column, allowed us to deduce that after 1h 30 min the reaction came to completeness.

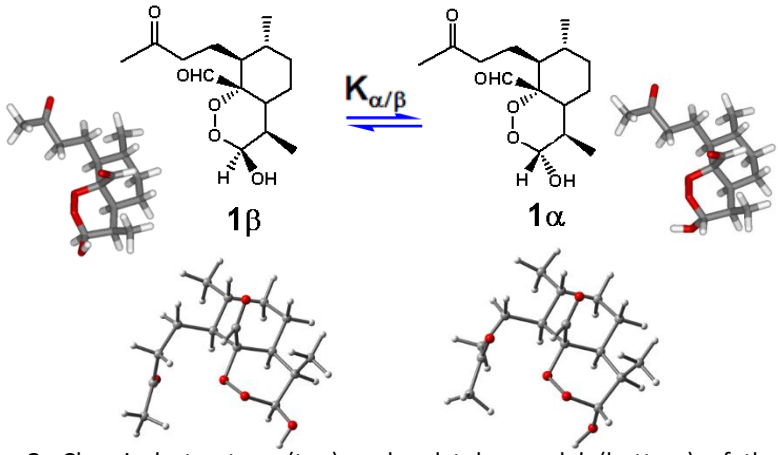

Figure 2. Chemical structure (top) and polytube model (bottom) of the interconverting epimers of **5**: the 5α-epimer bears the hydroxyl group in the axial position, whereas the 5β-epimer possesses an equatorial hydroxyl group. 3D models show the B3LYP/6-31G(d) optimized structures. Polytube models were derived by molecular mechanics optimization (MMFF force field as implemented in SPARTAN '04 1.0.0).

Purification was in this case quite easily obtained through preparative NP-HPLC with a 72 % yield and bearing a higher purity than the one obtained following pyrolysis of DHA **2**. It is worth of note, in this particular case, that MKA did not show any epimerization phenomena in normal phase, on the contrary of what happens with DHA **2**. This was probably due to a low selectivity of the chromatographic system. Once obtained in an almost pure state (95-99% purity), **5** was submitted to reversed-phase HPLC on a 100 × 4.6

mm I.D. Symmetry C_{18} column using a mobile phase made of 10mM NaH_2PO_4/MeCN/MeOH (55/35/10; v/v) with a ${}^{w}_{w}pH$ = 4.76 and a ${}^{s}_{w}pH$ = 5.61 (see experimental section for details). We performed the preliminary chromatographic runs by setting the temperature at *T* = 25 °C. A typical chromatogram obtained is reported in figure 4 (chromatogram on the left), where the UV trace was registered at 214 nm.

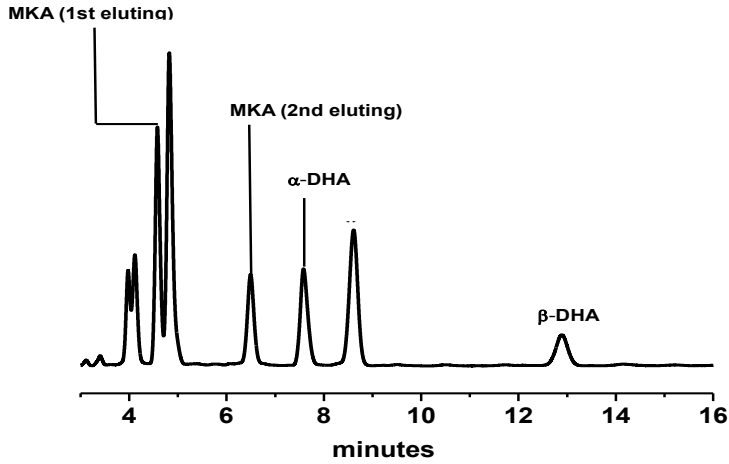

Figure 3. Chromatogram of the mixture obtained after pyrolysis. A C_{18} Acquity UPLC column (100 x 2.1 mm I.D.) was used. Eluent: 10 mM NaH_2PO_4 / MeOH/MeCN (65/5/30); Flow-rate: 0.4 ml/min; *T* = 25 °C. Detection: UV at 214 nm

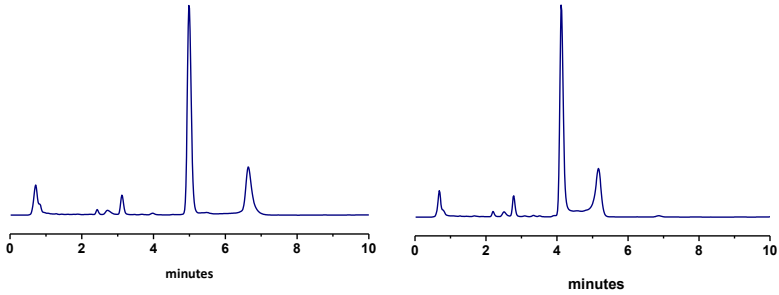

Figure 4. Chromatogram of purified MKA **5**. Column: Symmetry C18, 3.5 µm (100 x 4.6 mm I.D.). Eluent: 10mM NaH_2PO4/MeCN/MeOH (55/35/10; v/v) with a ${}^{w}_{w}pH$ = 4.76 and a ${}^{s}_{w}pH$ = 5.61. Flow: 1.00 ml/min. UV detection at 214 nm. Left: T = 25 °C. Right: T = 50 °C.

As it can be observed, two well resolved chromatographic peaks, corresponding to the two epimers, were obtained, with appealing retention (k'_1 = 5.73, k'_2 = 8.13) selectivity (α = 1.42) and resolution (R_s = 11.9). However, a visible plateau could be observed as the temperature was raised as can be seen in the right chromatogram of figure 4 (T = 50 °C).

At this point a full characterization of compound **5** became fundamental in order to assign the α- and β- configuration to the epimers. ^{1}HNMR and ^{13}CNMR, with special reference to NOE effects, were used to the purpose. Further studies were then needed to better understand the epimerization process.

2.2.2 Characterization of MKA

Compound **5** was fully characterized by comparison between its physico-chemical and spectroscopic properties and identified as a previously described product, obtained by exposure of the ethyl ether analogue of **2** (β-arteether) to simulated stomach acid [7], and, more recently, by heating solid 2 at 100 °C for 14 h under nitrogen[5].

The relative configuration of the two epimers at C-3 was determined by means of NOE spectra, performed in CD_3CN. For NMR assignments see figure 5.

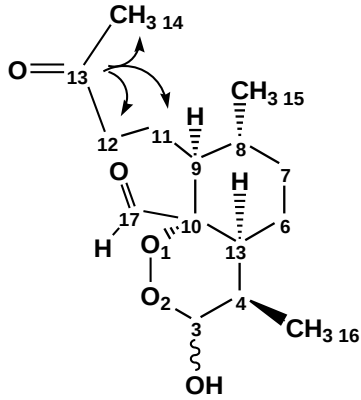

Figure 5. NMR assignments of MKA **5**.

Upon dissolution at 25 °C in acetonitrile and a suitable equilibration time (4h), a 2:1 ratio was observed between the two epimers. On

selective saturation of the minor Me-16 signal (trace b in Figure 6), significant NOE effects are observed only for H-4 and H-5. These signals act as “control” NOEs, since their spatial relationship with Me-16 is the same in both epimers. When the major signal of Me-16 (trace c in Figure 6) is saturated, NOEs are again observed on H-4 and H-5, and an additional strong NOE is observed on H-3. This indicates that in the major isomer the hemiacetalic proton H-3 is close to Me-16. The distance ratio obtained by integration of the experimental NOE intensities of H-3 and H-6 (1.01) matches very well the ratio calculated from the DFT optimized [11] structure (1.00). Analysis of the *J*-coupling in the two hemiacetalic protons H-3 reveals a $J = 2.3$ Hz in the case of the minor epimer, and a $J < 1$ Hz in the case of the major epimer. Starting from the optimized structure, direct DFT calculation of the *J*-couplings [11] of the two epimers yield a *J* coupling of 0.85 Hz for the α epimer, and 2.4 Hz for the β, in good agreement with the experimental values.

These results lead to assign the (*S*)-configuration (hydroxyl in the axial position, thus **5α**) to the C-3 center of MKA in the major isomer, and the (*R*)-configuration at the same carbon atom (hydroxyl in the equatorial position, thus **5β**) to the minor epimer. DFT calculations also indicated that the energies of the two epimers are very similar

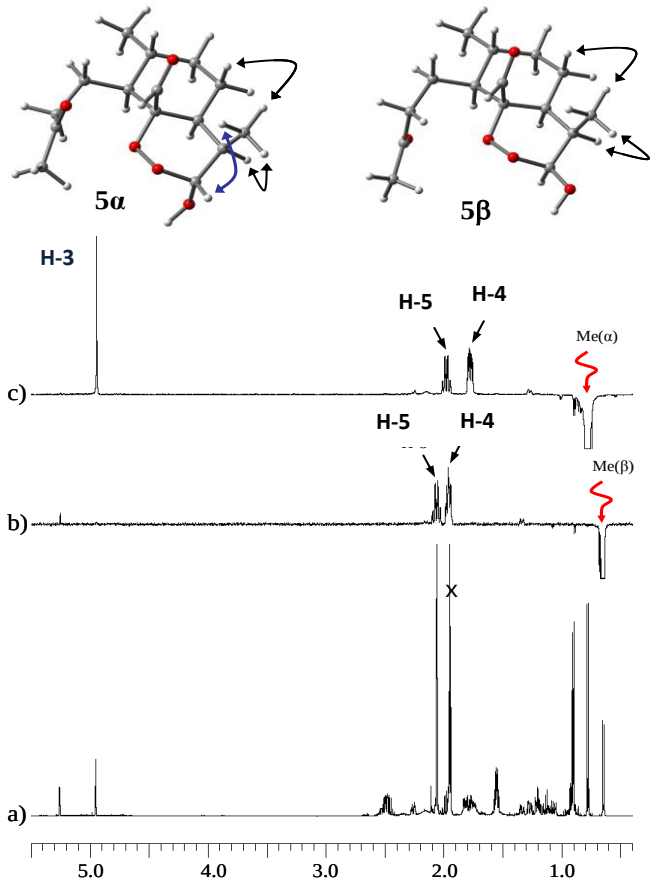

Figure 6. DPFGSE-NOE spectra of the aliphatic region of **5** (600 MHz in CD_3CN at +25 °C). Bottom: ^1H control spectrum. Trace b): NOE spectra obtained on saturation of the Me-16 of the minor epimer. Trace c): NOE spectra obtained on saturation of the Me-16 of the major epimer. The observed NOE are indicated by the arrows in the 3D structures ("control" NOEs in black, diagnostic NOEs in blue)

(being the **5β** less stable by 0.15 kcal/mol), therefore accounting for the ratio observed in solution.

A full characterization of MKA **5** is given in the experimental section, where the IR, NMR and mass spectra are reported together with elemental analysis and optical rotation data.

2.2.3 Determination of the equilibrium constant $K_{\alpha/\beta}$ of MKA in solution

The first experiments on MKA **5** with different solvents such as acetonitrile, water, hydro-organic mixtures, as well as our previous knowledge on DHA **2**, led us to investigate the relative abundance of the **5α** and **5β** epimers in a wide range of pure solvents and hydro-organic mixtures. In order to evaluate the molar ratio [α]/[β] (i.e., the equilibrium constant $K_{\alpha/\beta}$ of the $\beta \rightleftarrows \alpha$ process, see Figure 2), RP-HPLC was used. Further data were obtained by ^{1}HNMR, which was used to obtain the molar ratio between the **5α** and **5β** in those solvents where HPLC was not capable of separating the two epimers of MKA (dichloromethane and chloroform) and those were the solvent noise level interfered with the analysis (DMSO, THF).To conclude, 18 different media were selected within a wide range of permittivity

values (ε ranging between 80.2 and 4.8) to better evaluate the role of the solvent in the equilibrium between the **5α** and **5β** epimers. On the contrary of DHA **2**, where some data were present in literature, no such data were available for MKA, where only some generic observations on the abundance of the **5α** epimer in total absence of solvent could be found in previous publications.[7]

To the purpose, a cryo-HPLC-UV method was set in our lab in order to inhibit on-column epimerization of MKA, which accounts for plateau areas capable of interfering with the peak integration and thus [α]/[β] ratio determination. Following an initial experimental screening of different analytical conditions (including column temperature, buffer and pH variations), the chromatographic set-up was selected. In a previously published work [14], the Catalytic Effect of Stationary Phases (CESP) was defined as the percentage increasing (positive) or decreasing (negative) of the epimerization rate constant, with respect to the analogous value measured in mobile phase (see part C-1 for more details). On the basis of the results obtained for DHA, the Symmetry C_{18} column was selected for its capacity of decreasing the interconversion rate between **2α** and **2β** epimers. The column temperature was set at 5 °C while the mobile phase consisted of a ternary mixture of H_20:MeCN:MeOH (55/35/10; v/v/v), buffered at a ${}^{s}_{w}pH$ = 5.61 (${}^{w}_{w}pH$ = 4.76) with sodium dihydrogen phosphate. It

was, infact, experimentally observed that such pH was advantageous to our analysis (see figure 7). No visible interconversion was registered at this pH even at 25 °C, while at higher pH values ($_w^s pH$ = 8.02 and $_w^s pH$ = 9.38) a consistent plateau area or even coalescence were clearly identified.

Finally, a column temperature of 5 °C and a pH of $_w^s pH$ = 5.61 were selected in order to perform the calculation of the equilibrium constant of MKA in a range of solvents, including water, methanol, acetonitrile and 10 binary mixture of these three solvents (see Tab 1). After dissolution in the various media, MKA was allowed to equilibrate for up to 48 h (the monitoring of the solutions was performed on a regular basis) and was then injected into the column using the conditions described above. We were thus able to obtain the [α]/[β] ratios in 14 different media (see Table 1). However, no data could be obtained on the equilibrium constant through cryo-HPLC-UV in apolar solvents such as tetrahydrofuran, chloroform and dichloromethane because of the lack of separation of the **5α** and **5β** epimers under NP-HPLC conditions.

To overcome this limitation also present in the case of DMSO, where a high noise level was observed, ^{1}HNMR was used. As can be seen in Figure 8 (expansion of the spectrum obtained by dissolving MKA **5** in CD_2Cl_2), the ratio between the integration of the two different signals

obtained for the aldehyde proton was used to calculate $K_{\alpha/\beta}$. The integration of the two signals obtained for Me-16 (see figure 5) was also used, as a control signal.

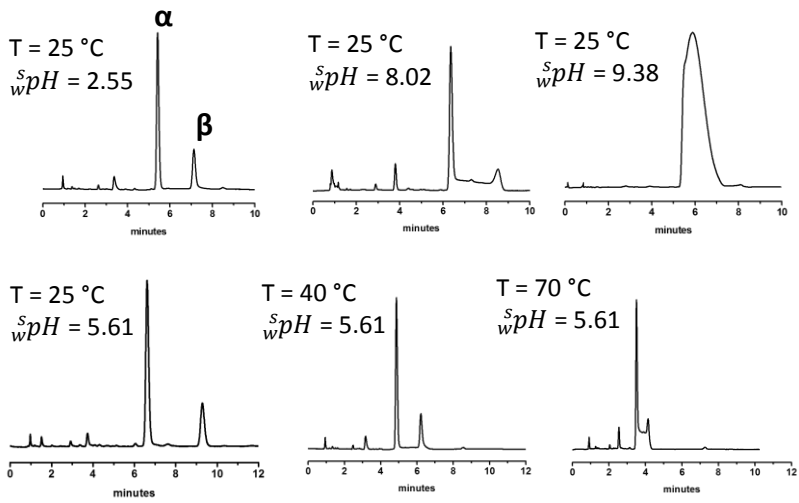

Figure 7. Chromatograms of MKA **5** obtained through D-HPLC at different temperatures and pH values. Column: Symmetry C18, 3.5 µm (100 x 4.6 mm I.D.). Eluent: 10mM NaH_2PO_4/MeCN/MeOH (55/35/10; v/v). Flow: 1.00 ml/min. UV detection at 214 nm.

The complete list of equilibrium constants obtained, together with the activation free energy barrier ($\Delta G^{\#}$) and the permittivity constant of each media is reported in Table 1.

Table 1. Equilibrium constants $K_{\alpha/\beta}$ obtained in 18 selected media and the corresponding free energies. The permittivity values of the solvents are also reported.

	ε	$K_{\alpha/\beta}$	$\Delta G°_{\alpha/\beta}$ (kcal/mol)
H_2O	80.200	4.41	-0.88
10/90 MeOH/H_2O	70.698	4.35	-0.87
10/90 MeCN/H_2O	69.391	4.06	-0.83
30/70 MeOH/ H_2O	56.860	3.70	-0.78
30/70 MeCN/H_2O	56.006	3.08	-0.67
50/50 MeCN/H_2O	48.042	2.70	-059
50/50 MeOH/ H_2O	47.269	2.98	-0.65
DMSO*	46.700	1.60	-0.28
70/30 MeCN/H_2O	42.760	2.15	-0.45
70/30 MeOH/ H_2O	40.230	2.91	-0.63
90/10 MeCN/H_2O	39.001	2.08	-0.43
MeCN	37.500	2.07	-0.43
90/10 MeOH/ H_2O	34.845	2.05	-0.43
MeOH	32.600	1.98	-0.40
EtOH	24.600	1.76	-0.33
CH_2Cl_2*	8.900	2.77	-0.60
THF*	7.600	2.17	-0.46
$CHCl_3$*	4.800	3.35	-0.72

* Obtained through ^{1}HNMR.

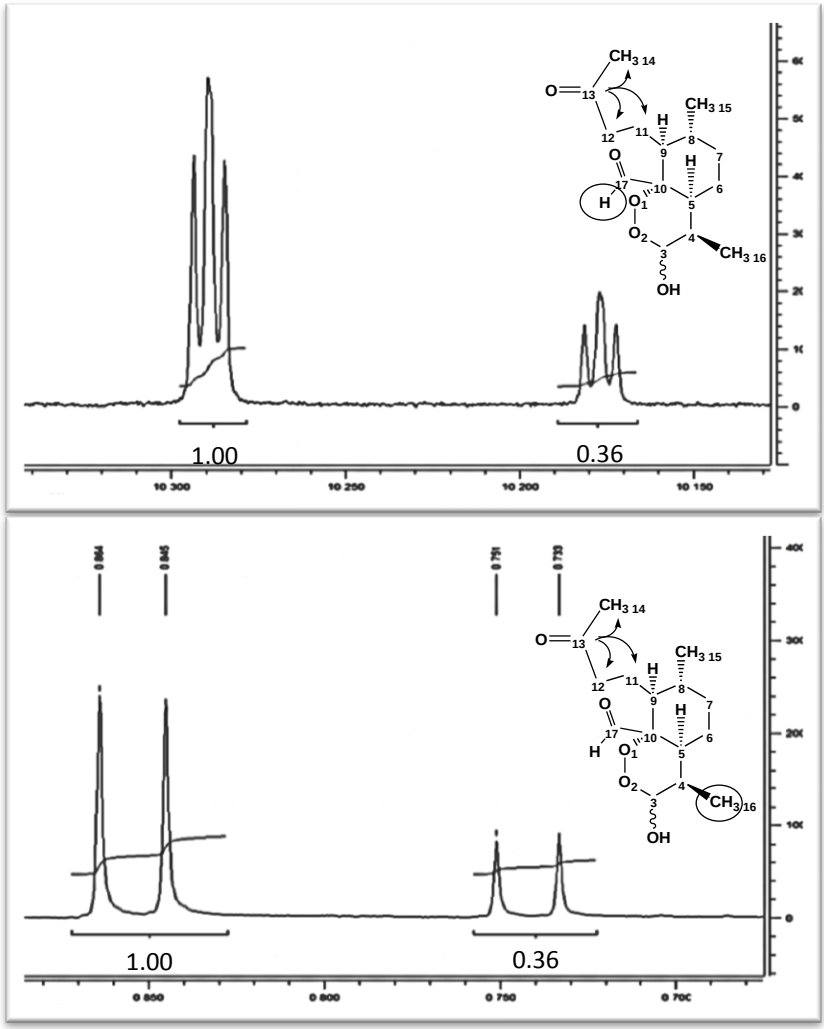

Figure 8. Molar ratio [α]/[β] calculated by integration of the signals obtained for the aldehyde proton H-17 (top) and for the protons of the methyl group C-16 (below). Solvent: CD_2Cl_2

2.2.4. Linear Solvation Energy Relationships (LSER) analysis

To gain insight into the main solute-solvent interactions responsible for the differential solvation of the two epimers, we decided to carry out an in depth linear solvation energy relationships (LSER) analysis. A similar investigation was performed on DHA **2** by our research group and has already been published [11]. In this thesis, a similar investigation performed on MKA will be reported, and the results will be compared to those previously obtained for dihydroartemisinin. As seen in Table 1, the solvents that were chosen, absolute or as a mixture, provide a wide typology of solute-solvent interactions, ranging from specific and non-specific Coulomb interactions to dispersive forces. The explored permittivity range relative to vacuum was very wide (from 80.2 to 4.8) and, among the selected solvents, thirteen were protic due to the presence of water and/or alcohols.

A quite regular permittivity distribution in the considered range was achieved by preparing suitable binary mixtures.

LSER analysis is based on the performance of a linear regression of a set of multiparameter equations, each of which can be expressed by the general formula:

$$^{x}\Delta G^{\circ} = {}^{gas}\Delta G^{\circ} + \sum f_i D_i = {}^{gas}\Delta G^{\circ} + {}^{x}\Delta G^{\circ solv} \qquad \text{(Eq. 1)}$$

where ${}^{x}\Delta G°$ is the change of standard free energy *(ΔG°)* relative to the considered process in solvent *x*, ${}^{gas}\Delta G°$ is the constant obtained by expressing *ΔG°* in absence of solvent, *Di* represents the generic *i* selected descriptor of solvation interactions, and *fi* corresponds to its regression coefficient. Descriptors *Di* are able to selectively monitor the ability of a solvent to interact with solute molecules by non-covalent interactions. The role played by each type of interaction associated to the generic descriptor *Di* is quantitatively expressed by the calculated value of the corresponding coefficient *fi*.

In the LSER study of DHA [11], the authors initially selected the following six *Di* descriptors of solvent effects to be inserted into Eq. 1, where, according to the monitored $\mathbf{2\alpha \rightleftarrows 2\beta}$ equilibrium, ${}^{x}\Delta G°$ corresponds to ${}^{x}\Delta G°_{\alpha/\beta}$: the permittivity ($\varepsilon$) and cohesive pressure (δ^2) of the solvent, and the four solvatochromic parameters ET_{30}, T_N, α (hereafter denoted as α_d), and β (hereafter denoted as β_d). These six descriptors (Table 2), considered in a multiparameter equation, may conveniently monitor different and complementary interactions/ effects arising between solute and solvent molecules, i.e., the capacity of electrostatic shielding of atomic charges (ε), the cavitational energy needed to host the solute molecules inside the solvent (δ^2), the electrostatic forces that, in general, may be

established in both specific and aspecific ways, also including the dispersive ones (ET_{30} and T_N), the solvent lone pair donor capacity (β_d), and the solvent lone pair acceptor capacity (α_d).

Table 2. Descriptors used in LSER analysis.

Descriptors used:	***sensitive to:***
ε	**shielding of charges**
δ^2	**cavitation energy**
ET_{30} and T_N	**establishment of specific and aspecific (dispersive and electrostatic) interactions**
α_d	**establishment of lone pair donation from substrate to solvent**
β_d	**establishment of lone pair donation from solvent to substrate**

The same descriptors used in the LSER study of DHA, were also employed initially in the analogous LSER study of MKA. A first indication as to the capacity of each single descriptor to correlate to the final $\Delta G°_{\alpha/\beta}$ independently is given by the results summarized in Table 3. This preliminary analysis clearly indicates that none of the considered descriptors is capable of monitoring the interactions that mainly contribute in defining the values assumed by $\Delta G°_{\alpha/\beta}$.

Table 3. Correlation between $\Delta G°_{\alpha/\beta}$ and the single descriptors. T is the result of the statistical T-test.

T=2.12	R^2	t_i	*F*
δ^2	**0.5785**	**4.69**	**1.7E-07**
ε	**0.2866**	**2.54**	**5.7E-04**
ET_{30}	**0.2197**	**2.12**	**3.8E-03**
T_N	**0.0596**	**1.01**	**4.7E-01**
α	**0.2922**	**2.57**	**4.8E-04**
β	**0.1684**	**1.80**	**1.8E-02**

In particular, ET_{30} and ε, which in the case of DHA [11] resulted dominant, thus clearly suggesting the decisive role of non-specific Coulomb interactions in the free energy variation of the epimerization, did not prove amongst the most significant parameters in the case of MKA **5**. On the contrary, the most significant descriptor seems to be the Hildebrand parameter, which led us to consider that in the equilibrium formation, the different cavitational value (and also the related differential cavitational energy) needed to host the two epimers in the various solvents was of great importance.

The significant difference between the epimerization processes of DHA **2** and MKA **5** is well described by plots correlating $\Delta G°_{\alpha/\beta}$ to

ε (see Figure 9). In the case of MKA, a series of interactions, significantly different in nature, must take part in the formation of the final $\Delta G°_{\alpha/\beta}$ value. Such interactions tend to prevail on one another passing from very polar, protic or aprotic, to totally apolar solvents with very low (≤9) permittivity values.

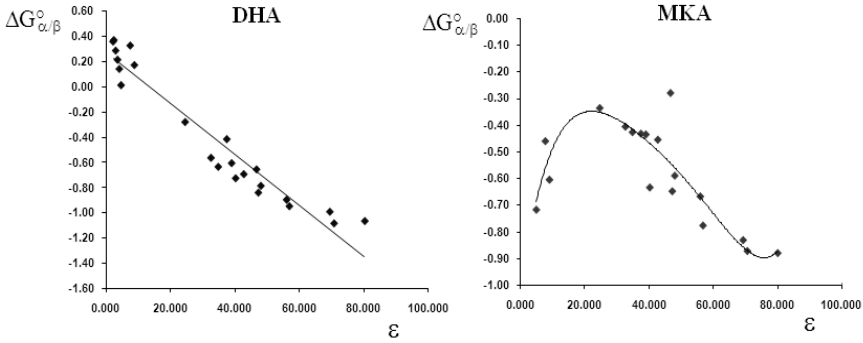

Figure 9. Plots $\Delta G°_{\alpha/\beta}$ vs. ε relative to the epimerization processes of DHA and MKA.

This accounts for the non-linear peak shape of the plot in figure 9 in the case of MKA. On the contrary, DHA has a linear correlation between the permittivity of the medium and the $\Delta G°_{\alpha/\beta}$ value.

Following this preliminary analysis, a more in detail LSER investigation was performed, considering a number of multiparameter equations that would describe the epimerization between **5α** and **5β** of MKA.

Numerous linear combinations of the cited descriptors (δ^2, α_d, β_d, ε, ET_{30} and T_N, values reported in Table 4), from 2 to 6 of them, have been considered, aimed at better understanding which parameters are really crucial in the solvation process, and dissecting the quantitative contribution coming from each relevant kind of interaction. Secondly, the regression results were analyzed according to statistics (F-test and T-test) to reasonably exclude casualness (index F) and to quantify the statistical weight of each used descriptor (index T and factor t_i). Having set at 0.05 the distribution probability of the analyzed data, the T index (calculated through function INV.T in Microsoft Excel 2003) varies between 2.20 (6 descriptors) and 2.13 (2 descriptors).

Equations endowed with all statistically significant descriptors have been selected and summarized in Table 5. Based on such reference, only 12 equations (2 with four descriptors, 4 with three descriptors and 6 with two descriptors) included all significant descriptors (Table 5). In all cases the F index was below 4×10^{-5}. In particular, no equation containing five, as well as the only equation with six descriptors, proved acceptable from a statistical point of view and amongst the 33 equations with 4 descriptors, only two passed the T-test.

Table 4. Thermodynamic ratios ($K_{\alpha/\beta}$) of **5α** and **5β** as function of solvent at 25 °C and values of descriptors used in the LSER analysis.

	$K_{\alpha/\beta}$	$\Delta G°_{\alpha/\beta}$ (kcal/mol)	ε	δ^2	ET_{30}	β	α	S_N^{OH}
H_2O	4.41	-0.88	80.2	552.3	63.1	0.47	1.17	1.00
10/90 MeOH/H_2O	4.35	-0.87	70.7	509.8	62.2	0.49	1.15	0.90
10/90 ACN/H_2O	4.06	-0.83	69.4	499.2	61.5	0.46	1.07	0.86
30/70 MeOH/ H_2O	3.70	-0.78	56.9	429.9	60.0	0.53	1.11	0.68
30/70 ACN/H_2O	3.08	-0.67	56.0	401.0	58.4	0.45	0.88	0.68
50/50 ACN/H_2O	2.70	-059	48.0	313.6	57.1	0.43	0.68	0.55
50/50 MeOH/ H_2O	2.98	-0.65	47.3	356.8	58.3	0.57	1.07	0.55
DMSO	1.60	-0.28	46.7	167.2	45.1	0.76	0.00	0.00
70/30 ACN/H_2O	2.15	-0.45	42.8	237.0	56.8	0.42	0.48	0.46
70/30 MeOH/ H_2O	2.91	-0.63	40.2	290.6	57.1	0.60	1.04	0.42
90/10 ACN/H_2O	2.08	-0.43	39.0	171.0	54.6	0.41	0.29	0.28
ACN	2.07	-0.43	37.5	142.1	45.6	0.40	0.19	0.00
90/10 MeOH/ H_2O	2.05	-0.43	34.8	231.1	56.1	0.64	1.00	0.34
MeOH	1.98	-0.40	32.6	203.9	55.4	0.66	0.98	0.30
EtOH	1.76	-0.33	24.6	166.9	51.9	0.75	0.86	0.21
CH_2Cl_2	2.77	-0.60	8.9	98.6	40.7	0.10	0.13	0.00
THF	2.17	-0.46	7.6	90.6	37.4	0.55	0.00	0.00
$CHCl_3$	3.35	-0.72	4.8	84.8	39.1	0.10	0.20	0.00

Among the two similar descriptors ET_{30} and T_N, the analysis performed clearly pointed out that only the former is important from

a statistical point of view. It was furthermore observed that the best correlation could be, within the same group of equations, by a joint use of β and δ^2.

Table 5. Multiparameter equations employed in the LSER analysis endowed with all statistically significant descriptors.

Entry	ET_{30}	ε	θ_d	δ^2	α_d	*T-index*	*F-index*	R^2
1	**3.83**		**3.59**			**2.13**	**4.0E-05**	**0.5799**
2		**4.32**	**3.73**				**1.0E-05**	**0.6299**
3			**4.60**		**5.24**		**1.0E-06**	**0.7064**
4	**2.87**			**5.29**			**5.0E-07**	**0.7279**
5		**3.53**		**5.61**			**1.2E-07**	**0.7697**
6			**5.75**	**8.93**			**9.5E-10**	**0.8684**
7		**2.25**	**5.33**		**3.17**	**2.14**	**2.7E-06**	**0.7864**
8	**2.47**	**3.13**		**6.95**			**2.6E-07**	**0.8397**
9		**5.14**		**7.13**	**2.98**		**9.7E-08**	**0.8592**
10		**3.88**	**6.07**	**8.23**			**2.6E-10**	**0.9366**
11	**3.56**	**4.69**	**7.26**		**5.41**	**2.16**	**3.3E-07**	**0.8909**
12	**2.44**	**3.96**	**5.91**	**9.64**			**6.8E-10**	**0.9565**

By adding a third descriptor, the multiparameter equation resulted in showing a significant increment in the correlation with the $\Delta G°_{\alpha/\beta}$ value, with R^2 passing from an initial value of 0.8684 (two-parameter equation containing β e δ^2) to 0.9366 after the addition of

the third descriptor, namely permittivity ε, or better still by adding both ε and ET_{30}, with R^2 reaching a maximum value of 0.9565.Noteworthy, little improvements could be obtained by employing the solvent lone pair acceptor capacity (α_d) jointly with β and δ^2. In fact, the four-parameter equation was used combining β, δ^2, ε and α_d achieved a value of R^2 of 0.9402. However, in this case, the t_i factor related to α_d resulted to be only 1.03 (against a *T-index* of 2.16) and the equation was thus considered statistically not significant.

In conclusion, the regressions performed with multi-descriptor equations showed that the best correlations could be obtained with the joined contributions of ε, β_d and δ^2 (i.e. that the most important interactions seem to be the donation of a lone pair from the single epimers to the solvent, the cavitational energy needed to host the solute and, finally, the charge shielding capacity of the solvent), while α_d was statistically inacceptable although capable of improving R^2. It was, at this point, hypothesized that the lone pair doning capacity of the solvent must also play an important role in the final equilibrium position, but that the α_d parameter was unable to describe such contribution in a satisfactory way, while the non-specific descriptor ET_{30} managed to do so in a better way. A more direct investigation of

the α_d values in the different media used in this study, especially in the hydro-organic mixtures, clearly demonstrates their low degree of diversification. In the range between 0 for DMSO and THF and 1.17 for water, a maximum difference of 0.3 units was observed between the various water/alcohol mixtures, which corresponds to a 26 % variation. The consequence of such low degree of diversification is that, although efficient in evaluating the lone pair donor capacity of solvents normally considered aprotic, such as dichloromethane, chloroform or acetonitrile, the α_d descriptor tends to compress the differences between highly protic solvents. Consequently, we explicitly defined to the purpose a new descriptor, named S_N^{OH}, using as molecular probe the organic salt DBUNCE, obtained reacting 2-nitrocyclohexane with 1,8-Diazabicyclo [5.4.0]undec-7-ene in ethyl ether (Figure 10).

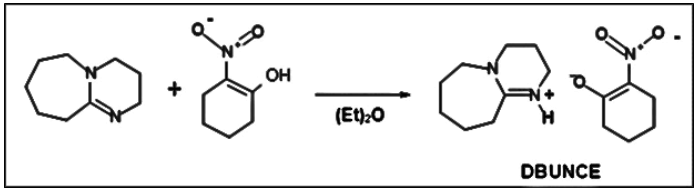

Figure 10. Preparation scheme for organic salt DBUNCE.

We were driven towards 2-nitrocyxlohexane due to its good discriminating behaviour with regards to the solvent lone pair

acceptor capacity when considering the solvatochromic T_N descriptor. On the other hand, DBU was chosen to give to the salt the necessary degree of solubility in a range of solvents as wide as possible, including those typically apolar. A full characterization of DBUNCE, including NMR, UV-vis and ESI-MS, was performed. The UV-vis spectra registered in the solvents reported in Table 6 show an unequivocal absorption slightly above 320 nm attributed to the $n \rightarrow \pi^*$ transition of one of the lone pair belonging to the oxygen atom present in the enolic function, on which the formal negative charge of the anion is localized. The lowest absorption wavelength was registered in *n*-hexane (λ_{max} = 321 nm). Among the aprotic solvents, the maximum quickly increases towards higher values with the increasing of the permittivity of the solvent, while it shows minimum modifications once the ε reaches value 10 (figure 11, red line). In protic solvents, however, λ_{max} increases only slightly up to ε = 20, and later quickly decreases reaching its minimum in water (λ_{max} = 337 nm, Figure 11, blue line).

This behaviour can be explained by considering the previously mentioned $n \rightarrow \pi^*$ transition which accounts for the formation of a more excited state of the salt which is more polar than its

fundamental state, thus more stable in those aprotic solvents which have a higher permittivity value (batochromic shift).

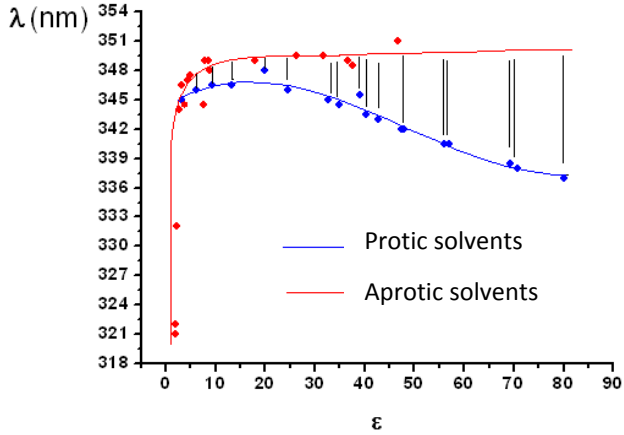

Figure 11. Plot of λ_{max} vs. permittivity values in solvents reported in Table 6.

When the solvent becomes protic, however, the formation of H-bonds between the solvent and the lone pairs of the oxygen in the anionic form of the salt, hinders the n→π* transition and produces an ipsochromic shift. The experimental batochromic shift observed in protic solvents is, in fact, the result of these two contrasting effects.

We can extrapolate the effect caused by the H-bond formation between the solvent and the molecular probe DBUNCE (hereafter named $\Delta\lambda_{max}^{H-bond}$) from the one strictly correlated to the permittivity of the solvent by subtracting from the λ_{max} determined in a protic

Table 6. S_N^{OH} values obtained for a series of protic and aprotic solvents.

	Solvents		ε	λ_{max}	$\Delta\lambda_{max}^{H\text{-bond}}$	S_N^{OH}
Protic	**H_2O**		80.2	337.0	-14.5	**1.00**
	MeOH-H_2O	10_90	70.7	338.0	-13.1	**0.90**
	ACN-H_2O	10_90	69.4	338.5	-12.5	**0.86**
	MeOH-H_2O	30_70	56.9	340.5	-10.0	**0.68**
	ACN-H_2O	30_70	56.0	340.5	-9.9	**0.68**
	ACN-H_2O	50_50	48.0	342.0	-8.1	**0.55**
	MeOH-H_2O	50_50	47.3	342.0	-8.1	**0.55**
	ACN-H_2O	70_30	42.8	343.0	-6.9	**0.46**
	MeOH-H_2O	70_30	40.2	343.5	-6.3	**0.42**
	ACN-H_2O	90_10	39.0	345.5	-4.2	**0.28**
	MeOH-H_2O	90_10	34.8	344.5	-5.0	**0.34**
	MeOH		32.6	345.0	-4.4	**0.30**
	EtOH		24.6	346.0	-3.1	**0.21**
	IPA		19.9	348.0	-0.9	**0.06**
	IPA-*n*-Hexane	70_30	13.2	346.5	-2.1	**0.14**
	IPA-*n*-Hexane	50_50	9.4	346.5	-1.9	**0.13**
	IPA-*n*-Hexane	30_70	6.1	346.0	-1.8	**0.12**
	IPA-*n*-Hexane	10_90	3.2	345.0	-1.1	**0.07**
Aprotic	**DMSO**		46.7	351.5	0.0	**0.00**
	ACN		37.5	348.5	0.0	**0.00**
	DMF		36.7	349.0	0.0	**0.00**
	CH_2Cl_2/DMF	20/80	31.7	349.5	0.0	**0.00**
	CH_2Cl_2/DMF	40/60	26.4	349.5	0.0	**0.00**
	CH_2Cl_2/DMF	70/30	18.0	349.0	0.0	**0.00**
	CH_2Cl_2		8.9	348.0	0.0	**0.00**
	$CHCl_3$/DMSO	90/10	8.5	349.0	0.0	**0.00**
	$CHCl_3$/DMF	90/10	7.9	349.0	0.0	**0.00**
	THF		7.6	344.5	0.0	**0.00**
	$CHCl_3$		4.8	347.5	0.0	**0.00**
	$CHCl_3$-Cyclohexane	90_10	4.4	347.0	0.0	**0.00**
	$CHCl_3$-Cyclohexane	70_30	3.8	344.5	0.0	**0.00**
	$CHCl_3$-Cyclohexane	50_50	3.2	346.5	0.0	**0.00**
	$CHCl_3$-Cyclohexane	30_70	2.7	344.0	0.0	**0.00**
	$CHCl_3$-Cyclohexane	10_90	2.2	332.0	0.0	**0.00**
	C_6H_{12}		2.0	322.0	0.0	**0.00**
	***n*-Hexane**		1.9	321.0	0.0	**0.00**

solvent ($^{p}\lambda_{max}$), the λ_{max} measured in an aprotic solvent having the same permittivity value ($^{a}\lambda_{max}$):

$$\Delta\lambda_{max}^{H-bond} = {}^{p}\lambda_{max} - {}^{a}\lambda_{max} \qquad \text{(Eq. 2)}$$

As it would probably be quite challenging, if not impossible, to find an aprotic solvent which would match in its permittivity value every protic solvent (pure or as a mixture), $^{a}\lambda_{max}$ will be obtained from interpolation on the red plot of figure 11. According to these assumptions, we calculated the $\Delta\lambda_{max}^{H-bond}$ values in all the protic solvent used in the LSER analysis of MKA, and normalized it the $\Delta\lambda_{max}^{H-bond}$ obtained in water, where such value proved higher with respect to the other solvents (see table 6).

$$^{i}S_{N}^{OH} = {}^{i}\Delta\lambda_{max}^{H-bond} / {}^{H2O}\Delta\lambda_{max}^{H-bond} \qquad \text{(Eq. 3)}$$

The S_N^{OH} parameter can be used as an alternative to α_d as it shows a higher degree of differentiation among strongly protic solvents with regards to their ability as lone pair donors. In figure 12 a bar diagram is reported, comparing the α_d and the S_N^{OH} values for the solvents involved in this study.

The new S_N^{OH} descriptor was, at this point, inserted in the LSER analysis, together with the other already described parameters, with the exclusion of T_N that proved unsuitable for the analysis. After the usual statistical tests, it was evident that when S_N^{OH} is used instead of α_d, the quality of the correlation increased sensibly (R^2 = 0.9554, line 2, Table 7), even higher than the correlation obtained in presence of the not so strongly specialized descriptor ET_{30}.

At this point we were able to choose the best multiparameter equation that would successfully describe the single contribution of the difference solute-solvent interactions to the final ${}^{x}\Delta G°_{\alpha/\beta}$ value.

$$ {}^{x}\Delta G°_{\alpha/\beta} = -0.499 + 0.00703\times\varepsilon + 0.477\times\beta - 0.0028\times\delta^2 + 0.400\times S_N^{OH} $$

(Eq. 4)

where 0.499 is the $\Delta G°_{\alpha/\beta}$ in the gas phase. It is noteworthy that all parameters present in equation 4 (ε, β, δ^2 and S_N^{OH}) are highly specialized, allowing an easier dissection of the contributions responsible of the final value of value ${}^{x}\Delta G°_{\alpha/\beta}$.

2.2.5. Discussion of the results of the LSER analysis

In the last paragraph, the multiparameter analysis provided us with the equation which best correlated the single contribution of each solute-solvent interaction in the determination of the $^{x}\Delta G°_{\alpha/\beta}$. At this point the solvent contributions to $^{x}\Delta G°_{\alpha/\beta}$ (i.e., the amount of energetic contribution $^{x}\Delta G°_{\alpha/\beta}{}^{solv}$ that the solvent brings to $^{x}\Delta G°_{\alpha/\beta}$) were accordingly calculated, and are schematically represented in Figure 13.

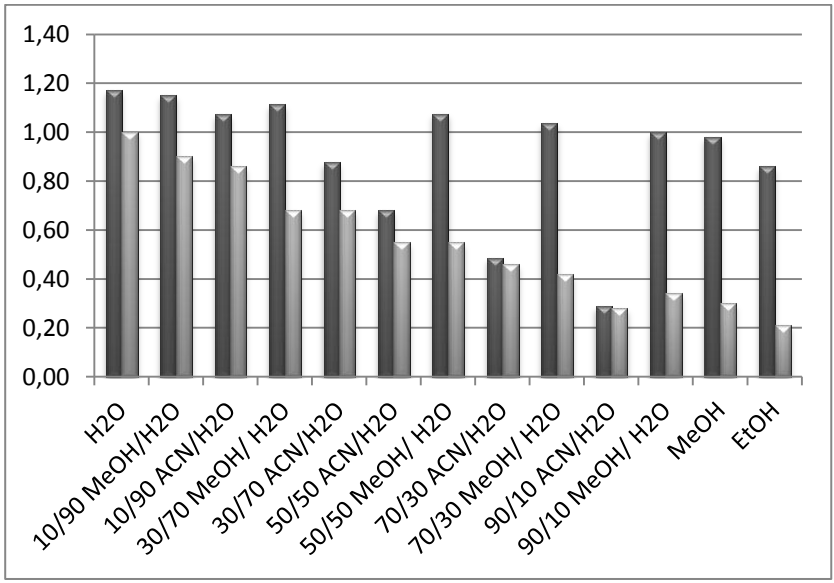

Figure 12. Bar Diagram of the α_d (blue) and S_N^{OH} (red) values for the solvents involved in LSER study.

Inspection of such data revealed that the solvent contribution governs the ${}^{x}\Delta G°_{\alpha/\beta}$ (from 60 to 85% of the total) when permittivity ε becomes greater than about 9, irrespective of the protic or aprotic nature of the medium. For chloroform, the contribution lowers up to 39 %, which indeed is still quite important.

Table 7. Multiparameter equations employed in the LSER analysis endowed with all statistically significant descriptors including S_N^{OH}.

Entry	ET_{30}	ε	β_d	δ^2	α_d	S_N^{OH}	*T-index*	*F-index*	R^2
			f_i coefficients					**Statistical parameters**	
1		5.03	7.49	6.97		2.66	2.16	4.6E-10	0.9590
2	4.49		4.42		3.21	6.26		2.1E-08	0.9270
3	2.71		2.94			5.56	2.14	5.5E-08	0.8692
4			4.37			6.90	2.13	3.2E-08	0.8008
5	4.14					6.35		5.4E-08	0.7887
6		1.59				3.35		1.7E-05	0.6123
7						4.40	2.12	4.4E-07	0.5570

Moreover, it was interesting to consider the algebraic sign of the coefficients associated to the descriptors. In fact, it was noted that the only contribute favourable to the **5α** epimer is the one monitored by δ^2, which is correlated to the smaller molar volume of this isomer when compared to the **5β** epimer of MKA.

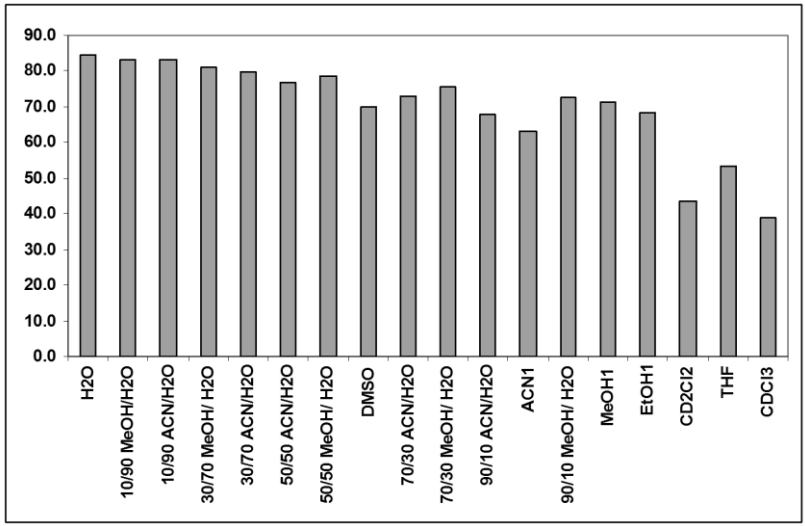

Figure 13. Bar plot of the percentage solvent contribution to ${}^{x}\Delta G^{\circ}_{\alpha/\beta}$

On the other hand, both electrostatic and H-bond interactions were favourable to the β epimer. In particular, the input in favour of the α epimer prevails on the sum of the contributions favourable to the β epimer (ε, β_d and S_N^{OH}) both in the more apolar solvents, such as chloroform and dichloromethane, and in solvents with a very high permittivity (ε > 47). In remaining solvents (9 < ε < 47), the β epimer would be the most abundant, were it not for the ${}^{gas}\Delta G^{\circ}_{\alpha/\beta}$, which prevails on the general contribution of the solvent. The natural conclusion of the interpretation of the LSER analysis is the explanation of the nonlinear plot $\Delta G^{\circ}_{\alpha/\beta}$ vs. ε obtained for MKA seen

in figure 9. In fact, the initial decrement of $\Delta G°_{\alpha/\beta}$, as ε increases from highly apolar solvents to solvents with ε ≈ 25, can be imputed to the concomitant increment of H-bond interactions, with the solvent acting mainly as an acceptor of H-bonds. (descriptor β_d, figure 14).

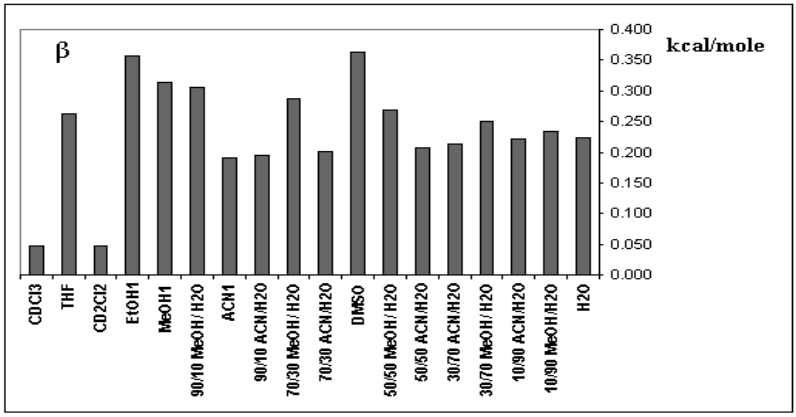

Figure 14. Absolute contributions coming from β_d to $\Delta G°_{\alpha/\beta}$

In these solvents, the cohesion energy monitored by δ^2 has not sufficiently increased to become predominant, and its effects can be contrasted by those favourable to the α epimer (figure 15). As the permittivity value rises above 25, the cavitational energy increases dramatically (descriptor δ^2, 15A) while the other interactions, favourable in this case to the β epimer, increase in a more steady way (combined effect of ε, β, and S_N^{OH}, figure 15A). The plot diagram of

figure 15B clearly reflects the profile obtained in figure 9. The same final results can also be more clearly understood by looking at figure 16, where the various contributions of solute-solvent interactions are reported as a mediated value within three different groups of solvents.

The so far examined solvents can, in fact, be divided into three groups:

Group 1: with a permittivity value lower than 9.

Group 2: with a permittivity value ranging between 9 and 47.

Group 3: with a permittivity value higher than 47.

From a strictly quantitative point of view, the analysis suggests that the cavitational effects are responsible in a 53% degree for the final value of $\Delta G°_{\alpha/\beta}$, with H-bond formation responsible in a 28% degree (19 % coming from interactions where the solvent acts as a donor of a lone pair to the solute and 9 % from interactions where the solvent is the acceptor of the lone pair deriving from the solute) and the remaining 19% coming from pure electrostatic interactions. These percentages do not change dramatically if, instead of the entire range of solvents, we consider each one of the three groups alone.

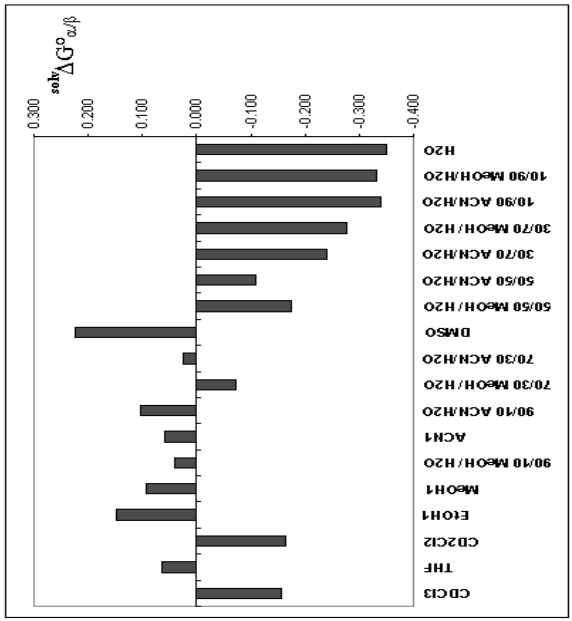

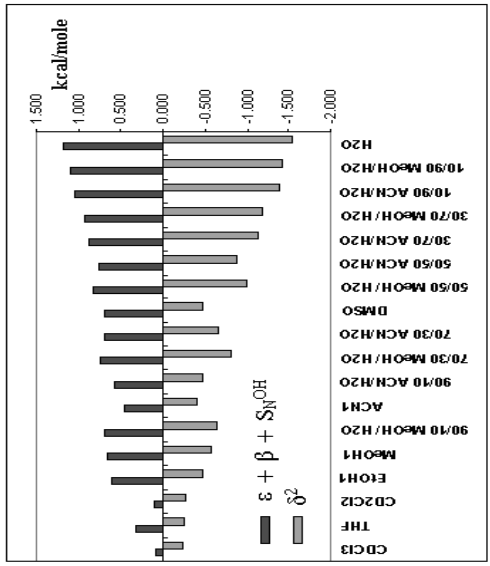

Figure 15. (A) Absolute contributions coming from the sum of ε, β_d and S_N^{OH} to $\Delta G^{\circ}_{\alpha/\beta}$ vs. δ^2. (B) Absolute contributions coming from all four interactions in the different solvents.

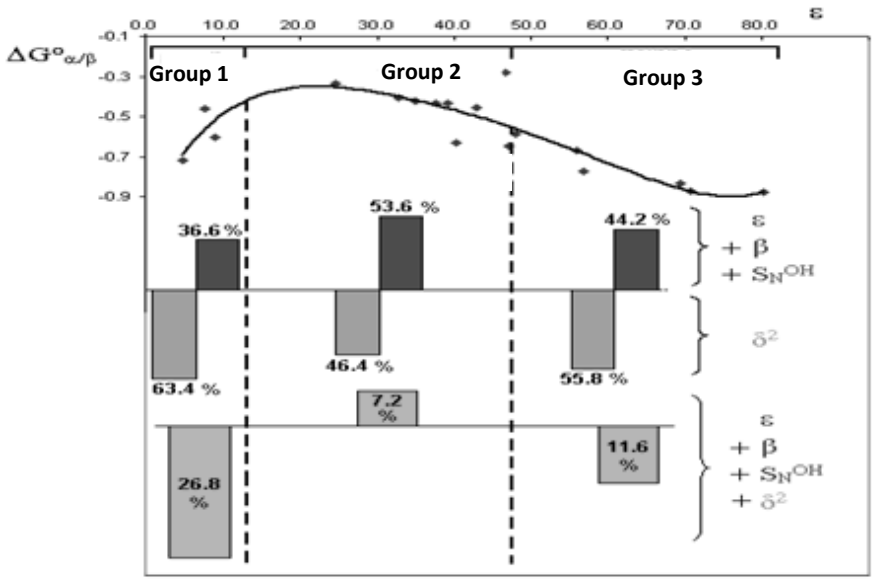

Figure 16. Percentage contributions coming from the four interactions considered (δ^2, ε, β, and S_N^{OH}) in the three groups of solvents investigated.

In comparing these results with the ones previously obtained in our lab for DHA **2** [11], it can be concluded that in the case of MKA **5**, the differentiation between epimers strongly depends on cavitational effects and differential acidity, while dispersive interactions do not seem to be important, as was the case with dihydroartemisinin **2**. This means that, in all the solvents, the thermodynamic position of epimerization must be significantly affected by a different acidity of the hemiacetal hydroxyl groups of **5α** and **5β**, and such effect must

be even more consistent that in the case of the **2α** and **2β** epimers of DHA. Such an interesting indication prompted us to investigate the acidity of **5α** and **5β** epimers through molecular modeling calculations.

Table 8. Percentage contributions coming from the four interactions considered (δ^2, ε, β, and S_N^{OH}) in the three groups of solvents investigated.

Groups of solvents	**Permittivity Interval**	**% of effect monitored by:**		
		$\delta^{[2]}$	**β + S_N^{OH}**	**ε**
Group 1	ε<9	55.8	24.5	19.7
Group 2	9<ε<47	46.4	31.2	22.4
Group 3	ε>47	63.4	24.5	12.1

2.2.6. Stability and acidity of the 5α and 5β epimers of MKA

The **5α** and **5β** MKA epimers were investigated using a theoretical approach apt to evaluate eventual differences between them in terms of dipolarity, molar volume and acidity. Due to the presence in the structure of **5** of an alkyl-ketonic moiety bearing a certain flexibility, it proved necessary to analyze the geometry of the two epimers using a conformational analysis, based on molecular

mechanics (force field: FFMM94, as implemented in Spartan '04). The analysis at 25 °C allowed us to obtain two conformations for the **5α** epimer, of comparable stability and representative for more than 90% of the entire Boltzmann population. Two other conformations were obtained for the **5β** epimer, in this case of different stability (relative abundances of about 79% and 8%, respectively), which represent 87 % of the entire Boltzmann population. These four structures have been further optimized, both on an *ab initio* level (HF-3-21G(*)) and using DFT, evaluating their energies both *in vacuum* and in water. The respective geometries, as well as relative energies in water and dipolar moments are reported in figure 17. The results obtained are quite similar to the experimental data on the stability in water (experimental value: $\Delta G°_{\alpha/\beta}$= -0.88; calculated value using HF-3-21G(*): $\Delta H_{\alpha/\beta}$= -0.84). Calculation of the dipolar moment in water yielded a significantly higher value for the β epimer, as the LSER analysis already hinted to. This explains the higher degree of stabilization observed in favour of the β epimer in solvents with higher permittivity values. Further confirmation of the interpretation of the data obtained using LSER analysis was provided by an approximate estimation of the molar volumes of the two epimers.

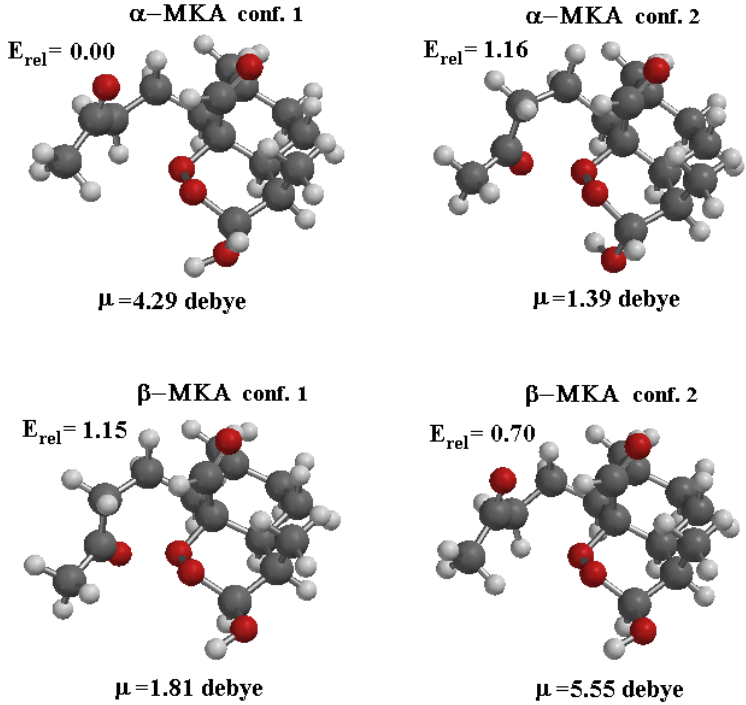

Figure 17. Four most stable conformations of the **5α** and the **5β** epimers of MKA.

The **5α** epimer was calculated to have a 1.6 cm^3/mol lower molar volume when compared to the **5β** epimer (calculated using the QSAR calculation module implemented in HyperChem Professional Release 7.5), again confirming the hypothesis that the only factor favourable to the **5α** epimer is cavitational energy.

Finally, the differential acidity of the two epimers was calculated using a multiparameter equation, based on values of atomic charge density, used as molecular descriptors of acidity. These values were expressly derived to allow the effective estimations of acidity of hemicetals and hemiketals [11]. The charge density on the hydroxyl group and on the vicinal atoms of **5α** and **5β** calculated according to the Mulliken approach at the HF-3-21G(*) level of theory, were inserted within the above multiparameter equation affording a pKa of 11.62 and 11.57 to the **5α** and the **5β** epimer, respectively. This difference, however, is too small (lower than the experimental error range) to be significant. For this reason, we decided to carry out further estimations of the differential acidity of the MKA epimers. To the purpose, we resorted to classical molecular modelling calculations, by assessing the thermodynamic stability of all the involved species in the ionization equilibria of **5α** and **5β**.

DFT calculations (GGA:BLYP/QZ4P large core, solvation by COSMO) resulted in a $\Delta pKa_{\alpha-\beta}$ value ranging between 2.35 (by taking into account the entropic effects and using ΔG) and 2.53 (by using ΔH and not considering entropic effects). The complete set of results of DFT calculations is reported in table 9. All data are in complete agreement with LSER analysis.

Table 9. Results of DFT calculations.

*DFT calculations**	*Calculated Values*
$^{H20}\Delta H_{\alpha-\beta}$ (Kcal*mol^{-1})	**-0.49**
$^{H20}\Delta G_{\alpha-\beta}$ (Kcal*mol^{-1})	**-0.38**
$^{gas}\Delta H_{\alpha-\beta}$ (Kcal*mol^{-1})	**-0.70**
$^{gas}\Delta G_{\alpha-\beta}$ (Kcal*mol^{-1})	**-0.84**
$^{H20}\Delta \mu_{\alpha-\beta}$ (Debye)	**-0.98**
$^{H20}\Delta Vm_{\alpha-\beta}$ (cm^3*mol^{-1})	**-1.60**
$\Delta pKa_{\alpha-\beta}$ (from ΔH)	**2.53**
$\Delta pKa_{\alpha-\beta}$ (from ΔG)	**2.35**

***** GGA:BLYP/QZ4P large core, solvation by COSMO

2.2.7. Kinetic investigation of the epimerization of MKA

In the past paragraphs, a comprehensive description of the thermodynamic aspects involved in the differential stabilization of the two epimers was provided. The results obtained have provided interesting information on the process; to reach a more complete knowledge of the epimerization phenomena taking place, a kinetic investigation is needed. In this thesis a preliminary study is presented. At present, all experimental data are available and in the near future

an adequate rationalization will be operated, providing material for a second publication on the stereodynamic investigations of MKA.

Owing to the biological activity of MKA **5** and its correlation with DHA **2**, it is, in fact, particularly significant to investigate the kinetic features of the **5**α⇄**5**β interconversion in aqueous media, which can be assimilated to biological fluids. Thus, we studied the epimerization in aqueous-organic mixtures as a function of both apparent pH and temperature, and measured the relevant forward and backward rate constants by DHPLC. Chromatographic conditions were selected in order to achieve the best simulation of the relevant dynamic chromatograms with the lower associated error.[14,15]. All the DHPLC experiments were carried out with a ternary mobile phase consisting of Water-Acetonitrile-Methanol 55:35:10 (v/v/v) (hereafter denoted as WAM solution), at controlled temperatures in a range between 10 and 80 °C. Solutions of **5** in mobile phase were buffered or not to apparent pH values (pH was measured in the ternary hydro-organic mixtures, while the electrode system was calibrated with aqueous standard buffers) ranging from 2.6 to 9.4 using 10 mM sodium phosphate. In figure 19 are reported examples of chromatograms (obtained using a non-buffered mobile phase) superimposed with the relevant simulated traces obtained using AutoDHPLCy2k. [16-21] Superimposed chromatograms of DHA **2**,

obtained under the same conditions, are reported in Figure 20 for comparison purposes. It can be clearly seen that the kinetic constants and the free energy activation barriers are different for the two compounds.

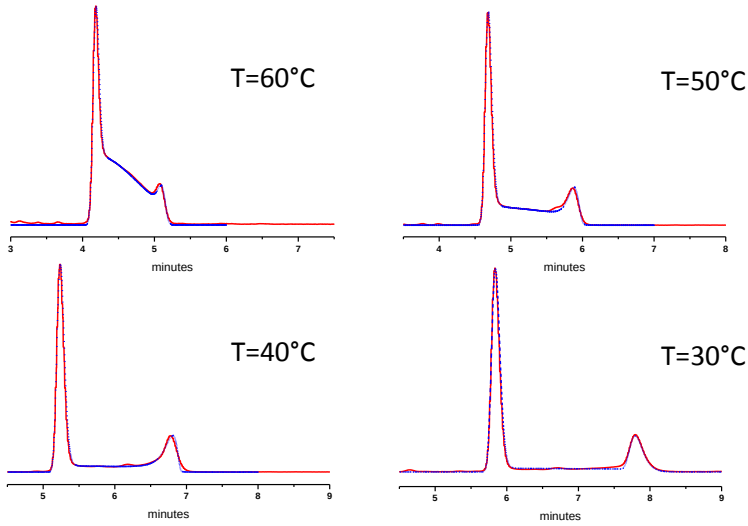

Figure 19. Superimposed experimental (red line) and simulated (blue line) dynamic chromatograms of **5** dissolved in mobile phase. Column: C18 Symmetry, 3.5 µm (75 × 4.6 mm I.D.). Eluent: water-acetonitrile-methanol 55:35:10 (v/v/v) + 10 mM NaH_2PO_4. ($^{s}_{w}pH = 6.95$). Flow-rate: 1.0 ml/min. Detection: UV at 214 nm.

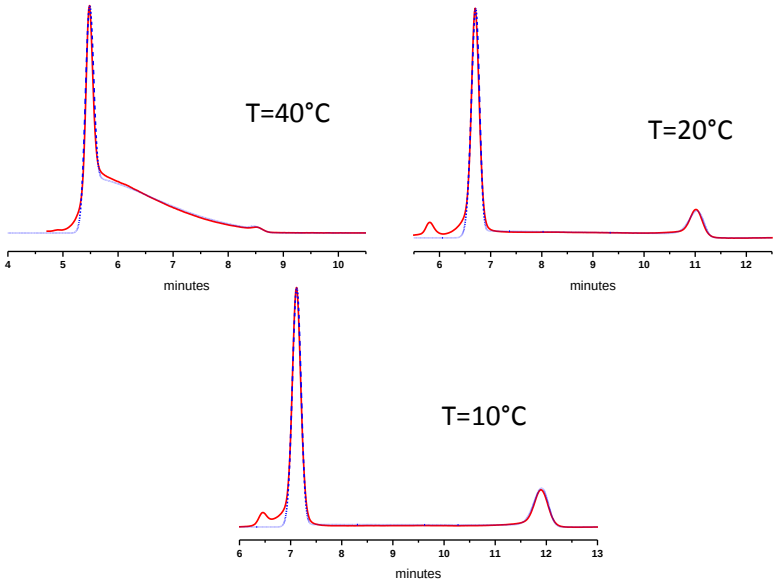

Figure 20. Superimposed experimental (*red line*) and simulated (*blue line*) dynamic chromatograms of DHA **2** dissolved in mobile phase. Column: C18 Symmetry, 3.5 µm (75 × 4.6 mm I.D.). Eluent: water-acetonitrile-methanol 55:35:10 (v/v/v) + 10 mM NaH_2PO_4. ($^{s}_{w}pH = 6.87$). Flow-rate: 1.0 ml/min. Detection: UV at 214 nm.

The measured first-order rate constants for the forward ($k_{\beta\rightarrow\alpha}$) and backward ($k_{\alpha\rightarrow\beta}$) interconversions are reported in Figure 21, whereas the corresponding free energy activation barriers have been calculated by the Eyring equation and are summarized in Table 10. In Figure 22 and Table 11 are reported the most relevant results obtained for dihydroartemisinin **2** under the same experimental

conditions. All simulations of dynamic chromatograms were performed using the classical stochastic mode, as implemented in AutoDHPLCy2k.[20] The same model was also used to calculate the rate contants for the forward and the backward epimerization processes.

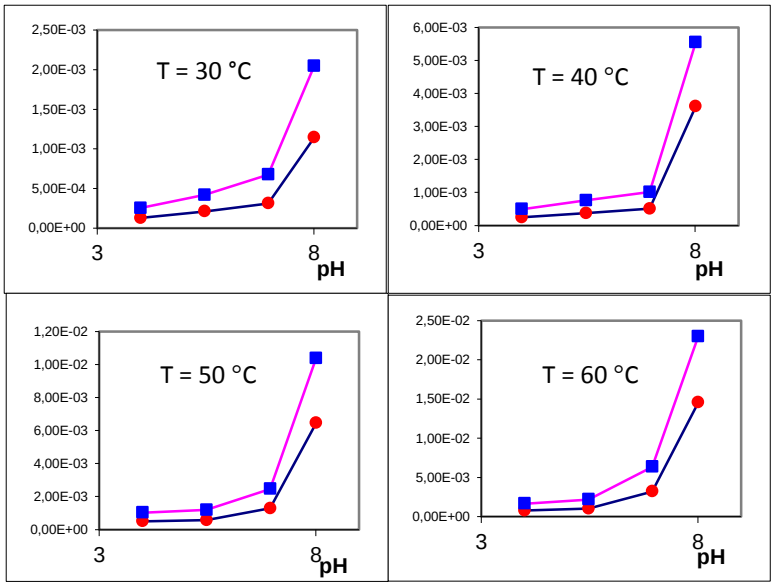

Figure 21. Rate-pH profiles of the **5β→5α** epimerization (*blue points*) and the **5α→5β** epimerization (*red points*) as a function of temperature, in the 30–60 °C range.

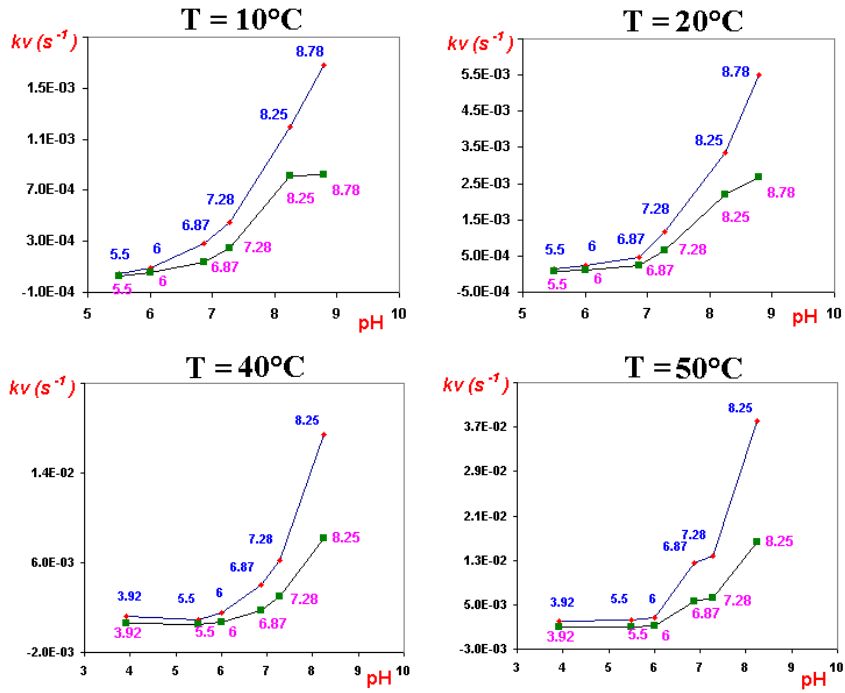

Figure 22. Rate-pH profiles of the **2β→2α** epimerization (*red points*) and the **2α→2β** epimerization (*blue points*) as a function of temperature, in the 10–50 °C range.

In a previous study on DHA performed in our lab [12], an in-depth study of the kinetic and mechanistic features of the **2α/2β** equilibration was found to be sensitive to both acids and bases, although the specific base-catalysis was demonstrated to be

much more effective than the specific acid one, as well as more influent than the corresponding general catalysis in the analyzed buffered ternary mixture. Instead, acid-catalysis by both specific and general species (H_3PO_4) showed to be of quite similar efficiency and dominant at pH < 4.5.

Table 10. $\Delta G^{\#}$ of activation of the **5α→5β** (*top*) interconversion and the **5β→5α** interconversion (*bottom*).

		5α→ 5β		$\Delta G^{\#}$ (kcal/mol)
T (°C)	pH 4.00	pH 5.48	pH 6.95	pH 8.01
10	23.5	23.1	23.3	22.2
20	22.9	22.6	22.5	21.8
30	22.8	22.5	22.2	21.5
40	22.4	22.1	21.9	20.8
50	22.0	21.9	21.4	20.4
60	21.7	21.5	20.9	20.0
70	21.3	21.2	20.4	19.5
80	20.8	20.9	20.0	19.0
		5β→5α		$\Delta G^{\#}$ (kcal/mol)
T (°C)	pH 4.00	pH 5.48	pH 6.95	pH 8.01
10	23.1	22.7	22.8	21.9
20	22.6	22.2	22.1	21.5
30	22.4	22.1	21.8	21.1
40	22.0	21.7	21.5	20.5
50	21.5	21.4	21.0	20.2
60	21.2	21.1	20.4	19.7
70	20.8	20.7	20.1	19.2
80	20.4	20.4	19.6	18.7

It was also found that the observed **2α/2β** concentration ratio has entropic origin, and this was related to a differential solvation of the transition states in the rate-limiting step of proton transfer, which, in turn, is induced by the different acidity of **2α** and **2β**. [12]

When considering the epimerization process **5β⇄5α** in comparison with the one involving DHA (*i.e.* **2β⇄2α**), we can clearly deduce that, at all the considered pH values, the dependence on the temperature of the stereolability is the opposite for the two species (see Figures 21 and 22, as well as Tables 10 and 11). This points to a different mechanism governing the stereomutation, involving a positive variation of entropy in the epimerization process of MKA and a negative one in the one of DHA. More precise indications about the **5β⇄5α** epimerization process, will require a much more extensive elaboration of the dynamic chromatograms already collected at different values of temperature and pH, as well as the conduction of calculations specifically aimed at better understanding the issue.

Table 11. $\Delta G^{\#}$ of activation of the **2α→2β** (*top*) interconversion and the **2β→2α** interconversion (*bottom*).

α-DHA→β-DHA							$\Delta G^{\#}$ (kcal/mol)
T °C	pH 3.92	pH 5.50	pH 6.00	pH 6.87	pH 7.28	pH 8.25	pH 8.78
10		22.49	22.11	21.56	21.22	20.55	20.54
20		22.71	22.42	22.04	21.43	20.72	20.60
30		22.96		22.16			
40	23.01	23.15	22.86	22.30	21.99	21.36	
50	23.45	23.39	23.27	22.30	22.23	21.61	
60		23.59					
70		23.87					
β-DHA→α-DHA							$\Delta G^{\#}$ (kcal/mol)
T °C	pH 3.92	pH 5.50	pH 6.00	pH 6.87	pH 7.28	pH 8.25	pH 8.78
10		22.12	21.76	21.15	20.89	20.33	20.14
20		22.31	22.03	21.61	21.08	20.47	20.18
30		22.53		21.69			
40	22.55	22.69	22.39	21.80	21.52	20.88	
50	22.96	22.90	22.77	21.78	21.72	21.07	
60		23.07					
70		23.33					

2.3 Conclusions

Part of this PhD thesis was conceived to achieve a deeper understanding of the thermodynamics and kinetics of the **5α/5β**

equilibration, by both experimental and theoretical approaches. MKA is a scarcely known metabolite of DHA, which has been obtained following pyrolysis or acidic treatment of DHA. Few literature data are available on this active and seemingly less toxic degradation product of **2**. In this work, we provide a full characterization of **5** by NMR, IR, Elemental analysis, ESI-MS.

A new and facile preparation technique through basic decomposition of DHA has been used to obtain pure MKA in high yields. The **5α/5β** epimerization process has been thoroughly studied from a thermodynamic point of view. By LSER analysis, it was elucidated that the ratio of the **5α** and **5β** epimers in different media is strictly related to three properties of the solvent: (*i*) the permittivity, which modulates the formation of aspecific electrostatic solute-solvent interactions, (*ii*) the cohesive pressure, which influences the cavitational energy needed to host the solute inside the solvent, and (*iii*) the capacity to establish H-bonds with the solute. In particular, it can be concluded that in the case of **5**, the differentiation between epimers strongly depends on cavitational effects and differential acidity, while dispersive interactions do not seem to be important, as was the case with dihydroartemisinin **2**. It was concluded that the only contribute favourable to the **5α** epimer is the one that monitors cavitational effects. This contribute is correlated to the smaller molar

volume of the **5α** isomer when compared to the **5β** epimer of MKA. On the other hand, both electrostatic and H-bond formation where favourable to the **β** epimer. In particular, the input in favour of the α epimer prevails on the sum of the contributions favourable to the β epimer (ε, β_d and S_N^{OH}) both in the more apolar solvents, such as chloroform and dichloromethane, and in solvents with a very high permittivity (ε > 47). In remaining solvents (9 < ε < 47), the β epimer would be the most abundant, were it not for the $^{gas}\Delta G°_{\alpha/\beta}$, which prevails on the general contribution of the solvent. This means that, in all the solvents, the thermodynamic position of epimerization must be significantly affected by a different acidity of the hemiacetal hydroxyl groups of **5α** and **5β**, and such effect must be even more consistent that in the case of the **2α** and **2β** epimers of DHA. In fact, both *ab initio* and DFT studies were performed to evaluate the differential acidity of the two MKA epimers, which resulted sensibly higher than the one observed for DHA.

Finally, we introduced a new descriptor S_N^{OH} capable of better differentiating among solvents with high permittivity values when considering the solvent lone pair acceptor capacity (traditionally monitored using α_d). Especially for hydro-organic mixtures, in fact, the α_d descriptor was not able to fully discriminate among different

solvents. Consequently, we explicitly defined to the purpose S_N^{OH}, using as molecular probe the organic salt DBUNCE, obtained reacting 2-nitrocyclohexane with 1,8-Diazabicyclo [5.4.0]undec-7-ene in ethyl ether. These results are to be the subject of a paper for *J. Org. Chem.*, now in course in preparation. Preliminary kinetic studies have also been performed on the **5α⇆5β** process. The effects of solvent, pH, ionic strength and temperature on the rate of the event, as well as of unattended details on the involved mechanism of epimerization are now being elucidated through *ad hoc* calculations and will be the subject of another future publication.

We believe that the present results on the stereolability of **5** may contribute to shed some light on the mechanism of action and/or bioavailability of the drug at molecular level, and, together with the already published results on DHA, represent a promising starting point for future studies and rational design of semi-synthetic artemisinin derivatives.

2.4 Experimental Section

2.4.1 Apparatus

Analytical liquid chromatography was performed using an HPLC separation module coupled with a Photodiode Array Detector. Chromatographic data were collected and processed using Empower2 software. Variable temperature HPLC (DHPLC) was performed by using a lab-made thermally insulated container cooled by the expansion of liquid carbon dioxide (CO_2). Flow of liquid CO_2 and column temperature were regulated by a solenoid valve, thermocouple, and electric controller. Temperature variations after thermal equilibration were within ± 0.2 °C.

Semi-preparative LC separations were carried out on a Waters Delta Prep 3000 chromatographic system, equipped with a Rheodyne Model 7010-5 ml loop injector, and a differential refractometer (RI) detector. All DHPLC experiments were performed on a C18 Symmetry, 3.5 µm (75 × 4.6 mm I.D.) column, with different binary and ternary hydro-organic mobile phases delivered at 1.0 ml/min and UV detection at 214 nm.

2.4.2 Preparation of MKA

Dihydroartemisinin (DHA, **2**) samples were supplied by sigma-tau S.p.A., Pomezia (Italy). Monoketo-aldehyde (MKA, **5**) was obtained in two different ways: by thermal degradation of **2** or by basic rearrangement of **2**.

Thermal Degradation: A screw-cap vial containing crystalline 2 (1.0 g; 3.5 mmol) was placed in an aluminum block pre-heated to 120 °C and left for 1h. Periodic withdrawals of the reaction mixture were made for the HPLC monitoring, under the following normal-phase conditions: column Reprosil Si 120, 3 µm (150 × 4.6 mm I.D.), *n*-hexane-ethanol 95:5 (v/v), flow-rate 1.0 ml/min, and UV detection at 214 nm. An evaporative light scattering detection (ELSD) system was also used (P = 45 psi; T = 45 °C; spray gun scale: 70%; gain = 9). The brown pyrolysate obtained (0.82 g) was allowed to cool to room temperature and dissolved in 10 ml of *n*-hexane-ethanol-dichloromethane 72:8:20 (v/v/v). Afterwards, it was submitted to semi-preparative HPLC, under the following normal-phase conditions: *n*-hexane-ethanol 95:5 (v/v), flow-rate 20.0 ml/min, and UV detection at 220 nm. A further purification of the last eluting fraction (0.11 g) gave MKA (**5**) as one major product (13%, 99% purity). An axially compressed column (500 × 20 mm I.D.) packed with LiChrosorb Si

100, 10 µm silica gel was used for the purification of the brown pyrolysate.

Rearrangement of DHA under basic conditions: To 42 ml of a MeCN/H_20 (70/30) mixture were added 0.351 g of pure crystallized DHA at room temperature. A catalytic amount of NaOH was then added (concentration in the final solution = 2 mM) and the reaction was complete after 1.5h. Reversed-phase HPLC was used to monitor the reaction. RP-HPLC was performed on a C18 Symmetry, 3.5 µm (100 × 4.6 mm I.D.) column, with a mobile phase composed of water-acetonitrile-methanol 55:35:10 (v/v/v) buffered using 10 mM sodium phosphate ($^{w}_{w}pH$ = 4.76; $^{s}_{w}pH$ = 5.61) delivered at 1.0 ml/min, and UV detection at 214 nm (*T* = 5 °C). The mixture was diluted with water, extracted with CH_2Cl_2 (3 × 60 ml), dried over anhydrous Na_2SO_4, filtered, and concentrated *in vacuo*. We obtained 0.322 g of a pale yellow oil. Afterwards 0.245 g of the crude oil obtained were dissoluted in a mixture of 4.75 ml of *n*-hexane, 0.25 ml of EtOH and 0.4 ml of dichloromethane (conc = 45 mg/ml) and were purified by NP preparative chromatography, obtaining 0.18 g of pure MKA. Yield = 72%; 99 % purity.

All solvents, both analytical and HPLC grade, as well as Na_2SO_4, Na_2HPO_4, NaH_2PO_4, H_3PO_4 and NaOH were acquired by Sigma Aldrich (Milano, Italy).

2.4.3 NMR Measurements

NMR spectra were recorded in CD_3CN at T = 25 °C on a Varian INOVA 600 MHz spectrometer equipped with a triple resonance indirect probe. The standard pulse sequence and phase cycling were used for gradient-enhanced COSY [22-24], HSQC [25,26] and HMBC [27,28] spectra. NOE spectra were acquired in CD_3CN at +25°C by means of the DPFGSE-NOE sequence [29-32], using a mixing time of 2.0 s and two "rsnob" 50 Hz-wide selective pulses. Data acquisition, Fourier transformation, and spectra elaboration were performed using the Varian software VNMRJ, 1.1D.

Calculations. Geometry optimization were carried out at the B3LYP/6-31G(d) level by means of the Gaussian 03 series of programs [13]. The reported energy values are not ZPE corrected. Harmonic vibrational frequencies were calculated for all the stationary points. For each optimized ground state the frequency analysis showed the absence of imaginary frequencies, *J*-coupling calculations were obtained with the GIAO method at the B3LYP/6-311++G(2d,p)//B3LYP/6-31G(d) level, and including the Fermi contact term.

2.4.4 Characterization of MKA

*ESI-MS (+):*experimental 307.1 m/z ($[M + Na]^+$),

$C_{15}H_{24}O_5$ requires 284.1697 (monoisotopic).

$[\alpha]_{D20}$ = −166 (c = 2.0; CH_3CN). Data never reported in literature.

Elemental analysis for $C_{15}H_{24}O_5$:

	% C	% H
Calculated	63.36	8.51
Experimental	63.91	8.59

IR: 3417, 2923, 1718, 1454, 1357, 1286, 1169, 1141, 1088, 958, 893, 820, 764.

NMR Assignment of 5

A sample suitable for NMR analysis was prepared in CD_3CN and analyzed at + 25 °C. Chemical shift references were the residual peaks of CD_3CN (1.95 ppm for ^1H, 0.54 ppm for ^{13}C). Standard high resolution ^{13}C-NMR and DEPT-135 spectra were acquired in order to table the exact chemical shifts and multiplicity of the two epimers of **5**.

^1H-^{13}C HSQC bi-dimensional spectrum allowed the correlation of each carbon with the corresponding protons. Protons belonging to C-6 and C-4 were assigned from the NOE spectra acquired on saturation of Me-16 (see text). COSY correlation from Me-16 and Me-15 assigned

the chemical shifts of H-4 and H-8, hence the corresponding carbons from HSQC. HMBC correlation (^{3}J) from the protons of Me-16 (doublet) assigned the shift of C-5, and confirmed the assignment of C-3. HMBC correlation (^{3}J) from the protons of Me-15 (doublet) assigned the shift of C-7 and C-9. HMBC correlation (^{3}J) from the protons of Me-14 (singlet) assigned the carbons C-13 and C-12. HMBC correlation (^{3}J) from C-13 assigned the shift of C-11.

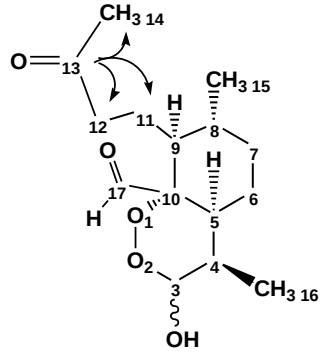

Full structural assignment of **5α** and **5β** is reported in the following tables.

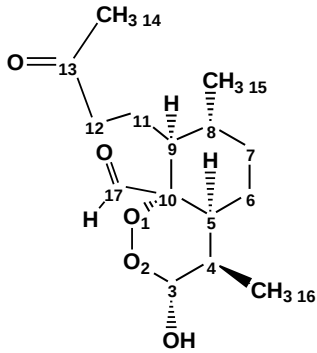

5α

	^{13}C δ	^{1}H δ, multiplicity, *J*
C12	43.32	2.49, m
C11	21.43	1.55, m
C9	50.40	1.21, m
C8	34.19	1.75, m
C7	35.18	1.82, 1.20, m
C6	23.85	1.98, 1.27, m
C5	41.42	2.26, m
C4	35.34	1.78, m
C3	101.31	4.95, s
C10	89.13	-
C15	19.91	0.904, d *J* = 6.5 Hz
C16	13.48	0.78, d, *J* = 7.5 Hz
C14	29.27	2.06, s
CHO	208.07	10.23, dd, *J*= 1.9, 1.5 Hz
C13	208.12	-
OH	-	

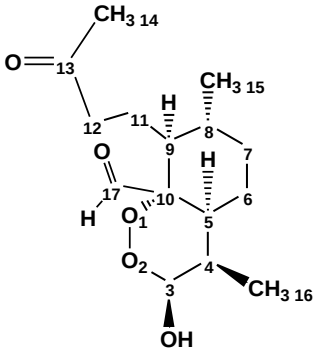

5β

	^{13}C δ	^{1}H δ, multiplicity, *J*
C12	43.28	2.49, m
C11	21.59	1.55, m
C9	50.35	1.11, m
C8	34.10	1.75, m
C7	35.21	1.82, 1.20, m
C6	24.50	2.06, 1.34, m
C5	49.19	1.95, m
C4	36.97	1.96, m
C3	100.26	5.26, d, *J* = 2.4 Hz
C10	88.97	-
C15	19.65	0.906, d, *J* = 6.5 Hz
C16	7.31	0.65, d, *J* = 7.4 Hz
C14	29.26	2.06, s
CHO	207.33	10.12, t, *J* = 1.7 Hz
C13	208.11	-
OH	-	

^{1}H spectrum of **5**

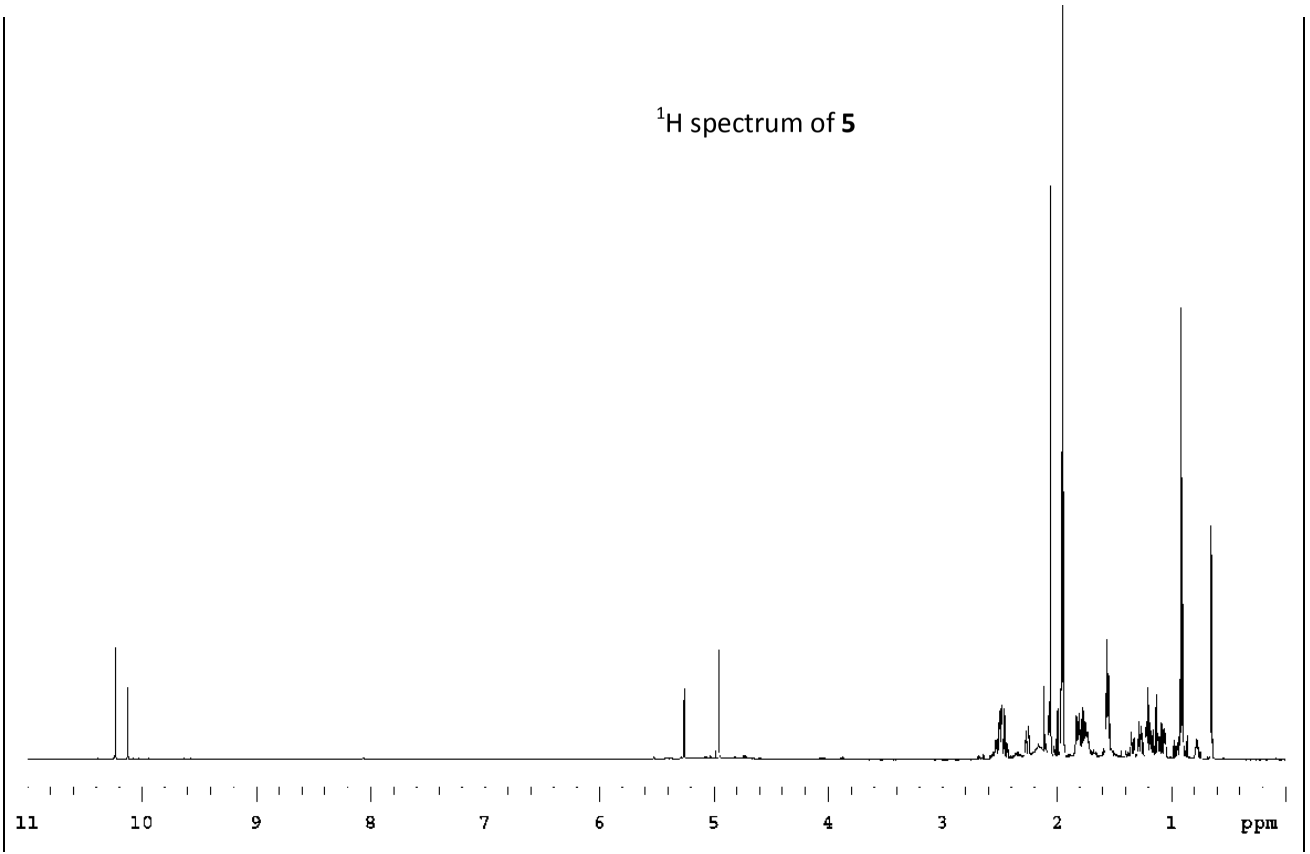

^{1}H spectrum of **5**, expansion of aliphatic region

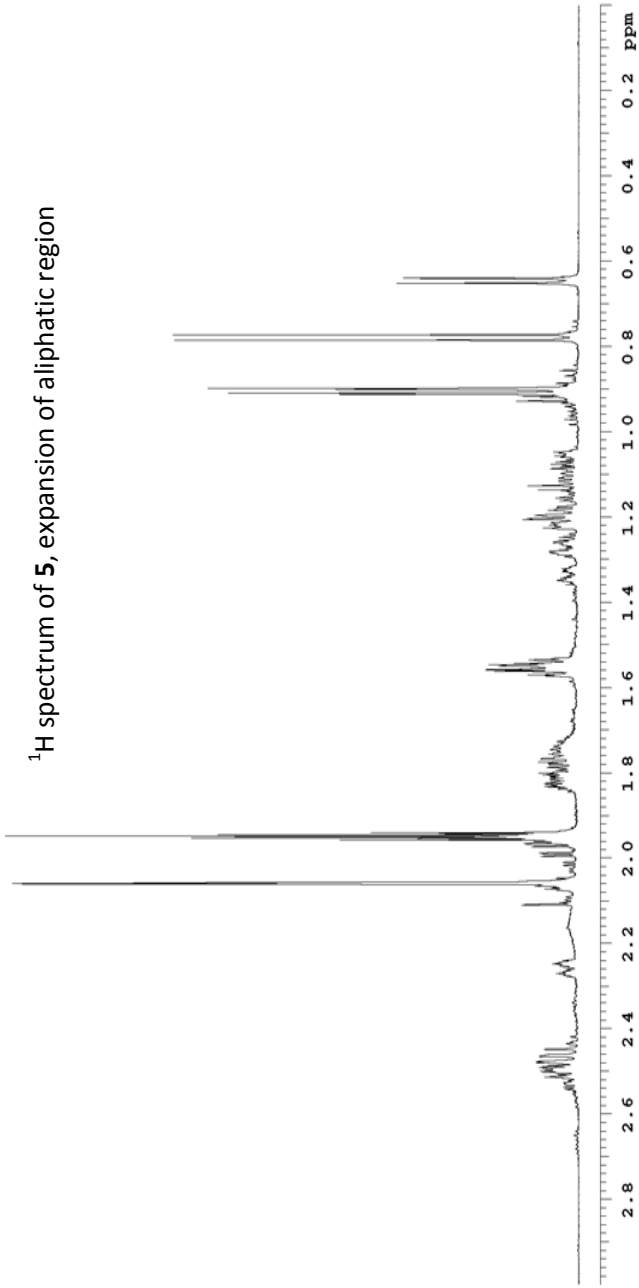

^{13}C spectrum of **5**, expansion of aliphatic region

INDEX	FREQUENCY	PPM	HEIGHT
1	15278.073	101.311	67.1
2	15120.423	100.265	41.1
3	13442.101	89.136	26.7
4	13417.513	88.973	21.6
5	7612.809	50.481	97.5
6	7594.296	50.359	61.3
7	7418.423	49.192	61.4
8	6529.797	43.300	90.4
9	6526.904	43.281	55.2
10	6246.316	41.420	94.7
11	5575.797	36.974	51.8
12	5329.921	35.343	85.3
13	5309.672	35.209	63.7
14	5306.201	35.186	105.7
15	5157.518	34.200	97.6
16	5142.477	34.100	60.3
17	4415.261	29.278	57.2
18	4412.947	29.263	31.5
19	3695.278	24.504	60.1
20	3596.060	23.846	102.2
21	3255.593	21.588	60.3
22	3231.584	21.429	95.7
23	3002.196	19.908	97.2
24	2963.724	19.653	62.8
25	2032.287	13.476	92.8
26	1101.718	7.306	56.3

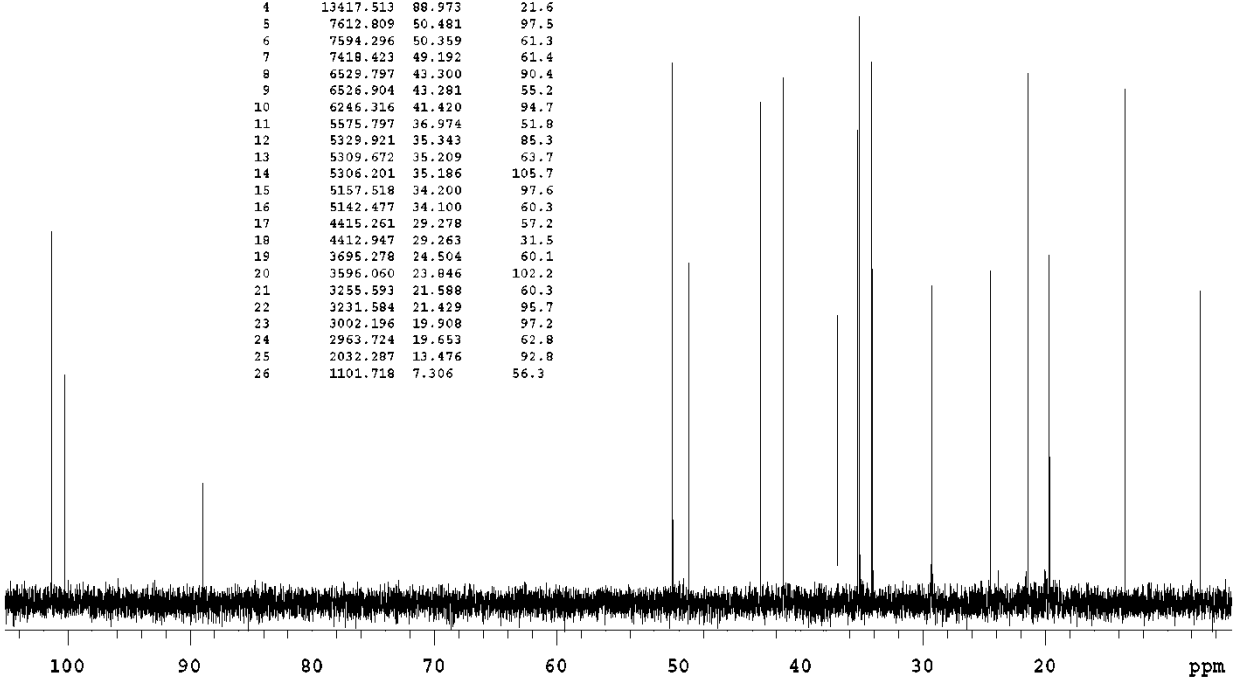

^{13}C spectrum of **5**, expansion of carbonylic region

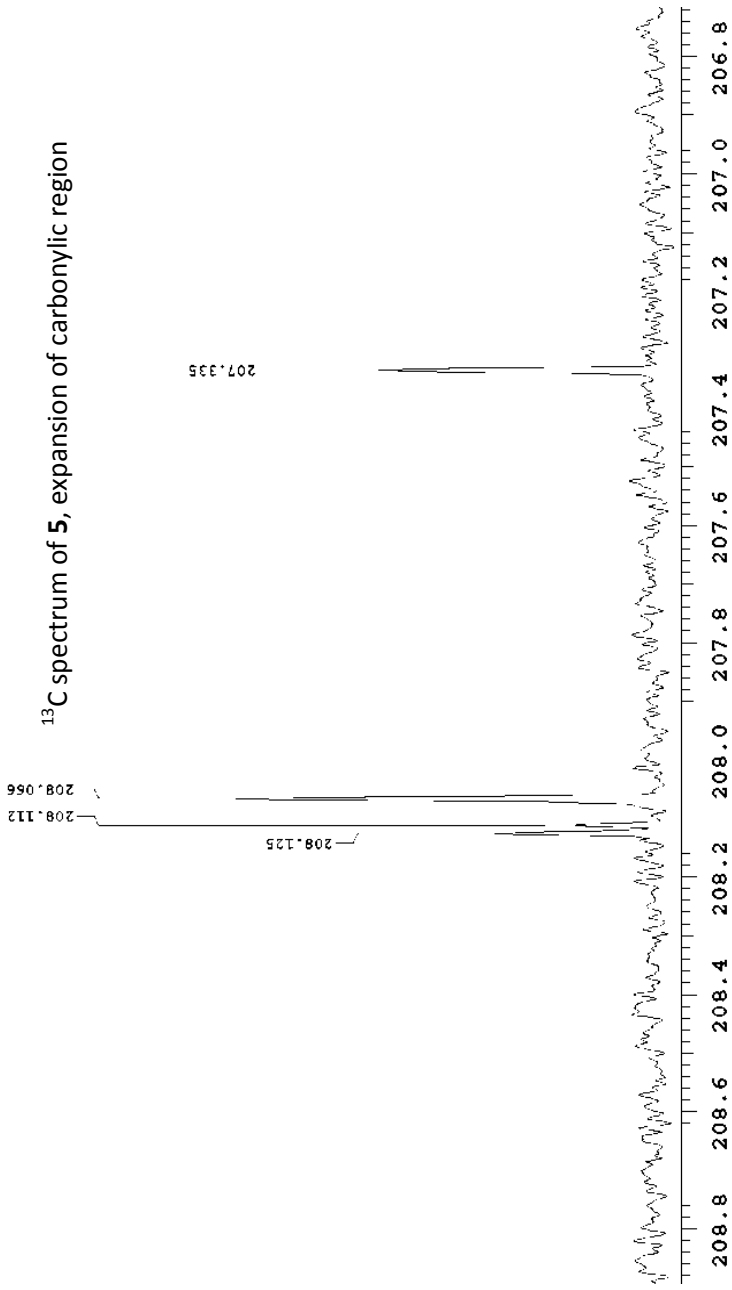

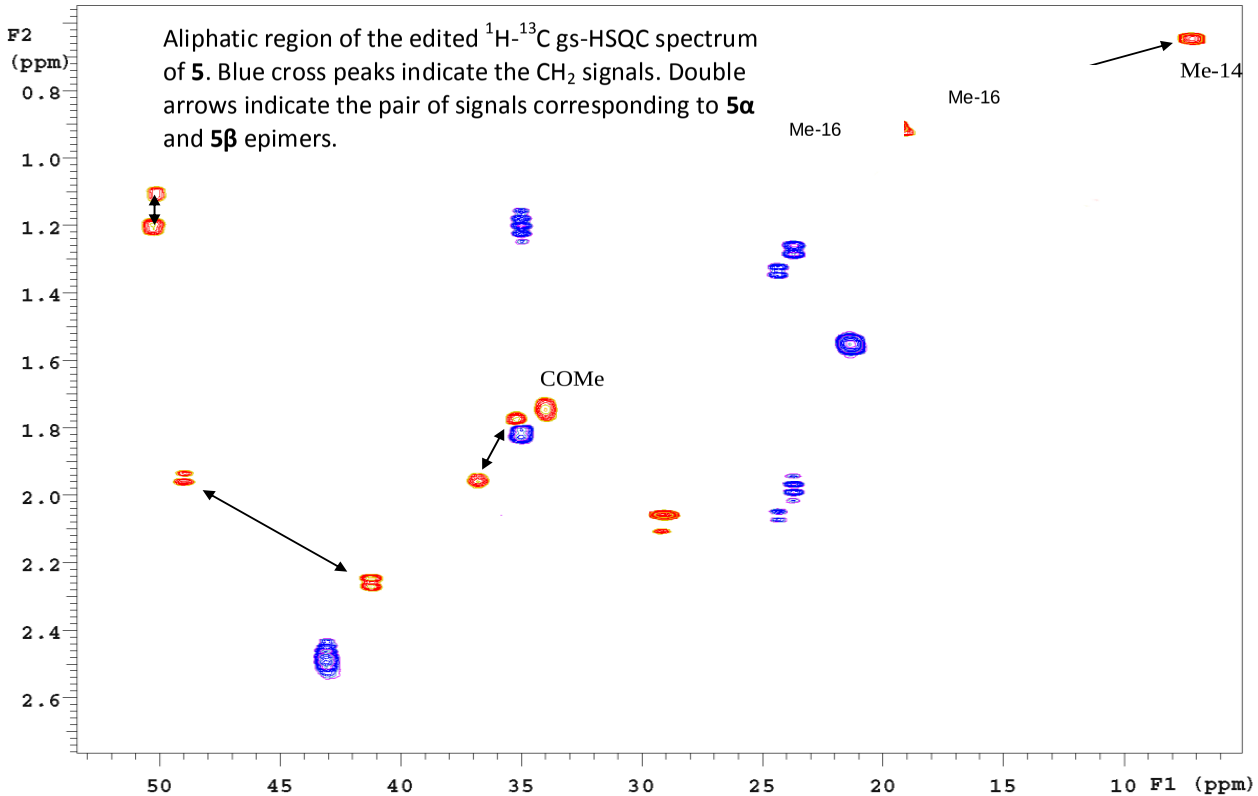
Aliphatic region of the edited ^{1}H-^{13}C gs-HSQC spectrum of **5**. Blue cross peaks indicate the CH_2 signals. Double arrows indicate the pair of signals corresponding to **5α** and **5β** epimers.
Me-14
Me-16
Me-16
COMe
F2 (ppm)
0.8
1.0
1.2
1.4
1.6
1.8
2.0
2.2
2.4
2.6
50
45
40
35
30
25
20
15
10
F1 (ppm)

Aliphatic region of the ^{1}H-^{1}H g-COSY spectrum of **5.**

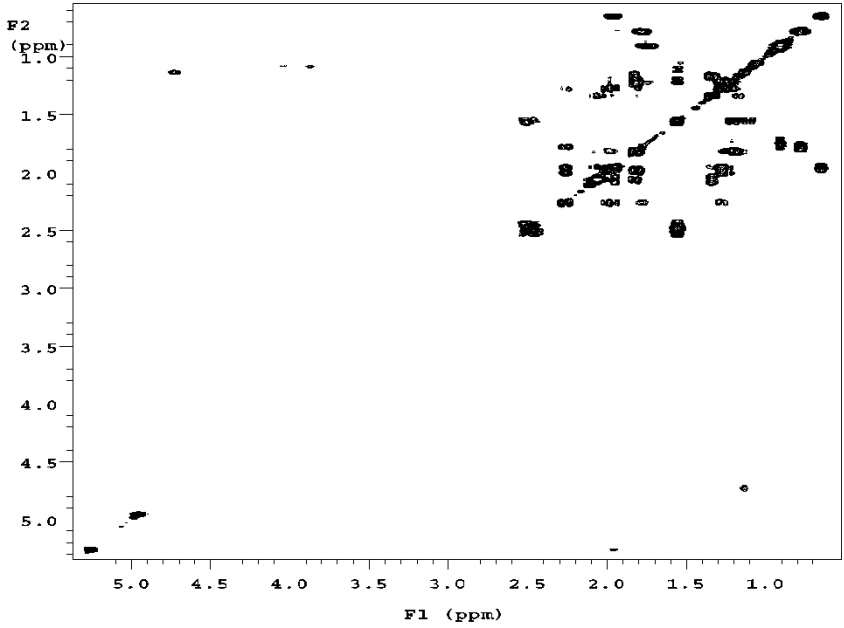

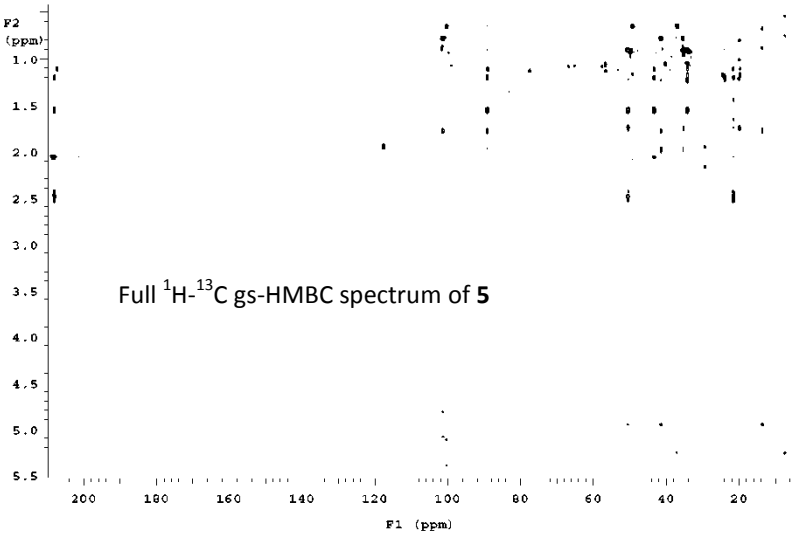

Full ^{1}H-^{13}C gs-HMBC spectrum of **5**

2.4.5 LSER Analyses

Both linear regression analyses and F-test and T-test statistical evaluations were performed by the dedicated functions implemented in the Microsoft Office Excel 2003 program. Probability related to the t-Student distribution in T-test was set to 0.05.

2.4.6 Molecular Modeling Calculations

All molecular modeling calculations were performed on a PC equipped with Intel Pentium 4, CPU 3.40 GHz, 2 GB of RAM and OS Windows 2000 Professional. Geometries of **5α**, **5β**, **5α**$^{-}$, and **5β**$^{-}$ were optimized at the SCF level by the semiempirical and Hartree-Fock/3-21G(*) methods implemented within the computer program SPARTAN 04 (Wavefunction Inc. 18401 Von Karman Avenue, Suite 370, Irvine, CA 92612, USA). With the same package were evaluated the relative hydration energies by the SM5.4/A solvation model. Geometries of **5α**, **5β**, **5α**$^{-}$, and **5β**$^{-}$ were further optimized at the SCF level by DFT calculations run with the Amsterdam Density Functional (ADF) package v. 2007.01 at two different levels of precision. Calculations at the lower level were carried out by the GGA-BLYP method with DZP medium core basis set, whereas the GGA-BLYP

method with QZ4P large core basis set was used for calculations at the higher level (only on **5α**, **5β**, **5α⁻**, and **5β⁻**). All the relative solvation energies in *n*-hexane, acetonitrile and water were computed with the same program by the COnductor like Screening MOdel (COSMO), with the cavity defined according to the Solvent Excluding Surface (SES) algorithm. Approximate assessments of molar volumes for **5α** and **5β** were based on the estimation of the respective molecular volumes performed by both SPARTAN 04 and the QSAR Properties calculator implemented in the computer program HyperChem Professional release 7.5.

2.4.7 Simulation of Dynamic Chromatograms

Simulation of variable-temperature experimental chromato-grams was performed by using the lab-made [16–21] computer program Auto DHPLC y2k which implements both stochastic [33] and theoretical plate models. [34] The developed algorithm may take into account all types of first-order interconversions, i.e., enantiomerizations as well as diastereomerizations or constitutional isomerizations (e.g., pseudo first-order tautomerizations). Within non-enantiomeric isomerizations, forward and backward interconversion occur at different rates in the achiral mobile phase,

where the two isomerizing species are present in differing amounts. According to the thermodynamic cycle involved inside a virtual chromatographic theoretical plate for a generic first-order isomerization concomitant with the chromatographic repartition equilibrium, we applied in the algorithm the following general equation:

$k_{-1}^{m}/k_{1}^{m} \times k_{1}^{s}/k_{-1}^{s} = k'_B/k'_A$,

where k'_A and k'_B are the retention factors of the first (A) and the second (B) eluting species, k_{-1}^{m} and k_{1}^{m} are the rate constants for the backward and forward interconversion in mobile phase, respectively, and k_{1}^{s} and k_{-1}^{s} are the rate constants for the forward and backward interconversion in stationary phase, respectively.

Program functionality was validated on several first-order isomerizations (both enantiomerization and non-enantiomerization) by comparing DHPLC results with those obtained by DNMR technique [16-19] or by classical method.[21] The algorithm developed also allowed to take tailing effects into account.

2.5 References and Notes

[1] Jansen, F. H. *Malaria Journal* **2010**, *9*, 212-216.

[2] Zeng, M.; Li, L.; Chen, S.; Li, C.; Liang, X.; Chen, M.; Clardy, J. *Tetrahedron* **1983**, *39*, 2941-2946.

[3] Lin, A. J.; Klayman, D. L.; Hoch, J. M.; Silverton, J. V.; George, C. F. *J. Org. Chem.* **1985**, *50*, 4504-4508.

[4] Lin, A. J.; Theoharides, A. D.; Klayman, D. L. *Tetrahedron* **1986**, *42*, 2181-2184.

[5] Haynes, R. K.; Chan, H.-W.; Lung, C.-M.; Ng, N.-C.; Wong, H.-N.; Shek, L. Y.; Williams, I. D.; Cartwright, A.; Gomes, M. F. *ChemMedChem* **2007**, *2*, 1448-1463.

[6] Dhooghe, L.; Van Miert, S.; Jansen, H.; Vlietinck, A.; Pieters, L. *Pharmazie* **2007**, *62*, 900-901.

[7] Baker, J. K.; McChesney, J. D.; Chi, H. T. *Pharm. Res.* **1993**, *10*, 662-666.

[8] El-Feraly, F.S.; Ayalp, A.; Al-Yahya, M.A. *J. Nat. Products.* **1990**, *53*, 920-925.

[9] Cabri, W.; Ciogli, A.; D'Acquarica, I.; Di Mattia, M.; Gasparrini, F.; Giorgi, F.; Mazzanti, A.; Pierini, M.; Quaglia, M. presented at the 19th Int. Symp. on Chirality. San Diego (USA), July, 8-11, 2007.

[10] Wesche, D.L.; De Coster, M. A.; Tortella, F.C.; Brewer, Tl G. *Antimicrob. Agents. Chemother.*, **1994**, *38*, 1813-1819.

[11] Cabri, W.; D'Acquarica, I.; Simone, P.; Di Iorio, M.; Di Mattia, M.; Gasparrini, F.; Giorgi, F.; Mazzanti, A.; Pierini, M.; Quaglia, M.; Villani, C. *J. Org. Chem.* **2011**, *76*, 1751-1758.

[12] Cabri, W.; D'Acquarica, I.; Simone, P.; Di Iorio, M.; Di Mattia, M.; Gasparrini, F.; Giorgi, F.; Mazzanti, A.; Pierini, M.; Quaglia, M.; Villani, C. *J. Org. Chem.* **2011**, *76*, 4831-4840.

[13] Gaussian 03, Revision E.01, Frisch, M. J.; Trucks, G. W.; Schlegel, H. B.; Scuseria, G. E.; Robb, M. A.; Cheeseman, J. R.; Montgomery, Jr., J. A.; Vreven, T.; Kudin, K. N.; Burant, J. C.; Millam, J. M.; Iyengar, S. S.; Tomasi, J.; Barone, V.; Mennucci, B.; Cossi, M.; Scalmani, G.; Rega, N.; Petersson, G. A.; Nakatsuji, H.; Hada, M.; Ehara, M.; Toyota, K.; Fukuda, R.; Hasegawa, J.; Ishida, M.; Nakajima, T.; Honda, Y.; Kitao, O.; Nakai, H.; Klene, M.; Li, X.; Knox, J. E.; Hratchian, H. P.; Cross, J. B.; Bakken, V.; Adamo, C.; Jaramillo, J.; Gomperts, R.; Stratmann, R. E.; Yazyev, O.; Austin, A. J.; Cammi, R.; Pomelli, C.; Ochterski, J. W.; Ayala, P. Y.; Morokuma, K.; Voth, G. A.; Salvador, P.; Dannenberg, J. J.; Zakrzewski, V. G.; Dapprich, S.; Daniels, A. D.; Strain, M. C.; Farkas, O.; Malick, D. K.; Rabuck, A. D.; Raghavachari, K.; Foresman, J. B.; Ortiz, J. V.; Cui, Q.; Baboul, A. G.; Clifford, S.; Cioslowski, J.; Stefanov, B. B.; Liu, G.; Liashenko, A.; Piskorz, P.; Komaromi, I.; Martin, R. L.; Fox, D. J.;

Keith, T.; Al-Laham, M. A.; Peng, C. Y.; Nanayakkara, A.; Challacombe, M.; Gill, P. M. W.; Johnson, B.; Chen, W.; Wong, M. W.; Gonzalez, C.; Pople, J. A.; Gaussian, Inc., Wallingford CT, 2004.

[14] Cabri, W.; Ciogli, A.; D'Acquarica, I.; Di Mattia, M.; Galletti, B.; Gasparrini, F.; Giorgi, F.; Lalli, S.; Pierini, M.; Simone, P. *J. Chromatogr. B.* **2008**, *875,*180-191.

[15] D'Acquarica, I.; Gasparrini, F.; Kotoni, D.; Pierini, M.; Villani, C.; Cabri, W.; Di Mattia, M.; Giorgi, F. *Molecules* **2010**, *15*, 1309-1323.

[16] Gasparrini, F.; Lunazzi, L.; Mazzanti, A.; Pierini, M.; Pietrusiewicz, K. M.; Villani, C. *J. Am. Chem. Soc.* **2000**, *122*, 4776-4780.

[17] Dell'Erba, C.; Gasparrini, F.; Grilli, S.; Lunazzi, L.; Mazzanti, A.; Novi, M.; Pierini, M.; Tavani, C.; Villani, C. *J. Org. Chem.* **2002**, *67*, 1663-1668.

[18] Gasparrini, F.; Grilli, S.; Leardini, R.; Lunazzi, L.; Mazzanti, A.; Nanni, D.; Pierini, M.; Pinamonti, M. *J. Org. Chem.* **2002**, *67*, 3089-3095.

[19] Dalla Cort, A.; Gasparrini, F.; Lunazzi, L.; Mandolini, L.; Mazzanti, A.; Pasquini, C.; Pierini, M.; Rompietti, R.; Schiaffino, L. *J. Org. Chem.* **2005**, *70*, 8877-8883.

[20] Ciogli, A.; Dalla Cort, A.; Gasparrini, F.; Lunazzi, L.; Mandolini, L.; Mazzanti, A.; Pasquini, C.; Pierini, M.; Schiaffino, L.; Yafteh Mihan, F. *J. Org. Chem.* **2008**, *73*, 6108-6118.

[21] Cirilli, R.; Ferretti, R.; La Torre, F.; Secci, D.; Bolasco, A.; Carradori, S.; Pierini, M. *J. Chromatogr. A* **2007**, *1172*, 160-169.

[22 Hurd, R.E. *J. Magn. Reson.* **1990**, *87*, 422-428.

[23] von Kielin, M.; Moonen, C.T.W.; van der Toorn, A.; van Zijl, P.C.M. *J. Magn. Reson.* **1991**, *93*, 423-429.

[24] Reynolds, W.F.; Enrìquez, R.G. *J. Nat. Prod.* **2002**, *65*, 221-244.

[25] Bradley, S. A.; Krishnamurthy, K. Magn. Res. Chem. 2005, 43, 117-123.

[26] Kontaxis, G.; Stonehouse, J.; Laue, E.D.; Keeler, J. *J. Magn. Reson. Ser. A* **1994**, *111*, 70-76.

[27] Hurd, R. E.; John, B. K. *J. Magn. Reson.* **1991**, *91*, 648-653.

[28] Willker, W.; Leibfritz, D.; Kerssebaum, R.; Bermel, W. *Magn. Res. Chem.* **1993**, *31*, 287-292.

[29] Stott, K.; Stonehouse, J.; Keeler, J.; Hwand, T.-L.; Shaka, A. J. *J. Am. Chem. Soc.* **1995**, *117*, 4199-4200.

[30] Stott, K.; Keeler, J.; Van, Q. N.; Shaka, A. J. *J. Magn. Resonance* **1997**, *125*, 302-324.

[31] Van, Q. N.; Smith, E. M.; Shaka, A. J. *J. Magn. Resonance* **1999**, *141*, 191-194.

[32] Claridge, T.D.W. High Resolution NMR Techniques in Organic Chemistry; Pergamon: Amsterdam, 1999.

[33] Jung, M. *QCPE Bull.* **1992**, *12*, 52.

[34] Trapp, O.; Schurig, V. *Comput. Chem.* **2001**, *25*, 187-195.

Acknowledgments

To my professor for his adventurous spirit and for always being where the action takes place. You have been such a great example!
To Ilaria for working next to me and talking with me, not only about chemistry: I learned a lot and shared a lot. The best wishes to you and your family.
To Prof. Pierini for the excellent advice (and the good chocolate). To Alessia for taking the pain to explain everything that was new to me and for being enthusiastic while doing it. To Signora Giovanna for her good spirits, her organization and her care.
To Nina, for the last 9 years.